Author:
Al-Jawoosh, Sara

Title:
Fabrication and characterisation of a novel biomimetic interpenetrating composite – a potential orthodontic bracket material

Fabrication and characterisation of a novel biomimetic interpenetrating composite – a potential orthodontic bracket material

by

Sara Al-Jawoosh

A dissertation submitted to the University of Bristol in accordance with the requirements for award of Doctor of Philosophy in the Faculty of Health Science

Submitted February 2019

Bristol Dental School
Lower Maudlin Street
Bristol BS1 2LY

Word count 61289

Abstract

Objective. To fabricate and characterise a novel biomimetic interpenetrating phase ceramic/polymer composite material consisting of aligned honeycomb-like porous ceramic preforms infiltrated with polymer for potential orthodontic bracket material applications.

Method. Unidirectional freeze-casting with a temperature gradient was used to fabricate and control the microstructure and porosity of alumina ceramic preforms, which were subsequently infiltrated with 40 to 80% by volume UDMA-TEGDMA and PC polymers. The composite materials had a gradient structure with a more dense bottom part (ceramic-rich) while the top part was more porous (ceramic-poor). These composite materials were then subjected to characterisation, namely ceramic volume fraction, density, compression, three-point bend, fracture toughness, hardness, surface roughness, abrasivity testing and surface loss. Samples were also subjected to scanning electron microscopy and micro computerised tomography (MicroCT).

Results. Three-dimensional aligned honeycomb-like ceramic structures were produced and full interpenetration of the polymer phase was observed using MicroCT. Depending on the volume fraction of the ceramic preform, the ceramic volume fraction of the final interpenetrating composites ranged from 18.83 to 61.17%, density ranged from 1.73 to 3.36 g/cm^3, compressive strength ranged from 26.31 to 253.97 MPa, flexural strength from 28.28 to 145.65 MPa, fracture toughness from 3.91 to 4.86 $MPa.m^{½}$, hardness ranged from 1.46 to 1.62 GPa, surface roughness following toothbrushing from 0.99 to 1.43 µm and surface loss from 0.56 to 1.40 µm.

Significance. Freeze-casting provides a novel method to engineer composite materials with a unique aligned honeycomb-like interpenetrating structure, consisting of two continuous phases, inorganic and organic. There was a correlation between the ceramic fraction and the subsequent, density, strength, fracture toughness, hardness and abrasivity of the composite materials. These composite structures could be potentially used as a composite bracket material to compete with the current aesthetic orthodontic brackets.

Dedication and Acknowledgements

I would like to dedicate this work to my mother and late father, Thanaa Matlak and Mohamed Al-Jawoosh, whose hard work and dedication to our family have proved inspirational and encouraged me to progress.

I declare my sincere gratitude to the Higher Committee of Education Development in Iraq who provided me with an incredible opportunity to develop as a researcher.

I would like to express my sincere gratitude to my supervisor, Professor Bo Su for his continuous support of my PhD study.

To my supervisor Professor Anthony Ireland, I wish to express my heartfelt thanks. Your scientific rigor, mentorship and unwavering support have made this work possible. The enthusiasm and diligence you present every day is truly admirable.

I would like to acknowledge all members of the Biomaterials Engineering group who have supported me throughout my time at Bristol. I have been lucky enough to meet a team committed researchers who have continually helped and encouraged me to make my time in the laboratory thoroughly enjoyable.

I would like to thank Mrs Judith Mantell for her assistance with the SEM imaging, Dr Tom Davies for his assistance with MicroCT imaging and Mr Nicholas Chapman for his assistance with preparing the human teeth.

Finally, I would like to thank my guarantors, my mother, Thanaa, my uncle Jamal and my aunt Maha for all their continued love, support and inspiration. I like to declare my deepest appreciation to my sisters Israa and Shahad and my brother Hussein for all their continued love and encouragement.

Author’s Declaration

I declare that the work in this dissertation was carried out in accordance with the requirements of the University's *Regulations and Code of Practice for Research Degree Programmes* and that it has not been submitted for any other academic award. Except where indicated by specific reference in the text, the work is the candidate's own work. Work done in collaboration with, or with the assistance of, others, is indicated as such. Any views expressed in the dissertation are those of the author.

SIGNED: ……. DATE: ……

Contents

List of Figures

List of Tables

Abbreviations

2D	Two-Dimension
3D	Three-Dimension
°C	Cellulose degrees
Al_2O_3	Alumina
Bis-GMA	Bisphenol A-glycidyl methacrylate
cm	Centimetre
g	Gram
GPa	Gigapascal
hrs	Hours
kV	Kilovolt
µA	Microampere
MicroCT	Micro Computerised Tomography
mins	Minutes
ml	Millilitre
mm	Millimetre
µm	Micrometre
mol	Mole
MPa	Megapascal
N	Newton
PC	polycarbonate
ppm	Parts per million
psi	Pounds per square inch
PVA	Polyvinyl alcohol
rpm	Revolutions per minute
SD	Standard Deviation
sec	Seconds
SEM	Scanning Electron Microscopy
SiC	Silicon Carbide

TEGDMA	Triethylene glycol dimethacrylate
UDMA	Urethane dimethacrylate
vol	Volume
wt	Weight

Chapter 1. Introduction

Within both restorative dentistry and orthodontics there is a need for biomimetic materials that more closely mimic the properties of natural tooth tissue. In restorative dentistry such a material could be used to restore tooth tissue lost through trauma or caries. A hybrid dental ceramic composite (i.e. VITA Enamic®) is commercially available (He and Swain, 2011; Coldea *et al.*, 2013) for use with CAD/ CAM technology to mill dental restorations. In orthodontics such a material with a more aesthetic appearance and matched mechanical properties to natural tooth might also have advantages when compared to currently available aesthetic bracket materials, such as ceramics or polymers.

Orthodontic brackets are used to transmit loads from the archwire to the tooth (Rahiotis and Schricker, 2017), and are most commonly metallic and bonded to the labial surfaces of the teeth, which makes them highly visible. In the United States, from 1981 to 2013, the number of adults seeking orthodontic treatment grew from 15% to 23% (Christensen and Luther, 2015) and as a result there have been increasing demands for more aesthetic, non-metallic bracket materials. Currently available aesthetic orthodontic brackets are either made from a polymer e.g. polycarbonate or polyurethane, or a ceramic, usually alumina, and the latter are either mono or polycrystalline in structure (Feldner *et al.*, 1994; Kusy, 2002).

Polymeric brackets, although aesthetically good at the start of treatment, are not popular due to poor dimensional stability under applied load (creep), staining and low

wear resistance (Feldner *et al.*, 1994; Zinelis *et al.*, 2005). Although ceramic brackets do not suffer from the same disadvantages, they are brittle with a tendency to fracture in-service, have a high surface hardness which can lead to abrasion of opposing teeth, and there is an increased risk of enamel fracture during bracket removal (Buzzitta *et al.*, 1982; Douglass, 1989).

An ideal aesthetic orthodontic bracket would combine all of the advantages and none of the disadvantages of currently available polymeric and ceramic brackets. These would include improved wear resistance, whilst minimising damage to opposing teeth, good stain resistance, good dimensional stability with minimal creep, and ease of removal from the tooth surface at completion of treatment. Although brackets comprising two material phases have been produced in the past, they are essentially a ceramic bracket with a thin polymer bonding base. Such a bracket still possesses many of the unwanted properties of ceramic brackets, namely brittleness and wear of opposing teeth. In addition, the polymeric base can delaminate during clinical service, leading to loss of tooth control and the need to bond a new replacement bracket (Olsen *et al.*, 1997; Elekdag-Turk *et al.*, 2009). Consequently, the development of a composite material that exhibits the advantages of both polymeric and ceramic brackets in a single interconnected network is desirable.

Certain naturally occurring biomaterials, including enamel and dentine, exhibit an interconnected dual phase structure leading to remarkable mechanical properties, which enable them to meet the biological functional needs of the organism (Munch *et al.*, 2008). Dental enamel is the hardest, most mineralised structure in the human body.

It is composed of 96% to 97% hydroxyapatite, 1% collagen and 2% to 3% water. Throughout a lifetime, enamel can endure the forces of mastication over millions of cycles (He *et al.*, 2013). By contrast, the underlying dentine is a porous, less well mineralised, but tougher material composed of 70% hydroxyapatite, 20% collagen and 10% water by weight (Zaslansky *et al.*, 2010). When joined together these two materials provide a biomechanically, long lasting, compatible system.

The aim of the present study is to produce a novel biomimetic ceramic/polymer composite for use as a possible orthodontic bracket material. The novelty of such a material would be defined by its unique microstructure, characterised by two continuous interconnected inorganic and organic phases as shown in Figure 1-1. The polymer rich surface attached to the tooth surface will aid bonding and debonding, and the ceramic rich surface, directly exposed to the oral environment, will provide the mechanical stability and durability in clinical use. In this way the final composite material will ideally combine the desirable properties of both ceramics and polymers, creating a durable, safe and aesthetically pleasing orthodontic bracket.

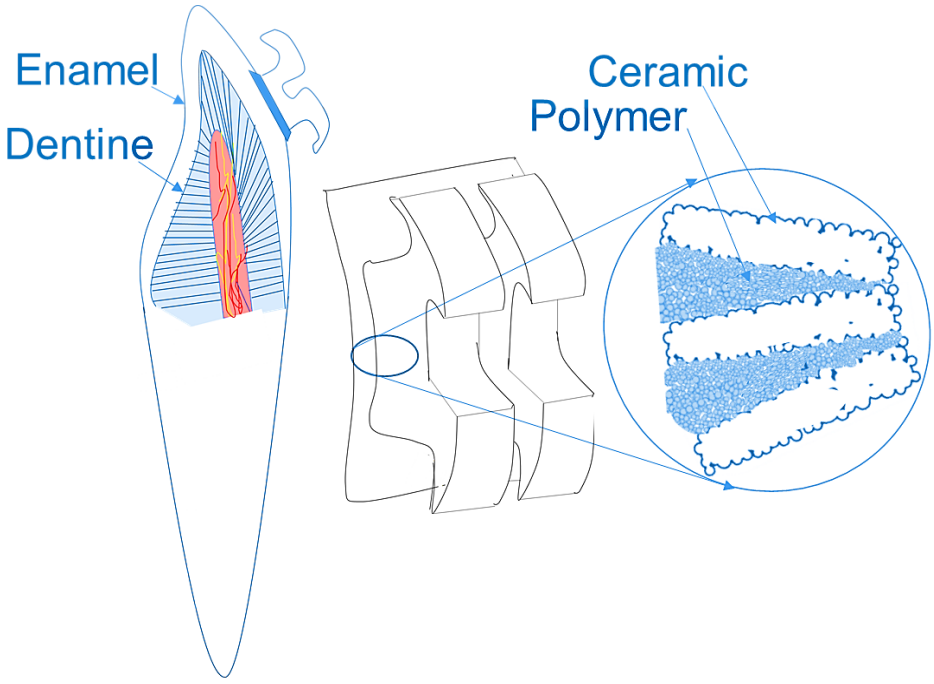

Figure 1-1. Schematic of the structure of the central incisor with the anisotropic feature of the biomimetic composite orthodontic bracket.

Freeze-casting is a well-established technique that can be used to fabricate porous scaffolds with complex microstructures. The process utilises the directional solidification of a ceramic suspension in a double-sided cooling/freezing device. The suspension is placed in a mould between two cooled surfaces, one of which is colder than the other and from this surface ice crystals begin to form in a unidirectional fashion. As the suspension continues to freeze the ice crystals grow from the coldest to the least cold surface. In doing so they compress the ceramic particles within the suspension to form an interconnected scaffold, which is then freeze-dried and sintered. The technique is relatively simple, cost efficient, environmentally friendly and offers the ability to produce a porous material with a controlled-size and interconnection of the pores. A

large number of processing parameters are used to tailor the final architecture of the porous scaffold, by controlling the crystal growth of ice (Zhang *et al.*, 2009; Deville, 2010).

The principal aim of the current study is to produce a biomimetic ceramic/polymer-infiltrated composite material using the freeze-casting technique, followed by its infiltration with UDMA-TEGDMA and polycarbonate (PC) polymers. The effect of the initial ceramic solid loading used during the freeze-casting phase on the microstructure, physical, mechanical and surface properties of the final ceramic polymer composite were then investigated.

Chapter 2. Literature review

2.1 Adult Orthodontics

Dental aesthetics is a key factor in overall physical attractiveness, it contributes to self-esteem and this is one of the main reasons patients undergo orthodontic treatment (Kerosuo *et al.*, 1995; Gazit-Rappaport *et al.*, 2010). The number of adults seeking orthodontic treatment has been increasing in recent years and in 2009 the number who underwent orthodontic treatment in the UK reached more than 51,000. This number continues to rise (Christensen and Luther, 2015) and this trend is also being seen worldwide (Pabari *et al.*, 2011; Johal *et al.*, 2014; Christensen and Luther, 2015; Tang *et al.*, 2015; Kim, 2017). A large number of adults also refuse to undergo orthodontic treatment on the basis of the negative appearance associated with conventional metallic fixed orthodontic appliances. However, they are often willing to pay more for appliances they consider aesthetic (Rosvall *et al.*, 2009).

The evolution and availability of aesthetic appliances, including the introduction of aligners and lingual appliances, may explain some of this increase in demand (Pabari *et al.*, 2011). Labial fixed appliances also now use smaller brackets and many are also tooth coloured (Cunningham *et al.*, 2000; Scott *et al.*, 2007). A cross-sectional survey of orthodontic specialists in the UK by Cedro *et al.* (2010) showed that the increasing options and number of aesthetic appliances had a positive impact on the number of adults seeking orthodontic treatment, and that many were willing to pay for it. Other possible reasons include improved accessibility to orthodontic services, as well as

improved awareness and a more progressive, positive attitude toward the treatment possibilities for adult patients (Scott *et al.*, 2007; Pabari *et al.*, 2011; Christensen and Luther, 2015). A survey by the British Orthodontic Society in June 2016 revealed the rising number of adults seeking orthodontic treatment in the UK. The survey illustrated that the key drivers for treatment appear to be the awareness of the possibility of adult orthodontics alongside rising expectations on how treatment can positively impact on appearance and well-being (Mianger, 2016). The number of orthodontists providing adult orthodontic treatment is also on the increase. A survey conducted in March 2018 among UK orthodontists revealed an increase in private adult treatment from 75% in 2016 to 80% in 2018 (Scully, 2018).

For the orthodontist, an advantage of treating adults is that they are more self-motivated towards the treatment when compared to children, as their principal motivation is the desire to improve dental appearance (Pabari *et al.*, 2011). However, the disadvantage is being able to meet their often higher treatment expectations. Previous studies have shown that satisfaction with facial and body image decreases with increasing age, which might explain the higher expectations, not only of the in treatment appliance appearance, but also the final treatment outcome (Bos *et al.*, 2003; Al-Omiri and Abu Alhaija, 2006). Furthermore, media can have a significant influence, especially with the increased demand to look good (Nattrass and Sandy, 1995). This can also explain the rise in the number of patients who are seeking re-treatment following previous orthodontic treatment.

2.2 Perception of orthodontic appliances

Although fixed orthodontic appliances have been modified in recent years to improve in treatment aesthetics e.g. bonded rather than banded appliances and reduced mesio-distal bracket dimensions, the appearance of these appliances still directly affects the perception of facial attractiveness. Studies have found that there is a general acceptance that invisible and tooth-coloured orthodontic appliances are preferable in terms of appearance to more traditional metal appliances (Newton *et al.*, 2003; Jeremiah *et al.*, 2010). According to Cedro *et al*. (2010) the most common complicating factor in orthodontic treatment is the appearance of orthodontic appliances, affecting more than 59% of private and 32% of NHS patients.

Furthermore, in a survey of 27-year-olds in Sweden, 33% of patients would not wear visible braces. Interestingly, 84% said they would have worn visible appliances as an adolescent (Bergström *et al.*, 1998), which supports the suggestions that adult patients are less likely to consider non-aesthetic appliances than adolescents. This is further supported by another study where 97% of adult Chinese female patients stated that they were seeking orthodontic treatment to improve their aesthetics, but 67% would not consider orthodontics due to the visibility of the appliance (Tang *et al.*, 2015). Furthermore Walton *et al.* (2010) reported that older patients tended to rate clear orthodontic appliances higher than did younger subjects. The acceptability of different orthodontic appliances by adults was also investigated by Rosvall *et al.* (2009) using a computer-based survey. The authors found that lingual appliances and clear aligners were the most acceptable, followed by labial ceramic and finally labial metal appliances.

Indeed, 90% of those included in the survey stated that they found labial ceramic appliances acceptable.

2.3 Currently available aesthetic appliances

2.3.1 Invisalign™/clear aligners

The use of clear aligners and most notably Invisalign™ started to become widespread in the early 2000s with the introduction of a sequential series of computer generated clear removable aligners by Align Technology Inc. The aligners are produced on a series of casts, with teeth reset in small increments as the patient progress from one aligner to the next in the series (Kuo and Miller, 2003; Weir, 2017).

By 2007, 300,000 cases had been treated using this technique in the USA alone (Kuncio *et al.*, 2007). Although initially released for use by specialists in orthodontics, they are now being marketed for use by general practitioners, which is not without risk.

Indications for the use of Invisalign™ include cases with mild to moderate crowding/spacing, mild open and deep bites, treatment of relapse following orthodontic treatment and in cases where there is no skeletal constriction of the arches (Clements *et al.*, 2003; Boyd *et al.*, 2006; Boyd, 2008; Rossini *et al.*, 2014; Li *et al.*, 2015). Contraindications include complex malocclusions, cases where there is a large antero-posterior discrepancy, anterior extrusion, rotation and severe deep bite cases (Clements *et al.*, 2003; Djeu *et al.*, 2005; Rossini *et al.*, 2014).

The advantages of clear aligners are their aesthetic appearance, the ability to remove them for cleaning and being comfortable to wear (Djeu *et al.*, 2005). However, the principal disadvantage is that treatment results rely on patient compliance. If they fail to wear them as instructed, treatment will not progress and if they do not remove them as instructed for cleaning, they may compromise both enamel and gingival health. Patients must also be monitored carefully to verify that tooth movement is tracking with the series of aligners. Some specific tooth movements with clear aligners still require the use and placement of composite tags and the wear of elastics and auxiliaries. Although tooth coloured they can still be visible and therefore these appliances are not completely invisible (Djeu *et al.*, 2005).

Nevertheless, despite thousands of completed cases and published case reports, orthodontists still generally feel that clear aligners produce inferior results when compared to fixed orthodontic appliances (Djeu *et al.*, 2005; Maganzini, 2006). Interestingly a recent survey in the USA that investigated differences in case selection and treatment management between orthodontists and general practitioners showed that orthodontists were more likely to identify the better treatment outcomes that can be achieved for their patients with fixed appliances when compared to Invisalign™ (Best *et al.*, 2016).

Other retrospective studies comparing the outcomes of Invisalign™ treatment versus fixed appliances treatment in adult patients have confirmed that treatment with fixed appliances is significantly more effective. Invisalign™ treatment was often quicker, but at the expense of the final occlusal result (Djeu *et al.*, 2005; Maganzini, 2006; Gu *et al.*,

2017). Clinicians are therefore often advised to ask for patients' consent to wear fixed appliances for a short period following Invisalign™ treatment (Giancotti *et al.*, 2006). Indeed, Kravitz *et al.* (2009) reported that 70% to 80% of clinicians considered the need for refinement with fixed appliances to finish such cases. More recently Gu *et al*., (2017) reported a lower refinement rate, although still 37.5%, and attributed this reduction to improvements in the aligner material and increased clinician experience.

2.3.2 Lingual orthodontics

Lingual orthodontic appliances are placed on the lingual and palatal surfaces of the teeth using the indirect bonding technique. They were introduced in the early 1970s, and initially they were merely labial brackets bonded to the lingual surfaces of the teeth (Fujita, 1979). In recent years a number of new systems have been introduced, either off the shelf systems, for example the 2D lingual bracket system (Forestadent, Pforzheim, Germany), or custom-made such as Incognito (3M, USA), as can be seen in Figure 2-1, which uses CAD/CAM technology to produce customised lingual appliances.

Figure 2-1. Lingual orthodontic appliance (Melsen, 2012).

These fully customised lingual orthodontic systems are marketed as achieving accurate results with enhanced patient comfort (Wiechmann *et al.*, 2003; Grauer and Proffit, 2011; Knösel *et al.*, 2014). Although lingual appliances are much more popular in Europe and Asia than in the United States, in the UK only 0.3% of specialist orthodontists use lingual appliances (Banks *et al.*, 2010). However, this number is growing and now about 10% of specialist orthodontists offer lingual orthodontic treatment (British Orthodontic Society, 2018).

Advantages of lingual appliances include: aesthetics, no labial gingival hypertrophy, reduced risk of caries, no damage to the labial surfaces of the teeth and better visualisation of the bucco-lingual position of the teeth (Fujita, 1979; Creekmore, 1989; Van der Veen *et al.*, 2010; Pauls *et al.*, 2017).

However, lingual appliances are not without their problems. These include: different mechanics and therefore treatment planning, a shorter arch perimeter leading to a smaller inter-bracket distance and consequently smaller cross sectional dimension archwires must be used (Moran, 1987; Park *et al.*, 2015). Also, placement of the appliance requires change in the clinician position and as such posture is different (Creekmore, 1989). Difficulties in the placement of brackets have as well been encountered due to the irregular and inconsistent lingual surface which can result in longer chairside time (Wiechmann *et al.*, 2003).

Furthermore, the bracket loss rate is substantially higher than in labial cases, indirect rebonding is complex and imprecise, the finishing process is time-consuming (Rummel *et*

al., 1999; Stamm *et al.*, 2000) and patients often have difficulty adapting to the appliance, especially when undergoing lingual treatment in both arches. Other difficulties include maintaining a good standard of oral hygiene, greater pain experience and problems eating and speaking (Miyawaki *et al.*, 1999; Kluemper *et al.*, 2002; Hohoff *et al.*, 2003; Hohoff *et al.*, 2004; Shalish *et al.*, 2011).

Recent systematic reviews have also shown that clinical trials investigating lingual appliance treatment showed a high risk of bias, with poor study designs, heterogeneity and small sample sizes (Mistakidis *et al.*, 2015; Papageorgiou *et al.*, 2016).

Despite these disadvantages, it is likely that lingual appliances will continue to develop in order to overcome the current shortcomings, thereby improving their acceptability to both orthodontists and patients alike.

2.3.3 Aesthetic labial appliances

There are many types of aesthetic orthodontic labial appliances and whatever the material used in their construction, ideal orthodontic brackets should have a number of desirable properties (Table 2-1). These properties will influence and affect the clinician's choice and perhaps ultimately the patient's choice as to what bracket to use. Britton *et al.* (1990) has described how orthodontists choose brackets based upon a combination of smooth edges, aesthetics and the design of the bracket base.

Although there is an ideal list of properties for orthodontic brackets, to date no single bracket or material possesses all of these properties. With these ideal bracket

characteristics in mind, polymeric and ceramic labial brackets will now be discussed in turn.

	Bracket type	
Ideal property	**Ceramic**	**Polymer**
Good biocompatibility and poor bio host	+	+
High fracture toughness	–	+
High strength	+	–
Good aesthetics and stain resistance	+	–
Low friction	–	–
Low risk of iatrogenic wear of enamel	–	+
Good bonding ability	–	+
Ease of debonding	–	+
Good abrasion resistance	+	–
Cost effective and environmentally friendly	–	+

Table 2-1. Properties of ideal and available aesthetic orthodontic brackets.

2.3.4 Polymeric orthodontic brackets

The first commercially available aesthetic brackets were polymeric brackets introduced as the aesthetic alternative to metal brackets during the early 1970s. These early polymeric brackets were made from unfilled polycarbonate but were soon known for their many disadvantages. Although they were relatively transparent and capable of resembling the shade of the underlying tooth, they had a tendency to stain easily (Figure 2-2) and also become odorous as a result of exposure to different foods and coloured mouth rinses.

Figure 2-2. Polycarbonate brackets staining and loss of aesthetic properties rendering them anaesthetic and uncomfortable to the patient (Brantley and Eliades, 2001).

Of equal concern was their tendency to deform or creep under constant load. As a result, torqueing forces generated by rectangular wires are not effectively transmitted to the teeth (Dobrin *et al.*, 1975; Swartz, 1988; Birnie, 1990; Faltermeier *et al.*, 2007a; Nishio *et al.*, 2009; Möller *et al.*, 2009). The distortion of the arch wire slot also leads to increased frictional resistance (Thorstenson and Kusy, 2003). According to Feldner *et al.* (1994), approximately 12% to 15% of torqueing force is lost due to creep in the case of the polycarbonate brackets. Therefore, additional torque applied to the archwire was suggested in order to obtain the expected torque when using polycarbonate brackets.

Other potential problems with polymeric brackets include a relatively poor abrasion resistance, poor frictional characteristics and plasticisation due to water absorption (Tselepis *et al.*, 1994; Arici and Regan, 1997; Thorstenson and Kusy, 2003; Cacciafesta *et al.*, 2003; Ali *et al.*, 2011). This means that they are susceptible to wear not only from toothbrushing, but also from contact with opposing teeth.

Therefore it is not unusual for the tie wings to wear away during the course of treatment, resulting in difficulties in retaining the archwire in the bracket slot (Aird and

Durning, 1987; Winchester, 1992a; Faltermeier *et al.*, 2007a; Wriedt *et al.*, 2007; Ali *et al.*, 2011).

As a result, treatment time is likely to be extended, and the mechanics of tooth movement compromised. It is partly for these reasons the use of polymeric brackets, in particular by American orthodontists, was reported to have decreased over the period 1986 to 2014, from 58% to only 4% (Keim *et al.*, 2014). Moreover, this decrease can be attributed to the steady improvement in ceramic brackets including good aesthetics, enhanced mechanical properties and advances in the bonding systems.

To date polymeric brackets have been manufactured using either polycarbonate, polyurethane or polyoxymethylene and all suffer from the disadvantages already described. However, further concerns have been raised with respect to the use of polyoxymethylene as an aesthetic bracket material (Reynolds, 1975; Bishara and Fehr, 1997). Although polyoxymethylene was said to provide stronger bracket tie wings, have improved abrasion resistance, less discolouration and better sliding mechanics, the principal disadvantage is that under certain conditions polyoxymethylene can degrade and release formaldehyde. This includes response to thermal stimuli, acids such as fizzy drinks, mechanical stimuli from the archwire or mastication, and background radiation. This is a real problem as formaldehyde is mutagenic and carcinogenic and its vapour alone can result in mucosal irritation and dermatitis. Furthermore, if formaldehyde is combined with water and ingested it can lead to abdominal pain and even death (Kusy and Whitley, 2005).

To summarise, polymeric brackets are best restricted to cases requiring minimal tooth movement (Jena *et al.*, 2007). In an attempt to overcome the problems of polymeric brackets, in particular the problem of creep, manufacturers have altered the polymer, introduced fillers and also added metal slot liners.

2.3.4.1 Metal slot liners

Metal slot liners added to polymeric brackets reduce the effect of creep, improve torque transfer when in rectangular wires and improve the frictional characteristics of the brackets. A study comparing seven polymeric brackets, with or without various modifications including metal slot liners, found that those with a metal slot liner demonstrated the lowest degree of creep under load. As a result the authors concluded that polymeric brackets were only suitable for clinical use if they possessed a metal slot liner (Sadat-Khonsari *et al.*, 2004). This finding was supported by other similar studies (Alkire *et al.*, 1997; Harzer *et al.*, 2004; Möller *et al.*, 2009; Nishio *et al.*, 2009; Matsui *et al.*, 2015).

Choi *et al.* (2013) measured the *in vitro* frictional resistance during sliding mechanics of three types of polymeric brackets, including glass fibre-reinforced polycarbonate, filler-reinforced polycarbonate, and a hybrid polycarbonate/polyethylene polymer with a metal slot insert, and compared them with stainless-steel and ceramic brackets. They found that the polymeric brackets with a metal slot liner showed the lowest frictional values, including the stainless-steel control bracket. Although they concluded that polymeric brackets with metal slot liners were the best choice among polymeric

brackets for low frictional resistance, this finding was not supported by the earlier work of Thorstenson and Kusy (2003), who found that the addition of these inserts did not considerably improve the frictional resistance over those without inserts. Indeed Ali *et al.* (2011) found the slot periphery in some metal slot liners to be particularly rough, such that it may affect sliding mechanics.

2.3.4.2 Fibre/filler reinforcements

To overcome the problems of low wear resistance, creep and staining, polymeric brackets have been reinforced with fillers and/or fibres. Of the fillers, the most commonly used is silica. Several different types of fibre have also been used including carbon, polyethylene and fibreglass, with the latter said to have the most reinforcing effect (Faltermeier *et al.*, 2007b). Interestingly the presence of fillers in polycarbonate brackets was associated with the highest degree of deformation under torqueing stress (Sadat-Khonsari *et al.*, 2004).

Choi *et al.* (2013) analysed the surface roughness and friction of the slot floors of polymeric brackets, with and without slot liners, and compared them to stainless-steel and ceramic brackets. They found that filler-reinforced polymeric brackets showed higher frictional resistance to sliding than polymeric brackets with metal slot liners and stainless-steel brackets but lower than that of the ceramic brackets.

2.3.5 Ceramic orthodontic brackets

Since their introduction in the 1980s, ceramic brackets have become very popular, with their use in the USA reportedly increasing during the period 1986 to 2014, from 6% to 70%. At the same time, the use of polymeric brackets declined significantly (Keim *et al.*, 2014). Properties such as good torque control and improved wear resistance meant they quickly superseded polymeric brackets as the labial aesthetic appliance of choice (Sinha and Nanda, 1997b).

Although the term 'ceramic' encompasses many different compounds, most of the currently available ceramic brackets are composed of aluminium oxide. Two basic types of alumina bracket exist, based on two different manufacturing processes. The first brackets were milled from single crystals of sapphire using diamond tools (Swartz, 1988). As a result, they were termed monocrystalline and were completely transparent in appearance. The second type, known as polycrystalline, were manufactured from alumina powder that was combined with special binders, packed into a bracket shaped mould and then thermally fused in a firing process known as sintering. The most apparent difference between the two is their optical clarity, with the monocrystalline brackets being more translucent. However, the polycrystalline variety tends to be more widely available due to their relative ease of manufacture (Swartz, 1988; Saunders and Kusy, 1994; Russell, 2005).

Polycrystalline zirconia brackets have been offered as an alternative to alumina ceramic brackets. They are characterised by a higher fracture toughness and therefore a lesser

tendency to in service failures and also improved frictional characteristics when compared to alumina (Keith *et al.*, 1994). However, they are aesthetically unacceptable due to their greater opacity which in addition may adversely affect bond strength with light-cured adhesive (Springate and Winchester, 1991). As the clinical performance of alumina ceramic brackets has continued to improve over recent years, zirconia brackets are rarely used (Russell, 2005).

Properties such as excellent aesthetics, good colour stability and minimal slot distortion have made ceramic brackets very popular in contemporary orthodontics. They are durable, can resist deformation and allow adequate force control over long treatment periods leading to good treatment outcomes (Karamouzos *et al.*, 1997; Meguro *et al.*, 2006; Eliades, 2007). However, they have a number of disadvantages. These can be listed under four main headings, namely: their chemically inert nature, brittleness, hardness and friction.

2.3.5.1 Chemically inert nature

A disadvantage of ceramics is their inert nature and a failure to form chemical bonds with resin adhesives (Olsen *et al.*, 1996). As a result, bonding occurs either mechanically, chemically (with an intermediate silane coupling agent), or a combination of the two.

Chemical bonding can be achieved via an intermediate silane coupling agent. To facilitate this, glass is usually added to the ceramic bracket base during manufacture. The silane is able to bond to both the glass of the ceramic and to the glass filler particles

in the resin adhesive (Jena *et al.*, 2007). When first introduced, ceramic brackets had smooth silane coated bonding bases.

Although this might initially appear to be an advantage in terms of bracket manufacture, a smooth bracket base leads to a wide distribution of stress over the whole enamel/bracket interface, which requires a greater force to debond. The use of silane on smooth ceramic bracket bases resulted in unacceptably high bond strengths in clinical use (Bishara *et al.*, 1993; Wang *et al.*, 1997; Pudyani and Widiarsanti, 2016), such that debonding ceramic brackets increased the risk of failure at the enamel adhesive interface, rather than at the bracket adhesive interface, resulting in enamel damage (Jeiroudi, 1991; Karamouzos *et al.*, 1997; Årtun, 1997; Jena *et al.*, 2007; Kitahara-Céia *et al.*, 2008; Eslamian *et al.*, 2011). It is the brittle and rigid nature of both the ceramic and the enamel which increases the risk of enamel fracture at debond (Swartz, 1988; Elekdag-Turk *et al.*, 2009).

Second generation ceramic brackets with a mechanical bonding base using undercuts were introduced in 1991. Mechanical bonding at the bracket base can be achieved using various designs such as dovetails, balls and dimples. These second generation brackets have been shown to have significantly lower bond strengths, with a concomitant reduced risk of enamel fracture when compared with the first-generation brackets (Forsberg and Hagberg, 1992; Redd and Shivapuja, 1991; Årtun, 1997). However, there is a greater probability of bond failure when not coated with silane (Fernandez and Canut, 1999). Laboratory testing showed that ceramic brackets have fewer mechanical undercuts when compared to mesh based metal brackets, leading to localised stress

concentration of the adhesive and thereby increased bond failure (Swartz, 1988; Karamouzos *et al.*, 1997).

Interestingly this is not a universal finding, as some studies have reported no bond strength differences between ceramic brackets with chemical or mechanical retention (Blalock and Powers, 1995), or between ceramic brackets and polycarbonate brackets (Özcan *et al.*, 2008) or between ceramic brackets and stainless-steel brackets (Habibi *et al.*, 2007).

2.3.5.2 Fracture toughness

Although ceramic brackets are rigid materials, another problem they possess is their low fracture toughness and a tendency to fracture during clinical use (Bishara, 2000; Sinha and Nanda, 1997b; Holt *et al.*, 1991; Karamouzos *et al.*, 1997). Ceramics are susceptible to crack propagation caused by minute surface imperfections or material impurities (Kelly *et al.*, 1989; Matsui *et al.*, 2015). Surface cracks can arise from something as simple as a scratch from a misplaced instrument. The fracture toughness of ceramics is 20 to 40 times less than stainless-steel (Swartz, 1988; Scott, 1988). Additionally, stainless-steel brackets can undergo approximately 20% deformation before failing, whilst ceramic bracket failure occurs at less than 1% deformation (Bishara and Trulove, 1990a; Bishara *et al.*, 1997). Of the two ceramic bracket types in use, polycrystalline alumina displays a higher fracture toughness than monocrystalline alumina (Viazis *et al.*, 1993). This lower fracture toughness of the monocrystalline brackets is attributed to the lack of grain boundaries capable of inhibiting crack propagation, and therefore an

inability to absorb energy during loading, leading to increased risk of failure (Scott, 1988; Swartz, 1988; Ghafari *et al.*, 1992).

Tie wings areas are the most common areas of ceramic bracket fracture (Figure 2-3). This can occur either due to tensile forces produced directly by steel ligatures, or when a large rectangular steel archwire is used to apply torque (Scott, 1988; Holt *et al.*, 1991; Johnson *et al.*, 2005). Fracture of the tie wings during treatment can increase chairside time, lead to loss of tooth control, increased patient discomfort and the potential risk of swallowing or aspiration of a radiolucent bracket fragment (Aknin *et al.*, 1996).

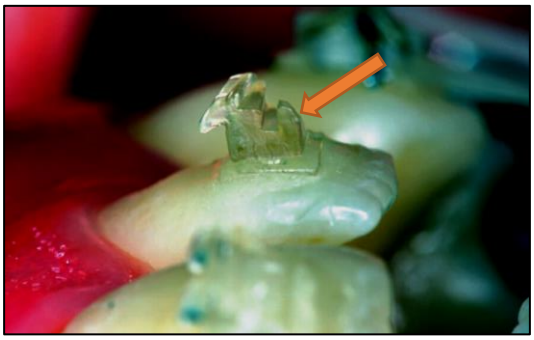

Figure 2-3. Fracture of the two tie wings in a ceramic orthodontic bracket (Melsen, 2012).

This low fracture toughness can also result in problems at debond, with failures occurring cohesively within the bracket or enamel (Viazis *et al.*, 1990). When ceramic bracket fracture occurs at debond it leaves fragments on the enamel, which then require removal using a high speed handpiece and a diamond bur. This increases the debond appointment time, the risk of direct enamel damage (Suliman *et al.*, 2014), the risk of pulpal damage by overheating (Karamouzos *et al.*, 1997) and exposure of both the patient and operator to inhalation of ceramic fragments and dust (Johnston *et al.*, 2009).

2.3.5.3 Hardness

Ceramic brackets, being second in hardness only to diamond, are significantly harder than enamel. Although it means they are not susceptible to toothbrush abrasion, unlike polymeric brackets, excessive tooth wear can occur when ceramic brackets come into contact with the opposing teeth (Figure 2-4) (Swartz, 1988; Douglass, 1989; Viazis *et al.*, 1990; Bishara and Fehr, 1997; Ogaard, 2004).

Figure 2-4. Enamel wear of maxillary incisors due to occlusal contact with the ceramic brackets on the lower incisors (Melsen, 2012).

As a consequence, it is recommended to avoid the use of ceramic brackets in the lower arch in cases where there is a deep overbite (Douglass, 1989; Birnie, 1990; Viazis *et al.*, 1990). Viazis *et al.* (1990) conducted an *in vitro* study on 64 premolars looking at the effect of enamel abrasion damage from ceramic and stainless-steel brackets and reported that enamel abrasion was 9 to 38 times greater in the case of ceramic brackets. Another purported disadvantage of ceramic brackets is excessive archwire wear, particularly at the slot margin, leading to notching of the wire and increased friction (Bishara and Fehr, 1997).

2.3.5.4 Friction

Friction is the force resisting motional sliding when one object moves against another (Kusy and Whitley, 1990; Burrow, 2009; Géminard and Bertin, 2010). Ceramic brackets present relatively increased friction due to their rougher, more porous surfaces (Angolkar *et al.*, 1990; Ghafari *et al.*, 1992; Gioka and Eliades, 2004; Rashid, 2014; Carrion-Vilches *et al.*, 2015). An increase in friction between the bracket and the archwire, which might affect the rate of tooth movement, has been suggested as a problem with ceramic brackets compared to metal brackets (Schumacher *et al.*, 1990; Bazakidou *et al.*, 1997). Additionally, polycrystalline brackets have been reported to produce greater friction than monocrystalline brackets (Arash *et al.*, 2015).

In a study by Pratten *et al.* (1990), the frictional resistance of ceramic and steel brackets in dry and wet environments was evaluated. They concluded that ceramic brackets produce greater friction than stainless-steel brackets in both environments. Ireland *et al.* (1991) compared friction in conventional and ceramic brackets using steel and nickel titanium wires. Their findings showed that frictional resistance was greater with ceramic brackets compared to metal brackets but only when used with smaller dimension rectangular wires.

However, it is worth noting that increased friction has been only demonstrated in laboratory studies. There is no clinical evidence to suggest this to be a problem affecting tooth movement. Friction in orthodontics is more complex than just the two materials in contact. Factors that will also affect friction include the mesio-distal bracket width, the

critical angle between wire and the slot, the surface topography of the slot, the slot lining e.g. stainless-steel and whether there is any rounding of the slot base (Kapur Wadhwa *et al.*, 2004; Arici *et al.*, 2015).

2.3.6 Ceramic bracket modifications

In order to overcome some of the aforementioned disadvantages of ceramic brackets, a number of modifications have been introduced including:

- The addition of a thin polycarbonate base to facilitate easier/safer debonding
- A metal reinforced slot to reduce friction
- A prestressed vertical notch to act as a stress raiser to facilitate easier/safer debonding

These will now be described in greater detail.

2.3.6.1 Addition of a thin polycarbonate base

The benefit of combining two materials, namely a polycarbonate base to a ceramic bracket, is to produce a final product that is superior to either of its principal components alone (Kusy, 1998). In this case the aesthetics, abrasion resistance and resistance to creep under continuous load of the ceramic bracket are retained, whilst the relative ease of debond of a polymeric bracket is utilised by incorporating a polycarbonate shim as the base of the ceramic bracket. The shear bond strengths of such brackets are significantly lower than those observed during the debond of single

component ceramic brackets (Olsen *et al.*, 1997; Elekdag-Turk *et al.*, 2009), making them as easy to remove as metallic brackets and reducing the risk of enamel damage *in vivo* (Winchester, 1992b; Franklin and Garcia-Godoy, 1993; Olsen *et al.*, 1997). However, in clinical use the presence of a well-defined boundary between the polymer phase and the ceramic phase often resulted in premature delamination of the base during clinical use (Bordeaux *et al.*, 1994; Olsen *et al.*, 1997). This can subsequently result in loss of tooth control during orthodontic treatment, increased treatment time and the probability of enamel damage due to the repeated removal of residual adhesive following unwanted debond (Bishara *et al.*, 1999).

2.3.6.2 Metal reinforced slot

Metal slot liners have been placed in some ceramic brackets, not to reduce the creep as is the case with polymeric brackets, but in an attempt to reduce friction (Pratten *et al.*, 1990).

Studies have shown that ceramic brackets with a metal slot liner demonstrate equivalent or lower frictional resistance values than conventional ceramic brackets without a liner (Loftus *et al.*, 1999; Guerrero *et al.*, 2010). Arici *et al.* (2015) compared the friction of ceramic brackets with and without a steel slot liner to stainless-steel brackets and reported that the ceramic bracket with the slot liner showed the lowest friction, while the unlined ceramic bracket showed the highest friction. Although Cacciafesta *et al.* (2003) also reported that ceramic brackets with a slot liner significantly

reduced friction compared to ceramic brackets, they reported it was still higher than with stainless-steel brackets.

2.3.6.3 Prestressed vertical notches

A ceramic bracket incorporating a vertical slot in the base was introduced in 1997 and this bracket was designed to help create a consistent site and mode of failure during debond, thereby reducing the risk of enamel damage (Bishara *et al.*, 1997). This vertical slot acts as a stress raiser, making debonding easier and more predictable (Figure 2-5). The notch concentrates the stress applied to the bracket and promotes failure within the bracket and adhesive at the bracket-adhesive interface, rather than within the enamel.

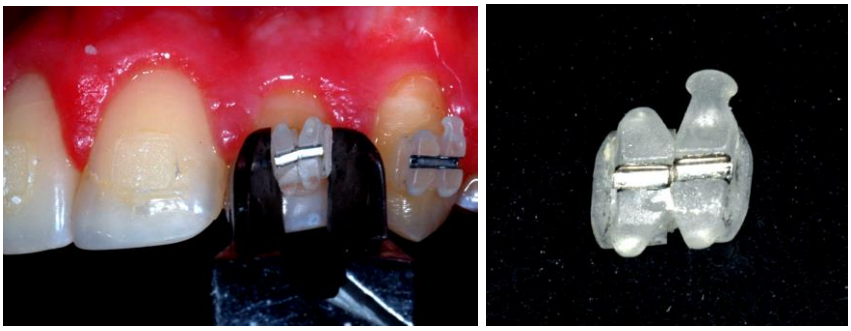

Figure 2-5. Debonding procedure using Clarity™ brackets: note that the bracket collapses in the middle part of the slot (Melsen, 2012).

2.3.7 Debonding ceramic brackets

Various techniques for debonding ceramic brackets have been suggested including the conventional mechanical method using specialised debonding pliers, ultrasonic, electrothermal and laser aided methods (Bishara and Trulove, 1990a; Bishara and Trulove, 1990b).

2.3.7.1 The mechanical method

This technique requires the use of specially designed pliers that work either through deformation of the bracket, or by stressing the adhesive to cause failure. This is probably the most popular method of ceramic bracket removal. Failure is anticipated to be adhesive at the bracket-adhesive interface or cohesive within the adhesive, or a mixture of the two.

A peeling movement is used and therefore debonding occurs as a result of shear, tensile and torsional forces (Katona, 1997). Various methods are used to mechanically debond ceramic brackets including the “lift off” bracket technique using a pistol grip plier and tensile forces, the delamination technique using a sharp instrument and a peeling force and a wrench with torsional forces applied to the bracket base. The “lift off” debonding method produces the most bracket fractures, whereas delamination and torsional forces allow for minimal residual adhesive to be left on the tooth (Bishara *et al.*, 1994; Sinha and Nanda, 1997a), but possibly greater risk of patient discomfort and enamel damage.

Whichever method is used, there is the potential risk of cracks being created within the enamel (Ghafari *et al.*, 1992). Since ceramic brackets are much more brittle than stainless-steel, unwanted failure can occur at the adhesive-enamel interface, or within the enamel surface. Therefore, particular care should be taken in the use of ceramic brackets on teeth that are compromised by the presence of developmental defects, enamel cracks, and large restorations (Sinha and Nanda, 1997a; Karamouzos *et al.*, 1997).

2.3.7.2 Ultrasonic debonding technique

In this method debonding of ceramic brackets is facilitated by removing the excess bonding adhesive around the bracket base using an ultrasonic scaler. The advantage of ultrasonic scalers is that they may decrease the chance of enamel damage and bracket failure. However, the disadvantages of this technique include: increased chairside time, patient discomfort and equipment cost in terms of damage to expensive ultrasonic tips on the hard ceramic brackets (Bishara and Trulove, 1990a; Krell *et al.*, 1993). Additionally, excessive heat may potentially cause pulpal irritation and possible necrosis.

2.3.7.3 Electrothermal debonding

During electrothermal debonding, heat is generated by the instrument tip in contact with the ceramic bracket which raises the temperature of the bonding adhesive above its glass transition temperature, making it relatively easy to then slide the bracket off the tooth surface. Thermal debonding is therefore effective in reducing the risk of enamel and bracket fracture, but the potential for pulpal damage is greater (Kraut *et al.*, 1991; Stratmann *et al.*, 1996; Kearns *et al.*, 1997; Crooks *et al.*, 1997; Yogesh *et al.*, 2016). Currently, electrothermal debonding is still not sufficiently efficient for routine clinical use. This is because the instrument must be cooled down after the removal of just a few brackets and before the debonding procedure can be continued (Strobl *et al.*, 1992).

2.3.7.4 Laser aided debonding

In this type of debonding, the labial surface of the bracket is irradiated by a laser in order to once again soften the composite bonding adhesive by raising its temperature above the glass transition temperature. Reports have shown that this technique also reduces the risk of enamel damage and decreases the incidence of bracket fractures (Tocchio *et al.*, 1993; Strobl *et al.*, 1992; Feldon *et al.*, 2010; Tehranchi *et al.*, 2011). However, early research into the dental use of lasers showed that laser irradiation generates high temperatures that can result in pulpal damage (Tocchio *et al.*, 1993). However, improvements in understanding and advances in laser technology have resulted in a reduction in this undesirable heating during use (Obata *et al.*, 1999; Azzeh and Feldon, 2003; Ural *et al.*, 2010). Nevertheless, the cost of the equipment and time taken to perform the debond means this technique has not proven popular in practice.

Regardless of the technique used to debond ceramic brackets, special care and consideration should always be taken due to the extreme hardness and low fracture toughness of the ceramic material. Ideally the enamel should be protected from damage leaving only a small amount of residual adhesive on the enamel surface at debond. If a considerable amount of adhesive remains on the enamel surface, the risk of enamel damage may well be reduced, but this adhesive then needs to be removed by the clinician.

2.4 Biological and biomimetic materials

Biological materials such as teeth and bone exhibit interpenetrating network microstructures consisting of multiphase constituents (Weinkamer and Fratzl, 2011; Porter *et al.*, 2013). Many of these structures show a unique combination of mechanical properties being strong, tough and light at the same time *(Wegst et al., 2015).* The experimental ceramic/polymer composites analysed in this study were chosen to emulate the mechanical properties of natural human dentine and enamel. Their composition and structure, as well as mechanical properties, will be discussed in the following literature review.

2.4.1 Constituent materials and composition

Teeth are complex multi-layered structures comprising enamel, dentine, cementum and pulp. The enamel and dentine are joined together at a complex interface called the dentine-enamel junction (Meyers *et al.*, 2011; Chan *et al.*, 2011).

Enamel, the external surface of the tooth, is the hardest and most highly mineralised tissue in the human body. It is composed of largely inorganic calcium phosphate in the form of hydroxyapatite crystals (96 to 97% by weight), surrounded by an organic mainly protein phase which includes amelogenins, enamelins (2 to 3% by weight) and finally water (1% by weight). Enamel provides a protective hard and wear resistant cover for the dentine and the pulp, allowing the tooth to withstand the masticatory forces throughout lifetime (Spears *et al.*, 1993) . At the microstructural level, enamel is uniquely composed of aligned mineral rich rods 3 to 6 μm in cross sectional diameter

with varying orientation and diameters (Figure 2-6). The rods are arranged throughout the enamel and embedded in the interrod enamel, which is protein rich (Young, 1974; Braly *et al.*, 2007).

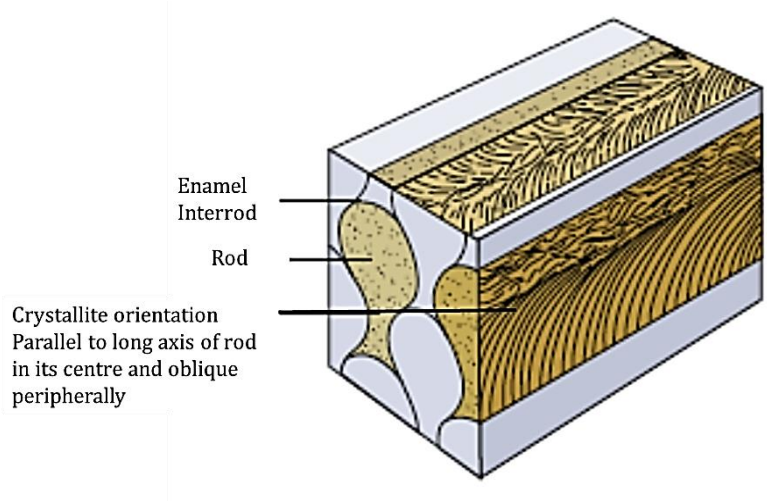

Figure 2-6. Schematic illustration of enamel's microstructure showing the enamel rods (Habelitz *et al.*, 2001).

Dentine on the other hand, is a mineralised tissue that forms the bulk of the tooth. It consists of 70% by weight hydroxyapatite, 20% by weight organic phase, mainly type I and type V collagen, with the remainder made up of non-collagen proteins and lipids and 10% by weight water. The hydroxyapatite crystals in dentine are smaller than those in enamel (Rasmussen *et al.*, 1976; Van Meerbeek *et al.*, 2003).

2.4.2 Structure of teeth

An anisotropic microstructure is the main characteristic of natural enamel and dentine, as well as many other natural biological materials. This results in an anisotropic response upon loading (Kinney *et al.*, 2003).

The structure of teeth is characterised by an organised inorganic-organic network, resulting in the formation of lightweight frameworks (Chen *et al.*, 2008; McKittrick *et al.*, 2010; Lee *et al.*, 2011). The combination of the hierarchical structure, the organic matrix and the inorganic constituents of biological materials leads to superior mechanical properties, while in fact the individual inorganic phases are often by themselves relatively weak (Chen *et al.*, 2008; Studart, 2012).

2.4.3 Mechanical properties of biological materials

Different purposes are served by different biological materials, and in the case of enamel and dentine, these include mastication and protection of underlying pulpal tissue (Goel *et al.*, 1990; McKittrick *et al.*, 2010). Under normal oral conditions, opposing teeth may have a critical contact area of 0.4 to 2.2 mm^2 with a bite force reaching 1000 N (Waltimo and Kononen, 1995; Hayasaki *et al.*, 2004). Unlike other calcified skeletal structures, any damage to the enamel is not repairable. The fracture toughness of enamel and dentine is higher than their constituent hydroxyapatite phases, implying a reinforcement mechanism resulting from a structural combination of inorganic and organic phases (Studart, 2012). Dentine is characterised by its compliant nature and low modulus of elasticity. Therefore, dentine serves as an elastic foundation for the hard, brittle outermost enamel, thus absorbing stress applied to the teeth. Table 2-2 shows a summary of the properties of human enamel and dentine.

Property	Enamel	Dentine
Density (g/cm^3)	**3.02** (Wilson *et al.*, 1999)	**1.9 to 2.4** (Lin *et al.*, 2010)
Compressive strength	**62 to 89** (Chun *et al.*, 2014)	**194 to 224** (Chun *et al.*, 2014)
Elastic Modulus (GPa)	**82 to 100** (He and Swain, 2008)	**20.3** (Xu *et al.*, 1998)
Fracture toughness (MPa.m^{½})	**0.6 to 0.9** (Park *et al.*, 2008)	**2.2 to 2.4** (Yan *et al.*, 2009)
Hardness (GPa)	**3.4** (Min *et al.*, 2016)	**0.6 to 0.9** (Lawn and Lee, 2009)

Table 2-2 Summary of the properties of human enamel and dentine.

2.4.4 A biomimetic approach – interpenetrating phase composites

Biomimetic materials refer to synthetically engineered materials that are inspired by one or more aspects of design, function or properties of natural biological materials (Meyers *et al.*, 2008; Chen *et al.*, 2012; Porter *et al.*, 2013). The potential of using a microstructural design to produce materials characterised by innovative mechanical properties will now be described, along with examples of the interpenetrating multi-phase composite materials.

In order to design dental materials characterised with tooth-like properties, novel CAD/CAM composites consisting of polymer-infiltrated-ceramic-network materials have been introduced in recent years (He and Swain, 2011; Coldea *et al.*, 2013; Nguyen *et al.*, 2014). In 2008, Munch *et al.* described the fabrication of ceramic/polymer composites by producing a porous alumina scaffold infiltrated with polymethyl methacrylate. They described the resultant product as having very similar features to natural nacre. The mechanical properties of this composite material included a high toughness and elastic strain, both of which would be desirable in orthodontic brackets. They concluded that the production of a porous structure, by using the technique of

freeze-casting, and then infiltrating it with a second phase organic could produce composites with a strength that could match that of an aluminium alloy. Later work by Launey *et al.* (2009; 2010) showed that composites fabricated by freeze-casting porous alumina scaffolds which were then infiltrated with a second more ductile phase, exhibited a higher fracture toughness than pure alumina.

Two phase bioinspired composites were fabricated by Naleway *et al.* (2015) using a freeze-casting technique of aqueous suspensions consisting of 10 vol.% zirconia ceramic powder. The resultant porous scaffolds were then infiltrated with epoxy polymer as the second more flexible phase. They found that these composites exhibited higher mechanical strength when compared to both constituents, a phenomenon that is common to biological composites. The authors suggested that the composite material could mimic the mechanical behaviour of natural biological materials and could serve in applications as biological implants. Moreover, An *et al.* (2016) fabricated composite materials either with or without hierarchical architectures inspired by bone. They found that hierarchical structural properties enhanced the mechanical properties of the composite, with a combination of high strength and toughness. The fracture toughness was more than double that of the composite without the hierarchical architecture.

Dental interpenetrating phase composites can be defined as materials that combine the characteristics of both dental ceramics and composites, which are the most commonly used materials in dentistry. A recent review that investigated the properties of such materials stated that they demonstrated good mechanical properties and showed

resistance to degradation when cemented to the teeth (Facenda *et al.*, 2018). Three dental interpenetrating materials currently available on the market are:

- Captek (Argen Edelmetalle GmbH, Duesseldorf, Germany).
- In-Ceram Alumina (VITA Zahnfabrik, Bad Saeckingen, Germany).
- Enamic (VITA Zahnfabrik, Bad Saeckingen, Germany).

Captek is used as a restorative core material and comprises a porous gold-platinum-palladium scaffold infiltrated with gold (Goodson *et al.*, 2001). The gold acts as an antibacterial agent that inhibits plaque accumulation in the oral environment, while the mechanical strength and toughness are provided by the matrix scaffold. This composite material is later covered by a ceramic to improve its aesthetics.

In-Ceram Alumina is an interpenetrating phase composite that is fabricated from a porous alumina preform infiltrated with glass. It is therefore a ceramic/glass composite and is used for restorative crown and bridge frameworks. The material is characterised by superior mechanical properties when compared to conventional dental ceramics (Campbell *et al.*, 1995; Giordano *et al.*, 1995; Hornberger *et al.*, 1996).

Based on this In-Ceram material, VITA has since developed porous ceramic scaffolds and infiltrated these with a polymer instead of glass. He and Swain (2011) investigated the mechanical properties of these polymer/ceramic composite materials including modulus of elasticity, hardness, and fracture toughness. They suggested that the interpenetrating composite materials produced were characterised by similar properties to human teeth. Coldea *et al.* (2013) tested the same polymer infiltrated ceramic networks but with

differing ceramic to polymer volume contents. They measured mechanical properties such as flexural strength and hardness and considered these materials to more closely imitate natural tooth properties compared with existing dental restorative materials. They also suggested that during hardness testing, the induced cracks were arrested by the polymer network causing greater crack deflection than the dense ceramic material.

The resultant material, namely Enamic, was later marketed by VITA as a restorative material and is described as mimicking natural teeth (Mörmann and Swain, 2014; Della Bona *et al.*, 2014). Enamic comprises a sintered porous ceramic matrix (86% by weight) infiltrated with a UDMA-TEGDMA polymer matrix (14% by weight) (Figure 2-7) (Leung *et al.*, 2015).

A review by Swain *et al.* (2016) evaluated the different properties of this material and found that crowns fabricated using it were more resistant to cracking induced by masticatory forces. Previous studies had observed microcracks between the phases of the material, which could have a critical effect on the microstructure and hence the mechanical behaviour of the composite (Della Bona *et al.*, 2014; Stawarczyk *et al.*, 2016; Swain *et al.*, 2016).

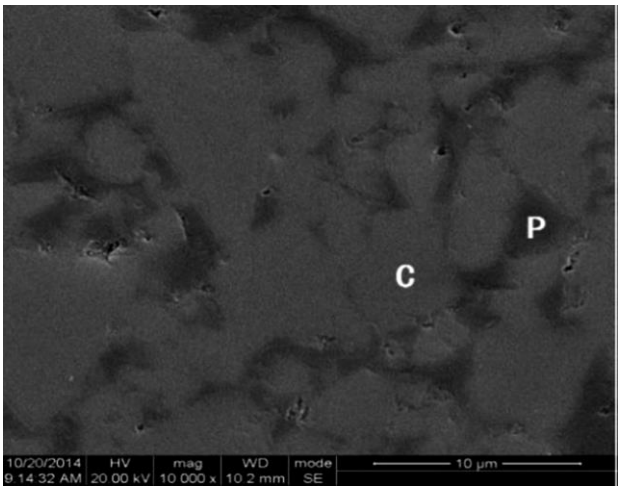

Figure 2-7. Microstructure of polymer-infiltrated-ceramic-network materials. Polymer matrix and ceramic matrix are labelled P and C, respectively (Min *et al.*, 2016).

In addition to the commercially available materials described, experimental two phase interpenetrating composites have also been produced and evaluated. Porous ceramic scaffolds fabricated using freeze-casting and subsequently infiltrated with epoxy polymer have been investigated as possible indirect dental restorations (Petrini *et al.* (2013). Silica scaffolds with UDMA-TEGDMA as the organic phase, this time created using the press moulding technique and heat polymerised to produce the final composite blocks, have been suggested as a permanent crown restoration material. The inorganic phase was relatively high at 70% by weight and the flexural strength measured 200 MPa (Okada *et al.*, 2014).

An experimental glass ceramic porous network produced by slip-casting and then infiltrating with UDMA polymer, followed by *in situ* high temperature/high pressure polymerisation, was described by Nguyen *et al.* (2014). They investigated the material properties and compared them to commercially available composite CAD/CAM block

material. The results of the study revealed that the mechanical properties of the resin infiltrated glass ceramic network were superior with respect to fracture toughness, strength and hardness.

A more recent study conducted by Li *et al.* (2017) produced tough polymer-infiltrated zirconia composites using a pressing technique, followed by infiltration with a BisGMA/TEGDMA monomer mixture. They stated that the resultant interpenetrating phase composite materials demonstrated high strength and toughness.

2.5 Fabrication techniques of porous ceramics

Porous ceramics with tailored open pore structures that can mimic natural structures are of potentially great use in the biomedical field. They can also be utilised as preforms that can be infiltrated with a second phase, such as a polymer or metal, to produce interpenetrating composites for different biological and engineering applications. Ceramic as the scaffold material for biomedical applications brings the advantages of biocompatibility, high strength and wear resistance (Green and Colombo, 2003). The less resilient interpenetrating polymer phase brings its own advantages, principally improving the toughness of the composite material, whilst itself being protected by the more durable ceramic phase.

Typical methods used to produce open porous ceramics are partial sintering, replica templating, direct foaming or sacrificial fugitives (Ohji and Fukushima, 2012). Whatever the method of production, the ideal properties of the porous ceramic scaffold are good

mechanical properties, chemical stability and an interconnected pore network (Hammel *et al.*, 2014; Scotti and Dunand, 2018).

Partial sintering, the most traditional technique, can produce homogenous porous ceramics with reasonably good mechanical properties. However, the main disadvantage of this method is that the ceramic scaffold often has a low porosity and the pore structures cannot be controlled (Ohji and Fukushima, 2012).

The replica template technique has been used to fabricate porous ceramics with a high porosity and large interconnected pores by using a porous polymeric sponge as a template. However, the mechanical performance of the resultant structures is usually poor (Studart *et al.*, 2006; Ohji and Fukushima, 2012).

The direct foaming technique offers easy low cost production of the porous ceramic framework. However, it is difficult to achieve a graded structure, the porosity is limited and interconnectivity control is poor (Barg *et al.*, 2009; Ohji and Fukushima, 2012).

The freeze-casting technique, based on the principle of using a sacrificial fugitive such as water, has been the most popular method of producing ceramic scaffolds in recent years. Using this method, it is possible to create unique porous ceramics with excellent properties. It is this method that forms the basis of the research in the present study and so it will now be described in greater detail.

2.5.1 Freeze-casting technique

Freeze-casting is a well-established technique that can be used to fabricate porous scaffolds with complex microstructures from a ceramic powder suspension (Deville *et al.*, 2015). It is relatively simple, cost efficient, environmentally friendly and offers the ability to produce a porous material with controlled-size and interconnectivity of the pores. A large number of processing parameters are generally used to tailor the final architecture of the porous scaffolds (Zhang *et al.*, 2009; Deville, 2010).

The pores are produced by controlling the solidification of a solvent, for example water within a powder suspension, followed by sublimation and solidification via sintering (Deville, 2008; Wegst *et al.*, 2010), as can be seen in Figure 2-8.

For aqueous ceramic suspensions, the ice crystals in the porous structure are usually removed by freeze-drying, leaving the pores as a negative replica of the initial ice crystals formed during freezing. The most commonly reported microstructures of freeze-cast materials are: lamellar, dendritic, and honeycomb (Scotti and Dunand, 2018).

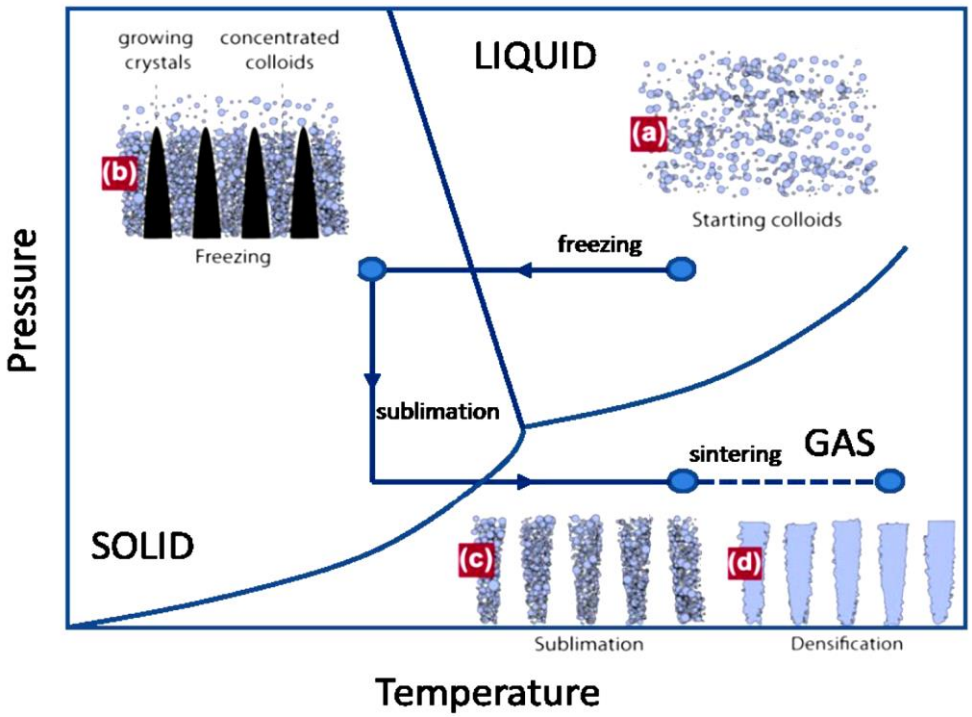

Figure 2-8. The fundamental steps in the production of a freeze-cast ceramic scaffold. a) stable ceramic suspension; b) freezing of the suspension; c) sublimation of the ice crystals to create a green body; d) densification of the green body through sintering (Deville, 2013).

The use of freeze-casting to produce porous materials began in the 1980s. Mahler and Bechtold (1980) produced silica fibres by phase separation during the freezing of aqueous polysilicic acid. A few years later Tong and Gryte (1985) studied the mechanisms of lamellar ice crystal growth in frozen agar gels, and specifically the influence of the freezing rate on the crystal structure and final porosity. However, it was only in 2001, with the work of Fukasawa, that the idea of using freeze-casting to fabricate porous ceramic structures from a water based ceramic suspension was formulated (Fukasawa *et al.*, 2001a). Since then a large number of papers have been published in this field.

Of particular interest in the current project is the utilisation of freeze-cast alumina ceramic porous scaffolds (Fukasawa *et al.*, 2001a; Fukasawa *et al.*, 2001b; Deville *et al.*, 2007; Preiss *et al.*, 2012; Petrini *et al.*, 2013), and the production of interpenetrating composite materials with the potential for use as two phase orthodontic bracket materials.

There are many advantages of freeze-casting, particularly when using a water based ceramic suspension. These include: the flexibility of the freeze-casting process, the variety of attainable pore structures, the possibility of tuning the templated microstructure during the process, the potential applications and its cost effectiveness (Deville, 2010; Wegst *et al.*, 2010; Scotti and Dunand, 2018). However, freeze-casting of porous ceramics is not without issues and the main disadvantage is the complexity when attempting to understand the underlying principles that govern the microstructure template during freeze-casting. Other problems include the volume expansion of water on solidification and the use of a high solid content (> 60%), which makes processing more difficult and expensive due to the need for a pressurised production system (Sofie and Dogan, 2001; Scotti and Dunand, 2018).

2.5.2 Freeze-casting process

2.5.2.1 Creation of suspension

The first part of the freeze-casting process involves the creation of a ceramic suspension. The ceramic powder used in the suspension comprises either micro or nanoparticles dispersed in a liquid medium. A dispersant and other additives may also be added to the

suspension to reduce any tendency to particle segregation and help control the stability of the suspension. This in turn will help create the density gradients and final porosity of the ceramic scaffold (Deville, 2010; Deville *et al.*, 2015). Typical ceramic powders used in freeze-casting include alumina and hydroxyapatite (Deville, 2008). Particle size can influence ice crystal nucleation and thereby pore structure. Smaller particles provide more nucleation points during solidification, better particle redistribution and packing during solidification, resulting in thinner ceramic walls and ultimately lower porosity values for identical solid loadings (Deville *et al.*, 2009; Deville *et al.*, 2010; Zhou *et al.*, 2011; Zamanian *et al.*, 2014).

2.5.2.2 Freezing conditions

Freeze-casting techniques can be categorised as anisotropic or isotropic. Isotropic freeze-casting is used for the production of non-aligned porosity (Prakobna *et al.*, 2016). The anisotropic technique is of interest in this study as it allows the production of aligned pores.

Once created the ceramic suspension is poured into a mould within a custom-built machine. The mould comprises thermally insulating sides and a thermally conductive base. In this initial stage of solidification, the base of the mould is cooled, which promotes ice crystal nucleation and directional solidification within the suspension from the bottom to the top across a temperature controlled gradient. This is the critical stage where the structure of the final scaffold is determined, namely the pore size, their orientation and interconnection (Deville *et al.*, 2015; Scotti and Dunand, 2018).

Two types of freeze-cast systems have been described: one-sided and two-sided freeze-casting. The most commonly used is the two-sided freezing system where the top and the bottom temperatures can be pre-set, providing a better control over the freeze-casting system. Solidification typically takes place vertically from the bottom to the top. The one-sided freezing system only has a controlled temperature at the base, meaning less overall control of the structure of the final scaffold (Deville *et al.*, 2006a; Wegst *et al.*, 2010; Scotti and Dunand, 2018). With either system, a temperature gradient forms and it is along this temperature gradient that ice crystals then form within the ceramic suspension. According to Deville (2008), three different zones have been identified during the freeze-cast process, namely: the dense zone, the intermediate columnar zone and the lamellar structure zone.

2.5.2.3 Freeze-drying

Once the ceramic suspension has been freeze-cast, it is then placed into a freeze-dryer within its mould. Here it is kept under conditions of low temperature and low-pressure, which results in the elimination of the solvent and evaporation of the ice crystals (Szepes *et al.*, 2007; Deville, 2008; Launey *et al.*, 2010; Wegst *et al.*, 2010). After the sublimation of the ice, a ceramic scaffold is obtained where the porous spaces are replicas of the original frozen solvent. For different solvents different sublimation conditions are required. The green body obtained retains its shape due to the action of the binder that holds the ceramic particles together.

2.5.2.4 Sintering

In order to obtain a strong freeze-cast ceramic scaffold, a sintering step is required in which densification is achieved by elimination of any micro porosity between the ceramic particles within the walls, while maintaining the macro porosity. This will decrease the total porosity and improve the overall mechanical strength. Sintering conditions are not believed to have a significant impact on other pore network characteristics (Deville *et al.*, 2006b; Deville *et al.*, 2007; Fu *et al.*, 2008).

Following sintering, the freeze-cast porous ceramic scaffold, with its aligned porosity, is ready to be used as a preform and infiltrated with a variety of materials, including metals or polymers, depending upon the intended final application.

2.5.3 Control parameters in the freeze-casting method

The most important parameters involved in the freeze-casting technique are the suspension solid loading, the solvent system, additives, the temperature gradient and the freezing rate (Fukasawa *et al.*, 2002; Koch *et al.*, 2003; Deville *et al.*, 2007; Sofie, 2007; Deville, 2008; Munch *et al.*, 2009; Rodríguez-Parra *et al.*, 2012). These will be described in turn.

2.5.3.1 The solid ceramic loading

The solid content is the primary factor that determines the total porosity, pore size and the pore connectivity of the final scaffold (Deville *et al.*, 2015). Higher solid loading

results in an increased particle-particle interaction. This increased interaction affects the viscosity, which in turn plays an important role in determining the microstructural and mechanical properties of the material. A higher solid loading will reduce overall porosity, reduce the pore size and increase the ceramic wall width. Conversely, lower solid loading allows for increased pore connectivity (Deville, 2008; Zuo *et al.*, 2011). There is a trade off between the porosity and the mechanical strength that is required for the desired application. Lower solid loadings will result in an increase in the dimension of the pores and as such the mechanical properties will be affected, despite the porous structure being more easily infiltrated with a second phase material. However, there is an optimal range of suspension solid loadings (15% to 40%) required to produce a porous scaffold that maintains a solid shape and can be a handled safely without disintegrating (Fukasawa *et al.*, 2002; Sofie, 2007).

2.5.3.2 The solvent system

The solvent plays the role of structuring agent, binder and pore forming agent. The precise pattern of pore morphology, freezing temperature, costs, and environmental consequences are dependent upon the solvent used during freeze-casting. Three such solvents are water, camphene and tert-butyl alcohol (TBA) (Scotti and Dunand, 2018) and each leads to the production of different pore structures (Lee *et al.*, 2007; Peko *et al.*, 2010; Souza *et al.*, 2014). Water based systems result in lamellar pore structures due to the hexagonal growth of the ice crystals developing parallel to the direction of the freezing, while camphene based systems show dendritic pore morphologies, and TBA-based systems have prismatic pores (Yook *et al.*, 2008; Hu *et al.*, 2010).

Of particular interest in this study is water, as it is the most popular solvent for freeze-casting due to its environmental friendliness, low cost, and bio-inertness. In addition, water is a polar solvent and as such the surface charge on the particles aid their dispersion within the suspension, which improves the overall homogeneity of the suspension (Wegst *et al.*, 2010; Scotti and Dunand, 2018). A disadvantage of using water as the solvent is that it is more time consuming, relatively more expensive, requires an additional freeze-drying process to remove it, and the growth of ice crystals is more sensitive to impurities (Deville *et al.*, 2007). The principal disadvantage of using solvents other than water, is that they form different crystal structures that are not necessarily lamellar and are therefore more difficult to infiltrate with a second polymer phase (Deville *et al.*, 2006b).

2.5.3.3 Polymer additives

Additives are substances used to control the stability of the particles in the suspension, pores characteristics, the freezing behaviour and the strength, both in the green and sintered conditions (Deville *et al.*, 2010). The role of the additive depends on the interaction and chemical compatibility between the additive, the solvent and the ceramic powder. Dispersants and binders are the two most common additives used in freeze-casting. Dispersants are usually employed to produce a stable suspension and reduce particle aggregation and settling during solidification, reducing heterogeneities within the final product and consequent defect formation (Yoon *et al.*, 2007).

In the preparation of the alumina suspension, the ceramic powder may aggregate to form clumps when added to any suspension medium (Gaudillere and Serra, 2016). This results in a suspension with a higher viscosity, which makes processing more difficult and reduces the mechanical properties of the material. Therefore, the prevention or elimination of agglomeration, and the uniform distribution of the particles within the ceramic suspension before the fabrication of the green body, is crucial to the integrity of the final porous ceramic scaffold (Fu *et al.*, 2008).

The dispersants used in freeze-casting are ionic polymers, which once added to the solution are absorbed on the surface of the particles (Cesarano *et al.*, 1988; Scotti and Dunand, 2018) and therefore their concentration in the ceramic suspension has to be well determined (Lu *et al.*, 2006; Zou *et al.*, 2011).

Additives are used to increase the strength of the ceramic green body and aid control of the final pore structure during the freezing (Munch *et al.*, 2009). Gelatine is one such additive that is used as a binder during freeze-casting, and previous research has shown that its use leads to the production of ceramic structures characterised by a porosity of more than 70%, with micro-sized pores, good pore orientation and with a final honeycomb-like structure (Figure 2-9) (Fukushima *et al.*, 2008; Fukushima *et al.*, 2010; Arabi and Zamanian, 2013; Fukushima *et al.*, 2014).

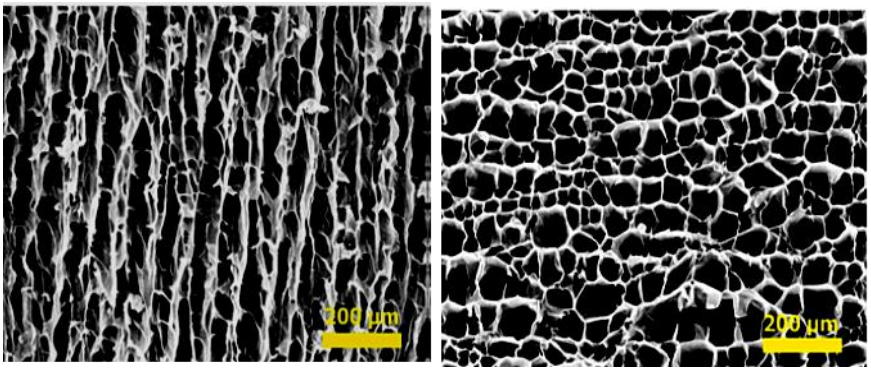

Figure 2-9. The honeycomb pore structure obtained using an aqueous suspension containing 5 wt.% gelatine and anisotropic freeze-casting. The direction of cross section is perpendicular and parallel to the ice growth direction (Arabi and Zamanian, 2013).

Polyvinyl alcohol (PVA) and glycerol are the most frequently used additives for freeze-casting (Scotti and Dunand, 2018). PVA, a water soluble polymer, has been used to transform the structure of the scaffold to create small, interconnected lamellar pores (Zuo *et al.*, 2008; Peko *et al.*, 2010) as can be seen in Figure 2-10.

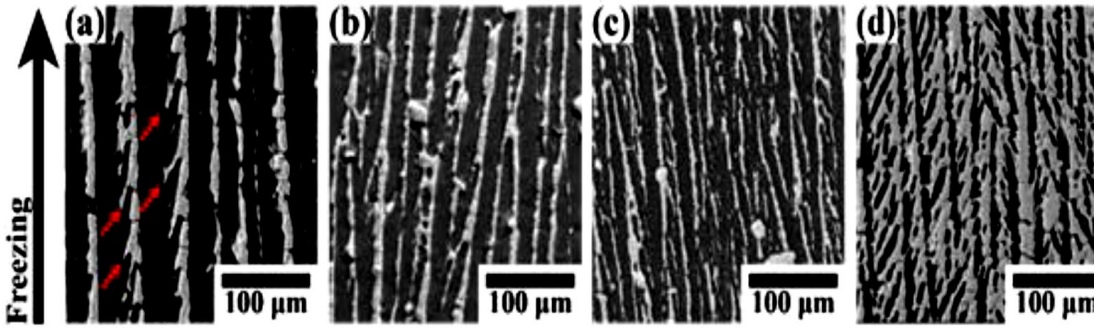

Figure 2-10. Effect of PVA as a binder on anisotropic freeze-cast porous alumina prepared from aqueous suspensions. Cross sections are taken parallel to the freezing direction; dark regions represent pores and the light regions alumina walls. (a). shows the microstructure obtained when no binder is added; the pores have lamellar morphology and dendritic bridges (red arrows). Microstructures obtained with the inclusion of 5, 15, and 20 wt.% PVA are shown in b, c and d respectively (Peko *et al.*, 2010).

In a study by Liu *et al.* (2015), they looked at the effect on the microstructure of using PVA as a binder and changing the cooling rate in aqueous suspensions consisting of 25 vol.% alumina. They found that both affected the microstructure, with PVA decreasing the pore size and as such increasing the porosity.

Glycerol binds to water molecules, reducing the size of the growing ice crystals (Fu *et al.*, 2008; Rahaman and Fu, 2008; Zhang *et al.*, 2010). Sofie and Dogan (2001) investigated the effect of adding glycerol to an aqueous alumina suspension and found that the addition of glycerol led to scaffolds with increased density and a more uniform microstructure.

As previously described, of particular interest to the present study is the use of gelatine as a binder. Previous studies showed that gelatine addition could result in porous freeze-cast ceramic scaffolds with excellent mechanical properties and high pore connectivity. Increased interconnectivity is often desired as it improves the material's compressive response (Fukushima *et al.*, 2014; Bouville *et al.*, 2014; Fukushima and Yoshizawa, 2015; Fukushima *et al.*, 2017). Fukasawa *et al.* (2001b) used unidirectional freeze-casting and gelatine to process a water based alumina ceramic suspension to produce porous materials that could be used in filters and catalysts. The resultant porous scaffolds were characterised by macroscopically aligned open pores. They concluded that this fabrication technique was advantageous in terms of applicability and environmental friendliness. In a more recent study by Wu *et al.* (2018), the effect on the microstructure and compressive strength of using different concentrations of gelatine as a binder

showed that as the concentration of gelatine increased, so the pore connectivity increased, porosity decreased and compressive strength increased.

2.5.3.4 Freezing temperature and freezing rate

The parameter with the greatest effect on the orientation and dimensions of the pores is the freezing temperature and the freezing rate (Koch *et al.*, 2003; Deville *et al.*, 2007; Munch *et al.*, 2009). Setting the freezing device to a constant temperature over the course of an experiment is a key parameter for fabricating materials with predefined microstructural characteristics (Scotti and Dunand, 2018).

A low freezing temperature reduces pore size by increasing the freezing front velocity of the suspension. Likewise, when faster cooling rates are applied, pore size is again decreased (Fukasawa *et al.*, 2001b; Deville *et al.*, 2006b). Freezing rate can be defined as the rate at which the freezing device is cooled down to the final, lowest temperature. When the freezing is performed at a constant rate, a porous structure with unidirectional channels is obtained (Deville, 2008; Scotti and Dunand, 2018).

Freezing rates may also affect pore structure. Previous studies have shown that as rates increase, a cellular morphology develops (Waschkies *et al.*, 2011; Deville *et al.*, 2007). Yoon *et al.* (2007) demonstrated that through the use of a high freezing temperature and low freezing rate, highly porous samples can be produced with enhanced compressive strength. In a study by Arabi and Zamanian (2013), they described the use of unidirectional freeze-casting to fabricate porous gelatine scaffolds and used different

cooling rates of 1, 3, and 6°C/min; the solvent was water. They found that the increase in cooling rate resulted in higher compressive strength of the final scaffolds.

2.5.4 Application of freeze-casting

Fabrication of materials with application-specific microstructures is possible via freeze-casting. Freeze-cast ceramic-based materials have many applications, including: filtration membranes (Fukasawa *et al.*, 2001b; Gaudillere *et al.*, 2014) , fuel cell electrodes (Mansor *et al.*, 2016), photocatalysis (Xing *et al.*, 2013), pressure sensors (Kuang *et al.*, 2015) and batteries (de Hazan, 2012).

However, the most extensively investigated discipline in which the application of freeze-casting as a technique of material fabrication has been studied is biomaterials. More than 44 papers were published between 2000 and 2017 on this subject (Scotti and Dunand, 2018). The production of highly porous biomimetic ceramics through the utilisation of freeze-casting has been the focus of much research to date. Current research has focused on the production of freeze-cast hydroxyapatite scaffolds as bone scaffolds and therefore bone substitutes (Landi *et al.*, 2008; Lee *et al.*, 2017; Deville *et al.*, 2006b). Freeze-casting has also been used for drug carrier production through the use of channel-like structures, which can allow for better dispersion of drugs (Szepes *et al.*, 2007; Frohberg *et al.*, 2016) and foodstuffs (Nguyen and Ulrich, 2014).

Furusawa *et al.* (2016) conducted a study aimed at making porous hydroxyapatite scaffolds coated with gelatine, using freeze-casting, and for use as dental implants. In

laboratory tests on rats they found that the scaffolds were characterised by high porosity and good compressive strength and were biocompatible.

In restorative dentistry, freeze-casting has already been used to fabricate materials with the potential for use as dental restoratives. Petrini *et al.* (2013) produced a biomimetic composite material characterised by an anisotropic structure resembling that of human dentine. The composite material consisted of a porous lamellar alumina preform with graded porosity, produced by freezing alumina aqueous suspension using the freeze-casting technique. A vacuum impregnation system was then used to infiltrate the preforms with an epoxy resin, resulting in an interpenetrating composite material. The authors suggested that the advantages of this composite could be minimally invasive tooth preparation and the possibility of *in vivo* repair. The authors reported that the strength of the material was comparable to that of dentine. They concluded that freeze-casting offers a viable route for the fabrication of biomimetic complex composite materials through the control of microstructural and mechanical properties, which could potentially be useful in the production of dental restorations.

More recently, Noguchi *et al.* (2014) produced porous hydroxyapatite scaffolds with a unidirectional and interconnected pore structure, and an average porosity of 75%, using a freeze-casting technique. The authors implanted the porous scaffold into dogs for 1, 2 and 3 years and found it to be suitable to promote bone growth. They concluded that freeze-casting is a promising technique for the fabrication of porous ceramic scaffolds that can mimic bone tissues.

2.5.5 Creation of interpenetrating ceramic/polymer orthodontic brackets

So far, the advantages and disadvantages of aesthetic orthodontic brackets have been described, along with manufacturer's attempts to try to maintain the desirable properties, while eliminating the undesirable properties. A potential novel method to achieve this is to create a true interpenetrating polymer/ceramic composite bracket. The ideal aesthetic orthodontic bracket should satisfy both mechanics and aesthetics. It should have a largely ceramic body and largely polymeric base, so that it is strong enough to withstand the oral environment and transfer the applied stresses during orthodontic treatment, maintain a good appearance/colour and be easy to remove at the completion of treatment, with little risk to the enamel surface. Previous attempts at producing hybrid ceramic polymeric brackets have led to poor clinical performance as a result of the lack of intimate contact of the two phases throughout the body of the bracket, leading instead to premature delamination at the single ceramic/polymer interface (Olsen *et al.*, 1997; Elekdag-Turk *et al.*, 2009).

More recently, Alrejaye *et al.* (2016) fabricated orthodontic brackets by milling aesthetic restorative CAD/CAM ceramic composite blocks, including Paradigm MZ100 (3M ESPE, USA), Lava Ultimate (3M ESPE, USA), Mark II (VITA Zahnfabrik, Germany) and In-Ceram (VITA Zahnfabrik, Germany). They found that the torsional strength of Paradigm and Lava Ultimate brackets was comparable to commercially available alumina ceramic brackets. Their results show the potential of using interpenetrating phase composite materials as an orthodontic bracket *in vitro*.

Freeze-casting is a promising technique that has been used to produce porous ceramic scaffolds characterised by a gradient structure, with open porosity. This means they can then be infiltrated with a more flexible second phase material to produce a biomimetic composite. In this way it might be possible to create an orthodontic bracket characterised by a mainly ceramic outer structure, with good aesthetic properties, good abrasion resistance, good resistance to creep, but with a relatively lower hardness polymer inner phase to aid in facilitating safer bonding and debonding.

2.6 Aims and Objectives

This study aims to produce novel biomimetic interpenetrating ceramic/polymer composites, using the technique of freeze-casting, with mechanical properties that would make them suitable for use as potential aesthetic orthodontic bracket materials. Unlike previous studies, this work focuses on the development of an interpenetrating phase composite consisting of graded alumina freeze-cast preforms with a honeycomb-like microstructure, by using a combination of gelatine and freeze-casting to replicate the graded structure found in natural teeth. The specific objectives are:

- To produce and optimise graded porous ceramic scaffolds suitable for use as a preform for interpenetrating composite materials that could be used as an orthodontic bracket material using the technique of freeze-casting.
- To produce biomimetic interpenetrating ceramic/polymer composites using either vacuum infiltration or heat/pressure infiltration.
- To characterise the biomimetic interpenetrating ceramic/polymer composites using compressive strength, flexural strength, modulus of elasticity, fracture toughness,

hardness and wear resistance testing, along with microstructural assessment using SEM and MicroCT.

- To investigate the effect of different processing parameters, such as initial solid ceramic loadings on the final structure and properties of the biomimetic ceramic/polymer interpenetrating phase composite material.
- To ultimately produce a biomimetic composite material with mechanical properties that would make it suitable for clinical use as an orthodontic aesthetic bracket.

•

Chapter 3. Materials and methods

3.1 Preparation of the porous ceramic scaffolds

3.1.1 Preparation of the ceramic suspensions

The ceramic suspension, a colloidal suspension of solid particles in a liquid, comprises mainly aluminium oxide powder (alumina) dissolved in water along with a specific volume of additives (dispersant and binder). The quantity of alumina, water and additives within the formulation was initially based on the specification within the freeze-casting patent by Jones and Todhunter (2010). The amount of any additive used in the present study is expressed in relation to the dry weight of the alumina powder.

All the suspensions were prepared at room temperature and pressure. Suspensions with different initial solid ceramic loadings (10, 15, 20, 25, 30 and 35 vol.%) were prepared for freeze-casting using alumina powder (CT3000, Almatis AC, Inc. Germany) with an average particle size of 0.6 µm. In order to produce the ceramic suspension in each experiment, 40 g of alumina powder was dispersed in deionised water using an anionic dispersant (DOLAPIX CE 64, Zschimmer and Schwarz GmbH KG Chemische Fabriken, Lahnstein, Germany) at a ratio of 0.6 wt.%. Once prepared the ceramic suspensions were ball milled in 500 ml polyethylene bottles, using zirconia balls (with diameters of 5 and 10 mm) with a total weight of 300 g, in a roller mixer ball milling machine (SRT6, Stuart, UK) at a speed of 400 rpm. This was completed overnight, in order to break down any agglomerations and achieve a homogenous dispersion in each case.

3.1.2 Preparation of the gelatine/ceramic suspensions

Gelatine powder (Type A, G2500, Sigma-Aldrich, St. Louis, USA) was used as a binder to increase the strength of green ceramic scaffolds. The gelatine concentration used in the present study to fabricate the porous ceramic scaffolds was constant (2.5 wt.%). The gelatine solution used in each experiment was made of gelatine powder added incrementally to 5 ml of deionised water. The resulting solution was then heated to 55°C in a 200 ml glass beaker on a hot plate using a magnetic stirrer (Fisher Scientific, UK) until a clear homogenous solution was obtained.

This solution was then added to the ceramic suspension, which also contained Octanol (Fisher Scientific, UK). Octanol is a de-gassing agent and had been previously added to the ceramic suspension at a ratio of 0.1 wt.% of the dry alumina powder weight, in order to prevent any bubble formation. This is because bubbles can result in the formation of closed pores in the final porous scaffold, which can act as areas of weakness. The gelatine/alumina suspension was then ball milled in a roller mixer machine (Stuart SRT6, six-rollers, UK) at a very low speed of 25 rpm/min, while being heated to 50°C in a temperature controlled programmable oven (Eurotherm, Thermo Scientific, UK) for 4 hrs. The volume of deionised water varied depending on the desired solid ceramic loading of the suspension, as shown in Table 3-1.

Initial solid ceramic loading (vol.%)	Volume of water (ml)	Volume of Gelatine solution (ml)	Dolapix dispersant (ml)
10	84.76	5	0.24
15	51.43	5	0.24
20	34.76	5	0.24
25	24.76	5	0.24
30	18.09	5	0.24
35	13.33	5	0.24

Table 3-1. Recipes used for the preparation of the different solid ceramic loadings of the aqueous ceramic suspension prior to freeze-casting.

Finally, the bubble-free colloidal suspension was poured into a 100 mm diameter mould comprising a stainless-steel base and an acrylic jacket. This mould measured 70 mm in height, 20 mm in thickness and 60 mm in inner diameter. The mould was pre-greased at the margins using Vaseline grease (Unilever, UK) to prevent any leakage and the ceramic suspension was poured in to a standardised height of 20 mm. Once poured into its mould, each suspension was held at rest at room temperature overnight to form a stable gel suspension. Figure 3-1 is a flow chart of the suspension preparation procedures.

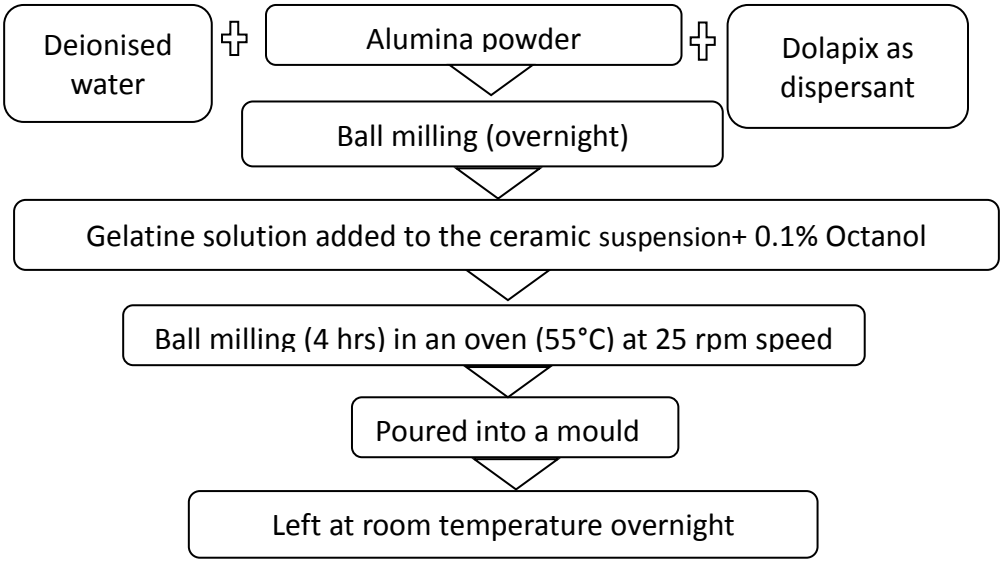

Figure 3-1. Flow chart illustration of the aqueous alumina/gelatine suspension preparation technique.

In the second part of the experiment, investigating gelatine as a binder, the initial solid ceramic loading was kept constant, at 10 vol.% and the gelatine concentrations were altered. Gelatine was used in concentrations by weight of 2.5%, 3.75%, 5%, 7.5% and 10%.

3.1.3 Freeze-casting procedures

Freeze-casting was carried out in a custom-built freeze-casting machine (Figure 3-2) as previously described (Preiss *et al.*, 2012). The freezing apparatus used for the unidirectional freeze-casting in this experiment comprised a double-sided cooling system. The mould containing the ceramic suspension was placed onto the lower copper rod of the freeze-casting machine and the upper copper rod was lowered into the mould so that it was positioned just above the ceramic suspension, without touching it. The bottom rod was cooled using a lab immersion cooler (Polyscience, USA) at a controlled rate of 1°C/min whilst the temperature of the top rod was maintained at a constant temperature using another immersion cooler (Julabo FT 200, Germany).

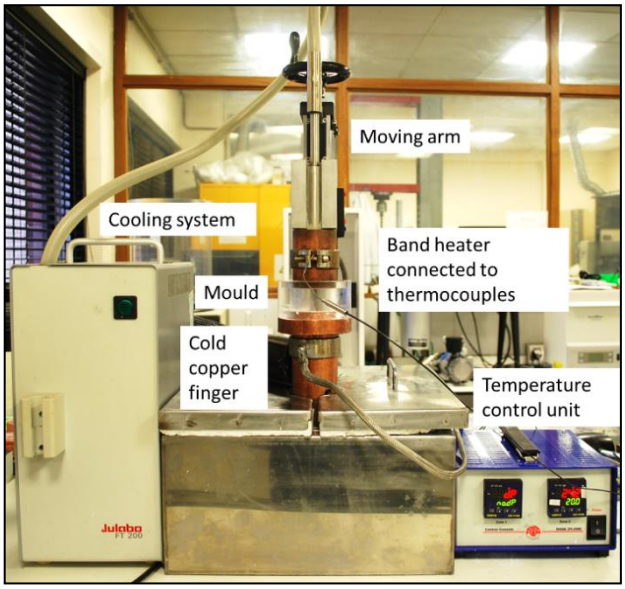

Figure 3-2. Custom-made double-sided device used for unidirectional freeze-casting.

Solidification took place from the bottom to the top rod with a temperature gradient from -10°C up to +20°C. This was controlled using band heaters (MI, 400W, Watlow, USA) and thermocouples attached to the copper rods (TPC-2000 type J, Tempco, USA). The mould was covered with aluminium foil so that the ceramic suspension was appropriately isolated from the room temperature changes.

Before placing the specimen on the copper rod to start the freezing process, the portable temperature control console was turned on for 20 mins and the programme allowed to run in order to reduce the temperature to -10°C. Silicon grease (Rocol, RS, Taiwan) was used to facilitate the removal of the mould from the freeze-cast machine.

The freeze-casting process utilises the principle of directional solidification of suspensions. The temperature gradient used allows ice crystals to grow unidirectionally along the temperature gradient, as can be seen in Figure 3-3. As the suspension

continues to freeze the ice crystals grow from the coldest to the least cold surface, forcing the ceramic particles together to create a continuous ceramic framework.

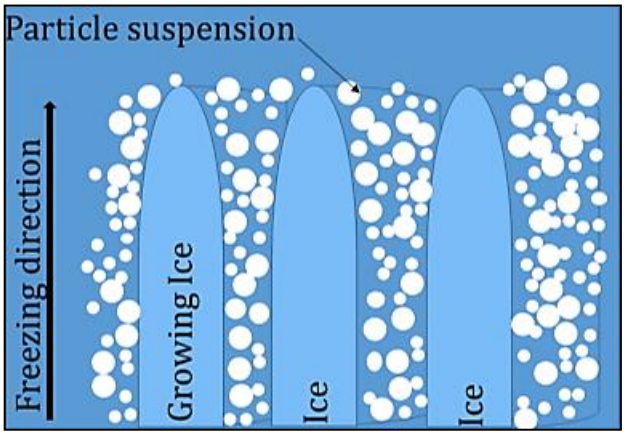

Figure 3-3. Schematic illustration showing the principle of freeze-casting, with the growing ice crystals compressing the ceramic particles to form a porous scaffold.

3.1.4 Freeze-drying procedures

Following freeze-casting, the mould containing the freeze-cast sample was carefully and quickly transferred to the vacuum freeze-drier (Edwards Modulyo, XDS 10, Crawley, UK). The freeze-drier had been turned on for at least 30 mins previously, in order to reach the desired temperature prior to the placement of the sample. Freeze-drying then took place at a pressure of 10^{-1} mbar and a temperature of -55°C for 48 hrs, following which the vacuum was released and the mould containing the frozen specimen was removed from the machine. Finally, the specimen was removed from the mould using a custom-made stainless-steel device, revealing the green body scaffold, which was then ready for sintering.

3.1.5 Sintering

Sintering was performed in two steps using a laboratory chamber furnace (Eurotherm 2416 temperature controlled programmer, Elite Thermal System Ltd, UK). In order to burn out the binder, the specimens were initially heated to 450°C at a rate of 60°C/hr. They were then left to dwell at this temperature for 2 hrs followed by further heating at a rate of 600°C/hr up to 1600°C, and again dwelled for 2 hrs. Cooling down took place with the specimen in the furnace, turned off, overnight. The whole sintering process took approximately 24 hrs to complete. A schematic of the microstructural changes from freeze-casting, to final sintering, is illustrated in Figure 3-4 and a typical final sintered specimen in Figure 3-5.

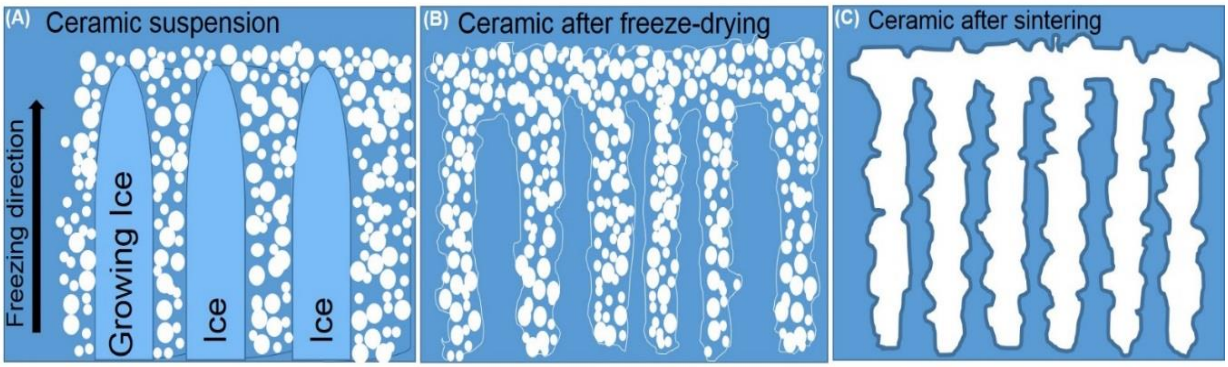

Figure 3-4. Schematic illustration of microstructural evolution of ice in freeze-casting (a), after freeze-drying (b) and finally sintering (c).

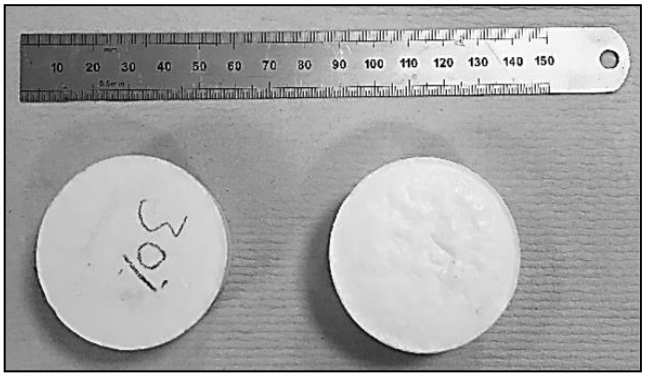

Figure 3-5. Typical sintered specimens (at 1600°C, 2 hrs) obtained from initial solid ceramic loading suspension of 30 vol.% through directional freeze-casting.

3.2 Polymer Infiltration

In the present study, 3 types of polymers were used to infiltrate the ceramic scaffolds namely: epoxy, UDMA-TEGDMA and polycarbonate (PC). Epoxy was used for microstructural evaluation of the porous ceramic scaffold, while UDMA-TEGDMA and PC were used to investigate the microstructural, physical, mechanical and surface properties of the biomimetic ceramic/polymer interpenetrating phase composite materials.

3.2.1 Epoxy polymer infiltration

In order to evaluate the microstructure of the porous ceramic scaffolds, the specimens were infiltrated with epoxy polymer. Infiltration was performed using a self-contained vacuum machine (Bueheler Cast n'Vac, USA). The epoxy was mixed in a ratio of 1-part curing agent (2-methyl-1, 5-pentamethylendiamine, Rotherham, UK) to 7-parts base monomer (Bisphenol-A-epichlohydrin, molecular weight: 700, Rotherham, UK) using a

wooden spatula for 5 mins. Two drops of methylene blue dye were then added to facilitate better imaging contrast and also mixed in for 1 min. The ceramic scaffold was then placed in the Cast n'Vac machine, at a vacuum pressure of 4 x 10^{-1} psi for 15 mins, following which the machine was turned off and the epoxy monomer was allowed to infiltrate the specimen. Once the epoxy fully covered the ceramic scaffold, the vacuum was released, and the specimen was maintained at room temperature overnight in order to fully cure the material.

3.2.2 UDMA-TEGDMA polymer infiltration

3.2.2.1 Chemical treatment with silane coupling agent

For the UDMA-TEGDMA infiltrated ceramic scaffolds, it was decided to treat the samples with a silane to improve interpenetration of the polymer into the ceramic scaffold, as suggested by (Nguyen *et al.*, 2014). The silane solution was prepared by mixing 1 ml of 3-Methacryloxyproply-trimethoxysilane (Sigma Aldrich, UK), 93.8 ml of 1-methoxy-2-propanol (Sigma Aldrich, UK), 5 ml of deionised water and 0.2 ml of acetic acid (Sigma Aldrich, UK). The pH of the final solution was adjusted to 4 using acetic acid and measured by pH meter (Mettler Toledo, Keison International Ltd, UK) to allow silane hydrolysation. This was then stirred for 1 hr in a 200 ml glass beaker with a magnetic stirring machine (Fisher Scientific, UK) and a magnetic flea.

After cooling, the sintered porous ceramic scaffolds were immersed in this silane solution in a small plastic container, ensuring that it was fully submerged. The beaker was then covered with a plastic sheet overnight. Finally, the ceramic scaffold was

removed from the silane solution and dried at 140°C for 6 hrs in an oven (Heratherm, temperature controlled programmer, ThermoScientific, UK).

3.2.2.2 Polymer infiltration

As with epoxy polymer infiltration described earlier, a self-contained vacuum machine (Bueheler Cast n'Vac, USA) was used to backfill the ceramic scaffold with UDMA-TEGDMA monomers. The monomer used in this part of the study was prepared by adding 49.5 g of UDMA (Molecular weight: 470.56 g/mol, Density: 1.11 g/ml, Sigma-Aldrich, UK) to 49.5 g of TEGDMA (Molecular weight: 286.32 g/mol, Density: 1.09 g/ml, Sigma-Aldrich, UK). This was initially mixed in a glass beaker using a wooden spatula for 5 mins and then on a magnetic stirrer (Fisher Scientific, UK) using a magnetic flea for 1 hr. Luperox Benzoyl peroxide (Molecular weight: 242.23, Sigma-Aldrich, UK), used as a heat initiator, was then added to the mixture in the weight of 1 g. This was followed by further stirring at room temperature until a clear homogeneous solution was obtained. Infiltration of the ceramic scaffold was then carried out in the same manner using the vacuum casting machine as was described for the epoxy specimens.

Finally, the ceramic/monomer specimens were placed in an oven (Heratherm, temperature controlled programmer, ThermoScientific, UK) to cure, initially at 50°C for 1 hr, followed by 60°C for 1 hr, 70°C for 1 hr, 80°C for 1 hr and finally 90°C for 12 hrs to allow complete polymerisation. Figure 3-6 shows the steps used to initially fabricate the porous ceramic preform followed by the steps to create the ceramic/polymer (UDMA-TEGDMA) interpenetrating phase composite.

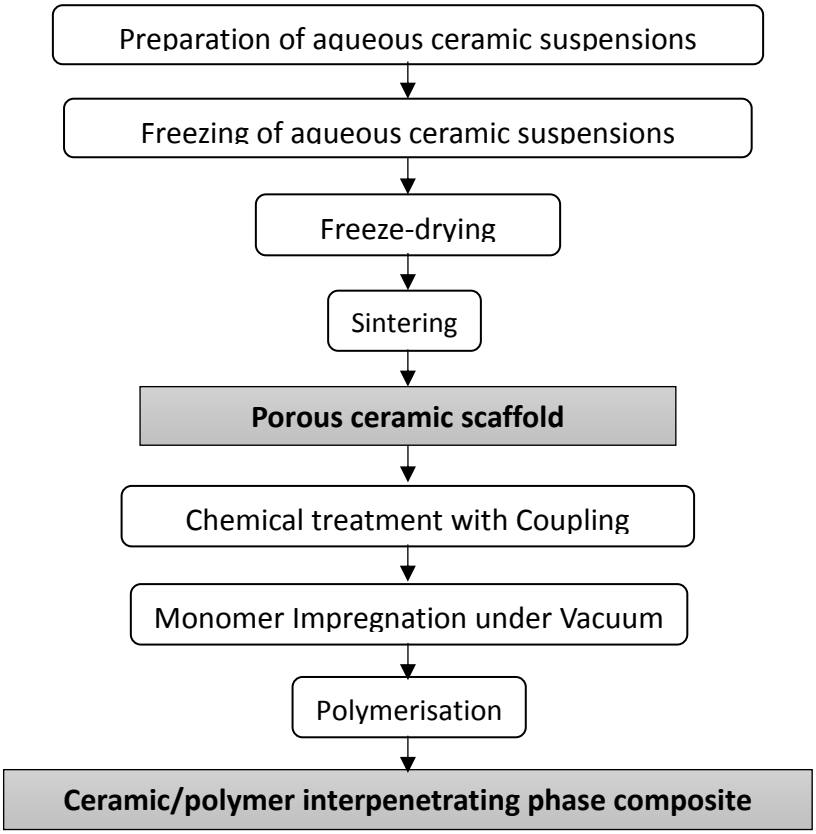

Figure 3-6. Diagram showing the steps for Al_2O_3-UDMA-TEGDMA composite materials fabrication.

3.2.3 PC polymer infiltration

Polycarbonate (Density: 1.20 g/cm³, Good Fellow, UK) is a thermoplastic polymer that becomes less viscous at higher temperatures. Using this property two different infiltration methods were tested, namely loading using a tablet dye-presser machine and loading using a series of weights. In all cases the weight of the PC polymer utilised was equal to the weight of the porous ceramic preform for each specimen, and polymer infiltration was tested at 5 different experimental temperatures, namely 200, 225, 250,

270 and 300°C. Figure 3-7 shows the steps used to initially fabricate the porous ceramic preform followed by the steps to create the ceramic/polymer (PC) interpenetrating phase composite.

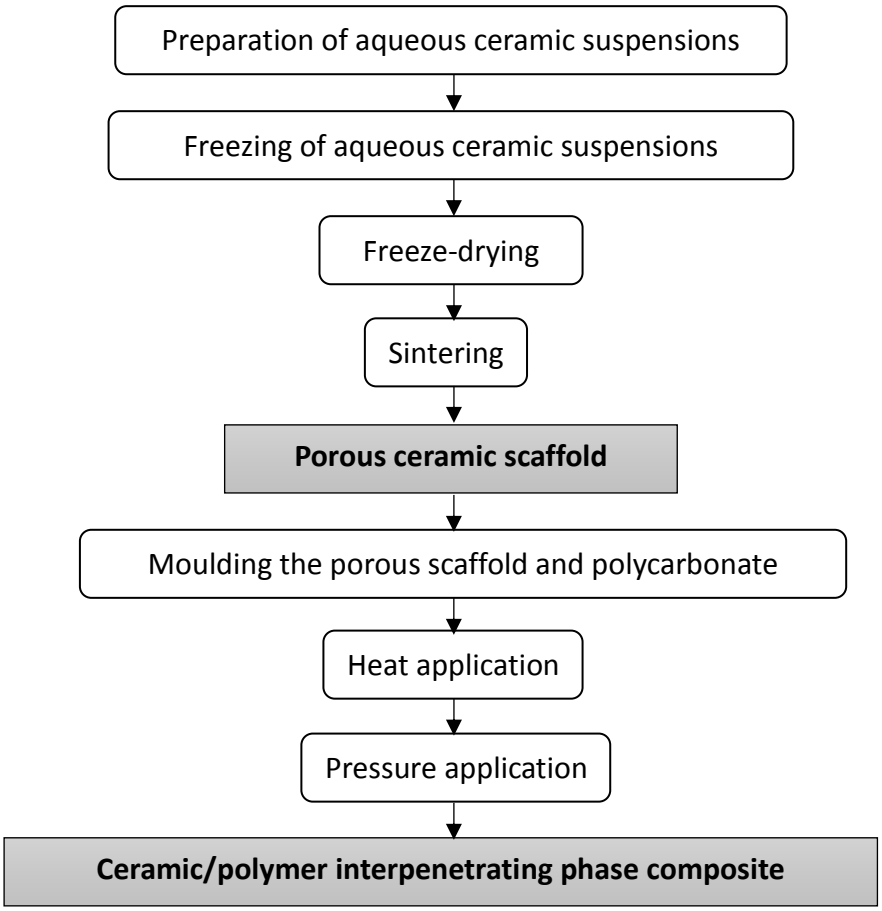

Figure 3-7. Diagram showing the steps for Al_2O_3-PC composite materials fabrication.

In the case of the first method, using the tablet dye-presser machine (PerkinElmer, Germany) (Figure 3-8), the porous ceramic preform was placed into a stainless-steel cylindrical mould with an inner diameter of 38 mm and covered with PC polymer. This was then placed into the pressing machine and using a single channel temperature controller device (WK-1, MTI CO, USA), the specimen was heated to the desired temperature (200, 225, 250, 270 or 300°C) before being subjected to one of 2 loads

namely 1000 or 2000 N. The heating element was then turned off and the mould allowed to cool to room temperature under pressure overnight.

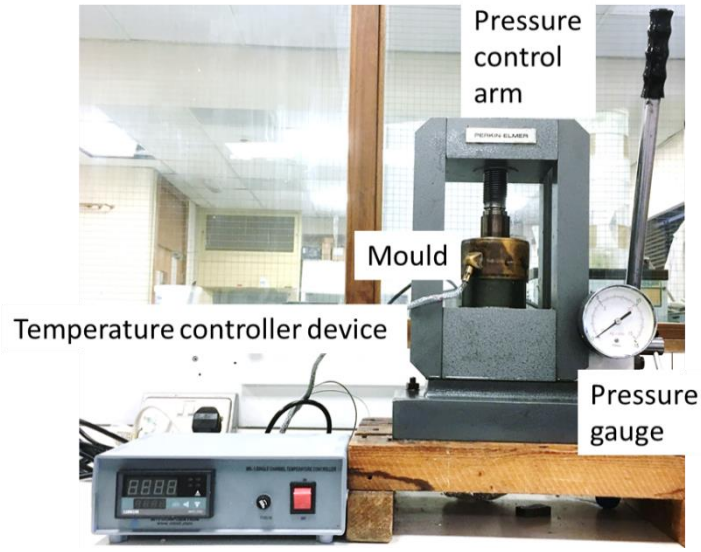

Figure 3-8. Dye-presser machine with a 38 mm diameter stainless-steel cylindrical mould and temperature controller used to fabricate Al_2O_3-PC interpenetrating phase composite materials.

In the second infiltration method, loading was achieved using stainless-steel cylindrical weights (Figure 3-9). The loads applied ranged from 100 to 400 N in 50 N increments. The specimens were placed into an oven (Heratherm, Thermo Scientific, UK) for 2 hrs at 250°C and then loaded for a further 2 hrs at 250°C. The specimen in its mould was then left in the oven overnight to cool down before being removed for testing.

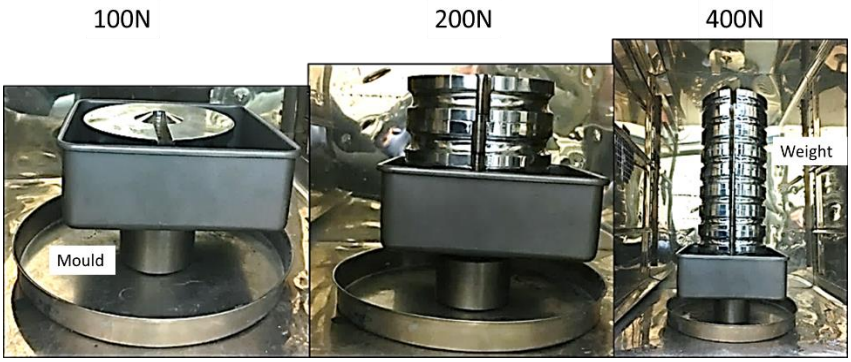

Figure 3-9. Stainless-steel cylindrical mould with Al_2O_3-PC composite specimen and weights on the top used to fabricate ceramic/polymer interpenetrating phase composite materials.

3.3 Preparation of the raw ceramic and polymer blocks

3.3.1 Dense alumina

Alumina powder (CT 3000, Almatis, USA), 2 wt.% Poly-Vinyl Alcohol used as a binder (hydrolysed 87-90%, molecular weight: 30,000 to 70,000 g/mol, Sigma–Aldrich, UK) and 2 wt.% Ethanol (⩾99.8%, Honeywell, UK) used as a solvent, were mixed by hand for 30 mins until a fluffy homogenous suspension was produced. The suspension was then placed in a 38 mm cylindrical stainless-steel mould before being pressed in a tablet dye-presser (PerkinElmer, Germany) with a load of 98066.5 N for 1 hr. The resultant green dense ceramic specimen was then carefully removed from the mould and transferred to a chamber furnace (temperature controlled programmer, Elite Thermal System Ltd, UK) for sintering. It was sintered from the room temperature to 450°C at a rate of 1°C/min, allowed to dwell at this temperature for 2 hrs before the temperature was then increased at a rate of 10°C/min up to 1600°C/min. Once again, this temperature was

maintained for a further 2 hrs before the furnace was the turned off and the specimen left to cool to room temperature overnight.

3.3.2 UDMA-TEGDMA

To prepare the pure UDMA-TEGDMA polymer blocks for testing, 49.5 ml of UDMA (Molecular weight: 470.56 g/mol, Density: 1.11 g/ml, Sigma-Aldrich, UK) and 49.5 ml of TEGDMA (Molecular weight: 286.32 g/mol, Density: 1.09 g/ml, Sigma-Aldrich, UK) were mixed using a wooden spatula for 5 mins and then stirred until the clear homogeneous mixture was seen. 1 ml of Luperox Benzoyl peroxide (Molecular weight: 242.23, Sigma-Aldrich, UK) was then added, as a heat initiator, and dissolved in the monomer mixture by stirring using a magnetic stirring (Fisher Scientific, UK) and a magnetic flea for 1 hr at room temperature. The mixture was then transferred to a 60 ml clear plastic container and placed in an oven (Heratherm, temperature controlled programmer, ThermoScientific, UK) and cured at 50°C for 1 hr, followed by 60°C for 1 hr, 70°C for 1 hr, 80°C for 1 hr and 90°C for 12 hrs to allow complete polymerisation.

3.3.3 Polycarbonate

Polycarbonate films (GoodFellow, UK) were placed into a stainless-steel cylindrical mould with an inner diameter of 38 mm and then transferred to tablet dye-presser (PerkinElmer, Germany). A single channel temperature controller device (WK-1, MTI CO, USA) was then used to heat the specimen to 200°C using a single channel temperature controller (WK-1, MTI CO, USA) for 1 hr. A load of 98066.5 N was then applied to the mould and maintained for a further hour. Once the pressure reached the desired level,

the heating element was turned off and the specimens removed and allowed to cool to room temperature.

The pure UDMA-TEGDMA, Polycarbonate and dense alumina blocks were then cut and polished ready for the physical, mechanical and surface characterisation experiments.

3.4 Preparation of the ceramic/polymer interpenetrating phase composites, ceramic and polymer specimens

3.4.1 Cutting the samples

Using an Accutom-50 (Stuers, Denmark) cutting and polishing machine, each of the ceramic/polymer interpenetrating phase composites, polymer and dense ceramic samples were cut into the relevant sizes according to the test to be performed. In addition, 3 mm of the ceramic rich layer close to the bottom cooling plate of each half was removed as it consisted of randomly packed ceramic particles and closed pores. During the freeze-cast process, it is to be expected that different layers of each specimen will possess different ceramic fractions and porosities as a result of the temperate gradient.

To determine the microstructural and mechanical properties of the ceramic/polymer interpenetrating phase composite specimens in this gradient manner, specimens of the Al_2O_3-UDMA-TEGDMA composites were sectioned at three different levels. The first level represented the bottom layer next to the cooling plate (ceramic-rich). The second level or middle level was cut 4 mm above the bottom layer and the third or top level

(polymer-rich) was again cut 4 mm above the middle layer. Each specimen was therefore divided into three separate specimens from top to bottom in order to evaluate the effect of the anisotropy in the ceramic/polymer interpenetrating phase composite material. The tests and respective sample sizes are shown in Table 3-2.

Test	**Dimensions (mm)**
Fraction	4 x 4 x 8
Density	4 x 4 x 8
Compression	4 x 4 x 2
Flexural	1.8 x 4 x 18
Fracture toughness	4 x 8 x 32
Hardness	4 x 10 x 12
Abrasivity	4 x 6 x 6
MicroCT	5 × 5 x various heights

Table 3-2. Different sample sizes prepared for each relevant test.

3.4.2 Polishing the samples

The second stage of specimen preparation was grinding and polishing to remove damaged material at the specimen surface and to produce a plane surface. Grinding and polishing were carried out using a grinding machine (Tegra Pol 15, Struers, UK) with SiC papers (Struers, Denmark) ranging from p500, p1200 to p2400 under water cooling at a speed of 40 rpm, for 1 min.

Manual polishing was also utilised (using the grinding machine, but with the manual-setting option) under water cooling when the specimen size was not suitable for machine polishing. All polishing procedures were carried out by the same researcher.

Final polishing took place using Al_2O_3 polishing paste (3 µm, Lagro 3, Dia Pro, Struers, Denmark) and the same grinding machine. The final step in specimen preparation was sonication in a digital ultrasonic water bath (Grant Scientific, UK). The specimens were placed in a glass beaker and fully immersed with deionised water, and then placed in the bath for 30 mins at a temperature of 40°C. This step was crucial to remove any remaining debris after cutting and polishing that could result in pore blockage.

3.4.3 Preparation of the human enamel specimens

Six extracted human third molars were used to produce enamel specimens in the present study. The tooth samples were sourced from an ethically approved tooth tissue bank (REC REF 16/NI/0192) held under HTA licence 12200, project reference: 75. The teeth were inspected for imperfections on the surface. Teeth with cracks, caries, discoloration or loss of hard tissue were excluded. When not being prepared the teeth were stored in 0.7% sodium chloride (NaCl) solution containing 0.1% thymol. For cutting, each tooth was attached to a metal holder using sticky wax as shown in Figure 3-10.

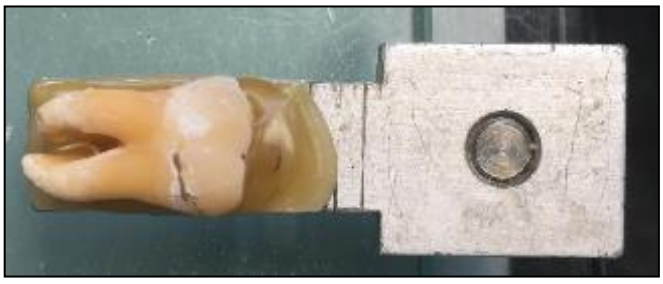

Figure 3-10. Tooth fixed to holder by wax prior to cutting.

The teeth were initially sectioned using an Accutom-50 water cooled high speed diamond saw (Struers, Denmark and MicroSlice; Metal Research, Cambridge, UK) to separate the crown from the root as illustrated in Figure 3-11. Following this the pulp chamber was removed from the crown of the tooth using a high speed rotatory hand air motor (NSK, Japan) as can be seen in Figure 3-12. Enamel specimens were prepared for surface hardness and abrasivity tests. All the enamel specimens were cut to the dimensions of 2 x 3 x 2 mm.

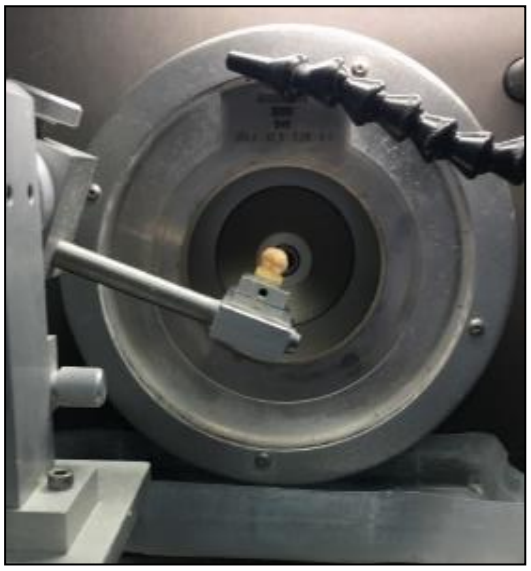

Figure 3-11. Tooth during the cutting procedures.

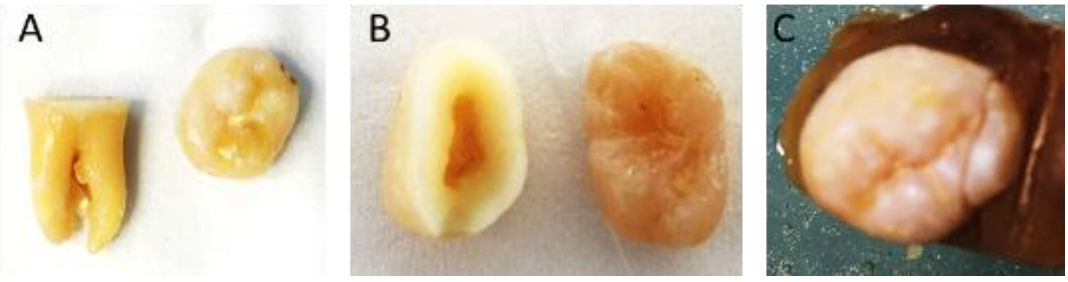

Figure 3-12. Tooth after cutting. A. Crown and root separated. B. The tooth pulp removed. C. The tooth crown fixed to holder by wax after specimen was cut.

Each enamel block was then mounted in epoxy resin (Stycast; Hitek Electronic Materials, Scunthorpe, UK) in a mould as illustrated in Figure 3-13 and left to set overnight.

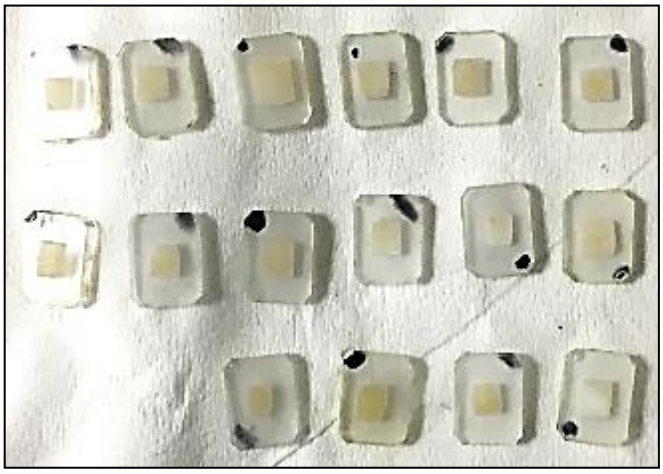

Figure 3-13. The final enamel specimens prepared, polished and set in epoxy resin. Specimens were marked with a spot for orientation during testing.

These specimens were then polished using a polishing machine (Struers, UK) with SiC discs: p1200 (Struers, UK) applied and finished by final hand polishing with Al_2O_3 powder (0.3 µm) as a suspension in deionised water on a glass slab to achieve a smooth flat surface. They were then ultrasonicated in deionised water between each polishing stage to remove any debris.

3.5 Microstructural characterisation

For qualitative evaluation of the microstructure, the cross sections perpendicular and parallel to the ice growth direction were observed using different imaging techniques.

3.5.1 Optical microscope

An optical microscope (Leica DMLB, USA) was used to characterise the specimens at x 40 magnification and images were viewed directly using the eyepiece and indirectly using the monitor screen. The images were captured using a digital camera (Olympus, Japan) coupled with the microscope. An external light source (Schott LED, KL1600, UK) was used to aid in the visualisation, and further analysis of the images was then performed using ImageJ image-analysis software (Fiji, Japan).

3.5.2 Scanning electron microscope

Backscatter SEM images were obtained using SEM (FEI Quanta 400, USA). In each case the specimens were coated prior to imaging with gold palladium using a sputter coater (Emitech K575X, Quorum Technology Ltd, UK).

3.5.3 Micro computerised tomography

Specimens were scanned using a MicroCT scanner (Nikon XTH225, Tungsten target, 225 reflection head, Japan) at 120 kV, with a current of 300 µA and an exposure rate of 1.4 µm/sec with no filter. VGstudio software (VGstudio MAX 3.1, Japan) was used to produce 3D models of the scaffolds from the 2D images obtained by the MicroCT. Rendered 3D images were subsequently obtained using Avizo Standard (version. 8.1, Thermo Fisher Scientific, UK) and Simpleware (Simpleware software, USA). The spatial resolutions utilised in the present study were different for each specimen due to different imaging results required: for the 20 vol.% Al_2O_3-PC, spatial resolution was 4

μm, for the 20 vol.% Al_2O_3-UDMA-TEGDMA and 30 vol.% Al_2O_3-PC, spatial resolution was 6 μm and for the 30 vol.% Al_2O_3-UDMA-TEGDMA, spatial resolution was 13 μm.

3.6 Physical characterisation

3.6.1 Density and porosity measurements

The densities of the porous ceramics, ceramic/polymer interpenetrating phase composites, dense alumina and pure polymers were obtained using the Archimedes' method according to ASTM standard C373−16, USA (2016). Six specimens were investigated from each experimental material. For the ceramic/polymer interpenetrating phase composites material, six initial solid ceramic loadings (10, 15, 20, 25, 30, and 35 vol.%), a fixed gelatine concentration (2.5 wt.%), a fixed freezing temperature gradient (bottom rod: -10°C to top rod: +20°C) and freezing rate (1°C/min) were evaluated to examine the effect of alumina solid loading.

The dry weight of the specimen was determined at the beginning by heating the specimens in an oven (Heratherm, temperature controlled programmer, Thermo Scientific, UK) at 150°C for a minimum of 24 hrs, followed by cooling in a vacuum desiccator with silica gel. Then the dry weight was determined using a balance (TE 1502S, Sartorius, Germany). To determine the suspended and the wet weight, the specimens were then boiled for 5 hrs ± 5 mins and allowed to continue to soak in the same deionised water for an additional 24 hrs ± 30 mins. Using a density kit (YDK 01, Sartorius, Germany) the suspended weight of the specimens was measured in water. To measure the suspended weight, the specimen was fully submerged in deionised water in

a stainless-steel container with the mass ratio of water to test specimens being at least 3:1. Weighing was then performed by placing the specimen in a wire loop that was suspended from one arm of the balance (TE 1502S, Sartorius, Germany). After the determination of the suspended mass, each specimen was lightly blotted with a damp leather chamois to remove all visible water droplets from the surface and the wet weight measured. Once all the measurements had been obtained, the following formulae were used to calculate the density, and the total porosity.

The density of the specimen was calculated using the following equation:

$$\text{Density} = \frac{\text{Dry weight x (Density of deionised water- Density of air)}}{\text{Wet weight-Suspended weight}}$$

The density of the deionised water was determined from the measurement of the water temperature and assuming the density of air was 0.0012 g/cm^3.

The porosity of the specimen was calculated using following equation:

$$\text{Porosity} = \frac{\text{Wet weight - Dry weight}}{\text{Wet weight - Suspended weight}} \text{ X } 100\%$$

3.6.2 Porosity measurement

The porosity values were obtained for specimens with a constant initial solid ceramic loading (10 vol.%), at gelatine concentrations of 2.5, 3.75, 5, 7.5, and 10 wt.%, a fixed freezing temperature (bottom rod: -10°C to top rod: +20°C) and freezing rate (1°C/min)

by image analysis using ImageJ (Fiji, Japan) image analysis software. The analysis was based on image specific contrast/brightness adjustments and the specimens were analysed at cross sections perpendicular to the direction of freezing at 4 mm intervals up to 20 mm, progressing from the ceramic rich layer to the most porous layer. For each specimen 5 images were captured using light microscopy from 5 different locations. The results were then collated and an average reading for porosity was determined.

3.6.3 Volumetric shrinkage

In order to determine the shrinkage as a result of sintering, the diameter of each specimen was measured before and after sintering using a laboratory digital calliper (Mitotoyo, UK). Six specimens for each initial solid ceramic loading (10, 15, 20, 25, 30, and 35 vol.%) with 2.5 wt.% gelatine concentration, a freezing temperature of -10°C to +20°C and a freezing rate of 1°C/min were used in this experiment. Measurements were performed immediately after freeze-drying at room temperature and then immediately after sintering. The following formula was used to calculate shrinkage:

$$\text{Shrinkage} = \frac{\text{Diameter}_{\text{before sintering}} - \text{Diameter}_{\text{after sintering}}}{\text{Diameter}_{\text{before sintering}}} \times 100\%$$

3.6.4 Ceramic fraction measurements

The ceramic fractions of the ceramic/polymer interpenetrating phase composites were determined by weighing each specimen and then heating them in an oven (Elite Thermal Systems Ltd., UK) to a temperature of 600°C at a rate of 1°C/min in order to ensure

complete removal of the organic polymer phase. Once cooled to room temperature over 24 hrs, the specimens were then reweighed and the weight fractions determined. The volume fractions could then be calculated from the specific densities of the principal constituents. To determine the volume fraction of the specimen the initial component densities, as provided by the manufacturer, were used. The alumina density was 3.90 g/cm³, PC was 1.20 g/cm³ and the UDMA-TEGDMA mixture was 1.11 g/ml.

3.7 Mechanical characterisation

3.7.1 Compression testing

Six rectangular specimens of each material were tested to failure using a universal testing machine (Zwick Roell Z020, Ulm, Germany) and preloaded software (TestExpert II V3.1). The compression force was directed along the long axis of the specimens and in the same direction as the freeze-casting, with the polymer rich surface at the top and the ceramic rich surface at the bottom. Before starting the test, all the specimens were placed in the centre of the plates of the universal testing machine (Figure 3-14). The mechanical compression properties were determined according to the EN ISO 604:2003 standard (2003).

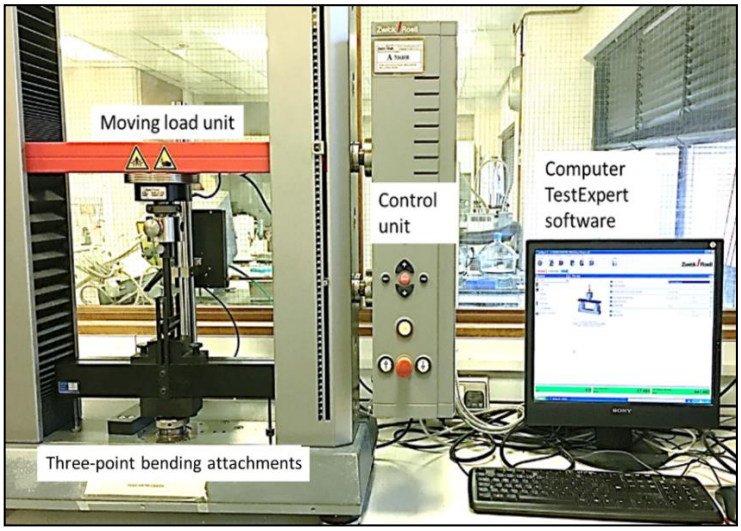

Figure 3-14. Zwick Roell Z020 test machine used for mechanical testing procedures.

All specimens were tested to failure. While the ceramic/polymer interpenetrating phase composite specimens seemed to maintain their shape and character, the dense ceramic specimens demonstrated sudden and catastrophic failure.

The compressive strength was calculated by using the following formula:

$$\text{Compressive strength} = \frac{\text{Force}}{\text{Cross sectional area}}$$

3.7.2 Flexural strength and modulus of elasticity

A three-point bend test was used to determine the flexural strength. Rectangular specimens were chamfered and polished according to British Standard, BS EN ISO 6872, (2008). Testing was again performed using a Zwick Roell (Z020, Ulm, Germany) universal testing machine, with a cross head speed of 0.5 mm/min. Specimens were tested to failure and then examined carefully to ensure failure had indeed taken place. This is

because the ceramic/polymer interpenetrating phase composite specimens often did not appear to fracture catastrophically. Flexural strength was calculated according to the formula:

$$\text{Flexural strength} = \frac{3 \times \text{Force} \times \text{Length}}{2 \times \text{Width} \times \text{Thickness}^2}$$

The modulus of elasticity was determined from the three-point bend test results using the formula:

$$\text{Modulus of elasticity} = \frac{\text{Force} \times \text{Length}^3}{4 \times \text{Deflection} \times \text{Width} \times \text{Thickness}^3}$$

3.7.3 Testing in 2 planes with respect to the freezing direction

For the ceramic/polymer (UDMA-TEGDMA) interpenetrating phase composite specimens, the three-point bend test was the test of choice for testing in 2 planes. For ceramic/polymer (PC) interpenetrating phase composite specimens, the compression test was the test of choice as it was not possible to obtain specimens of sufficient length (18 mm) due to the different infiltration technique.

The ceramic/polymer interpenetrating phase composite specimens were divided into 2 groups. In one group the force was directed parallel to the direction of freeze-casting and in the second group the force was applied perpendicular to the direction of freeze-casting (Figure 3-15).

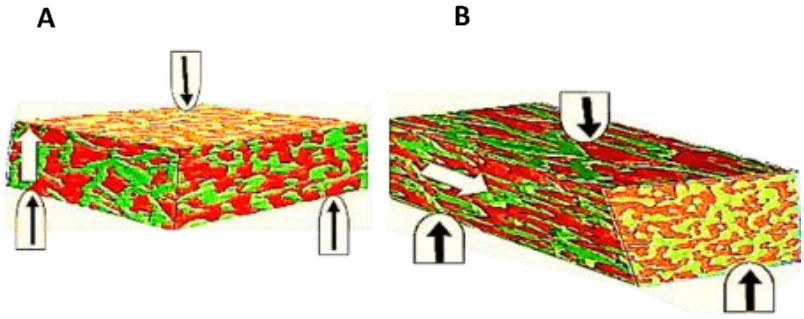

Figure 3-15. Schematic illustration of mechanical three-point bend test on the ceramic/polymer (UDMA-TEGDMA) interpenetrating phase composite specimens showing the direction of the test force in relation to the freezing direction: A. parallel and B. perpendicular. The white arrows indicate the freezing direction and the black arrows indicate the force direction.

3.7.4 Fracture toughness

Fracture toughness was determined for 4 of the ceramic/polymer interpenetrating phase composite materials, namely: ceramic/polymer (UDMA-TEGDMA) interpenetrating phase composite with initial solid ceramic loading of 30 and 35 vol.%, and ceramic/polymer (PC) interpenetrating phase composite with initial solid ceramic loading of 20 and 30 vol.%. For each specimen, a notch was prepared using a high speed cutting machine (Accutom-50, Struers, UK) according to the standards for a single-edge-notched beam, ASTM 1820.15.A,USA (2011). The notch depth was 3.9 mm and it was placed midway along the long axis of the specimen into the 8 mm length. A razor blade and diamond polishing paste (3 µm paste, Struers, Denmark) were then used to sharpen the notch and extend it an additional 200 to 350 µm. The final length of the notch was measured using an optical microscope (Lieca DMLB, USA). Each of the prepared

specimens were then tested to failure using a universal three-point bend test machine (Shimadzu-Tce-N300, Japan) with a support span of 32 mm and at a cross head speed of 1 mm/min (Figure 3-16).

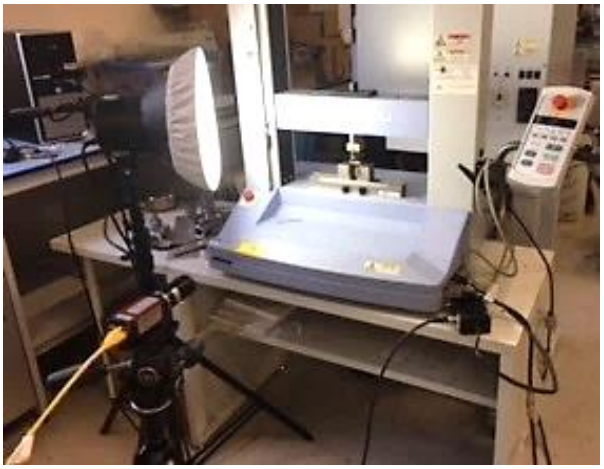

Figure 3-16. Universal testing machine with video system used for fracture toughness testing procedures.

As part of the test procedure the DIC system, computer-controlled video system (NAVITAR, Japan) and video gauge (Imetrum Ltd, UK) were used to record the fracture path as can be seen in Figure 3-17.

Figure 3-17. A ceramic/polymer interpenetrating phase composite specimen at the end of the fracture toughness testing procedure.

The following equation was used to calculate the fracture toughness for each specimen:

$$\text{Fracture toughness} = \frac{\text{Force} \times \text{Length}}{\text{Thickness} \times \text{Width}^{3/2}} \times f(a/W)$$

In which *f(a/W)* is the geometrical factor which can be calculated using the following equation:

$$f(\alpha/W) = 3\,(\alpha/W)^{1/2} \times (1.99-(a/W) \times (1-a/W) \times (2.15-3.93\,(a/W) + 2.7\,(a/W)^2))/2\,(1+2a/W)\,(1-a/W)^{3/2}$$

In which W is the width of the beam, and a is the length of the notch.

3.8 Characterisation of the surface properties

3.8.1 Vickers hardness

Vickers hardness tests were performed at a constant load with a calibrated Vickers indenter in a micro-based indentation system (Duramin Ver 0.08, Struers, UK). Rectangular specimens were cut and polished from ceramic/polymer (UDMA-TEGDMA) interpenetrating phase composite with initial solid ceramic loadings of 30 and 35 vol.%, ceramic/polymer (PC) interpenetrating phase composite with an initial solid ceramic loading of 20 and 30 vol.%, dense alumina and pure polymer specimens. Human enamel specimens were cut and polished to a size of 2 x 3 x 2 mm.

In the case of the ceramic/polymer interpenetrating phase composite materials the maximum load was applied parallel to the direction of freeze-casting. The maximum load was held for 20 sec and 30 determinations were made for each material as illustrated in Table 3-3.

Six indents were made on each specimen with an interval of 2 mm between indents to avoid the influence of residual stresses from neighbouring indents. Indentation diagonals and cracks emanating from the diagonals were measured by light microscopy and any irregular indentations were rejected, as advised by the Standards of Advanced Technical Ceramics, EN843-4: 2005. BSI (2007). The lengths of the two resultant diagonals of the surface indentations were measured and averaged for each measurement. Hardness was calculated according to the formula:

Hardness = 1.854 x Force/ indentation diagonal length^²

Parameter	Composite	Enamel	Alumina	Polymer
Hardness	HV 1	HV 0.2	HV 2	HV 0.2
Time	20 sec	20 sec	20 sec	20 sec
Load	9.807 N	1.961 N	19.807 N	1.961 N
Lens	X 40	X 40	X 40	X 40

Table 3-3. Parameters for Duramin Vickers hardness testing machine.

For the ceramic/polymer (PC) interpenetrating phase composite materials, further hardness evaluation was performed where the maximum load was applied

perpendicular to the direction of freeze-casting to the specimens to evaluate the anisotropy of the materials.

3.8.2 Abrasion testing

The aim of abrasion testing was to determine the maximum predicted wear of an orthodontic appliance constructed of a composite material over 2 years, when subjected to 2 mins of toothbrushing twice daily. This would equate to a total of 2 hrs and 50 mins of toothbrushing per bracket. Six flat specimens were prepared from human permanent tooth enamel, dense ceramic, pure polymers, ceramic/polymer (PC) interpenetrating phase composite specimens with initial solid ceramic loadings of 20 and 30 vol.% and ceramic/polymer (UDMA-TEGDMA) interpenetrating phase composite specimens with initial solid ceramic loadings of 30 and 35 vol.%. Each section was polished and finished using a 0.3 μm Al_2O_3 powder as a suspension in deionised water to achieve a smooth surface. A custom-made toothbrushing machine (Bristol University) was utilised for brushing the samples using a linear motion (Figure 3-18). In order to study surface loss, protective tape was applied to either end of the specimen leaving only an exposed window of the specimen that was subjected to abrasion testing.

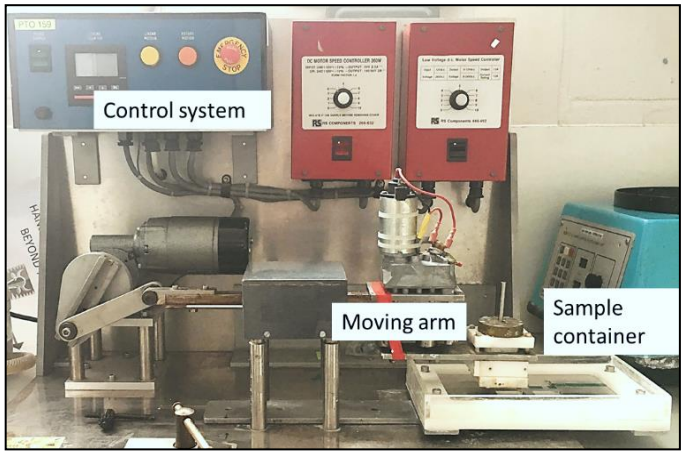

Figure 3-18. Custom-made abrasivity machine.

Within the testing machine custom-made supports were made using Elite Double 32, a vinylpolysiloxane duplicating material (ZhermCK SPa, Badia Polesine, Italy). The base and catalyst were mixed together in a ratio of 1:1 in a glass beaker and the mixture was poured into the pre-existing well on the abrasion testing machine. The mixing time was 1 min; the working time 10 mins and the total setting time was 20 mins. Once the material was tacky to touch, the specimens were placed in a row, split between the two wells along their long axis to create the mould.

Prior to abrasion testing, a toothpaste suspension was prepared using a ratio 25 g toothpaste (Colgate Total Everyday, 1450 ppm.F-, 27.6 µmol/L.F-, Colgate-Palmolive Ltd, Guildford, Surrey, UK) to 40 g deionised water, mixed using a stirrer and magnetic flea (Fisher Scientific, Loughborough, UK) until a homogenous suspension was obtained. This was then poured into the toothbrushing machine reservoir to ensure that each specimen was covered by at least 3 mm of dentifrice suspension. The tooth brushes (Oral B, standard medium, size 35, Procter & Gamble, Egham, Surrey, UK) were mounted

such that the toothbrush filament tip plane moved back and forth across the specimen. Each test group was allocated a new toothbrush head. A weight of 200 g was added to the brushes to simulate the everyday toothbrushing force according to International Standard, ISO 11609 (2017).

The specimens were brushed for 2 hrs 50 mins at 75 strokes per minute. The suspension was replaced every hour to ensure adequate coverage of the specimens. After brushing any remaining dentifrice suspension was removed using deionised water before the specimens were stored in deionised water prior to measurement.

3.8.3 Surface roughness and surface loss

Non-contact white light optical profilometer (Figure 3-19) (Proscan 2100 non-contact profilometer, Scantron Industrial Products Ltd, Taunton, Somerset, UK) and Proscan software (Scantron Industrial Products, Ltd, Taunton, Somerset, England) were used to measure the surface roughness before and after toothbrushing and the amount of surface loss after toothbrushing. Non-contact profilometry provide 2D measurements that are measured in micrometres. A dark reference background check was performed each time prior to scanning to achieve optimum sensitivity during measurements.

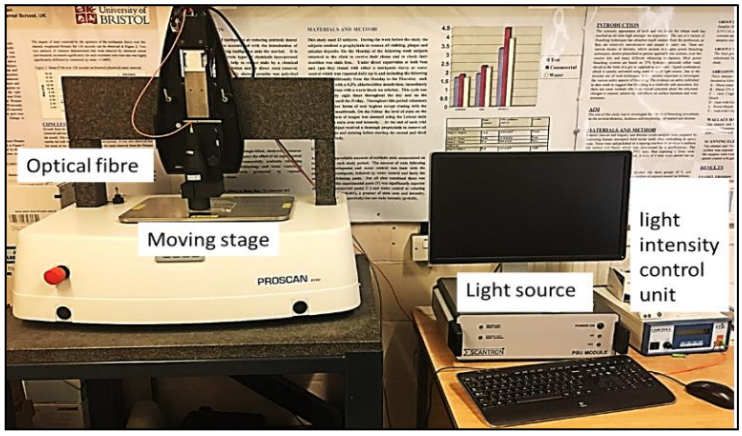

Figure 3-19. Proscan profilometer used for surface roughness and surface loss characterisations.

The non-contact profilometer software comprises a variety of ISO analytical tools for surface form, finish and feature geometry, as well as area and volume-based measurements. To determine the initial surface roughness before toothbrushing, surface scanning was performed for a scan area of 2 x 2 mm in dimension. The optimal step size for the scan area was 0.01 mm in both the horizontal and vertical scan directions and the number of steps was 200. A reference line was placed on one edge of each specimen in order to record the start position which was used for all scans pre-brushing and post-brushing. Six specimens from each material were examined. One measurement was conducted for each specimen in horizontal and vertical directions. Before the start of the brushing experiment, the ends of each specimen from all the different groups of the test materials were protected with adhesive tape providing two control areas and an approximate 1.5 mm^2 wide surface window following initial scanning. When the brushing testing procedures were completed, the protective tape was peeled away, and any tape residue was removed by briefly soaking in acetone (Fisher Scientific, Loughborough, UK) for 30 sec.

The non-contact profilometer detector is able to recognise surfaces properties as these affect the energy absorption of the material. The outline roughness of the tested surface would impact the detector light reflection which would help detector to recognise the degree of the surface roughness. Care was taken to choose the central area of each specimen to avoid edge effects. Surface roughness was measured by scanning the test materials prior and post toothbrushing. The sensor utilised for the measurements was S11 chromatic sensor. The scan measurements were completed by using Surface Filter and Auto levelling function.

The roughness parameters determined were the following:

- Ra, average roughness, which describes the overall surface roughness.
- Rz, which defines the average maximum peak-to-valley height of five consecutive sampling depths.
- Rmax, maximum roughness depth, which analyses isolated profile features on the surface.
- Rq, root mean square roughness, which represents the height distribution relative to the mean line.

To determine the amount of surface loss, A 1.5 x 1.5 mm^2 area was scanned and Proscan software used to highlight three areas, one in the centre across the brushed area (treated) and two from the specimen shoulder areas that were covered and protected initially with tape (control). This allowed for direct comparison between the brushed and unbrushed areas. Any flawed peaks were removed. Differences in height were calculated

using simulation of the area trace method (West *et al.*, 2000). The measurements were repeated 3 times and the mean value was considered as the surface loss value of the specimen. Six specimens from each specimen were investigated. Surface loss was measured by scanning the area that had been brushed (treated) along with the unbrushed areas (control) that had previously been protected by taping.

3.9 Statistical analysis

The statistical tests used on the results obtained from the abrasion testing were paired t-test. The data were analysed using Stata version 14 (Stata Corp, College Station, Texas, USA) with a 5% significance level.

Chapter 4. Fabrication and microstructure of porous ceramic scaffolds

4.1 Introduction

Porous ceramics with tailored open pore structures that can mimic natural structures show great promise for use in biomedical fields. They can be used as preforms to infiltrate with a second phase, such as a polymer or metal, to produce an interpenetrating phase composite for different biological and engineering applications. Due to the poor aesthetic properties of metals and poor mechanical properties of polymers when used as orthodontic bracket materials, pure ceramic, principally alumina, is frequently used (Jena *et al.*, 2007). Although ceramic brackets show good aesthetics and abrasion resistance, their brittle nature means there is the risk of bracket and enamel fracture at debond. The principal aim of the present study is to produce ceramic scaffolds with a graded porosity throughout the overall structure using a gelation/freeze-casting technique. This was the first stage in the development of the biomimetic composites, with the potential for use as an orthodontic bracket material. This was achieved by using a temperature gradient between the top and bottom cooling plates during fabrication, resulting in specimens with a porous composition and microstructure as a function of location. The results are presented both qualitatively, describing the outcome of the stepwise fabrication of the porous ceramic scaffold and its characteristic structural morphology, and quantitatively, describing the results of the density, porosity and shrinkage characterisation.

4.2 Results

4.2.1 Microstructural characterisation of porous ceramic scaffolds

4.2.1.1 Effect of initial solid ceramic loading

The initial solid ceramic loadings (by volume) in the aqueous suspension were found to affect the size and morphology of the pores in the porous ceramic scaffolds (Figure 4-1).

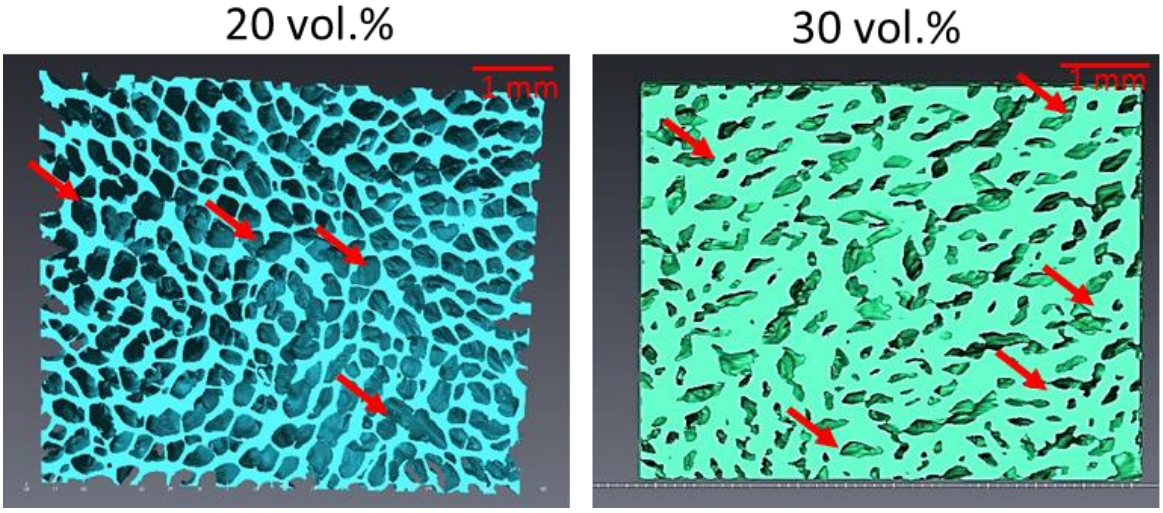

Figure 4-1. MicroCT images of porous ceramic scaffold with initial solid ceramic loading of 20 and 30 vol.% respectively. The images show the change in the pore dimensions and distribution due to changes in the initial solid ceramic loading. Red arrows indicate the different pores with different pore sizes.

When looking at Figure 4-1, we can see that as the initial solid ceramic loading increased, the pore size of the resulting scaffold decreased along with an increase in ceramic wall thickness. For example, porous scaffolds containing 20 vol.% ceramic as the initial solid loading were characterised by relatively bigger pores and the ceramic walls were thinner.

4.2.1.2 Effect of gelatine concentration

To determine the effect of different gelatine concentrations (by weight) on pore size and morphology, SEM images of the porous ceramic scaffold were obtained for six different specimens. These were prepared with constant initial solid ceramic loading in the aqueous suspension (10 vol.%), but with different gelatine concentrations (2.5 to 10 wt.%) and with PVA as a binder for comparison (Figure 4-2). Freezing temperature (-10°C to +20°C) as well as the cooling rate (1°C/min) were fixed in order to allow the comparison between the specimens. The SEM images were taken in two planes with respect to freezing direction: top and sagittal.

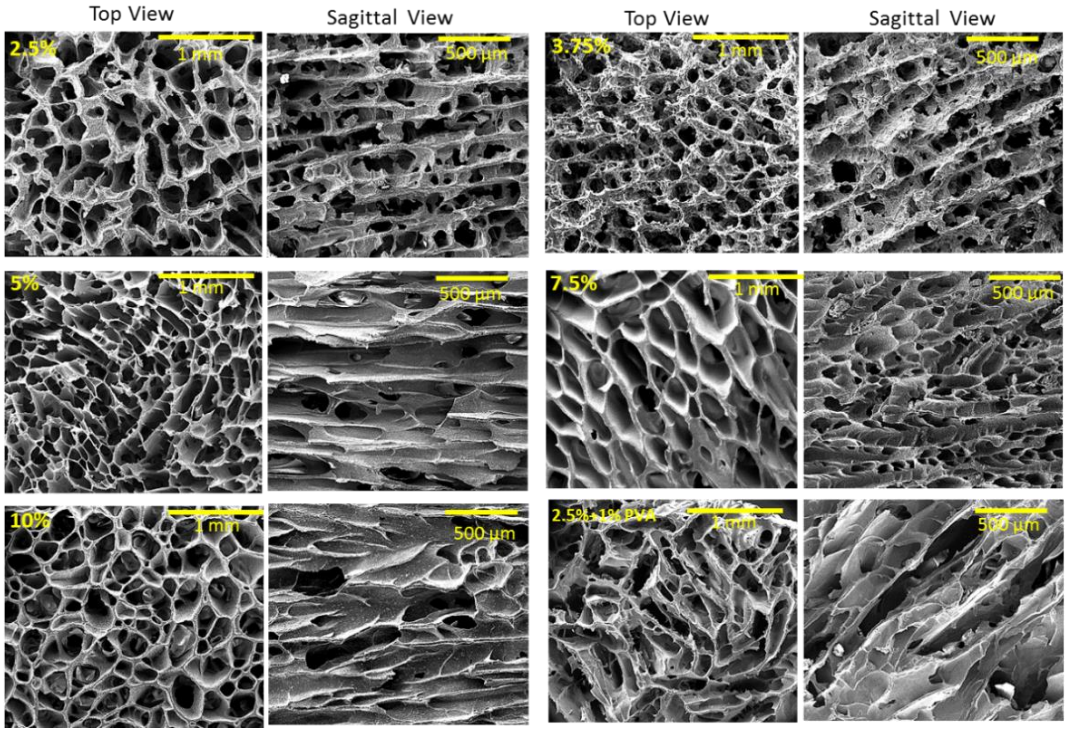

Figure 4-2. SEM images of porous ceramic scaffolds in two planes with respect to freezing direction: top and sagittal showing the morphology and dimensions of the unidirectional aligned pore channels. The porous ceramic scaffolds were produced with an initial solid ceramic loading of 10 vol.%, six different gelatine concentrations of 2.5%, 3.75%, 5%, 7.5%, 10% and both gelatine 2.5% and PVA 2%. A freezing temperature of -10°C to +20°C, and a cooling rate of 1°C/min.

The SEM images in Figure 4-2 demonstrate that the shape of the pores at the relatively lower gelatine concentrations looks less rounded and appear as polygons. With increasing gelatine concentration, the pore shape changed to a more rounded appearance.

It can be seen from the graph in Figure 4-3 that in each layer, as the concentration of the gelatine increased, so the porosity decreased. It is clear that the increase in the gelatine concentration leads to a reduction in the overall porosity, regardless of the size and the

shape of the pores. As might be expected there was a progressive increase in the porosity from ceramic-rich to the more porous layers along the direction of freezing.

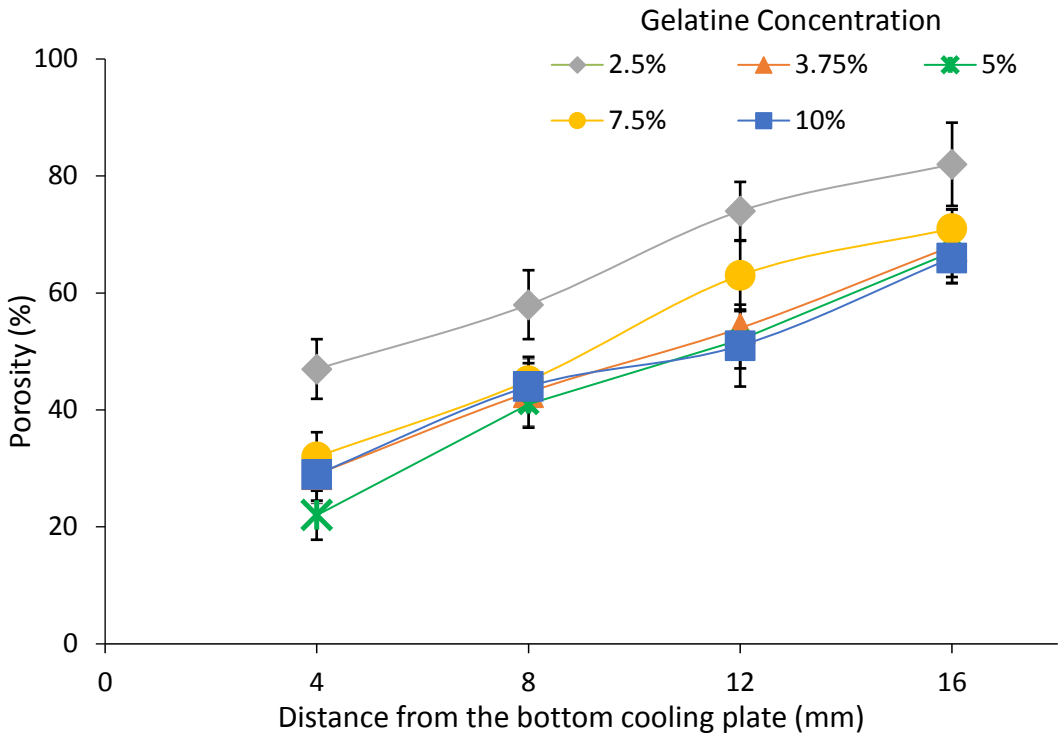

Figure 4-3. The overall mean and SD (%) of the porosities progressing from the ceramic-rich layer to the more porous layer of porous ceramic scaffolds with respect to anisotropy and different gelatine concentrations. The porous ceramic scaffolds were produced with an initial solid ceramic loading of 10 vol.%, five different gelatine concentrations of 2.5%, 3.75%, 5%, 7.5% and 10%, a freezing temperature of -10°C to +20°C, and a cooling rate of 1°C/min. The porosity analysis of these images was performed using ImageJ image-analysis software.

Specimens containing 20 vol.% initial solid ceramic loading, prepared at a freezing temperature gradient of -10°C to +20°C, a gelatine concentration of 2.5% and a cooling rate of 1°C/min were further cut into 4 mm thick sections, progressing from the ceramic-rich layer to the more porous layer. Specimens containing 20 vol.% initial solid ceramic

loading were chosen for this investigation to show the effect of the freeze-casting process on the gradient structure of the resultant porous scaffolds. Optical microscope images were obtained at a distance of 4, 8, 12, 16 and 20 mm from the bottom cooling plate, where freezing started, progressing from the ceramic-rich layer towards the top ceramic-poor (more porous) layer. Images were taken of each layer and ImageJ software was used to measure the porosity (Figure 4-4). It is clear that when progressing further from the bottom ceramic-rich layer, the ceramic component decreases in volume and become less dense, while the pores become bigger. The images show that the temperature gradient significantly influences pore structure with a gradual increase in the size of the pores.

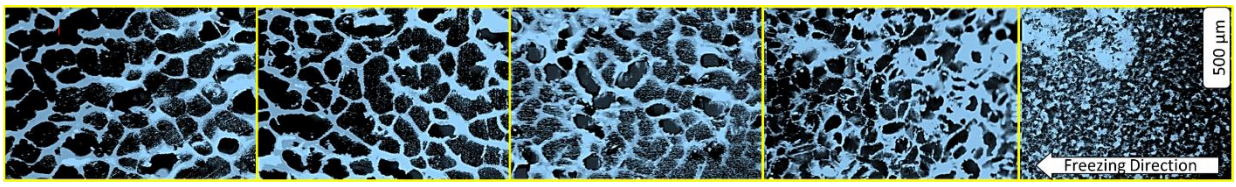

Figure 4-4. Optical images show the cross sections of porous freeze-cast scaffold produced with initial solid ceramic loading of 20 vol.%. At a distance of (a) 20 mm from the bottom, (b) 16 mm, (c) 12 mm, (d) 8 mm and (e) 4 mm.

4.2.1.3 Morphology of the pores

SEM images in Figure 4-5 show the microstructure of the porous ceramic scaffold. The morphology of the pores obtained by using the gelation/freeze-casting route was typically cylindrical and with the main structure characterised by pores of various sizes.

The pores were characterised by a hexagonal architecture arranged as a 3D honeycomb-like structure.

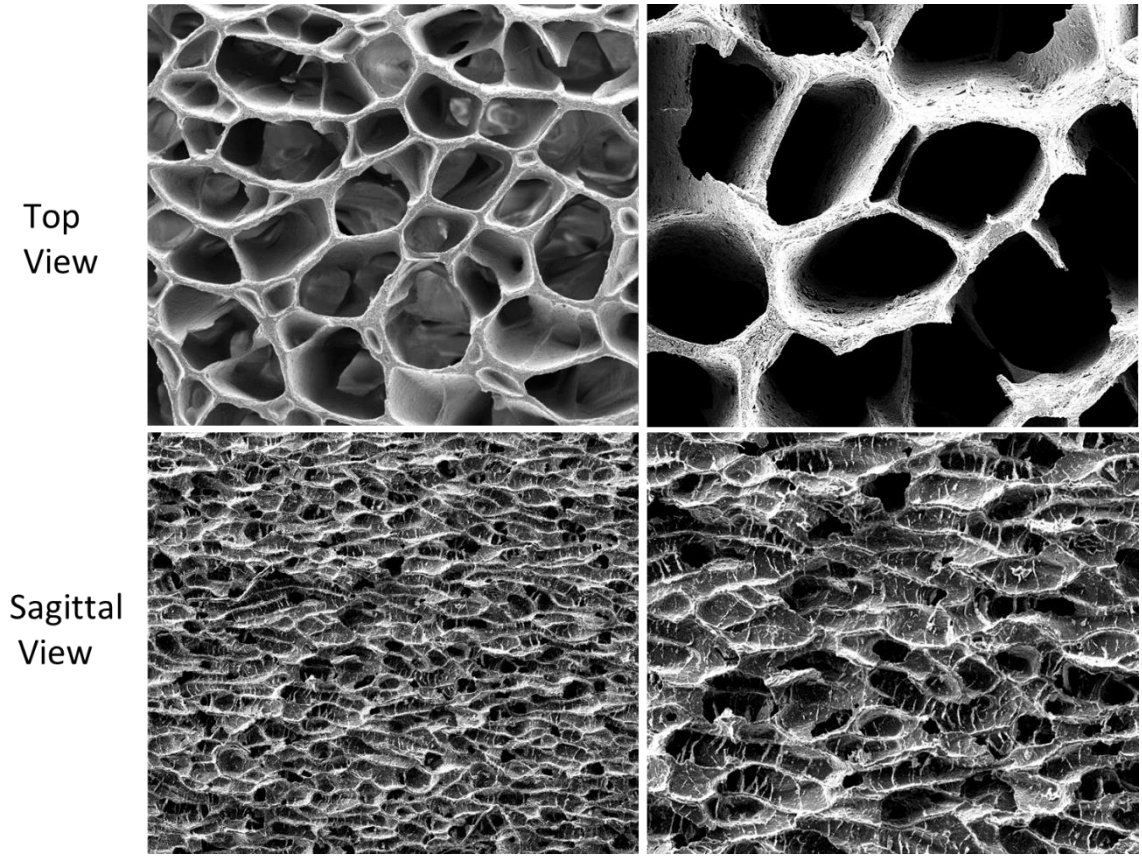

Figure 4-5. SEM images of the porous ceramic specimen for top and sagittal plane showing the unique 3D honeycomb-like structure. The porous ceramic scaffolds were prepared with initial solid ceramic loading of 20 vol.%, a freezing temperature of -10°C to +20°C, a gelatine concentration of 2.5 wt.% and a cooling rate of 1°C/min.
A: Magnification x 80. B: Magnification x 160.

4.2.1.4 The graded structure of the pores

MicroCT images (Figure 4-6) were produced for the porous scaffolds with 20 vol.% initial ceramic loading, a freezing temperature gradient of -10°C to +20°C, a gelatine concentration of 2.5% and a cooling rate of 1°C/min. MicroCT examination provided a

continuous image in the sagittal plane along the direction of freezing from the ceramic dense to the porous rich layer.

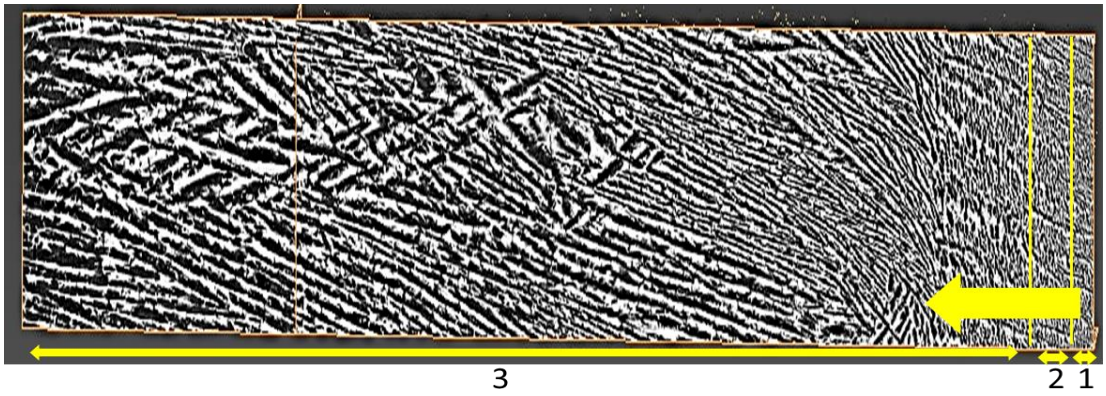

Figure 4-6. MicroCT 2D image of the sagittal cross section of freeze-cast porous alumina scaffold with initial solid ceramic loading of 20 vol.%. The scaffold shows a porosity gradient in the direction of freezing. The yellow arrow indicates the freezing direction. The numbers indicate the zone characteristics of the freeze-cast porous scaffold.

It is clear the temperature gradient significantly influences the pore size and structure. The image shows a unidirectional channelled structure exists in the entire ceramic scaffold, which is a typical feature of freeze-casting when using water as a solvent (Figure 4-6). As the distance from the cooling plate increases, so the porosity of the ceramic scaffold increases and in a graduated fashion from the bottom to the top of the specimen. We can also see three distinct zones:

- Zone 1, closest to the freezing plate where the freezing process starts, the scaffold is dense, and no porosity can be observed
- Zone 2, the scaffold has a randomised structure and closed pores

- Zone 3, the scaffold has open and interconnected porosity adapted to the direction of the freezing front.

These zones have been previously described by Deville *et al.* (2006b). The present study will focus only on the properties of the porous top zone.

4.2.2 Physical characterisation of porous ceramic scaffolds

4.2.2.1 Density and porosity (Archimedes' method)

The densities and porosities of specimens containing initial solid ceramic loading of 10, 15, 20, 25, 30 and 35 vol.%, a freezing temperature of -10°C to +20°C, a gelatine concentration of 2.5 wt.% and a cooling rate of 1°C/min were evaluated using the Archimedes' method and deionised water. The results for the densities and porosities obtained for these samples can be seen below in Figure 4-7.

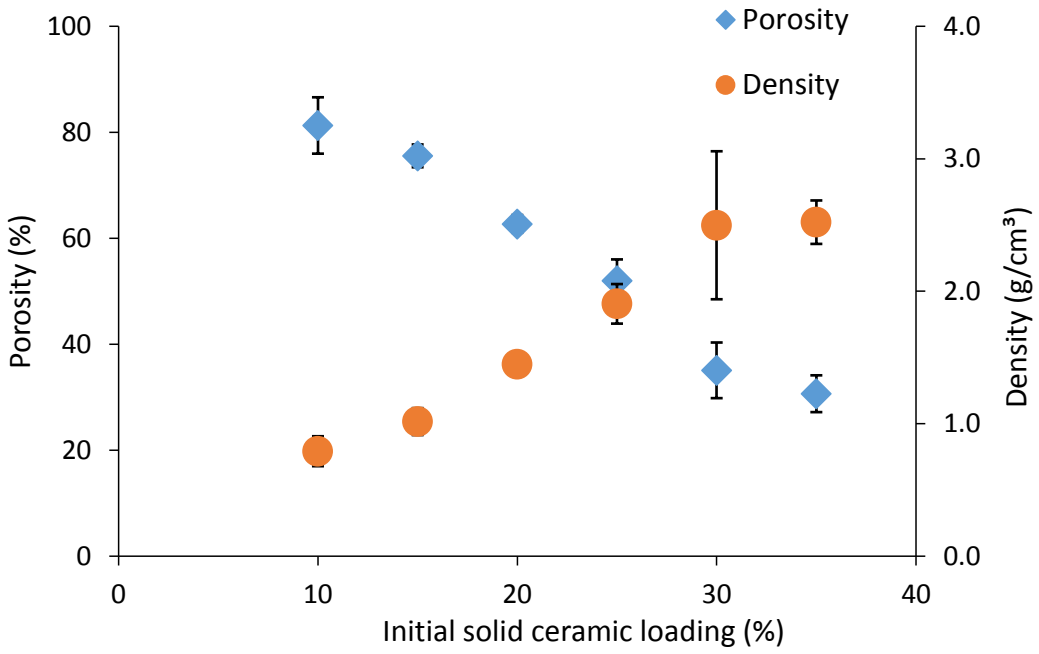

Figure 4-7. Graph illustrating change in the mean and SD of porosities (%) and densities (g/cm³) of the porous ceramic scaffolds in relation to the initial solid ceramic loading. The data were produced using the Archimedes' method.

It can be seen that the values of the densities for the samples were linearly related to the solid loading. This is to be expected as the density of a sample is a function of the solid loading in the initial suspension.

When looking at the graph in Figure 4-7, we can see the total porosity for these samples, which was calculated based on their weight, tended to increase with decreasing solid ceramic loading. This again is to be expected as the total porosity is a function of the amount of water present in the initial suspension.

4.2.2.2 Linear sintering shrinkage

Shrinkage evaluation was performed by measuring the specimen diameters at room temperature following freeze-drying, and again at room temperature after sintering (Figure 4-8).

Figure 4-8. Typical porous ceramic specimens before and after sintering respectively. Specimens obtained from initial solid ceramic loading of 30 vol.% through directional freeze-casting and subsequently sintered at a temperature of 1600°C for 2 hrs.

It can be seen in Figure 4-8 that the ceramic scaffold was sintered successfully with no apparent deformation or cracks.

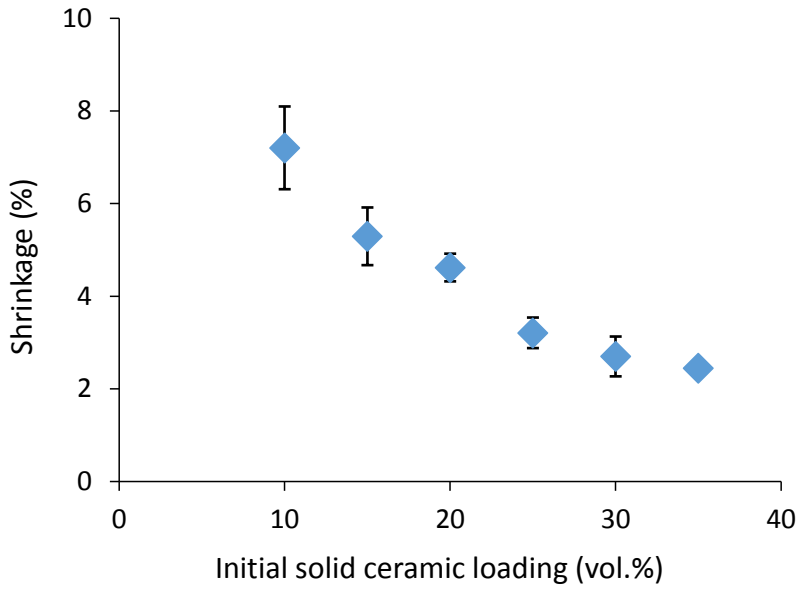

Figure 4-9. Graph illustrating the measurements of the mean and SD of the sintering shrinkage (%) values in relation to the initial solid ceramic loading.

By looking at Figure 4-9, we can see that as the initial solid ceramic loading increased, the volume shrinkage decreased. For example, the linear shrinkage was observed to be only 2% in the case of the specimens containing initial solid ceramic loading of 35 vol.%, while it was 7% in case of the specimens containing initial solid ceramic loading of 10 vol.%.

4.3 Discussion

In order to produce a biomimetic interpenetrating phase composite material, it was first necessary to fabricate a porous ceramic scaffold with graded open pores, which could subsequently be infiltrated with a polymer. In the present study a combination of gelatine/gelation and directional freeze-casting was used to produce the porous alumina

ceramic scaffolds. This method has the advantage of being able to produce a material with a variable porosity that is controlled by the initial solid ceramic loading in the aqueous suspension. The use of water as a principal component makes the process environmentally friendly and it is also applicable to various types of ceramics (Deville, 2010; Ohji and Fukushima, 2012).

In the present study, the porous alumina ceramic scaffolds created comprised anisotropic honeycomb-like porous microstructures, rather than the lamellar pore structure typically seen with freeze-casting (Park *et al.*, 2017). This was due to the use of gelatine as a binder and is in agreement with other studies that investigated the production of a microporous ceramic with a very high porosity and a honeycomb-like structure (Fukushima *et al.*, 2010). The characteristic honeycomb-like structure is believed to be formed as a result of the gelatine/gelation effect during the freezing process (Fukushima *et al.*, 2008). This mimics to some extent the distribution of the dental organic phase within the inorganic phase seen at the dentine-enamel junction in teeth (Amizuka *et al.*, 1992) and in the outer layer of the enamel (Wang *et al.*, 2012).

The honeycomb-like structure produced using this technique has the potential to improve the mechanical properties of any subsequent interpenetrating phase composite produced using other processing techniques (Wegst *et al.*, 2010). Similarly, the lamellar pores seen in the present study demonstrated more interconnections than are typically seen using other binders such as PVA (Preiss *et al.*, 2012), which again has the potential to improve the mechanical properties. This is because a connected porous structure typically results in increased strength and stiffness (Scotti and Dunand, 2018).

4.3.1 The gelatine freeze-casting process

Freeze-casting has been widely considered a useful technique for porous ceramic production from a fine ceramic powder aqueous suspension. The main mechanism is the rejection of particles from the growing solvent crystals in the suspension (Deville, 2010; Fukushima *et al.*, 2008). Moreover, it is a promising technique to mimic nature's toughening mechanisms, by fabricating composites characterised by higher mechanical properties than those of their individual component parts (Munch *et al.*, 2008; Launey *et al.*, 2010; Preiss *et al.*, 2012; Petrini *et al.*, 2013; Porter *et al.*, 2013).

In the present study, the specimens were produced to a standardised height of 20 mm, which was appropriate for microstructural and mechanical property analysis, as well as permitting a relatively short freeze-casting time to be used (Deville, 2008).

When the freeze-casting process was complete, the green body was then freeze-dried to facilitate sublimation of the water from the ice phase to the gas phase. Following freeze-drying, a porous ceramic green body was obtained where the ceramic particles were held together by the binder gelatine. This green body was sufficiently strong that it could be handled without fracturing, prior to sintering. During sintering, it is crucial to avoid crack formation within the specimen by using a slow heating phase, which permits slow evaporation of any residual water and the decomposition of the organic gelatine binder (Deville, 2008; Deville, 2013). The first step of the sintering phase was slow heating to up to 450°C at a rate of 1°C/min. This was followed by further heating up to 1600°C to allow

densification of the ceramic walls (Deville, 2008), the elimination of any micro-porosities and a potential improvement in the final mechanical properties (Nguyen *et al.*, 2012).

Alumina powder was used in the present study as it is the most popular ceramic material used to produce aesthetic orthodontic brackets. This is due to its chemical stability, excellent biocompatibility, high wear resistance, good optical properties and high mechanical strength (Moraes *et al.*, 2004). It has been used to produce well-defined porous ceramic scaffolds using the freeze-casting technique and the scaffolds have reportedly demonstrated excellent mechanical properties (Fukasawa *et al.*, 2001a; Fukasawa *et al.*, 2001b; Deville *et al.*, 2007; Preiss *et al.*, 2012; Petrini *et al.*, 2013). Ceramics have been successfully used in restorative dentistry in fabricating CAD/CAM indirect restorations, such as crowns and bridges, for decades (Miyazaki and Hotta, 2011), and more recently sintered alumina networks, infiltrated with a second phase, have been manufactured for potential use in dentistry (Chaiyabutr *et al.*, 2009; Preiss *et al.*, 2012; Petrini *et al.*, 2013; Giordano, 1998; Giordano, 2000).

4.3.2 Effect of the initial solid ceramic loading on the microstructure

In the present study, the effect of different solid ceramic loadings within the initial aqueous suspension was investigated, namely 10, 15, 20, 25, 30 and 35 vol.% of ceramic. Based on a previous study by Preiss *et al.* (2012), this range of solid loading is thought to be ideal for the fabrication of porous ceramic scaffolds and subsequent polymer infiltration. The higher the solid loading the greater the forces required for the growing ice crystals to push up through the ceramic suspension to create a porous ceramic

framework (Deville, 2008; Deville *et al.*, 2015). As a result, ceramic suspensions containing high initial solid ceramic loading (40 vol.%) may result in a porous ceramic scaffold with a very low porosity that might be difficult to infiltrate with a second polymeric phase. Conversely, ceramic aqueous suspensions with initial solid ceramic loading lower than 10% may result in scaffold with poor mechanical properties for clinical use, even after polymer infiltration (Deville, 2010). In the present study, it has been demonstrated that different initial solid ceramic loadings in the suspension can have a clear effect on the final porous scaffold microstructure with respect to pore size, morphology and wall thickness, as illustrated in Figure 4-1. With increasing solid loading there is a decrease in pore size and an increase in wall thickness. On the other hand, reducing the ceramic solid content lead to a decreased ceramic wall thickness and an increase in pore size. This can be explained by the presence of relatively high water content in the aqueous suspension, hence bigger ice crystals developed. These results agree with previous research that has examined the influence of the initial solid loading of the ceramic suspension on pore size and wall thickness (Deville *et al.*, 2007; Preiss *et al.*, 2012; Naleway *et al.*, 2016).

4.3.3 Effect of the binder on the microstructure

At the beginning of the present study, gelatine as a binder was added immediately to the alumina suspension. However, it did not completely dissolve, which resulted in an inhomogeneous suspension. It was therefore decided to initially dissolve the gelatine powder in water heated to 55°C and stirred for 1 hour. This solution was then added to the aqueous ceramic suspension, resulting in a more homogenous mixture. This

combination of freeze-casting and gelatine/gelation has been used previously in the fabrication of porous ceramic scaffolds (Fukushima *et al.*, 2008; Koch *et al.*, 2003; Fukushima *et al.*, 2014; Matsunaga *et al.*, 2017). Gelatine is a biopolymer that is widely used in composite materials due to its non-toxicity, biological origin and desirable mechanical properties. It is a denatured collagen, which undergoes physical gelation at temperatures below 20°C, forming a weakly crosslinked network.

In the present study, the effect of gelatine addition on the structure of freeze-cast scaffolds was to produce a more cylindrical pore structure, which is in agreement with previous work on porous scaffold fabrication (Fukasawa *et al.*, 2001a; Landi *et al.*, 2008; Fukushima *et al.*, 2008). Gelatine slowly gelatinises and hinders the anisotropic growth of ice crystals and so the pores evolve into spherical and reticulated shapes (Zhang *et al.*, 2009). These honeycomb-like porous structures are produced probably as a result of the increased resistance the gelatine affords, preventing the ice crystals created during the freeze-casting process from adopting their more usual plate-like morphology, and therefore lamellar structure within the ceramic suspension (Fukasawa *et al.*, 2001a; Landi *et al.*, 2008; Fukushima *et al.*, 2008; Liu *et al.*, 2015).

The pore size and porosity both decreased when the gelatine concentration was increased as can be seen in Figure 4-2 and 4-4. One possible reason is that with an increased concentration of gelatine, solution viscosity increases and therefore a higher force is required for the gelatine molecules and the ceramic particles to be expelled by the water molecules during ice crystal formation (Fukushima *et al.*, 2008). This is in agreement with previous studies in the literature, where ice crystal size was observed to

be reduced in the presence of gelatine molecules (Arabi and Zamanian, 2013; Wu *et al.*, 2010).

4.3.4 Morphology of pores

In the present study, examination of the sintered porous structure revealed macroscopic pores uniformly distributed over the entire scaffold. These pores were aligned along the direction of growth of the ice crystals and exhibited a well-defined honeycomb-like shape in their cross sectional view (Figure 4-4), more so than the pore structure typically seen for freeze-cast specimens produced using different binder systems (Li and Dunand, 2011). The dendritic structure, more typically seen with ice crystal growth where just water or a camphene-based suspension is used, was not seen (Fukasawa *et al.*, 2002; Ding *et al.*, 2007; Yoon *et al.*, 2007).

All specimens, independent of their initial solid ceramic loading, showed a progressive increase in pore size with increasing distance from the bottom cooling rod of the freeze-casting machine. This was associated with the slowing down of the freezing velocity of the growing ice front. This means that at distances further away from the cold surface of the lower cooling rod, the ice growth rate reduced due to the evolved ice which operates as an insulator and reduces the temperature gradient. The temperature ranged from -10°C to +20°C in the current investigation. The range from -7°C to 0°C is known as the zone of maximum ice crystal formation (Knight *et al.*, 1988; Yeh and Feeney, 1996). This anisotropic structure created as a result of the directional freeze-casting process

can result in mechanical properties that are significantly higher than those achieved by ceramic scaffolds created using non-directional freezing (Deville *et al.*, 2006a).

The pore sizes observed in the present study demonstrated a potential for polymer infiltration enabling the fabrication of a composite material. The graduated structure produced means that if this material were to be used in the construction of an orthodontic bracket, it may provide a polymer rich layer for bonding to the tooth surface, and a ceramic-rich layer exposed to the oral environment with improved wear and abrasion resistance. If this is to be the case, then the architecture of the framework must be tailored to provide suitable dimensions for the composite material to be fabricated into an orthodontic bracket.

4.3.5 The graded porous structure

The production of a homogenous specimen using freeze-casting, with a uniform temperature across the specimen would have a very little potential application as a bracket material, as the resultant scaffold would have a cellular microstructure with randomly orientated pores (Fu *et al.*, 2008). This would potentially affect polymer infiltration and reduce the mechanical properties. During the freeze-casting process in the present study, ice crystal growth was restrained by the application of a temperature gradient induced in the gelatine solution, resulting in a unidirectional gradient porous scaffold (Rodríguez-Parra *et al.*, 2012; Kang *et al.*, 1999; Jing *et al.*, 2010).This phenomenon is known as anisotropic ice crystal growth. This unique microstructure was achieved by having one end of the specimen at a lower temperature than the other, and

with the ceramic particles initially being rejected by the solidification front forming at the bottom cooling plate and progressing to the top cooling plate (Barr and Luijten, 2010). The resultant scaffold was characterised by a complex porous anisotropic microstructure, which can be easily infiltrated by another phase network (Han *et al.*, 2009). To visualize the pores inside the scaffold, specimens were cut transversely through the total length of the specimens and viewed with optical microscopy, as can be seen in Figure 4-3. The same was also viewed with MicroCT 2D imaging (Figures 4-6). In both cases it can be clearly seen that the scaffold exhibits a graduated porous structure in the direction of freeze-casting.

Freeze-cast porous scaffold are characterised by three distinct zones along the solidification front (Figure 4-6), as had been previously described by (Deville *et al.*, 2006a). The present study will only focus on the third porous zone. Looking at the image in Figure 4-6, it would appear that as we progress further from the ceramic-rich end, the pore size increases in this porous zone, and the ceramic component become less dense. Additionally, there was a transition from a random architecture to a 3D honeycomb-like structure. This channelled structure occurs in the entire sintered body from bottom towards the top, with the top layers characterised by a higher porosity.

In an aesthetic orthodontic bracket made from such a material, this characteristic gradient structure would allow the production of a polymer rich tooth facing layer, which would reduce the risk of enamel damage at debond. Conversely there would be a ceramic-rich outer layer, exposed to the oral environment, which would demonstrate

improved wear resistance compared to a conventional polymeric bracket, and tougher bracket tie wings compared with conventional ceramic orthodontic brackets.

4.3.6 Density and porosity of the porous ceramic structure

The density of a specimen is the proportion of its dry mass divided by the exterior volume including pores. The mean values of the density of the porous ceramic scaffolds reported in the present study ranged from 0.79 to 2.52 g/cm³. The mean density value of the porous scaffolds containing an initial solid ceramic loading of 20 vol.% was 1.45, and for a loading of 30 vol.% it was 2.5 g/cm³. These values are comparable to the mean density values reported for porous alumina scaffolds 1.43 and 2.06 g/cm³ respectively by Zhang *et al.* (2010). It can be seen from Figure 4-7 that the values of the densities for the samples were linearly related to the initial solid ceramic loading, and there was an increase in the density with increasing vol.% of ceramic. This may be attributed to a higher volume of alumina powder and thereby more densely packed ceramic particles.

The porosity of a material is the relationship of the volume of open pores of specimen to its exterior volume (Diamond, 2000). In the present study, for porous ceramic scaffolds the porosity was investigated in relation to the initial solid loading of the suspension, as illustrated in Figure 4-7. The porosity ranged from 31 to 81% when the initial ceramic solid loading decreased from 35 to 10 vol.%. The total porosity of the scaffold was strongly affected by the initial solid ceramic loading in the suspension. This indicates that the porosity results from the volume of water within the initial suspension (Fukasawa *et al.*, 2001a; Fukasawa *et al.*, 2001b; Deville *et al.*, 2007). Usually, the growing ice crystals

repel all particles, additives and impurities, concentrating them within the inter-crystal space (Deville, 2013). By altering the initial solid ceramic loading it was possible to customise the resultant ceramic scaffold porosities, meaning that freeze-casting shows promise for the development of porous ceramics tailored for orthodontic applications. These results observed are consistent with the range of mean porosities reported in the literature (40 to 97%), demonstrating that freeze-casting is a versatile technique that can produce a wide range of porous materials (Deville *et al.*, 2006a; Deville *et al.*, 2006b). When alumina suspensions were processed by freeze-casting and using gelatine gelation, Fukasawa *et al.* (2001b) showed the porosity of final scaffolds containing 28.0% and 33.3% ceramic sintered at 1600°C ranged from 52.8% and 45.8% respectively, which again are comparable with the data obtained in the present study (51.97% and 35.00% porosity with initial solid loading of 25 and 30 vol.% respectively).

4.3.7 Shrinkage and deformation of the porous ceramic structure

The final porous ceramic scaffolds produced in this study were successfully sintered with relatively low shrinkage. High sintering shrinkage can lead to internal and surface cracks, in the final ceramic scaffold (Tillman *et al.*, 2014). It can be seen from Figure 4-9 that shrinkage of the final porous scaffold decreased slightly as the initial solid ceramic loading in the original suspension increased, when the sintering temperature was fixed. This is probably due to the shrinkage of the specimen being determined almost entirely by the intrinsic shrinkage of alumina itself and densification of the ceramic walls of the porous scaffold. Previous research has shown that a higher initial solid ceramic loading is required to reduce the shrinkage of the ceramic green body during drying and sintering

(Sharifi *et al.*, 2014). Moreover, Fukasawa *et al.* (2001b) investigated the characteristics of porous alumina scaffolds produced by conventional freeze-casting and found that solid ceramic loading has very little effect on the sintering shrinkage, although they only investigated specimens with an initial solid ceramic loading of 30 to 45 vol.%.

4.4 Summary

In this part of the study, porous ceramic scaffolds were produced with a view to later infiltration with polymer in order to create a material that might be used for the fabrication of aesthetic orthodontic brackets. Porous alumina scaffolds with different ceramic volume fractions and anisotropic graded structures were successfully produced using a unidirectional freeze-casting technique and with gelatine as a binder. Freeze-casting, combined with the use of gelatine gelation created not only porous alumina scaffolds, but created scaffolds with a honeycomb-like structure that could be tailored by manipulating the processing and freezing conditions. Optical, SEM and MicroCT observations showed an aligned and graduated structure within the ceramic scaffolds, with 3D interconnected pores along the whole body of the scaffold.

Chapter 5. Fabrication and microstructural characterisation of ceramic/polymer interpenetrating phase composites

5.1 Introduction

An ideal orthodontic bracket should be strong enough to withstand the oral environment, be able to transfer the applied forces to the tooth during orthodontic treatment and satisfy the aesthetic needs of the patient. In the previous Chapter the fabrication and characterisation of the porous ceramic frameworks was described. The aim of this part of the study is to fabricate and characterise ceramic/polymer interpenetrating phase composites for use in aesthetic orthodontic brackets. These materials comprise a polymer infiltrated into a porous freeze-cast alumina preform with interconnected porosity and a graded structure. Two different types of polymers, namely UDMA-TEGDMA and PC, were used for the ceramic framework infiltration. These polymers were chosen as they are currently widely used in dentistry, possess good aesthetics, good mechanical properties and are biocompatible. The effect of different initial solid ceramic loadings on the ceramic structure and therefore polymer infiltration process was also investigated. The results are presented as both qualitative, describing the outcome of the stepwise fabrication of the ceramic/polymer interpenetrating phase composites and their characteristic structural morphology, and also quantitative, describing the effects of the ceramic volume fraction on the microstructure and density of the final interpenetrating phase composite materials.

5.2 Results

5.2.1 Microstructure of ceramic/polymer interpenetrating phase composite

5.2.1.1 Al_2O_3-UDMA-TEGDMA interpenetrating phase composite

In this study, UDMA-TEGDMA was infiltrated into the pores of the porous ceramic preform using vacuum infiltration followed by *in situ* heat polymerisation (as described in Chapter 3, page 68 to 69). Figure 5-1 shows an example of a freeze-cast porous preform and the ceramic/polymer infiltrated interpenetrating phase composite, as prepared for this study.

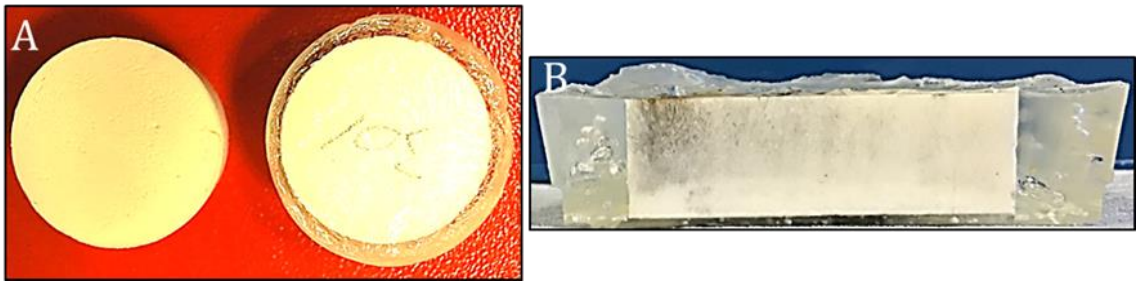

Figure 5-1. A: Top view of a sintered porous ceramic specimen before and after UDMA-TEGDMA infiltration. B: Sagittal view of a specimen after UDMA-TEGDMA infiltration.

The resultant ceramic/polymer interpenetrating phase composite is uniform showing that the monomers had completely penetrated the pores of the ceramic preform. SEM images in Figure 5-2 were obtained for the Al_2O_3-UDMA-TEGDMA interpenetrating phase composites with different initial solid ceramic loadings in the aqueous suspension.

It is clear from the images that with increasing ceramic volume fraction, the polymer volume decreases, probably due to reduced pore size.

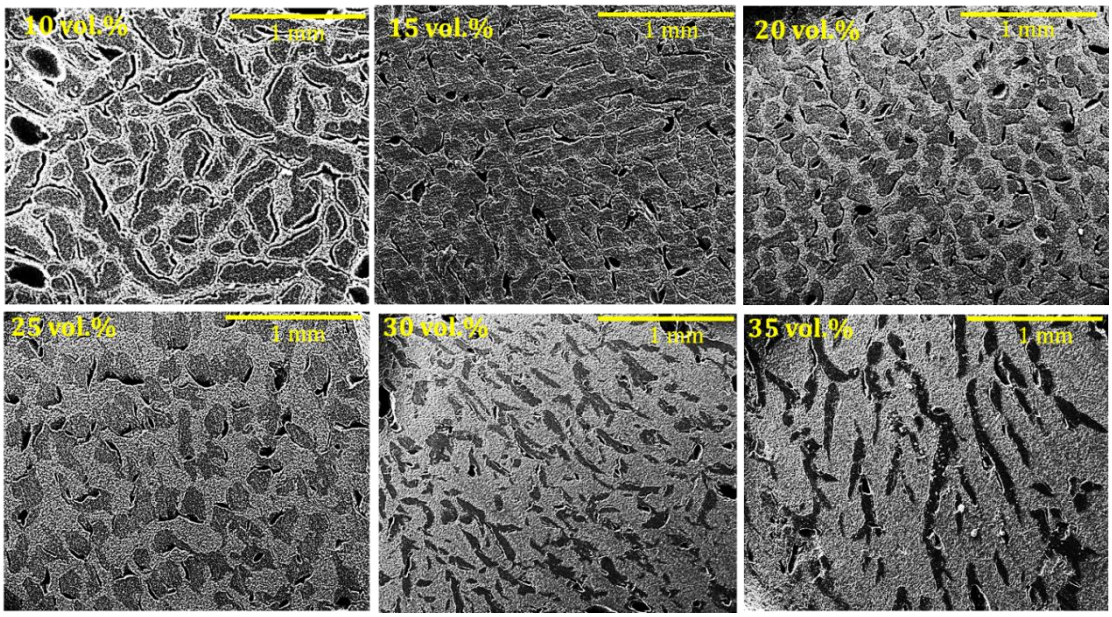

Figure 5-2. SEM images showing the change in the structure of the ceramic/polymer interpenetrating phase composite in relation to the ceramic fraction. With initial solid ceramic loadings :10, 15, 20, 25, 30 and 35 vol.% respectively.

When looking at SEM images for composites produced with an initial solid ceramic loading of 10 vol.%, we can see that the polymer matrix is more dominant, abundant and well distributed. It is also obvious that the polymer shape changes with increasing ceramic fraction, which is attributed to the change in the geometry of the original ice crystals.

5.2.1.2 Al_2O_3-PC interpenetrating phase composite

Unlike the UDMA-TEGDMA composite, PC was infiltrated into the pores of the ceramic preform using heat and an applied load. When looking at Figure 5-3 we can see that a temperature of less than 250°C did not result in successful PC infiltration, while 300°C caused decomposition of the PC and unwanted colour changes. As a result, 250°C was

the temperature of choice to perform the experiments in the present study. The effect of different loads on polymer PC penetration into the porous ceramic preform was also investigated. It can be seen in Figure 5-3 that applied loads of 200 N and 400 N resulted in polymer infiltration of the ceramic. However, at applied loads of 1000 N or more the ceramic fractured. An applied load of 400 N was therefore used in the present study.

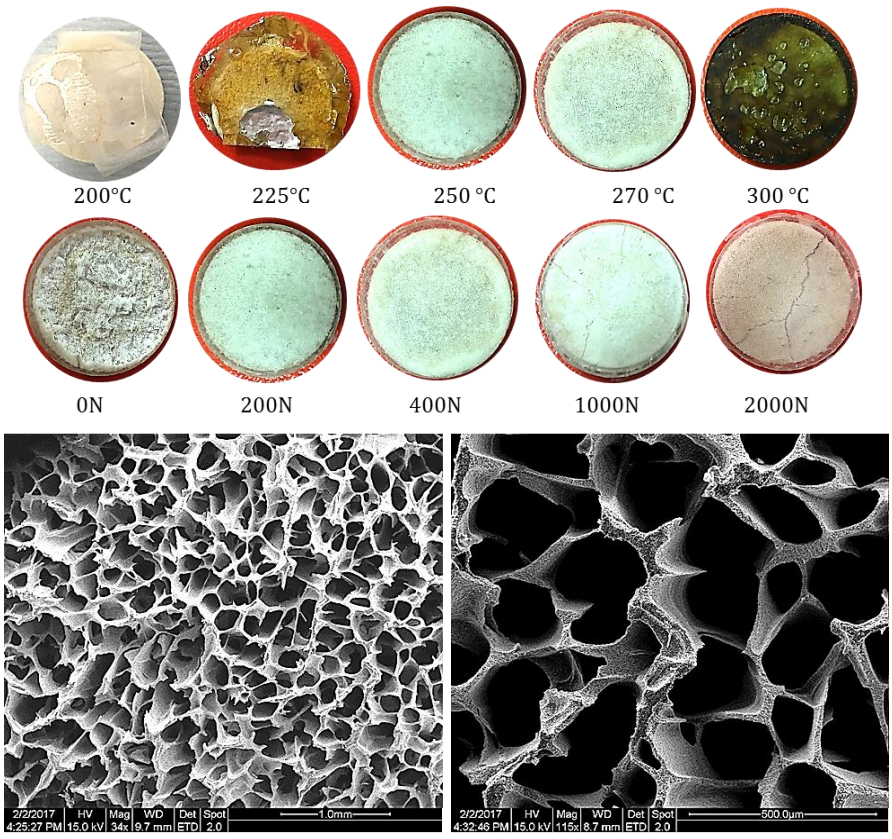

Figure 5-3. The effect of different temperatures and applied loads on the infiltration of PC into the porous ceramic preforms. Temperatures of 200 and 225°C did not result in a successful infiltration. Temperatures of 250 and 270°C resulted in a successful infiltration of PC to the porous ceramic preforms. Temperatures of 300°C resulted in decomposition of PC. No load resulted in no infiltration. Loads of 200 and 400 N resulted in a successful infiltration. Loads of 1000 and 2000 N resulted in the ceramic preform fracture. SEM images are presented here to illustrate the structure of the porous ceramic preform prior to infiltration.

The SEM images in Figure 5-4 confirmed that an applied load of 100 N resulted in improper infiltration. An applied force of 200 N resulted in limited PC infiltration into the porous ceramic preform of less than 4 mm, while an applied load of 400 N resulted in PC infiltration of approximately 4 mm.

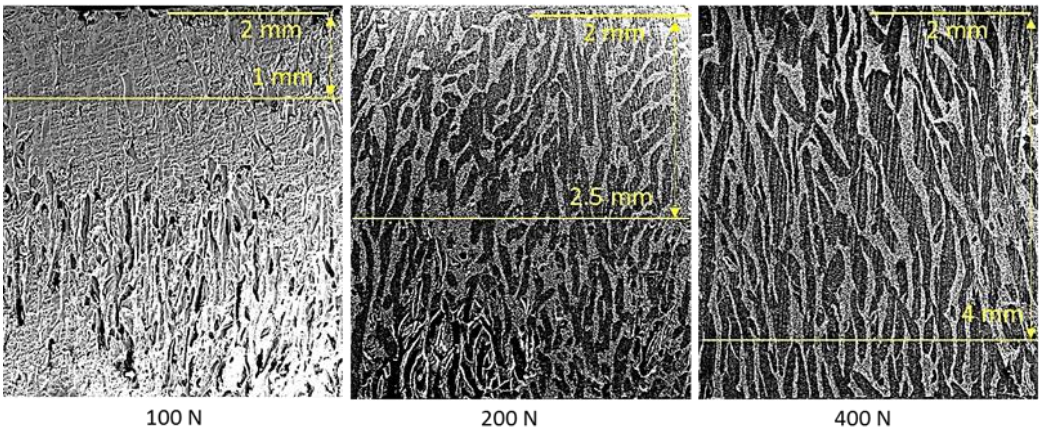

Figure 5-4. SEM images illustrating the effect of different load applications on the infiltration of PC into Al_2O_3-PC specimens. A: 100 N load resulted in less than 1 mm infiltration, B: 200 N load resulted in less than 2.5 mm infiltration, C: 400 N load resulted in 4 mm infiltration.

The SEM images in Figure 5-5 show the porous ceramic preform before and after infiltration with PC. The pores possess a honeycomb-like structure with good polymer infiltration and no closed pores. Different sizes and shapes of pores were successfully infiltrated with PC.

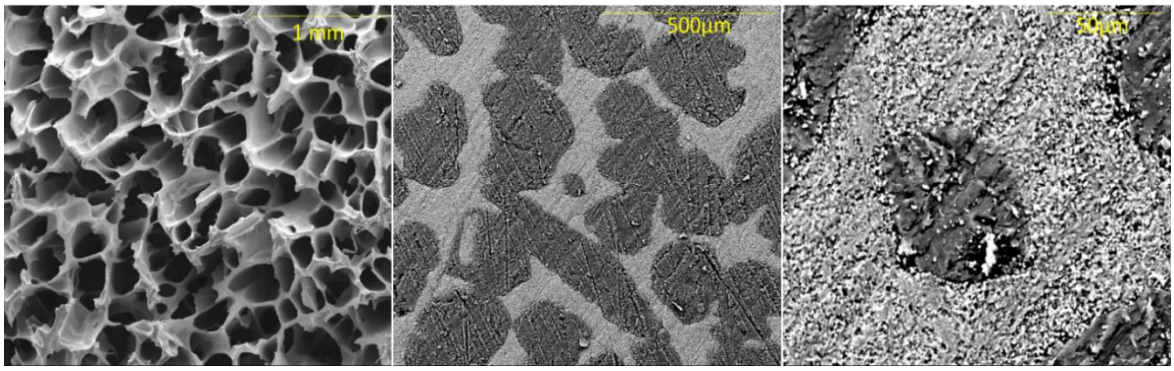

Figure 5-5. SEM images showing the pore structures of the porous ceramic preform before and after the infiltration with PC. A temperature of 250°C and a load of 400 N were used. Initial solid ceramic loading 20 vol.%.

When looking at Figure 5-6 it can be seen that for all three initial solid ceramic loadings 10, 20 and 30 vol.%, PC infiltration was good even though the ceramic microstructures differed. There was also an intimate ceramic/polymer interface in each case.

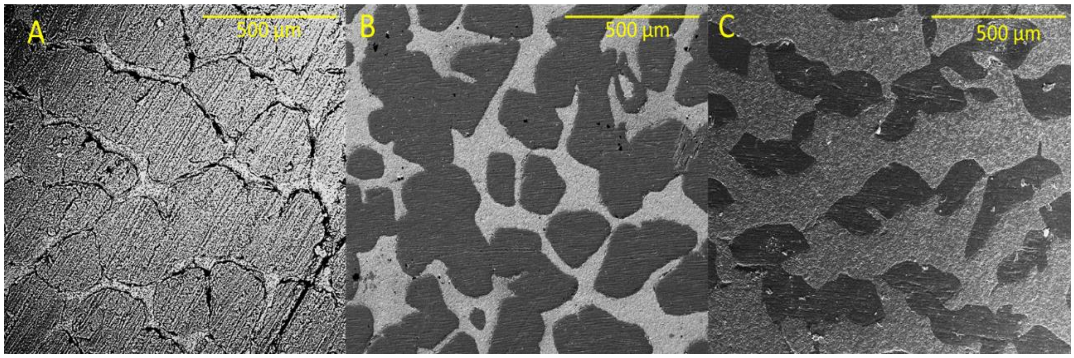

Figure 5-6. SEM images showing Al_2O_3-Pc interpenetrating phase composite infiltrations in porous ceramic preform made from different initial solid ceramic loadings. A. 10 vol.%, B. 20 vol.%, C. 30 vol.%.

However, the sagittal section SEM images in Figure 5-7, which show the specimens sectioned in the direction of the freeze-casting temperature gradient, illustrate how the different initial solid ceramic loadings of the porous ceramic preform affect the degree of PC infiltration. Preforms with an initial solid ceramic loading of 20 vol.% showed a

better PC infiltration of 4 mm into the preform than 30 vol.% solid ceramic loading, which showed a more limited PC infiltration of 3 mm.

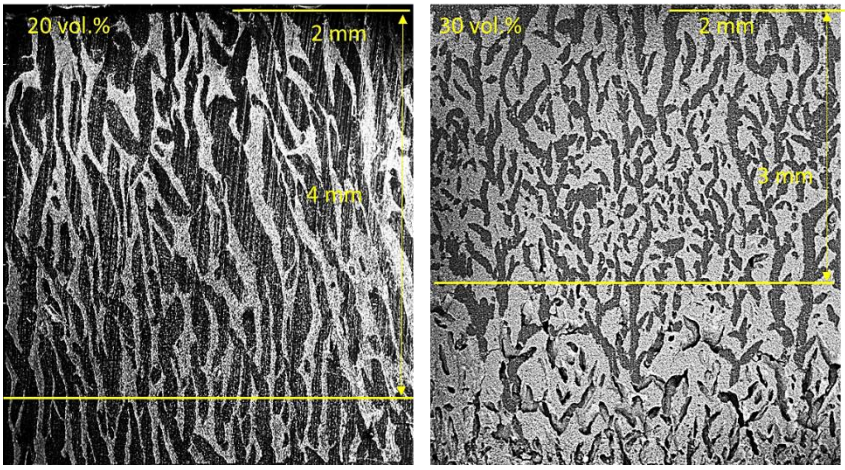

Figure 5-7.SEM images showing the effect of different initial solid ceramic loadings (20 and 30 vol.%) on PC infiltration process. Below the horizontal line are the areas where PC infiltration was less apparent.

5.2.2 Ceramic volume fraction

In this part of the study, the inorganic ceramic fraction of the specimens was measured following polymer burnout from the ceramic/polymer interpenetrating phase composites. The density value for alumina is 3.90 g/cm³, for UDMA-TEGDMA it is 1.15 g/cm³ and for PC it is 1.20 g/cm³. The observed volume fractions for the UDMA-TEGDMA composites in the top, middle and bottom sections of each of the specimens and the PC composites will now be described.

5.2.2.1 Al_2O_3-UDMA-TEGDMA ceramic fraction

Figure 5-8 shows the change in ceramic fraction with initial solid ceramic fraction, and from the top to bottom of the samples with the UDMA-TEGDMA polymer.

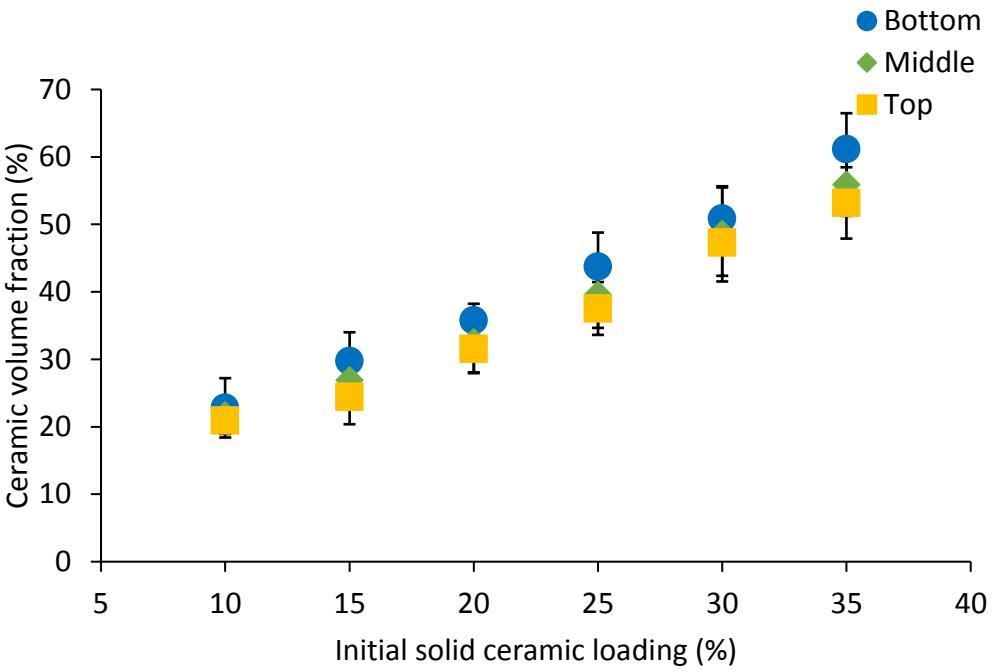

Figure 5-8. Mean and SD of ceramic volume fractions (%) in relation to the different layers and initial solid ceramic loading of the Al_2O_3-UDMA-TEGDMA interpenetrating phase composites.

When the residue left after burn out was measured, there was seen to be a linear relationship between the initial solid ceramic loading and the final ceramic volume fractions, with the overall ceramic fraction increasing with the higher initial solid ceramic loadings. For example, with an initial solid ceramic loading of 30 vol.%, the ceramic fraction was 50.89 vol.%, while an initial solid loading of 20 vol.% resulted in a ceramic fraction of only 35.38 vol.% in the bottom ceramic rich layer. Within each ceramic

loading there was a trend for a greater ceramic fraction at the bottom of the specimen, followed by the middle and then the top of the specimen, indicating a graded structure of the ceramic preforms.

5.2.2.2 Al_2O_3-PC ceramic fraction

For the Al_2O_3-PC composites it was not possible to evaluate the specimens from different levels, as it was only possible to infiltrate initial ceramic preforms to 4 mm in thickness. Figure 5-9 illustrates the effect of a different initial solid ceramic loading on ceramic volume for the Al_2O_3-PC composites. Once again there was a tendency for an increasing ceramic fraction with increasing initial solid loading. A 30 vol.% initial solid ceramic loading resulted in a ceramic fraction of 51.46 vol.% and an initial solid loading of 20 vol.% resulted in a 34.20 vol.% ceramic fraction.

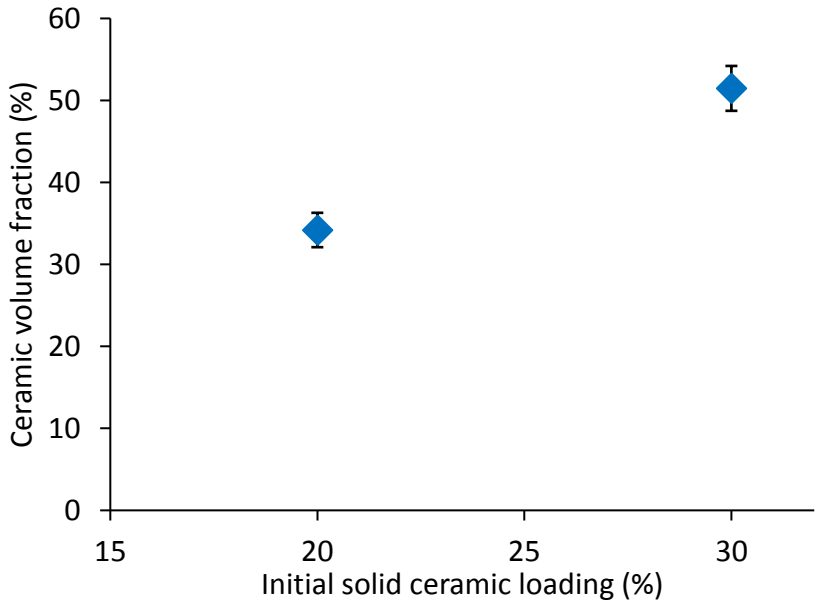

Figure 5-9. Mean and SD of ceramic volume fractions (%) relative to the initial solid ceramic loading of Al_2O_3-PC.

5.2.3 MicroCT analysis

MicroCT imaging was used for further characterisation of the samples and evaluation of the degree and pattern of polymer infiltration.

5.2.3.1 Al_2O_3-UDMA-TEGDMA MicroCT

A full interpenetration of the UDMA-TEGDMA polymer into the porous alumina preform can be seen in Figure 5-10.

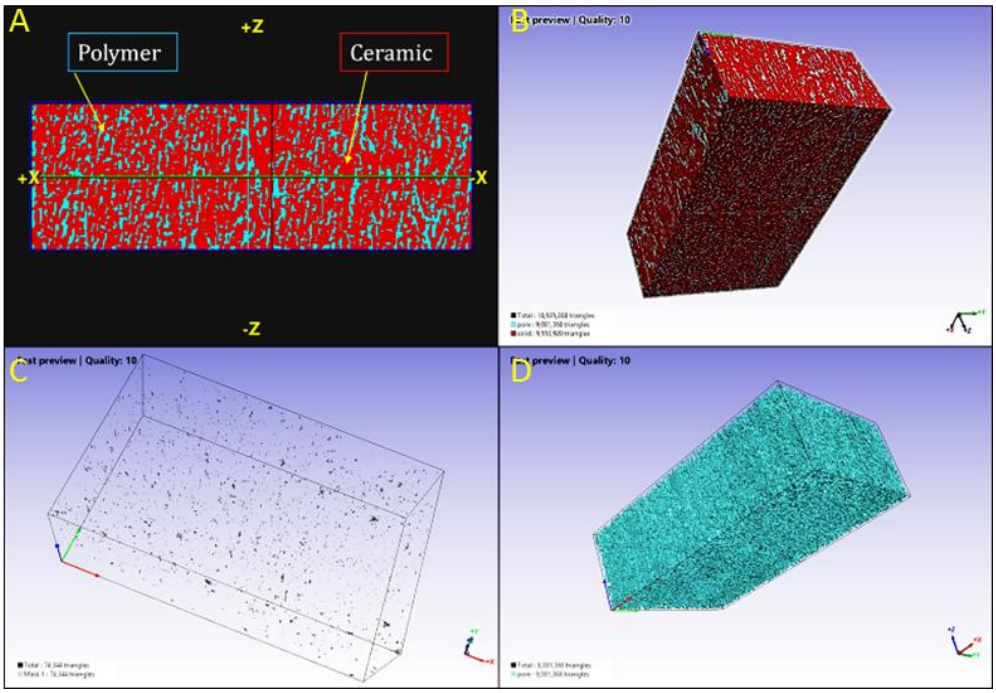

Figure 5-10. 3D MicroCT images of Al_2O_3-UDMA-TEGDMA interpenetrating phase composite produced from initial solid ceramic loading of 30 vol.%. Differences in the colours represent a difference in phase. A: Al_2O_3-UDMA-TEGDMA interpenetrating phase composite material containing 30 vol.% ceramic. Red represents the ceramic phase and green the polymer phase. B: The porous ceramic scaffold (ceramic only phase). C: The polymeric part of the composite (connected pores, polymer only phase) and D: The air part of the composite (closed pores).

By looking at the MicroCT images in Figure 5-10, we can see that the interpenetrating phase composite contains three phases: the ceramic phase, a polymer phase infiltrating the interconnected pores, and finally a lesser air phase representing the closed pores which could not be infiltrated with polymer.

Table 5-1 shows volume fractions as calculated from the MicroCT data. The values obtained from this method were based on the MicroCT identification of the different densities of the ceramic and polymer constituent phases of the interpenetrating phase composite material.

Constituent material	**Volume fraction**
Alumina	56.9%
UDMA-TEGDMA	42.9%
Air	0.2%

Table 5-1. Data representing constituent volume fraction of Al_2O_3-UDMA-TEGDMA interpenetrating phase composite produced from initial solid ceramic loading of 30 vol.% (bottom level).

5.2.3.2 Al_2O_3-PC MicroCT

MicroCT was used to evaluate Al_2O_3-PC composites containing 20 and 30 vol.% initial solid ceramic loadings (Figure 5-11). With PC there was once again good interpenetration into the pores of porous ceramic preform. A lesser third air phase could also be seen, once again probably as a result of air trapped between the ceramic preform and PC during the infiltration process.

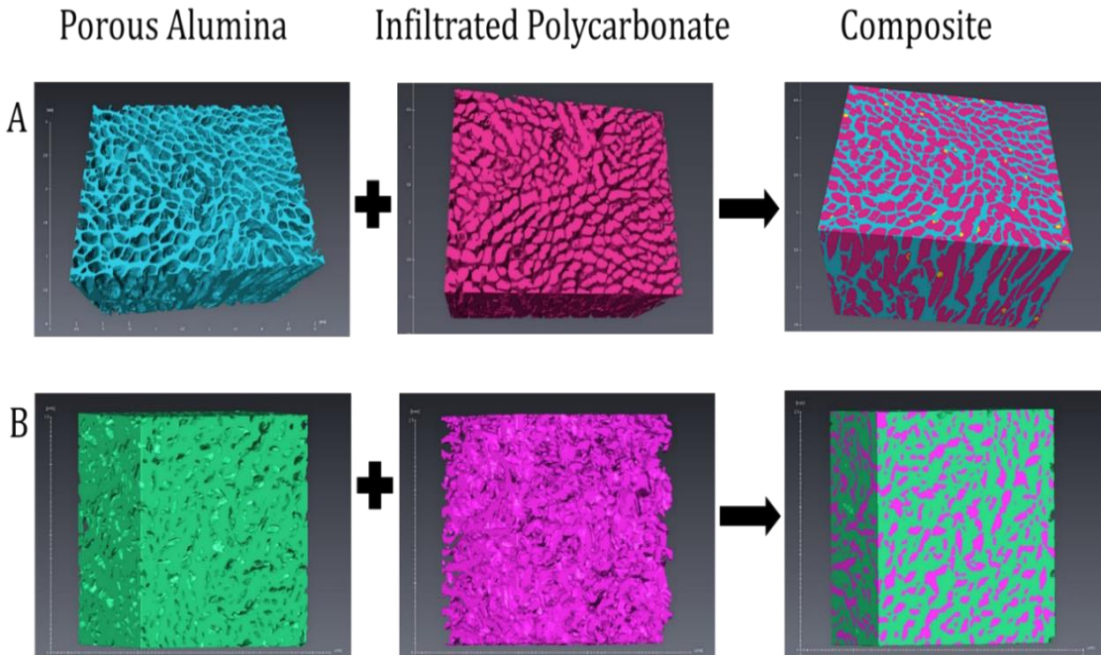

Figure 5-11. 3D MicroCT images of the porous alumina preform, infiltrated polycarbonate phase and the final interpenetrating phase composite material. A: Al_2O_3-PC interpenetrating phase composite material containing 20 vol.% ceramic, blue represents the ceramic phase and pink the polymer. B: Al_2O_3-PC interpenetrating phase composite material containing 30 vol.% ceramic, green represents the ceramic phase and pink represents the polymer phase.

When looking at Figure 5-11, we can see that the increase in the initial solid ceramic loading resulted in a significant change in the microstructure of the interpenetrating ceramic/polymer phase composite material. The pores are bigger and more rounded in shape when the initial solid ceramic loading was 20 vol.% compared with the composites produced with 30 vol.% initial solid ceramic loading.

5.2.4 The graded and anisotropic structure of the interpenetrating phase ceramic/polymer composites

To characterise the anisotropy of the Al_2O_3-UDMA-TEGDMA composites, different layers were cut and prepared from different locations of the specimens. Figure 5-12 illustrates the characteristics of specimens containing initial solid ceramic loadings of 30 vol.%. These specimens were taken from the top, middle and bottom layers of the ceramic/polymer composite.

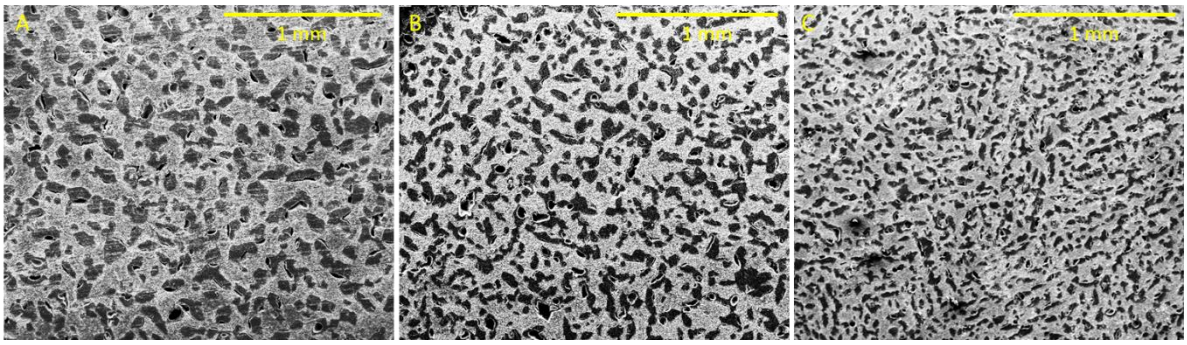

Figure 5-12. SEM images of Al_2O_3-UDMA-TEGDMA interpenetrating phase composite produced from initial solid ceramic loading of 30 vol.%. These images are showing the changes in the polymer distribution in the same specimen when evaluated from the top, A, (polymer rich), middle, B, and bottom, C, (ceramic rich) layers respectively (i.e. images left to right). These images illustrate the unique graded structure of the ceramic/polymer interpenetrating phase composites.

It is clear from the SEM images that the shape of the polymeric structure changes from one layer to another in the direction of freezing, leading to a graded structure. In the top layer the polymer appears to have a larger distribution than in the middle and bottom layers.

MicroCT imaging was also used to evaluate the anisotropic structure of the ceramic/polymer interpenetrating phase composites and they also show the graded porous structure (Figure 5-13).

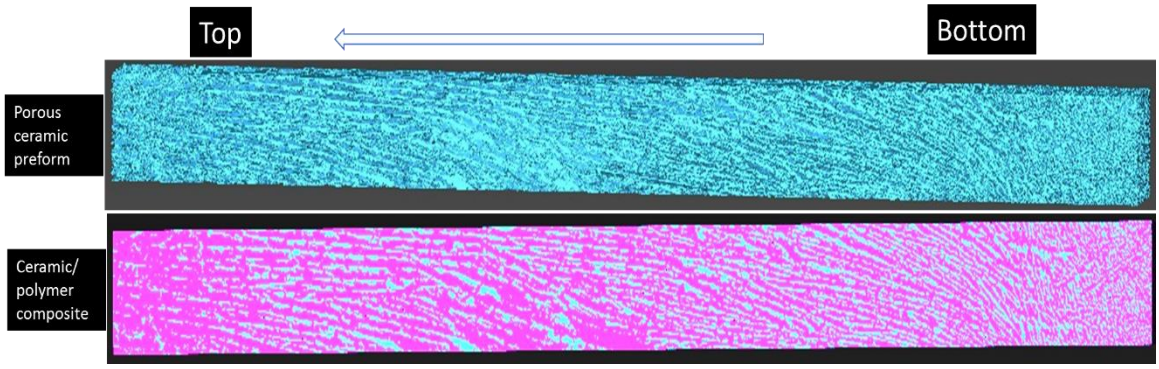

Figure 5-13. 3D MicroCT images of Al_2O_3-UDMA-TEGDMA interpenetrating phase composite obtained from 20 vol.% initial solid ceramic loading (lower picture), and its porous preform (upper picture). These images illustrate the unique anisotropy of the ceramic porous preform and the ceramic/polymer interpenetrating phase composites. Blue represents the ceramic phase and pink the polymer. White arrow indicates the freezing direction.

The anisotropic graded structure can be clearly seen in the porous ceramic preform related to the freezing direction (Figure 5-13) with a polymer rich layer at the top and a ceramic rich layer at the bottom. The interpenetrating phase composite material is again characterised by full interpenetration of the polymer into the pores of the ceramic preform.

5.2.5 Density measurements

5.2.5.1 Al_2O_3-UDMA-TEGDMA interpenetrating phase composite

The mean and SD of the densities of the Al_2O_3-UDMA-TEGDMA interpenetrating phase composite materials plotted against the ceramic volume fraction are illustrated in Figure 5-14.

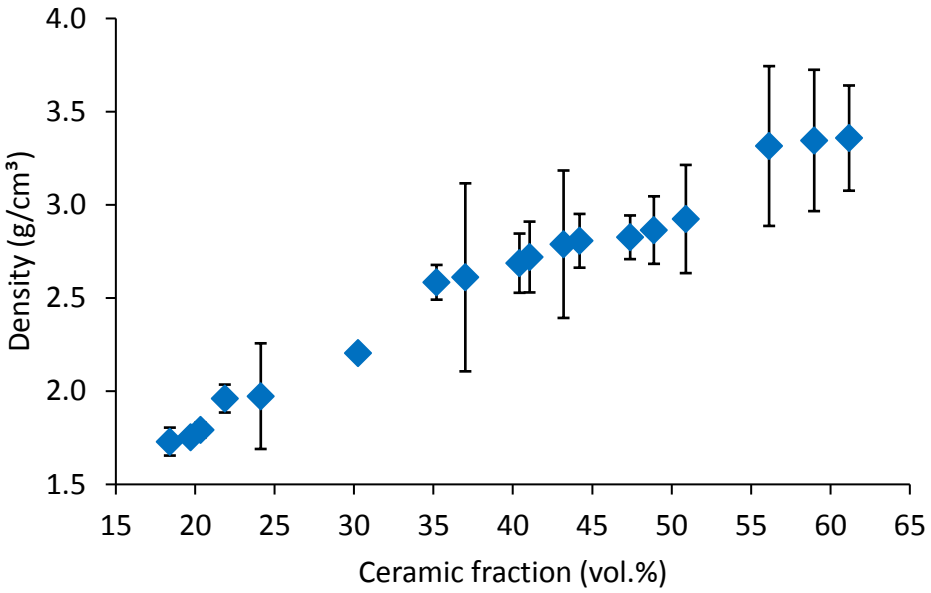

Figure 5-14. Mean and SD for density (g/cm³) of the Al_2O_3-UDMA-TEGDMA interpenetrating phase composites as a function of ceramic fraction (six specimens per group). (Density of alumina 3.90 g/cm³, density of UDMA-TEGDMA 1.15 g/cm³.)

As might be expected, Figure 5-14 shows a clear trend of increasing density with increasing ceramic fraction, and with the densities lying between those of pure alumina and UDMA-TEGDMA.

5.2.5.2 Al_2O_3-PC interpenetrating phase composite

As with the Al_2O_3-UDMA-TEGDMA interpenetrating phase composites, the density of Al_2O_3-PC composite materials increased with increasing ceramic fraction and was again between the densities of pure alumina and PC (Figure 5-15).

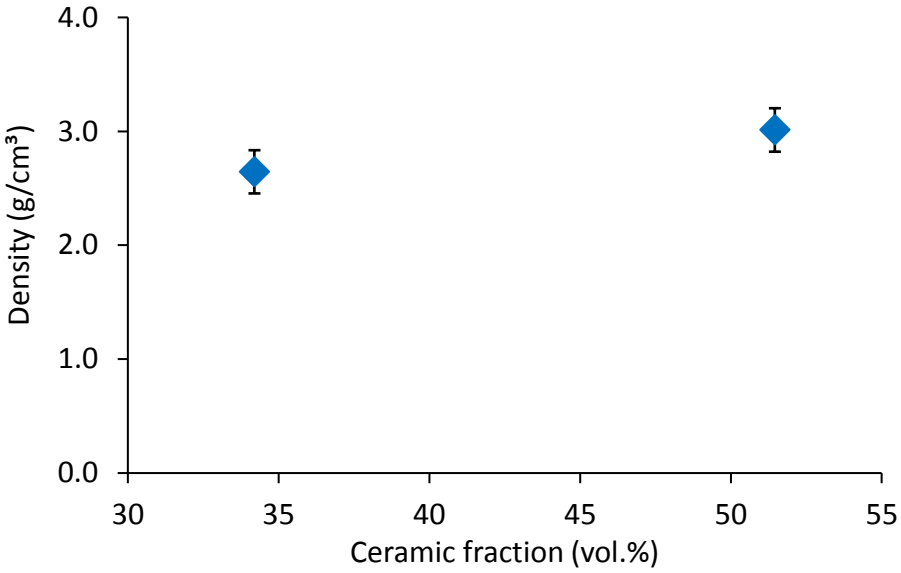

Figure 5-15. Mean and SD for density (g/cm³) of the Al_2O_3-PC interpenetrating phase composites as a function of ceramic fraction (six specimens per group). (Density of alumina 3.90 g/cm³, PC 1.20 g/cm³.)

5.3 Discussion

The mechanical properties of ceramics are very dependent on the presence of imperfections, either within their bulk or at their surface. Generally such imperfections, which might include porosity, are detrimental to properties such as flexural strength and fracture toughness (Guazzato *et al.*, 2004a; Guazzato *et al.*, 2004b). However, in terms of mechanical properties a composite material is often superior to a pure ceramic with

respect to such properties (Albakry *et al.*, 2003; Jongsma *et al.*, 2012). Traditional dental composites have a random arrangement of the inorganic phase within an organic matrix and are therefore unable to mimic the aligned structure of natural tissues such as dentine and enamel. In the present study we have been able to fabricate ceramic/polymer interpenetrating composites that more closely mimic the structure of these natural composites. They comprise not only an interpenetrating network of a polymer matrix within a sintered porous ceramic preform, but also a gradient structure from the top to the bottom of the specimens, with very few air inclusions.

5.3.1 Al_2O_3-UDMA-TEGDMA interpenetrating phase composite

In the production of the Al_2O_3-UDMA-TEGDMA composite used in this experiment, the two monomers were mixed in a 1:1 ratio by weight, before being added to the ceramic preform under vacuum. This ratio was based on the work of Okada et al., (2014). UDMA was chosen as the base polymer for a number of reasons. It was first introduced in 1974 as the base polymer for resin composites (Foster and Walker, 1974) and has since been widely used in dentistry. The absence of a phenol ring in the monomer chain leads to higher flexibility and improved toughness (Asmussen and Peutzfeldt, 1990; Asmussen and Peutzfeldt, 1998; Gajewski *et al.*, 2012) compared with Bis-GMA, another popular dental polymer. In addition, the lower molecular weight of UDMA (470 g/mol compared with 512 g/mol for Bis-GMA) makes infiltration into the ceramic preform easier (Gajewski *et al.*, 2012). It also shows less water absorption, a higher modulus of elasticity and increased flexural strength when compared to Bis-GMA (Gajewski *et al.*, 2012; Braden and Davy, 1986).

The main drawback of using UDMA as a base monomer is that it still has a high viscosity and multiple functional groups. It is for this reason that it is commonly combined with a less viscous monomer such as TEGDMA (Reed *et al.*, 1997; Ferracane, 1995). The disadvantage of the use of TEGDMA as a diluent monomer is that it leads to increased polymerisation shrinkage (Yap *et al.*, 2000). At the very beginning of the current study we followed the protocol of Okada *et al.* (2014), and the UDMA-TEGDMA was polymerised at a temperature of 120°C for 2 hrs. However, this led to the formation of cracks and bubbles within the polymer matrix. As a result we used a different heat cycle, following the work of Chaiyabutr *et al.* (2009) and modified by the author. This was achieved by curing initially at 50°C for 1 hr, followed by 60°C for 1 hr, 70°C for 1 hr, 80°C for 1 hr and finally 90°C for 12 hrs, to allow complete polymerisation with fewer cracks and bubbles.

SEM has been used previously to examine the microstructure of experimental dental interpenetrating phase composites (Coldea *et al.*, 2013; Della Bona *et al.*, 2014; Nguyen *et al.*, 2012). In the present study, SEM was used to evaluate the effect of the volume of ceramic in the initial solid loadings on the degree of porosity, along with any changes in the morphology of the pores themselves in the ceramic frameworks (Figure 5-2).

The SEM images show the presence of a small proportion of empty pores within the composite materials. The reasons for this might include: the hydrophobic nature of alumina, incomplete wetting of the ceramic walls by the silane coupling agent, the presence of closed pores and problems with the infiltration process itself, such as an incomplete vacuum, insufficient pressure or the incorrect temperature.

5.3.2 Al_2O_3-PC interpenetrating phase composite

Polycarbonate has been widely used to construct orthodontic brackets due to good aesthetics, biocompatibility and reasonably good mechanical properties (Freilich *et al.*, 1998; Russell, 2005). In terms of aesthetics the internal transmission of light in polycarbonate is almost the same as that of glass (Moretti *et al.*, 2017). However, the problem with pure polycarbonate brackets is the low abrasion resistance of the material and a tendency to creep under applied load (Feldner *et al.*, 1994; Ali *et al.*, 2011).

In this part of the study, in order to produce an Al_2O_3-PC interpenetrating phase composite, the PC was heat-pressed into the porous ceramic preforms. Polycarbonate is an amorphous thermoplastic, with a glass transition temperature of approximately 147°C, above which it softens until it begins to flow at approximately 155°C (Strabala, 2009). At this point it can be moulded and so can be infiltrated into a second phase to form a composite. This infiltration process can be affected by a number of parameters including the porosity and the thermal conductivity of the second phase, and the heat and load applied during processing. An incorrect combination of these parameters may result in incomplete infiltration.

The process of *in situ* infiltration of PC into a porous ceramic preform utilised in this study has not been reported elsewhere in literature, and as a result the parameters necessary for successful infiltration had to be investigated. One such parameter was the temperature for PC infiltration. Although the advice from the manufacturer of the PC was that it would begin to flow at a temperature of 150°C and above, it can be seen in

Figure 5-3 that it was necessary to experiment with temperatures of 200°C, 225°C, 250°C, 270°C and 300°C. At temperatures of less than 250°C no infiltration of the PC into the ceramic phase took place. At 250°C and 270°C, flow of the PC into the ceramic was effective. At a temperature above 300°C the PC underwent decomposition. For this reason, subsequent experiments used a temperature of 250°C.

The second important parameter for successful infiltration was the applied load. Initially in the present study, a dye machine was tested as a means of applying sufficient force for infiltration. Unfortunately, the force applied, as well as the heat control, was poorly suited to the purpose, as the machine was made to apply much higher forces for pharmaceutical applications. In addition, the heating device added to the machine used an external temperature controller, which resulted in poorly controlled heat distribution across the dye machine. The minimum load applied by the dye machine resulted in cracks and fracture lines within the ceramic preform (Figure 5-3).

As a result, the infiltration procedures were instead performed in an oven, with the ceramic and PC sitting in a mould, on top of which was a stainless-steel weight applying a maximum force of 400 N. This allowed for improved control of both heat and pressure, which was easily reproducible and resulted in infiltration of the polymer into the ceramic preform up to a depth of 5 mm, as can be seen in Figure 5-4. A disadvantage of this technique was the difficulty in manipulating both the weights and specimens at such high temperatures within the oven.

In this study, we were only able to infiltrate the PC to a depth of approximately 4 mm into the porous ceramic preforms. This was probably due to the viscous nature of PC (Senden *et al.*, 2012) and the inadequacy of the infiltration equipment and procedures used in this study. The high melting temperature and viscosity of PC makes fabricating composites difficult (Wang *et al.*, 2007). A higher load applied during the infiltration process might have been more effective, but no such equipment was available to us.

Porous ceramic preforms with different initial solid ceramic loadings of 10, 20 and 30 vol.% were infiltrated with PC in this study. Initially, when looking at the SEM images in Figures 5-5 and 5-6, the infiltration process of the PC into the ceramic frameworks was effective and appeared unaffected by the initial solid ceramic loadings. This was not the case when the specimens were studied in the direction of freeze-casting. It can be seen in Figure 5-7 that a deeper PC infiltration occurred where the initial solid loading of ceramic was less, and therefore the pore structure was larger. Therefore, penetration was deeper in the case of the 20 vol.% initial solid loading when compared with the 30% vol (Figure 5-7). However, where the initial ceramic solid loading was only 10 vol.%, the ceramic preform had a tendency to fracture during the infiltration process.

5.3.3 Ceramic volume fraction of the interpenetrating phase composite

The initial solid ceramic loading in the aqueous suspensions governed the overall volume of the ceramic in the resultant interpenetrating phase composite materials. The higher the initial solid loading, the higher the overall ceramic volume, as can be seen in Figures 5-8 and 5-9. To evaluate exclusively the volume fraction of ceramic in the

interpenetrating phase composite material, it was necessary to burn out the polymer phase. This was completed in an oven by heating to 600°C at a very slow rate of 2°C/min. The method has previously been shown to lead to complete degradation of both UDMA-TEGDMA and PC polymer contents, but with no significant effect on the ceramic content (Petrini *et al.*, 2013; McNeill and Rincon, 1993; Santana *et al.*, 2011).

Previously it has been shown that when the initial solid ceramic loading of the aqueous suspension increases, the porosity in the final porous ceramic preform decreases (Fukasawa *et al.*, 2001b; Sofie and Dogan, 2001; Deville *et al.*, 2007)**.** This reduction in porosity explains the reduction in the polymer volume in the interpenetrating phase composite with higher initial solid loading. Moreover, a higher solid ceramic loading in the suspension means a lower water content, resulting in smaller ice crystal formation, smaller pores with thicker ceramic walls and therefore an overall higher ceramic fraction.

5.3.4 MicroCT analysis of the interpenetrating phase composites

In order to fabricate a material that is inspired by nature, material architecture is of considerable importance, as this will be directly linked to its ultimate performance and mechanical properties (Hollister, 2005). The aim of using MicroCT in the present study is to characterise the structure of the ceramic/polymer interpenetrating phase composites. MicroCT has been previously used to investigate porous structures produced using freeze-casting (Cheng *et al.*, 2016; Lee *et al.*, 2017; Zhang *et al.*, 2017), as well as to examine orthodontic bracket materials (Öztürk *et al.*, 2015).

The MicroCT images (Figures 5-10), just like the SEM images, illustrate how the porous ceramic preforms comprised a 3D honeycomb-like porous structure, consisting of three distinct phases. In each case almost complete interpenetration of the polymeric matrix into the ceramic phase could be seen. Within the ceramic phase, the polymer phase occupies the space created by the original ice crystals produced during freeze-casting. The third, lesser phase seen in the image was entrapped air. This air, although comprising less than 2 vol.% of the composite, may well represent an area of weakness. Such air inclusions may well be due to air bubbles trapped during the polymerisation process, or they maybe as a result of closed pores within the porous ceramic preform. In the case of the latter, back pressure would prevent full penetration of the polymer. Although unwanted, even within more traditional interpenetrating phase composites used as dental restorations, the formation of some areas of void or air inclusion is almost inevitable (De Santis *et al.*, 2005). Table 5-1 shows the volume fraction of ceramic and polymer in the specimen based on the data provided by MicroCT (56.90 vol.% ceramic fraction). These results are slightly different from the physical values obtained by burning the polymeric phase (50.89 vol.% ceramic fraction). This can be attributed to the fact that MicroCT is a sensitive technique that depends on differences in material densities (McCollough *et al.*, 2015). Moreover, individual scanning parameters and the image reconstruction can influence quantitative results.

When looking at Figure 5-12, we can see that interpenetrating phase composite material produced from an initial solid ceramic loading of 20 vol.% was characterised by larger pores (originally ice crystals), when compared to interpenetrating phase composite

material produced from initial solid ceramic loading of 30 vol.%. This illustrates the effect of increasing initial solid ceramic loading in the aqueous suspension on the final structure of the ceramic preform in the novel interpenetrating phase composite.

5.3.5 The graded and anisotropic structure of the interpenetrating phase composite

It was anticipated that the microstructural properties, as well as the ceramic volume fractions, would differ according to distance from the initial freezing front and therefore the temperature gradient created within the freeze-casting apparatus. In order to test this, the material was tested at three levels with respect to the freezing direction, namely the bottom level (ceramic rich layer near the cooling plate), the middle level immediately above this bottom level, and the top layer (polymer rich layer). Measurements of mechanical and surface properties were made in order to determine which might be the best potential material for future clinical use. For example, a bracket that is characterised by a ceramic rich outer layer might help with the aesthetic properties and abrasion resistance, while a relatively low hardness polymer rich inner phase might aid bonding and also safer debonding.

A layer of 3 mm was removed from the base of the specimens prior to any preparation as this layer contained closed pores and random ceramic particle distribution with poor mechanical properties, as demonstrated by previous researchers (Petrini *et al.*, 2013; Deville *et al.*, 2007). The ceramic volume fractions of the remainder of the specimen in each case were higher at the bottom layer when compared to the middle and the top

layers. This might be explained by the presence of larger pores when moving away from the cooling plate and with a cooling temperature difference of -10°C to 20°C (Figure 5-13). Deville *et al.*, (2006a) reported such changes in freeze-cast porous ceramic structures. These changes could be attributed to differences in the solid ceramic loadings within the suspensions of the ceramic particles and the changing morphology of the growing ice crystals.

Moreover, a previous study by Petrini et al., (2013) confirmed the anisotropy of freeze-cast porous alumina preforms infiltrated with epoxy resin. Their results showed differing mechanical properties of specimens from two different levels with respect to the freezing direction. It is worth noting that the freeze-casting technique presented here creates a gradient from a denser to a more porous ceramic. By altering the processing parameters, it is possible to control the porosity and pore size within the preform, as can be seen from the MicroCT 3D images in Figure 5-14.

5.3.6 Effect of the interpenetrating phase composite characteristics on density

The density values of composite materials are usually closely related to their mechanical properties (Coldea *et al.*, 2013). The mean values of the density of the ceramic/polymer interpenetrating composites reported in the present study ranged from 1.79 to 3.36 g/cm³. When looking at these density values, we can see they range between those of the dense alumina and the pure polymers. The results obtained demonstrated an increase in the density of all interpenetrating phase composite materials with increasing

ceramic volume fractions, as might be expected, and as can be seen in Figures 5-15 and 5-16.

Coldea *et al.* (2013) reported the density of experimental polymer-infiltrated-ceramic networks ranged from 1.45 to 1.76 g/cm³, which is lower than the density reported in the present study. This may be due to the fact that they used feldspar ceramic as their primary ceramic preform with a density of 2.44 g/cm³, which is much lower than that of alumina (3.90 g/cm³). In addition, the density values of the interpenetrating phase composites in the present study were higher than the mean density value reported for VITA Enamic® (2.1 g/cm³) (Della Bona *et al.*, 2014), slightly lower than that of dentine (2.96 to 3.02 g/cm³) and comparable to that of enamel (1.96 to 2.4 g/cm³) (Lin *et al.*, 2010; Bajaj *et al.*, 2008). When comparing the density values of the Al_2O_3-UDMA-TEGDMA composites with those of the Al_2O_3-PC, there was little difference. This may be due to the fact that the density value of the pure PC (1.20 g/cm³) was similar to that of pure UDMA-TEGDMA (1.15 g/cm³), and that the biggest determinant of the density of the final composite was the ceramic fraction.

5.4 Summary

In the present study, ceramic/polymer interpenetrating phase composites with a unique graded structure have been developed, taking inspiration from natural materials. In the previous Chapters, it has been shown how a gradient structure can be created within the ceramic preform. It has also been shown that it is possible to infiltrate the preform with either UDMA-TEGDMA or PC. In the case of Al_2O_3-UDMA-TEGDMA, interpenetrating phase composites were fabricated by heating in the presence of a vacuum. This permitted infiltration of the ceramic preforms by the polymer, creating intimate contact at the interface of the two materials and with very few air inclusions, as shown by SEM and MicroCT. However, in the case of Al_2O_3-PC it was necessary to use a heavy weight in the presence of heat to achieve the same degree of polymer infiltration. Increasing the initial solid ceramic loading in the aqueous suspensions resulted in the production of interpenetrating phase composites with higher ceramic volume fractions, smaller pores and thicker pore walls. The densities followed a linear relationship with respect to the ceramic volume fraction, with higher ceramic volumes resulting in increased densities. The composites produced were characterised by a gradient structure. This unique structure could have potential in fabricating orthodontic brackets, with the ceramic rich layer exposed to the oral cavity able to resist wear and provide aesthetics, and the polymer rich layer in contact with the tooth able to facilitate easier bonding and safer debonding.

Chapter 6. Mechanical characterisation of ceramic/polymer interpenetrating phase composites

6.1 Introduction

Ideal dental materials should mimic tooth structure and its mechanical properties. An orthodontic bracket material that is strong enough to withstand and transfer the applied loads during orthodontic treatment and is aesthetically acceptable is desirable. The commercially available polymeric brackets have the disadvantages of slot deformation and creep during archwire ligation or tooth movements due to low strength properties (Dobrin *et al*., 1975, Russell, 2005, Faltermeier *et al*., 2007a, Nishio *et al*., 2009, Möller *et al*., 2009). Moreover, the major drawbacks of ceramic brackets are their low fracture toughness and brittleness leading to occasional fracture (Birnie, 1990, Jena *et al*., 2007).

In restorative dentistry, composites are widely used due to a combination of relatively good mechanical properties and good aesthetics. Since their introduction many efforts have been made to tailor their performance to clinical need (Ferracane, 2005). The mechanical properties of experimental polymer-infiltrated-ceramic-network materials, introduced for dental restorative applications, have previously been reported (He and Swain, 2011; Coldea *et al.*, 2013; Nguyen *et al.*, 2014; Okada *et al.*, 2014; Petrini *et al.*, 2013).

The aim of the present study is to produce a novel composite material, composed of porous alumina scaffold infiltrated with either UDMA-TEGDMA or PC polymers, that mimics the structure of teeth and that could be used as an aesthetic orthodontic bracket material. It is hoped such a material would have enhanced mechanical properties compared to conventional aesthetic orthodontic bracket materials.

In previous Chapters the fabrication and structure of two novel ceramic/polymer interpenetrating phase composites have been described. In this Chapter the results of mechanical testing to failure, both qualitative, describing the path of the crack propagation during fracture, and also quantitative, describing the effects of the ceramic volume fraction on the compressive and flexural strengths, modulus of elasticity and fracture toughness, will be described. The final volume fraction of the ceramic in the ceramic/polymer interpenetrating composites will be described here instead of the initial solid ceramic loading previously used in Chapters 3, 4 and 5.

6.2 Results

6.2.1 Compressive strength

Al_2O_3-UDMA-TEGDMA interpenetrating phase composites with different ceramic fractions, along with dense alumina and pure UDMA-TEGDMA blocks, were subjected to compression testing in a universal testing machine. The compression force was directed along the long axis of the specimens and parallel to the direction of the freeze-casting. The compressive strength measurements were plotted versus the ceramic volume fraction (Figure 6-1).

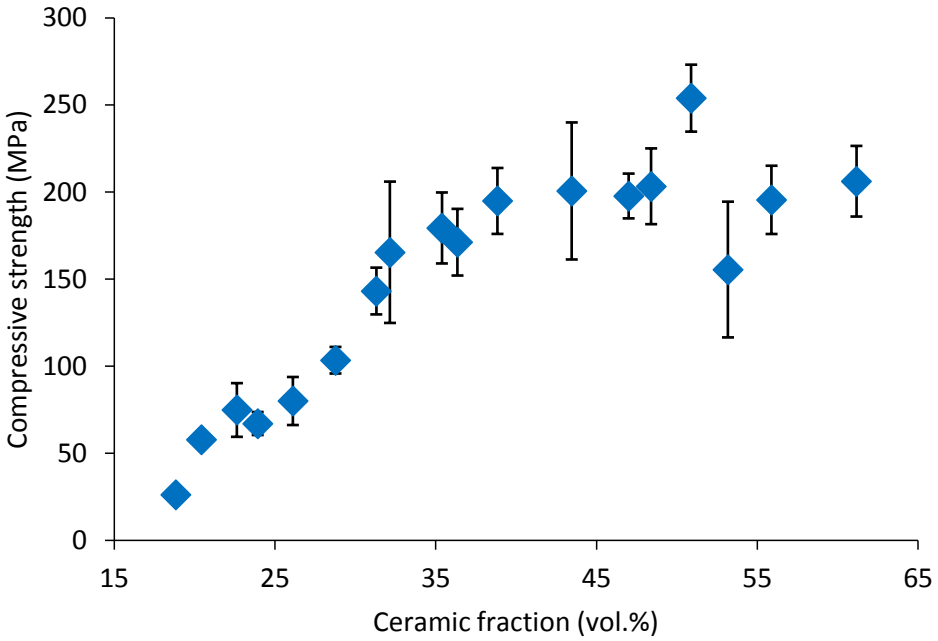

Figure 6-1. Means and SD for compressive strength (MPa) of the Al_2O_3-UDMA-TEGDMA interpenetrating phase composites in relation to the ceramic volume fractions (six specimens per material). The force was applied parallel to the freezing direction. The mean compressive strength of Al_2O_3 was 2358.08 ± 640.56 MPa, and for UDMA-TEGDMA was 129.95 ± 10.86 MPa.

When looking at the compressive strengths (MPa), we can see there is an increase with increasing ceramic fraction from 15 to 52 vol.%. However, above 52 vol.% ceramic fraction the compressive strength declined. The Al_2O_3-UDMA-TEGDMA interpenetrating phase composites containing 50.89 vol.% ceramic fraction showed the highest compressive strength when compared to the other composite materials.

For the Al_2O_3-PC interpenetrating phase composites, the compressive strength was evaluated only for composites containing 34.20 and 51.46 vol.% ceramic fraction. Once again compressive strength increased with increasing ceramic fraction (vol.%) as can be seen in Figure 6-2.

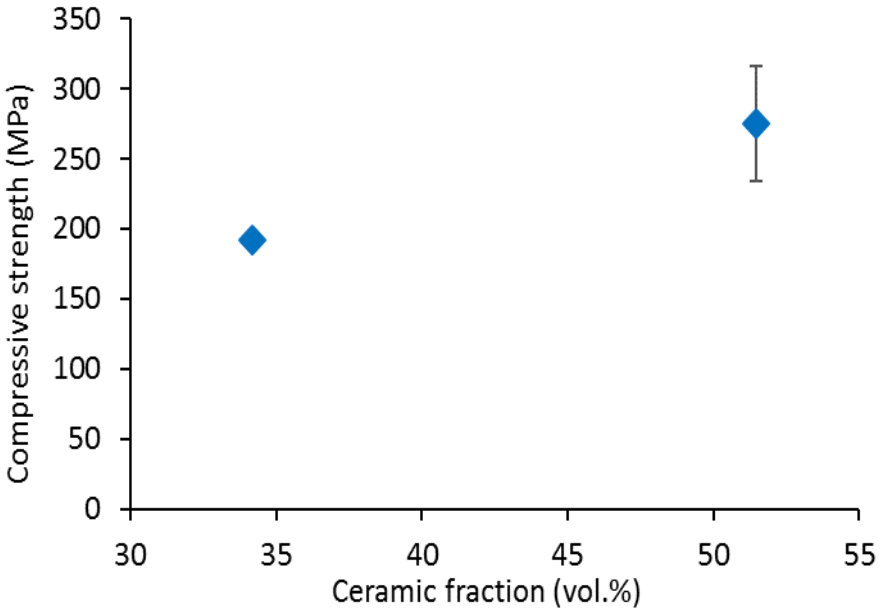

Figure 6-2 Means and SD for compressive strength (MPa) of Al_2O_3-PC interpenetrating phase composites in relation to the ceramic volume fractions. The force was applied parallel to the freezing direction. The mean compressive strength of Al_2O_3 was 2358.08 ± 640.56 MPa and for PC was 131.40 ± 11.21 MPa.

When comparing the mean compressive strength of 35.38 vol.% ceramic fraction Al_2O_3-UDMA-TEGDMA composite (179.42 MPa) with that of 34.20 vol.% ceramic Al_2O_3-PC composite (192.43 MPa), we can see Al_2O_3-PC was slightly higher than that of Al_2O_3-UDMA-TEGDMA. The same was true for 50.89 vol.% ceramic fraction Al_2O_3-UDMA-TEGDMA composite (253.97 MPa) and 51.46 vol.% ceramic Al_2O_3-PC composite (274.91

MPa. Pure UDMA-TEGDMA and PC had compressive strength values of 129.95 and 131.40 MPa respectively, which was higher than that of composite materials containing less than 30 vol.% ceramic fraction.

Although compressive strengths increased with increasing ceramic fraction, this relationship is complex. Below 30 vol.% ceramic fraction, the compressive strength is less than that of the pure polymers, while above 50 vol.% ceramic fraction, this positive correlation with ceramic fraction plateaus and may even fall. Although dense alumina showed mean compressive strength values of 2358.08 MPa, which was much higher that of the composite materials under test, when failure occurred it was sudden and catastrophic, unlike the composite materials where crack propagation was much more gradual before eventual failure.

6.2.2 Flexural strength

The flexural strength of each composite material was again investigated in relation to the ceramic volume fraction. Specimens were subjected to three-point bend tests and Figure 6-3 summarises the mean and SD (MPa) of flexural strength for Al_2O_3-UDMA-TEGDMA when the load was directed parallel to the freezing direction.

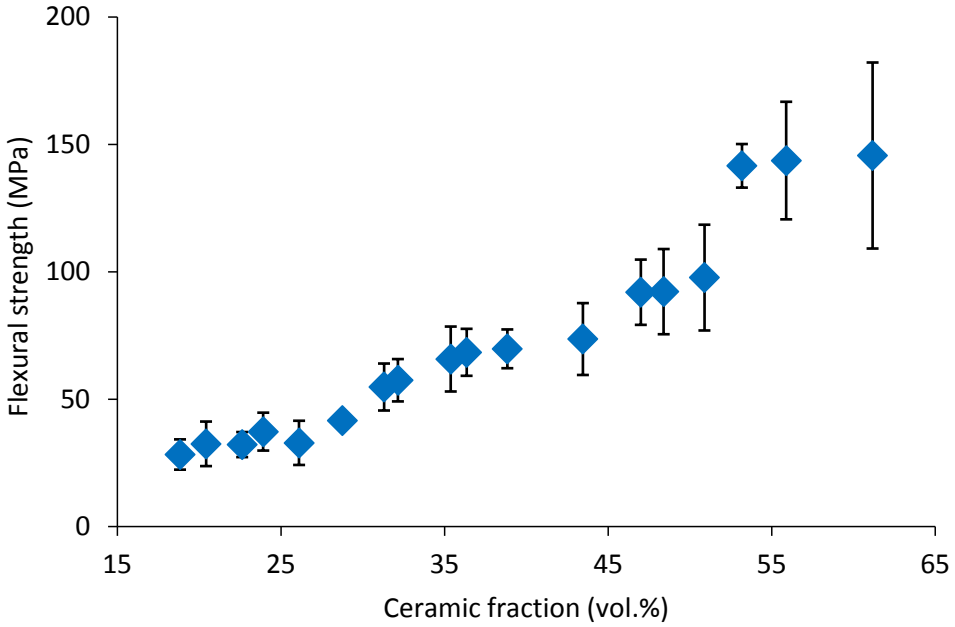

Figure 6-3. Means and SD for flexural strength (MPa) of the Al_2O_3-UDMA-TEGDMA interpenetrating phase composites in relation to the ceramic volume fraction (six specimens per material). The force was applied parallel to the freezing direction. The mean flexural strength of Al_2O_3 was 249.30 ± 72.15 MPa and for UDMA-TEGDMA was 111.91 ± 26.21 MPa.

The means and SD for flexural strength of the Al_2O_3-PC interpenetrating phase composite are presented in Table 6-1.

Ceramic fraction (vol.%)	Flexural strength	SD
34.20	192.43	5.97
51.46	274.91	41.05

Table 6-1. Means and SD for flexural strength (MPa) of the Al_2O_3-PC interpenetrating phase composites in relation to the ceramic volume fractions. The force was applied parallel to the freezing direction. The mean flexural strength of Al_2O_3 was 249.30 ± 72.15 MPa and of PC was 122.49 ± 5.73 MPa.

It is clear from Figures 6-3 and Table 6-1 that there is a difference in the flexural strength between different materials, with a clear trend for the flexural strength to increase with increasing ceramic volume fraction. Moreover, pure polymer specimens showed flexural strength values higher than those for composite materials with less than 30 vol.% ceramic fraction.

6.2.3 Modulus of elasticity

Modulus of elasticity was determined from the three-point bend tests. Figure 6-4 illustrates the modulus of elasticity of the of Al_2O_3-UDMA-TEGDMA interpenetrating phase composites with different ceramic fractions.

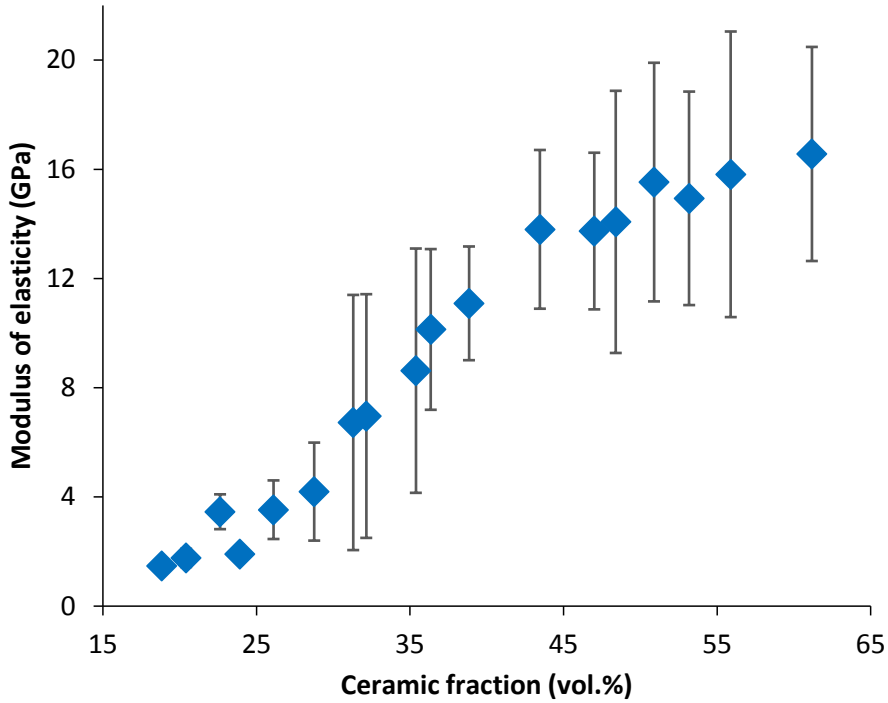

Figure 6-4. Means and SD for modulus of elasticity (GPa) of the Al_2O_3-UDMA-TEGDMA interpenetrating phase composites in relation to the ceramic volume fractions (six specimens per material). The force was applied parallel to the freezing direction. The mean modulus of elasticity value of Al_2O_3 was 118.50 ± 17.14 GPa and of UDMA-TEGDMA was 1.17 ± 0.01 GPa.

When looking at the modulus of elasticity of Al_2O_3-UDMA-TEGDMA composites (Figure 6-4) we can see that the modulus increases with increasing ceramic volume fraction, ranging from 1.48 to 16.56 GPa.

For the Al_2O_3-PC interpenetrating phase composite, again the modulus of elasticity increased from 0.72 to 15.17 GPa, with an increase in the ceramic fraction from 34.20 to 51.46 vol.% as can be seen in Figure 6-5.

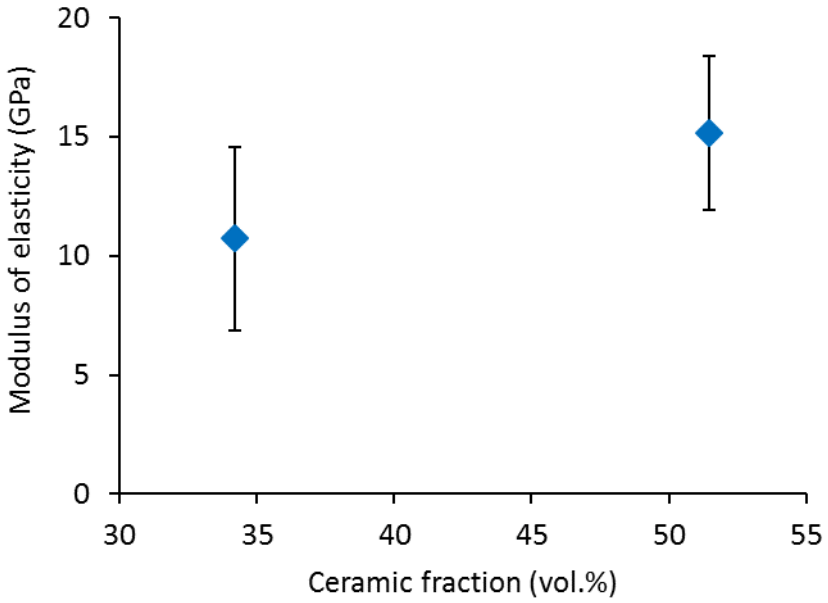

Figure 6-5. Means and SD for the modulus of elasticity (GPa) of the Al_2O_3-PC interpenetrating phase composites in relation to the ceramic volume fractions. The force was applied parallel to the freezing direction. The mean modulus of elasticity of Al_2O_3 was 118.50 ± 17.14 MPa and of PC was 1.50 ± 0.37 MPa.

6.2.4 Mechanical characterisation under different test conditions

When materials produced by freeze-casting are investigated, it is very important to test the materials with respect to their anisotropic characteristics. In other words, they should be tested both parallel and perpendicular to the direction of freeze-casting. For the Al_2O_3-UDMA-TEGDMA composite materials three-point bend tests were performed. For the Al_2O_3-PC composites compression testing was used due to the limited dimensions of the specimens produced with this polymer.

6.2.4.1 Al2O3-UDMA-TEGDMA interpenetrating phase composites

The flexural strength of each Al_2O_3-UDMA-TEGDMA composite was compared in two directions, namely parallel and perpendicular to the direction of freeze-casting, and with respect to the ceramic scaffold fraction by volume, as can be seen in Figure 6-6. When looking at Figure 6-6, we can see there was a slight increase in flexural strength when specimens were tested perpendicular to the direction of freeze-casting, compared to those tested parallel to this direction. This was the case for all specimens except for the 61.17 vol.% ceramic fraction. There was also a clear trend of increasing flexural strength with increasing ceramic volume fraction in both directions.

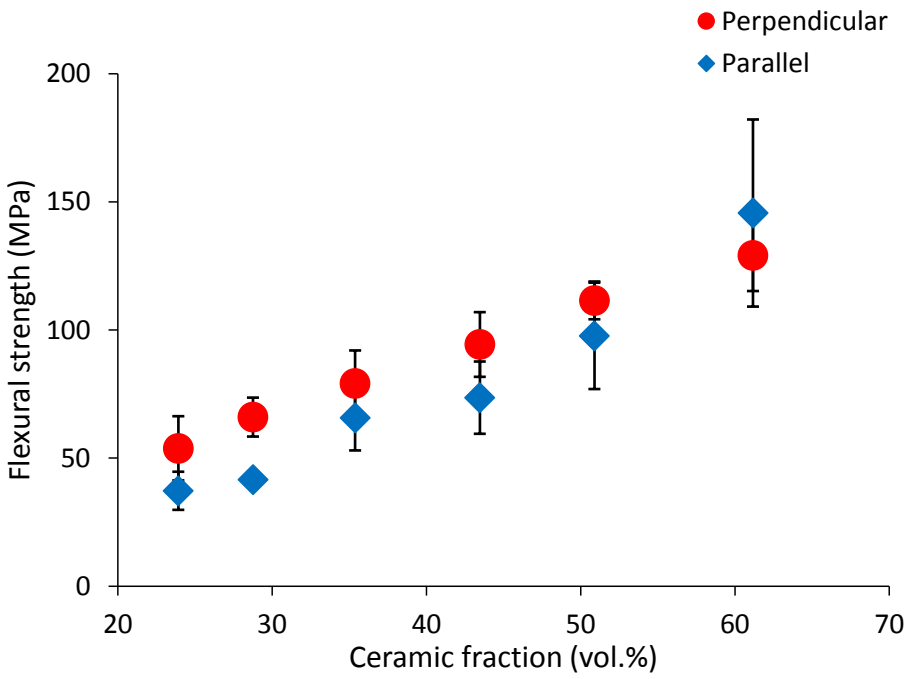

Figure 6-6. Means and SD for flexural strength (MPa) of the Al_2O_3-UDMA-TEGDMA interpenetrating phase composites in relation to the ceramic volume fractions. The three-point bend force was applied in 2 planes: parallel (Blue) and perpendicular (Red) to the freezing direction.

6.2.4.2 Al_2O_3-PC interpenetrating phase composites

When looking at the compressive strength with respect to the anisotropy of the material, we can see that with the Al_2O_3-PC interpenetrating phase composites there was again a slight increase in compressive strength when tested perpendicular to the direction of freeze-casting, as opposed to parallel to the direction of freeze-casting.

For the Al_2O_3-PC interpenetrating phase composites containing 51.46 vol.% ceramic fraction, there was a slight increase in strength from 274.91 to 285.15 MPa when the testing direction changed from parallel to perpendicular. For the Al_2O_3-PC interpenetrating phase composites containing 34.20 vol.%, the increase was from 192.43 to 198.26 MPa, as can be seen in Figure 6-7.

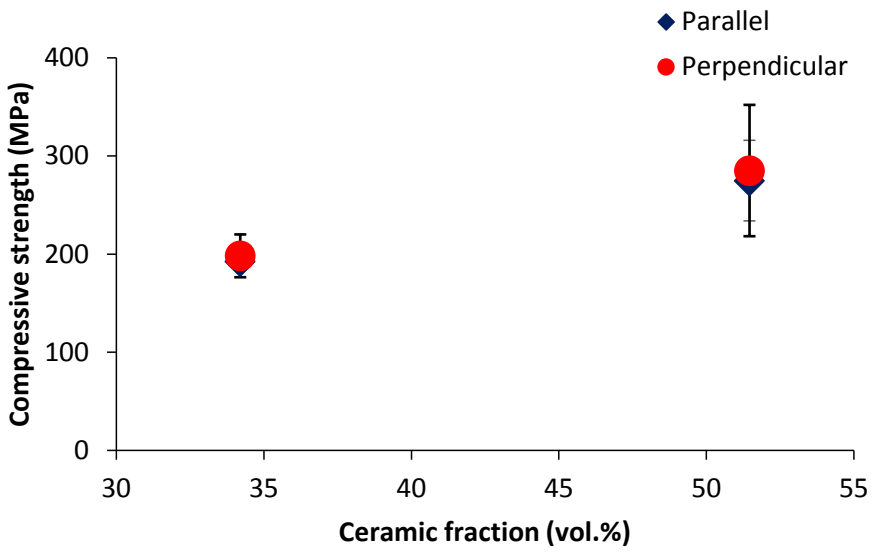

Figure 6-7. Means and SD for compressive strength (MPa) of the Al_2O_3-PC interpenetrating phase composites in relation to the ceramic volume fractions. The force was applied in 2 planes: parallel (Blue) and perpendicular (Red) to the freezing direction.

6.2.5 Crack propagation during three-point bend testing

SEM images in Figure 6-8 were taken for the 50.89 Al_2O_3-UDMA-TEGDMA interpenetrating phase composites after three-point bend testing in order to evaluate the nature of the fracture propagation.

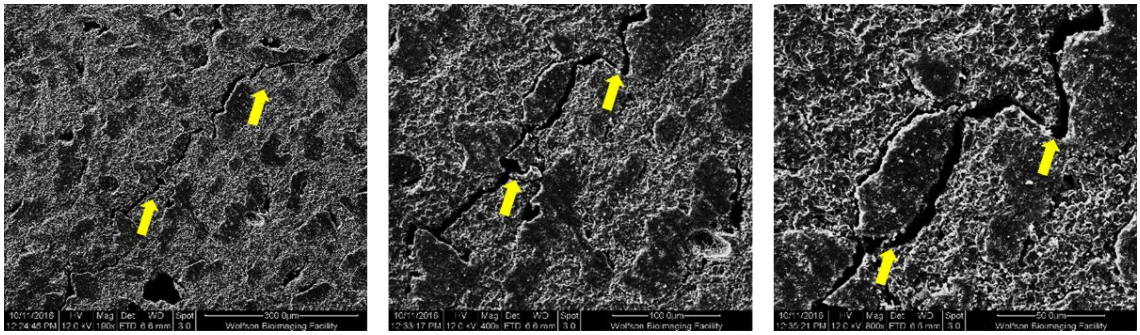

Figure 6-8. SEM images illustrating the fracture line after three-point bend testing. Yellow arrows indicate the areas of crack deflections. Magnification x 180, x 400, x 800.

When looking at the images in Figure 6-9, we can see that the fracture lines follow a tortuous path through the ceramic phase and also the ceramic/polymer interface. No cracks were observed purely in the polymer fraction.

6.2.6 Fracture toughness

Fracture toughness testing was performed on the Al_2O_3-UDMA-TEGDMA interpenetrating phase composite materials containing 61.17 and 50.89 vol.% ceramic fraction. For the Al_2O_3-PC interpenetrating phase composite materials, 51.46 and 34.20 vol.% were the materials of choice. The fracture toughness values for the Al_2O_3-UDMA-TEGDMA are illustrated in Figure 6-9.

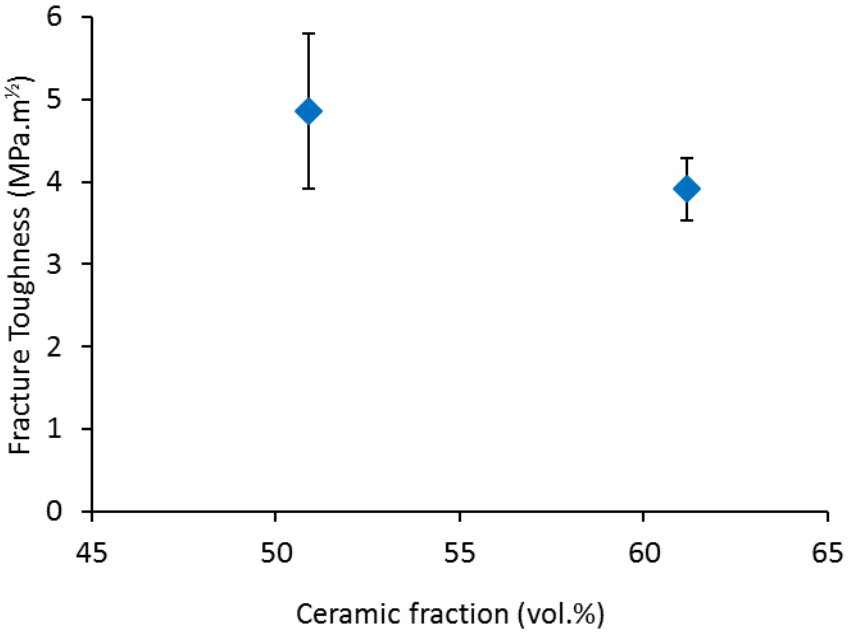

Figure 6-9. Means and SD for fracture toughness (MPa.m½) of Al_2O_3-UDMA-TEGDMA interpenetrating phase composites in relation to the ceramic volume fractions.

The DIC system was used to record the strain and the crack propagation behaviour to produce sequential images that show the crack propagation, as can be seen in Figure 6-10.

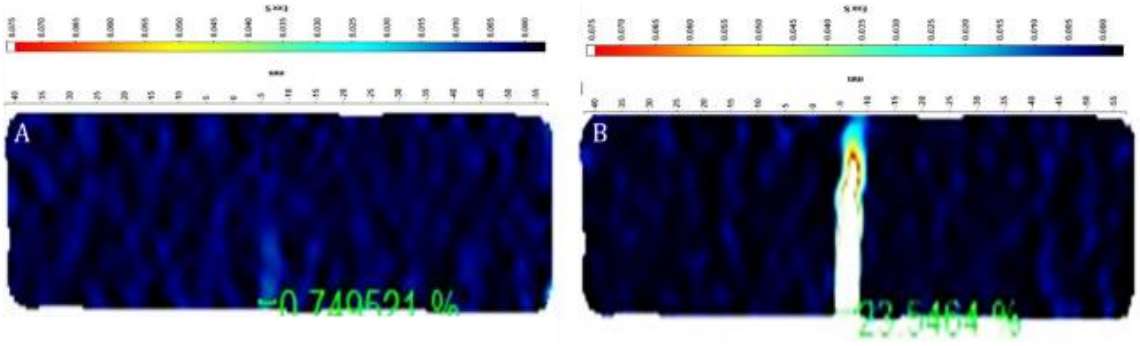

Figure 6-10. DIC images following fracture toughness measurements. A: Before failure. B: After failure.

For the Al_2O_3-PC interpenetrating phase composite, the fracture toughness measurements are illustrated in Figure 6-11.

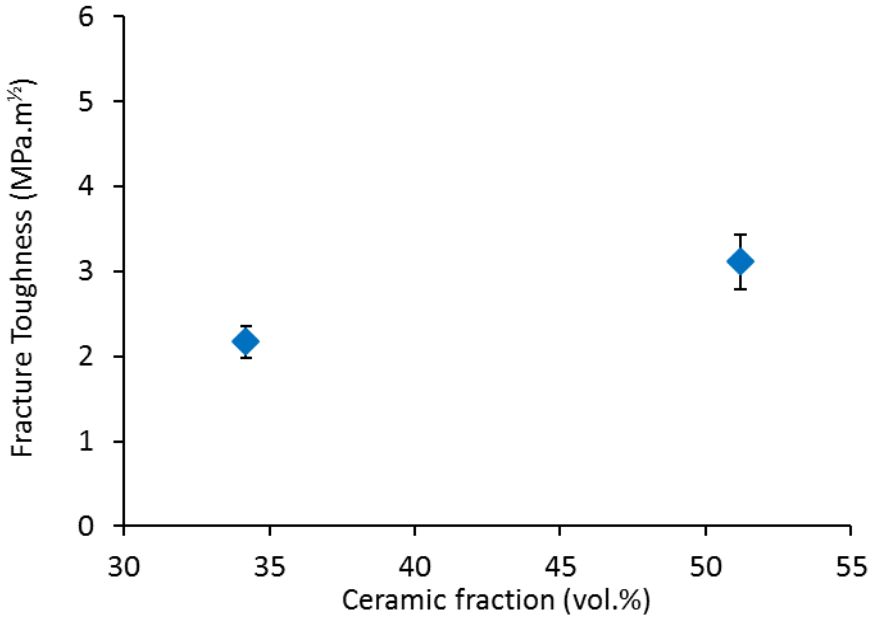

Figure 6-11. Means and SD for fracture toughness (MPa.m½) of Al_2O_3-PC interpenetrating phase composite in relation to the ceramic volume fractions.

It can be seen that the fracture toughness observed for the Al_2O_3-PC composite was lower than those for the Al_2O_3-UDMA-TEGDMA. This might be explained by the fact that the testing standard ASTM (2011) advised the depth of the specimen to be around 4 mm. In the case of the Al_2O_3-PC composite, consistent infiltration of the 12 test specimens to this depth was problematic. For the compression and three-point bend testing, materials were produced from specimens which were 2 mm in depth only, at which depth proper infiltration was less of an issue.

The MicroCT images (Figure 6-12) show the path of the crack propagation following the fracture toughness testing of the Al_2O_3-UDMA-TEGDMA composites. The fracture line can be seen to pass right through the composite.

The fracture lines can be seen as a black line which is highlighted in yellow in the adjacent images. The bulk of the composite structure remained stable and intact and unlike pure ceramic the failure was not sudden.

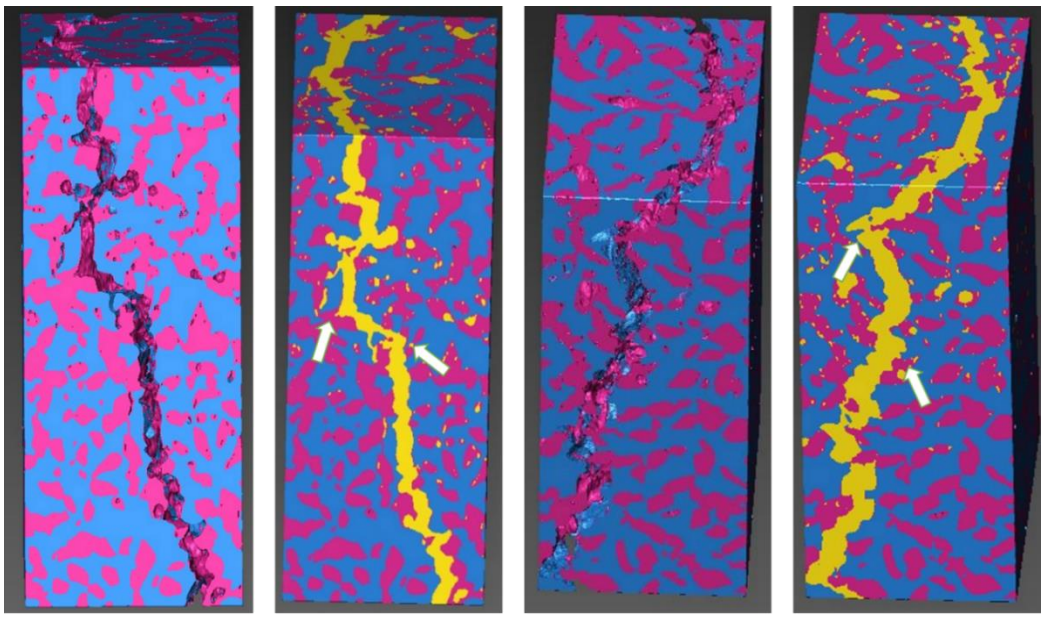

Figure 6-12. MicroCT 3D images showing the fracture line of the 51.46 vol.% ceramic fraction Al_2O_3-PC interpenetrating phase composite materials from two sides of the specimen. The yellow represents the fracture line propagation. White arrows indicate the crack deflection.

6.3 Discussion

Previous research has investigated the mechanical properties of hybrid materials produced using freeze-casting and isostatic pressing, but with restorative uses in mind rather than as possible orthodontic bracket materials (Petrini *et al.*, 2013; Li *et al.*, 2017). In addition, Petrini *et al.* (2013) used epoxy as the infiltrating polymer, which can be carcinogenic in the oral cavity, and Li *et al.* (2017) used a different ceramic material, namely zirconia. Pure zirconia has been used as an orthodontic bracket material, but has very poor aesthetic qualities (Keith *et al.*, 1994; Springate and Winchester, 1991). Also, none of the previous studies describe materials characterised by a honeycomb-like structure.

There is still limited data in the literature regarding a precise and thorough investigation of the mechanical behaviour of freeze-cast materials. The reason for this might be the number of the confounding factors when reporting such data. The mechanical properties of the material will depend on the nature of the material, the pore dimensions, the direction and morphology of the pores and their structural integrity. It is perhaps hardly surprising that mechanical testing and subsequent comparisons may not be straight forward. The role of the pore size, morphology and distribution over the mechanical response is complex and has not been fully investigated, but will likely play a critical role in the mechanical response and failure behaviour of the ceramic phase network (Deville, 2010). Furthermore, the strength of ceramic in general is a complex parameter that cannot be fully described by a single value (Evans, 1978; Lawn *et al.*, 1980).

The mechanical properties of the Al_2O_3-UDMA-TEGDMA interpenetrating phase composite materials (compressive test, three-point bend test and modulus of elasticity) were tested at three different levels within a single specimen: the bottom, middle and top. This was completed to determine the effect of distance from the freezing front, and therefore ceramic content on the properties of the final composite, and to see which might possess the best properties for use as an orthodontic bracket material.

As already described, the mechanical properties of polymer-infiltrated-ceramic composite materials can be enhanced by carefully designing their architecture and their constituent ceramic scaffolds (Launey *et al.*, 2009; Coldea *et al.*, 2013). An advantage of polymer-based materials is their property of plastic deformability, which can minimise the spontaneous fracture of the ceramic matrix (Alt *et al.*, 2011; Balkenhol *et al.*, 2008). For composite materials, the degree of polymer enhancement to the ceramic in the final structure depends on both the degree of polymer infiltration (connected porosity) and the polymer chemistry. For all the experimental composites the dimensions varied by ± 0.5 mm, due to the sensitive preparation techniques. However, every effort was made to ensure the specimens were flat and had parallel sides. This was important, as the conditions under which the mechanical properties were measured, such as specimen dimensions and experimental setup, are very important in the determination of the measured properties and their reproducibility in a uniform and consistent manner (Deville *et al.*, 2015).

6.3.1 Effect of the microstructure on compressive strength

Compressive strength testing is considered an important *in vitro* analysis to characterise dental materials and for simulating to some degree the forces they might be subjected to clinically (Kelly, 1999).

The compressive strength values of the ceramic/polymer composites containing more than 30 vol.% ceramic fraction ranged between 143 to 274.91 MPa, although lower than dense alumina (2358.08 MPa), were higher than that of PC (131.4 MPa), UDMA-TEGDMA (129.95 MPa) and enamel (62 to 89 MPa), and were comparable to that of dentine (194 to 224 MPa) and resin composite (265 to 290 MPa) (Chun *et al.*, 2014; Xu and Burgess, 2003). This may be attributed to the combination of the properties of alumina and the polymers and their complex interrelationship. For the experimental composite materials containing less than 30 vol.% ceramic fraction, the reduced mechanical properties are probably due to the lower volume fraction of ceramic, which provides the composites with their stiffness. Moreover, the primary ceramic preforms containing less than 30 vol.% ceramic fraction were characterised by relatively higher porosities, which resulted in increased brittleness of the composite materials despite the fact that they were toughened by a second flexible phase.

Interestingly the compressive strength values were lower than those reported by Petrini *et al.* (2013), which were 222 MPa for the composite materials produced from a porous alumina scaffold (with 20 vol.% initial solid ceramic loading). However, not only was their ceramic infiltrated with epoxy polymer as the second phase, which might have had

an effect, but they also used sapphire platelet-like alumina powder in addition to the alumina as the ceramic component in the initial aqueous suspension.

Regarding the effect of the ceramic volume fraction on the Al_2O_3-UDMA-TEGDMA interpenetrating phase composite material, there was a large difference between the compressive strengths of the Al_2O_3-UDMA-TEGDMA interpenetrating phase composites with an 18.83 vol.% ceramic fraction, compared with those with a 60.17 vol.% ceramic fraction (Figure 6-1). The interesting finding of the compressive strength results are that composites with 50.89 vol.% ceramic fraction showed the highest strength. This may be explained by the differences in the composition, microstructure and the presence of both ceramic and polymer in the same volume fractions in the composite material, leading to improved compressive load distribution. These results may also be attributed to the porous ceramic scaffold fabrication process (freeze-casting) and the resultant structure and porosity. When looking at the effect of the ceramic volume fraction for the Al_2O_3-PC interpenetrating phase composite material, we can see that the compressive strength increased from 192.43 to 274.91 MPa when the ceramic fraction in the composite increased from 34.20 to 51.46 vol.%. It has been reported in previous research that higher compressive strengths can be attained by changing the initial solid ceramic loading (Mozafari *et al.*, 2010; Deville *et al.*, 2015).

At the end of each test the composites, although appearing smaller in the direction of the applied force, did maintain their overall shape and structure, which might be the result of the presence of the flexible polymeric phase.

6.3.2 Effect of the microstructure on flexural strength

The flexural strength (three-point bend test) is the maximum observed stress of a material when loaded in the middle and supported at each end. This test determines both the strength and distortion of the specimen. The formation of cracks leading to failure of a material usually starts from a surface or internal flaw or void, and then penetrates to the interface of the grains or weaker phases in the material (Meyers *et al.*, 2008). Flexural strength is considered to be a critical mechanical parameter when brittle materials such as ceramics are being evaluated. According to Pereira *et al.* (2003), the flexural strength test deserves particular attention, because it measures tension and compression acting together, perhaps more closely simulating clinical conditions.

The three-point bend test is one of three standard tests used to determine the flexural strength of dental materials (with the others being the biaxial flexure test and the four-point bend test). Although composite materials are well known for presenting with highly variable flexural strengths due to their unpredictable flaw distribution (Rezwan *et al.*, 2006), the ISO standard test to determine the strength of ceramic based dental materials remains the three-point bend test.

In the present study, the mean flexural strength of UDMA-TEGDMA was 111.91 MPa and for PC was 122.49, whereas that of dense alumina was much greater at 246.3 MPa. The flexural strength of the Al_2O_3-UDMA-TEGDMA composite tested parallel to the direction of freezing was found to range from 28.28 to 145.65 MPa, as can be seen in Figure 6-3. The flexural strength of the Al_2O_3-Pc composite tested parallel to the direction of

freezing was found to be 105.54 MPa and 148.47 MPa for the 34.20 and 51.46 vol.% ceramic fractions respectively (Table 6-1). This would suggest that the greater the inorganic content in the novel composite material, the higher its flexural strength. This is in agreement with previous studies on dental composite materials (Inoue *et al.*, 1994; Kim *et al.*, 2002). Once again, the flexural strength mean values ranged between the values of the pure polymer, in both cases, and the dense ceramics, which implies a reinforcement mechanism of the two phase material compared to the single components. When the ceramic fraction was more than 53 vol.% of the Al_2O_3-UDMA-TEGDMA composite, the flexural strength was more than 140 MPa.

These results are comparable to the results reported by Coldea *et al.* (2013) for experimental UDMA-TEGDMA infiltrated porous sintered feldspar ceramic networks (125 to 160 MPa). But they were slightly lower than the values reported by Okada *et al.* (2014) (110 to 200 MPa). This might be explained by the fact that Okada *et al.* (2014) used a filler press moulding, rather than freeze-casting to produce their porous ceramic network, which could result in fewer flaws and also fewer micropores in the final composite material. It should be noted that the quality of press moulded porous ceramic structure is not always predictable due to residual pores that can occur as a result of incomplete compaction, density variation within the material, inhomogeneous pore distribution (Niesz, 1996) and the inability to produce graded porous structures, which is a significant advantage of using freeze-casting.

Li *et al.* (2017) reported the flexural strength of their BisGMA-TEGDMA-infiltrated zirconia networks ranged from 110 to 240 MPa, which again is higher than the values

obtained in the present study. However, zirconia was not used as it has been shown to demonstrate poor aesthetic properties when compared with the alumina used in the present study (Keith *et al.*, 1994; Springate and Winchester, 1991). It is also interesting to observe that composites obtained using a similar freeze-cast process by Petrini *et al.* (2013) showed higher flexural strengths (183 to 213 MPa) than our composites, even at lower ceramic loadings. This might be due to the use of different polymers, different binders (PVA) or different ceramics, such as sapphire platelet-like alumina powder that might enhance the mechanical performance (Petrini *et al.*, 2013). The values observed in the current study were nevertheless higher than that found for feldspathic porcelain(69 MPa) (Giordano II *et al.*, 1995), and slightly higher than traditional dental composites (103 to 107 MPa) (Yao *et al.*, 2014), but lower than dentine 212.9 MPa and commercially sintered polycrystalline alumina brackets (280 MPa) (Plotino *et al.*, 2007; Swartz, 1988).

The ceramic materials used in orthodontics are brittle since there is no mechanism that permits permanent deformation. As a result, a sudden catastrophic fracture under clinical conditions may occur, which poses a real concern to clinicians and patients. In order to improve the flexural strength, and to reduce the tendency to sudden failure, a propagating crack needs to be inhibited from progressing either by blunting, or by being deflected to take a more tortuous path through a material. Taking a more tortuous path requires more energy for the crack to propagate and therefore makes it less likely the material will fail. In the composite materials produced in this study, the cracks induced appeared to be deflected by the polymer-ceramic interfaces (Figure 6-8). As a result, the ceramic/polymer interpenetrating phase composites seem more likely to fail in a gradual

rather than sudden manner, which might otherwise result in soft tissue injury or a foreign body inhalation.

6.3.3 Effect of the microstructure on modulus of elasticity

Modulus of elasticity is useful as a measure of a material's resistance to elastic deformation when a force is applied and represents the stiffness of a material within the elastic range. Materials such as polymers have low values for modulus of elasticity, whereas ceramics have much higher values (Wong and Bollampally, 1999).

In the present study, the modulus of elasticity was found to range from 1.48 to 16.56 GPa for the experimental ceramic/polymer composite materials, 118.5 GPa for the dense pure alumina, 1.17 GPa for pure UDMA-TEGDMA and 1.5 GPa for pure PC (Figures 6-5 and 6-6). As expected, modulus of elasticity fell with increasing ceramic porosity (Asmani *et al.*, 2001). Even the pure alumina samples fabricated in the present study had a lower modulus of elasticity (118.5 GPa) than otherwise relatively pure alumina (300 GPa). It is to be expected that modulus of elasticity will fall with increasing ceramic porosity (Asmani *et al.*, 2001) and in this case the pure dense ceramic may have had some porosities present. The modulus of elasticity of PC was also lower that what had been reported previously (2.0 to 2.4 GPa) (Eliades, 2007), which again might be explained by different fabrication methods and the probability of the presence of micro pores in the specimens produced in the present study.

The modulus of elasticity for the Al_2O_3-UDMA-TEGDMA interpenetrating phase composite materials containing more than 40 vol.% of ceramic was found to range from

13.80 to 16.56 GPa, which is comparable to those of dentine 11 to 19 GPa, lower than those of other polymer infiltrated ceramic network materials 16 to 28 GPa (Coldea *et al.*, 2013) and comparable to those of hybrid filler resin composite restorative materials 6-21 GPa (Beun *et al.*, 2007) , and slightly higher than the values reported for other polymer-infiltrated-ceramic material (9 GPa) by Petrini *et al.* (2013)**.** These differences can be accounted for by the differences in the materials used to fabricate the porous ceramic scaffolds, the different fabrication methods and the different polymers used as the second phase. For example, zirconia was utilised by Coldea *et al.* (2013) to increase the toughness characteristics of the resultant composite material, and they used pressing to fabricate the porous scaffold. Also, Petrini *et al.* (2013) used sapphire platelet-like alumina powder in their ceramic scaffold to increase the strength and their porous scaffold and they were characterised by a lamella rather than a honeycomb-like structure.

6.3.4 Mechanical anisotropy of biomimetic ceramic/polymer interpenetrating phase composites

As the composite materials in the current study are primarily porous ceramic structures obtained by freeze-casting, testing in a direction perpendicular to the freeze-casting process not surprisingly produced results that differed to those observed when tested parallel to the direction of freeze-casting. Anisotropy was therefore observed both in structure and mechanical properties. Anisotropic porosity means that some aspects of the pores, e.g. shape and/or size, are directionally dependent. Even if the temperature gradient within the suspension is perfectly vertical, it is common to see tilting of the ice

crystals as they grow through the suspension during freeze-casting (Deville *et al.*, 2007; Deville, 2013).

When the mechanical properties were tested with respect to the direction of the freeze-casting, the results showed that values were slightly lower when the force was applied parallel to the direction of the freeze-casting when compared to perpendicular to this direction. This can be attributed to the arrangement of the ceramic walls and therefore polymer infiltrate within the composite, which resembles the effect seen with enamel and dentine (Miura *et al.*, 2009; Kinney *et al.*, 2003). This is very different to the pure ceramics or polymers found in currently available monolithic aesthetic orthodontic brackets. When the force was applied in the direction parallel to the freezing direction in any of the tests, it might be surmised that any crack is more likely pass down the length of a single pore rather than across multiple pores (filled with polymer) and their boundary ceramic walls when tested perpendicular to the direction of freeze-casting. Therefore, the mechanical properties in the perpendicular direction would be expected to be better than those in the parallel direction.

For Al_2O_3-UDMA-TEGDMA interpenetrating phase composite materials, flexural strength mean values ranged between the values of the pure polymer and dense alumina, which implies a reinforcement mechanism of the two phase material compared to the single components. The results observed were comparable to those of Launey *et al.* (2009). For Al_2O_3-PC interpenetrating phase composite material, the compressive strength test was the test of choice to evaluate anisotropy as the specimens produced were only 4 mm in depth.

6.3.5 Fracture toughness

Fracture toughness is the measure of a material's ability to absorb strain energy prior to fracture (Ritchie *et al.*, 1973). The importance of fracture toughness in the case of aesthetic orthodontic brackets is in the ability of the bracket to resist unwanted in-service failure, and this most commonly occurs at the tie wing (Johnson *et al.*, 2005). For ceramic brackets, it is essential to have sufficient strength to resist the forces imposed during bonding, the subsequent orthodontic treatment and at debond. Since ceramics used for brackets are brittle materials that fail by crack propagation, and ceramic brackets have historically shown a tendency for tie wing fracture, the fundamental mechanical property is fracture toughness (Scott, 1988; Kusy, 1988).

A convenient technique for measuring the fracture toughness of ceramic materials is the single edge-notch technique (Mante *et al.*, 1993). Digital image correlation (DIC) is a non-invasive optical measurement technique that analyses the displacement and gives a full three-dimensional field of strain (Sutton *et al.*, 1986; Shah and Kishen, 2011). The images are taken before and after the deformation by a digital camera from which the displacement at any point is computed, as can be seen in Figure 6-10. This technique has been used extensively for fracture testing of different materials such as composites (Sutton *et al.*, 1986; Abanto-Bueno and Lambros, 2002). In the present study, the use of the DIC system to record the strain and subsequent crack propagation behaviour was not entirely successful. The crack propagation was too rapid for the cameras to record it. Instead of having sequential images that show the crack propagation behaviour, only two useful images were obtained: one before the fracture and one immediately after

failure, as can be seen in Figure 6-10. For Al_2O_3-PC, MicroCT was used to investigate a specimen that had already fractured, as can be seen in Figure 6-12.

The mean values for the fracture toughness of Al_2O_3-UDMA-TEGDMA interpenetrating phase composite materials in the present study, containing 61.17 and 50.89 vol.% ceramic fraction, were 3.91 and 4.86 MPa.m^{½} respectively, as can be seen in Figure 6-9. The ratio between ceramic and polymer affected the resultant fracture toughness of the composite material. Fracture toughness increased as did the polymer volume, which was different to that observed with flexural strength. These results show that the addition of a ductile polymer phase contributes to the reinforcement mechanism of the final composite material.

The reported fracture toughness values for enamel and dentine are approximately 0.72 to 1.28 and 2.2 to 3.1 MPa.m^{½} respectively (Min *et al.*, 2016; Bajaj and Arola, 2009; Lawn and Lee, 2009). Previous studies have reported the fracture toughness of polycrystalline alumina to be in the range of 3.5 to 4.4 MPa.m½ (Gogotsi, 2003; Guazzato *et al.*, 2004a) and for monocrystalline alumina to be 2.1 to 2.5 MPa.m½ (Iwasa and Brandt, 1986; Anstis *et al.*, 1981). For zirconia toughened ceramic, fracture toughness values range between 4.8 to 4.9 MPa.m^{½} (Guazzato *et al.*, 2004b), while for zirconia brackets much lower mean fracture toughness values were reported at 3.92 MPa.m^{½} (Tilson, 1994). According to He and Swain (2011), where a series of polymer-infiltrated feldspar ceramics from VITA company were investigated, the fracture toughness ranged from 0.44 to 1.72 MPa.m^{½}, values which were far lower than those of the interpenetrating phase composite materials in the present study. Moreover, fracture toughness values

reported in the present study were slightly higher than the fracture toughness values reported for polymer infiltrated ceramic network materials by Chaiyabutr *et al.* (2009) (92.48 to 3.43 MPa.m^{½}), Li *et al.* (2017) (1.5 to 3.6 MPa.m^{½}), Della Bona *et al.* (2014) (1.09 MPa.m^{½}), and comparable to those reported by Launey *et al.* (2009) (3.1 to 5.1 MPa.m^{½}).

Alumina possesses strong, directional, covalent bonds that do not allow permanent deformation by dislocation (Christel, 1989). When these ceramics are subjected to their maximum elastic stress levels, brittle failure occurs. It has been demonstrated that the stress field at the crack tip, to allow the crack to re-enucleate in the subsequent ceramic layer, has to reach a critical value in order to fracture the brittle phase at some distance ahead (Tobler and Reed, 1977).

The unique structural architecture achieved by gelation and freeze-casting generates in these microstructures the activation of several toughening mechanisms and that makes them tougher as a pre-existing crack propagates. When load is applied to the material, plastic deformation of the flexible polymer will be constrained by the surrounding ceramic network with its higher modulus of elasticity, making crack bridging the dominant toughening mechanism (Rose, 1987; Erdogan and Joseph, 1989). As the polymer phase is less stiff than the ceramic matrix, both the plastic deformation of the polymer phase and the effect of polymer-ceramic phase debonding contributes to crack shielding (Gang and Chung-Yuen, 1990).

Whilst in the case of 61.17 vol.% the polymer layers were reduced as the ceramic contents increased, Al_2O_3-PC interpenetrating phase composite materials containing 51.46 vol.% ceramic fraction showed a fracture toughness value of 3.11 MPa·m^{½} (Figure 6-11), which was much lower than that of Al_2O_3-UDMA-TEGDMA interpenetrating phase composite materials containing 50.89 vol.% (4.86 MPa·m½). This may be explained by the fact that specimens used for fracture toughness testing were 4 x 32 x 8 mm in size, which was very hard to produce in the case of the Al_2O_3-PC interpenetrating phase composites due to the sensitive infiltration technique, which could have resulted in empty pores around the crack area and have led to faster crack propagation and more immediate failure.

6.4 Summary

In the present study, experimental ceramic/polymer interpenetrating phase composites with a good combination of strength and fracture toughness have been developed, taking inspiration from natural dental materials. The manipulation of the ceramic volume fraction affected the compressive strength, flexural strength, modulus of elasticity and the fracture toughness properties of the final composite materials. The anisotropic characteristic of the composite material affected their mechanical properties when the strength was tested in parallel and perpendicular directions with respect to freeze-casting. The mechanical properties of the final ceramic/polymer interpenetrating phase composite materials produced with 50.89 vol.% Al_2O_3-UDMA-TEGDMA exhibited the best combination of strength and toughness, with final values of 97.73 MPa and 4.86 MPa·m^{½} respectively. The Al_2O_3-PC interpenetrating phase composites showed slightly

higher compressive and flexural strengths when compared to Al_2O_3-UDMA-TEGDMA interpenetrating phase composites, while the modulus of elasticity showed almost the same values.

Chapter 7. Surface characterisation of biomimetic ceramic/polymer interpenetrating phase composites

7.1 Introduction

Surface characteristics of the orthodontic bracket materials plays an important role in determining their ability to maintain surface structural integrity in the presence of loads arising from mechanics such as archwire sliding, high torqueing moments, or masticatory forces produced by chewing hard food (Saunders and Kusy, 1994). Surface roughness changes and hardness instabilities can be considered as disadvantages that concern aesthetic brackets, reducing their clinical efficiency during treatment (Alkire *et al.*, 1997; Gioka and Eliades, 2004; Russell, 2005; Zinelis *et al.*, 2005).

Micro-indentation has been used to evaluate the surface hardness of hard tissue like dentine (Hosoya *et al.*, 2000) and enamel (Min *et al.*, 2016), ceramics (Seghi *et al.*, 1995), polymer (Amitay–Sadovsky and Wagner, 1999) as well as composite materials (Schulze *et al.*, 2003). Non-contact profilometer is a tool that is used to measure surface roughness and loss of dental hard tissues and was first introduced in 1972 (Marshall Jr *et al.*, 1997; Al-Radha *et al.*, 2012; Paepegaey *et al.*, 2013; Baysan *al.*, 2018). Non-contact profilometer Proscan software provides a variety of surface measurements and the technique is non-invasive.

The aim of this Chapter is to evaluate and compare surface properties of the novel biomimetic ceramic/polymer interpenetrating phase composites as a potential material

for orthodontic brackets and to compare them with the raw constituent materials (dense alumina, unfilled PC polymer and unfilled UDMA-TEGDMA polymer) and human enamel. The properties examined included surface hardness, surface roughness before and after toothbrushing and surface loss following toothbrushing. The ceramic/polymer interpenetrating phase composites investigated were: Al_2O_3-UDMA-TEGDMA composites containing 50.89 and 61.17 vol.% ceramic fractions and Al_2O_3-PC composites containing 34.20 and 51.46 vol.% ceramic fractions.

7.2 Results

7.2.1 Hardness

The mean and SD surface hardness values (GPa) of Al_2O_3-UDMA-TEGDMA composites and Al_2O_3-PC composites are shown in Figure 7-1. In addition, the surface hardness values of dense alumina, UDMA-TEGDMA and PC polymers and human enamel were also evaluated.

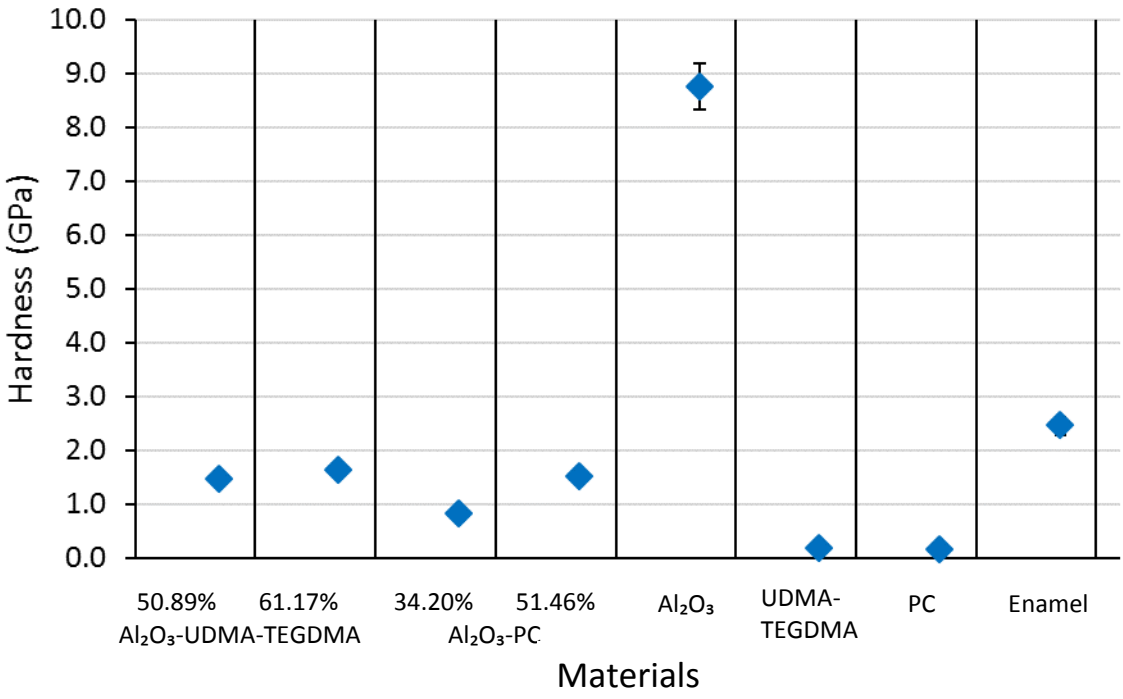

Figure 7-1. Mean and SD (GPa) for Vickers hardness (six specimens per material). The load was applied parallel to the freezing direction.

When looking at the hardness values in Figure 7-1, we can see that alumina had the highest hardness followed by human enamel, and the two polymers demonstrated the lowest values. The hardness values of the composites were between these two groups.

It is also apparent that increasing the ceramic volume fraction within the ceramic/polymer interpenetrating phase composite leads to an increase in the observed surface hardness of the materials. The mean Vickers hardness values of Al_2O_3-UDMA-TEGDMA interpenetrating phase composites containing 50.89 and 61.17 vol.% ceramic fraction were 1.46 and 1.62 ± 0.09 GPa respectively. The mean Vickers hardness values of Al_2O_3-PC interpenetrating phase composites containing 34.20 and 51.46 vol.% ceramic fraction were 0.82 ± 0.13 and 1.52 ± 0.09 GPa respectively.

The hardness of the Al_2O_3-PC interpenetrating phase composites was also measured, but with the force applied in two planes, perpendicular and parallel to the direction of freeze-casting of the porous ceramic preform. The results are illustrated in Figure 7-2.

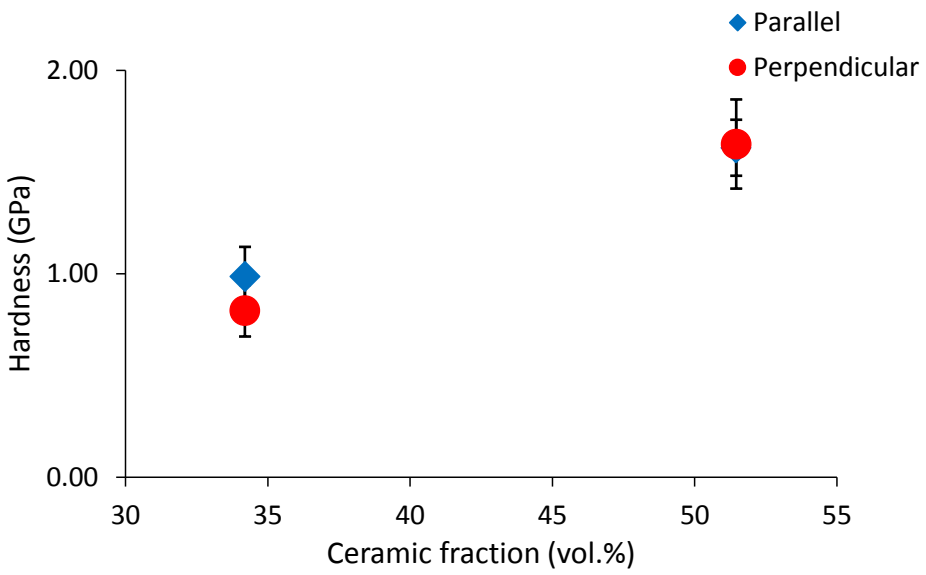

Figure 7-2. Mean and SD (GPa) for Vickers hardness (six specimens per material) when the indentation force was applied in two planes, parallel (Blue) and perpendicular (Red), for Al_2O_3-PC interpenetrating phase composites.

When looking at Figure 7-2, we can see that the hardness of Al_2O_3-PC interpenetrating phase composites containing 34.20 vol.% was higher when tested perpendicular rather than parallel to the direction of freeze-casting. For the same composite when the ceramic volume fraction was 51.46 vol.%, the direction of testing had no significant effect. Again, it is clear from Figure 7-2 that there is a clear trend for the hardness to increase with increasing ceramic volume fraction.

7.2.2 Surface roughness before and after simulated toothbrushing testing

In this part of the study, the surface roughness of each experimental material was tested before and after 2 hrs 50 mins of simulated toothbrushing. This was equivalent to two years in a clinical situation when subjected to 2 mins of toothbrushing twice daily. As a general rule aesthetic orthodontic brackets are not used on molar teeth and therefore this test was performed on twenty teeth in total (8 incisors, 4 canines and 8 premolars). Surface roughness was evaluated prior to and after toothbrushing. Paired t-tests were used to test for differences between pre and post toothbrushing measurements for each material ($p<z$).

7.2.2.1 Mean average roughness (Ra)

The mean and SD values for the average surface roughness (Ra) of each material before and after toothbrushing are illustrated in Figure 7-3.

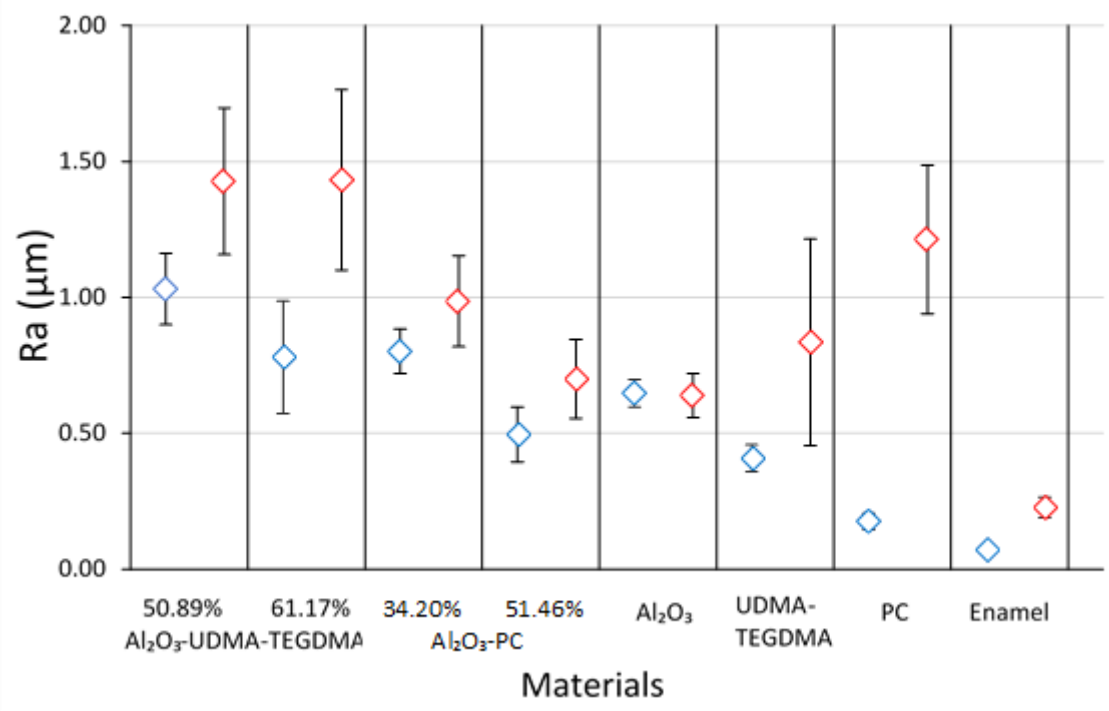

Figure 7-3. Mean and SD (µm) of surface roughness (Ra) for materials under test, pre (Blue) and post (Red) two years of simulated toothbrushing.

When looking at Figure 7-3 we can see that toothbrushing resulted in an increased Ra value for almost all specimens. Prior to brushing, human enamel and PC had the lowest Ra values, while Al_2O_3- UDMA-TEGDMA composite containing 50.89 vol.% showed the highest value. When looking at Al_2O_3-PC interpenetrating phase composite the 34.20 vol.% ceramic fraction specimens demonstrated significantly higher Ra values when compared to those of the 51.46 vol.% ceramic fraction.

Significant changes in the Ra values following brushing were found in Al_2O_3-UDMA-TEGDMA interpenetrating phase composites ($p=0.02$ for 50.89 vol.% ceramic fraction and $p=0.02$ for 61.17 vol.% ceramic fraction), Al_2O_3-PC interpenetrating phase composites containing 51.46 vol.% ($p=0.00$), pure polymers ($p=0.03$ for UDMA and

p=0.00 for PC) and human enamel (p=0.00). No significant changes were observed for the 34.20 vol.% Al_2O_3-PC interpenetrating phase composites (p=0.10). Interestingly, the surface roughness values for the dense alumina specimens were slightly lower following brushing but this effect was not statistically significant (p=0.65).

7.2.2.2 Average maximum peak-to-valley height of five consecutive sampling depths (Rz)

The mean and SD values for the average maximum peak-to-valley height of five consecutive sampling depths (Rz) of each material before and after toothbrushing are illustrated in Figure 7-4.

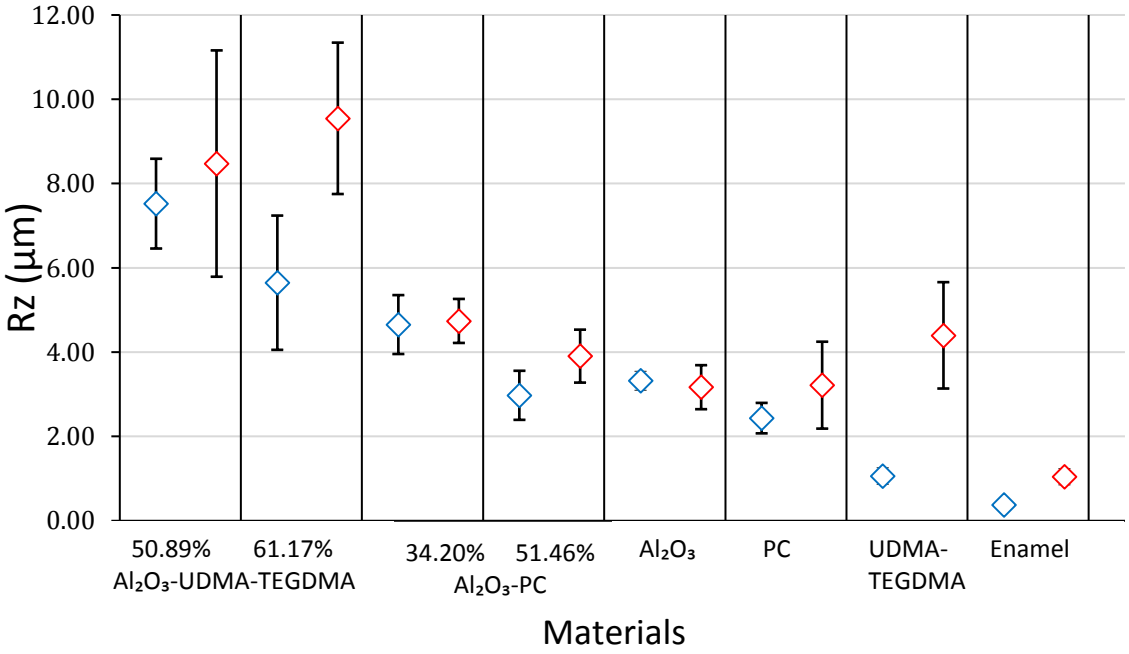

Figure 7-4. Mean and SD (µm) of the average maximum peak-to-valley height of five consecutive sampling depths (Rz) for materials under test, pre (Blue) and post (Red) two years of simulated toothbrushing.

When looking at Figure 7-4 we can see that toothbrushing resulted in an increased Rz value for almost all specimens. Prior to brushing, human enamel and UDMA-TEGDMA had the lowest Rz values, while Al_2O_3-UDMA-TEGDMA composite containing 50.89 vol.% showed the highest value. Significant changes in the Rz values following brushing were found in Al_2O_3-UDMA-TEGDMA interpenetrating phase composites containing 61.17 vol.% ceramic fraction (p=0.01), Al_2O_3-PC interpenetrating phase composites containing 51.46 vol.% (p=0.01), pure PC (p=0.00) and human enamel (p=0.00). No significant changes were observed for the Al_2O_3-UDMA-TEGDMA containing 50.89 vol.% ceramic fraction (p=0.43), Al_2O_3-PC interpenetrating phase composites containing 34.20 vol.% (p=0.84) and pure UDMA-TEGDMA (p=0.11). Interestingly, the surface roughness values for the dense alumina specimens were slightly lower following brushing (p=0.33) but again this was not statistically significant.

7.2.2.3 Root mean square roughness (Rq)

The mean and SD values for the root mean square roughness (Rq) of each material before and after toothbrushing are illustrated in Figure 7-5.

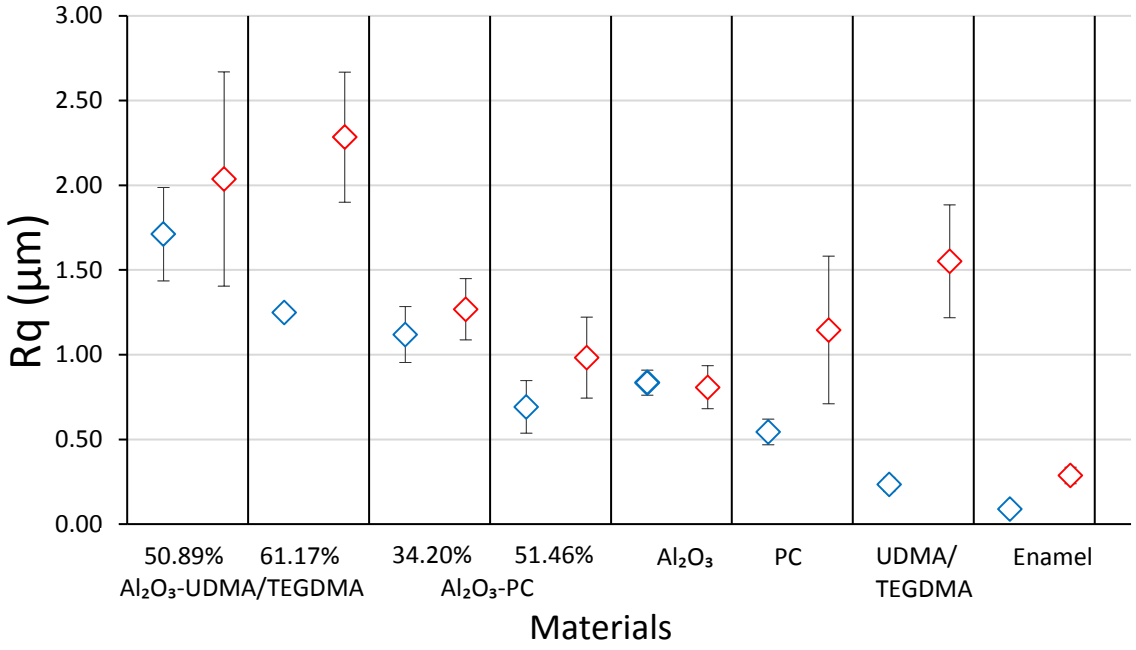

Figure 7-5. Mean and SD (µm) of root mean square roughness (Rq) for materials under test, pre (Blue) and post (Red) two years of simulated toothbrushing.

When looking at Figure 7-5 we can see that toothbrushing resulted in an increased Rq value for almost all specimens. Prior to brushing, human enamel and UDMA-TEGDMA had the lowest Rz values, while Al_2O_3- UDMA-TEGDMA composite containing 50.89 vol.% showed the highest value.

Significant changes in the Rq values following brushing were found in Al_2O_3-UDMA-TEGDMA interpenetrating phase composites containing 61.17 vol.% ceramic fraction ($p=0.01$), Al_2O_3-PC interpenetrating phase composites containing 51.46 vol.% ($p=0.03$), pure polymers ($p=0.01$ for UDMA-TEGDMA and $p=0.00$ for PC) and human enamel ($p=0.00$).

No significant changes were observed for the Al_2O_3-UDMA-TEGDMA containing 50.89 vol.% ceramic fraction (p=0.30) and Al_2O_3-PC interpenetrating phase composites containing 34.20 vol.% (p=0.26). Again, the surface roughness values for the dense alumina specimens were slightly lower following brushing (p=0.34).

7.2.2.4 Maximum roughness depth (Rmax)

The average and SD values for the root maximum roughness depth, Rmax, for each material before and after toothbrushing are illustrated in Figure 7-6.

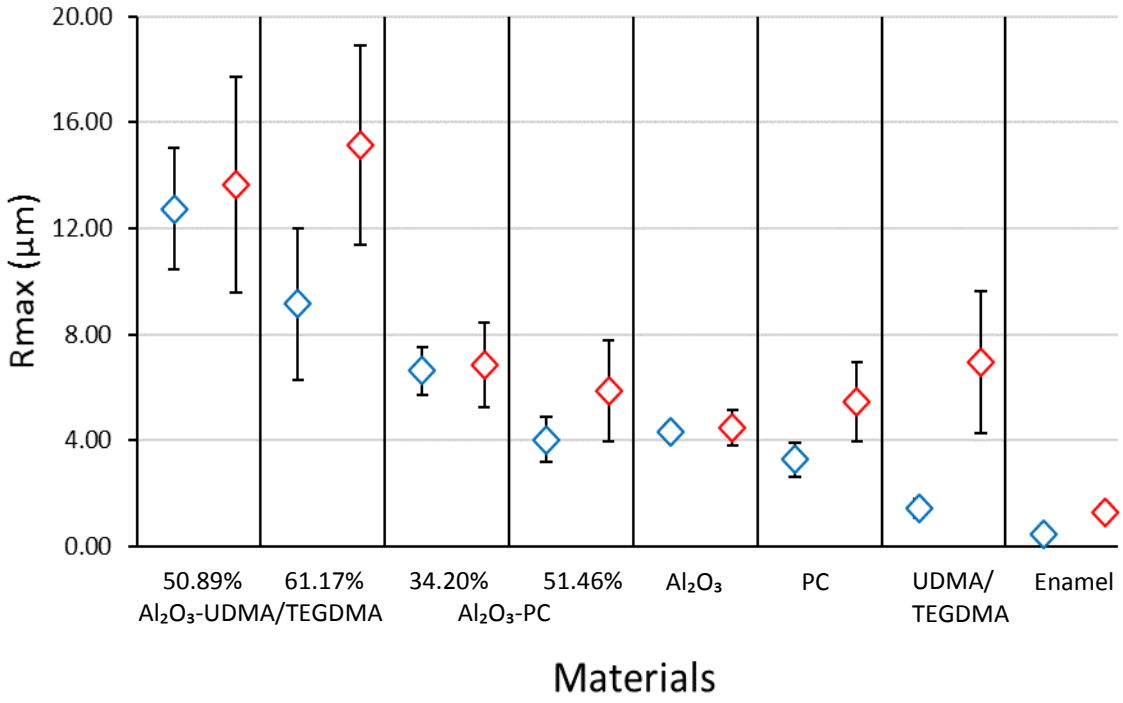

Figure 7-6. Mean and SD (µm) of the maximum roughness depth (Rmax) for materials under test, pre (Blue) and post (Red) two years of simulated toothbrushing.

When looking at Figure 7-6 we can see that toothbrushing resulted in an increased Rmax value for almost all specimens. Prior to brushing, human enamel and UDMA-TEGDMA

had the lowest Rmax values, while Al_2O_3- UDMA-TEGDMA composite containing 50.89 vol.% showed the highest value.

Significant changes in the Rmax values following brushing were found in Al_2O_3-UDMA-TEGDMA interpenetrating phase composites containing 61.17 vol.% ceramic fraction ($p=0.01$), pure polymers ($p=0.01$ for UDMA-TEGDMA and $p=0.01$ for PC) and human enamel ($p=0.00$). No significant changes were observed for the Al_2O_3-UDMA-TEGDMA containing 50.89 vol.% ceramic fraction ($p=0.63$), Al_2O_3-PC interpenetrating phase composites ($p=0.75$ for 34.20 vol.% ceramic fraction and $p=0.08$ for 51.46 vol.% ceramic fraction) and for the dense alumina ($p=0.43$).

7.2.3 SEM imaging following simulated toothbrushing

Using SEM to examine the specimens after simulated toothbrushing once again shows the distinct honeycomb-like structure of the ceramic/polymer composite samples. However, closer examination of the SEMs in Figure 7-7 shows that the polymer fraction in each case has surface striations that would appear to correspond with the direction of toothbrushing. No such surface effects are visible within the ceramic fractions. These results are also confirmed by the 3D profilometry images in Figure 7-8, where there are obvious differences between the post-brushing surface profile for the ceramic and polymer samples. Following brushing, the ceramic samples had a much smoother profile without the brushing grooves observed with the pure polymers.

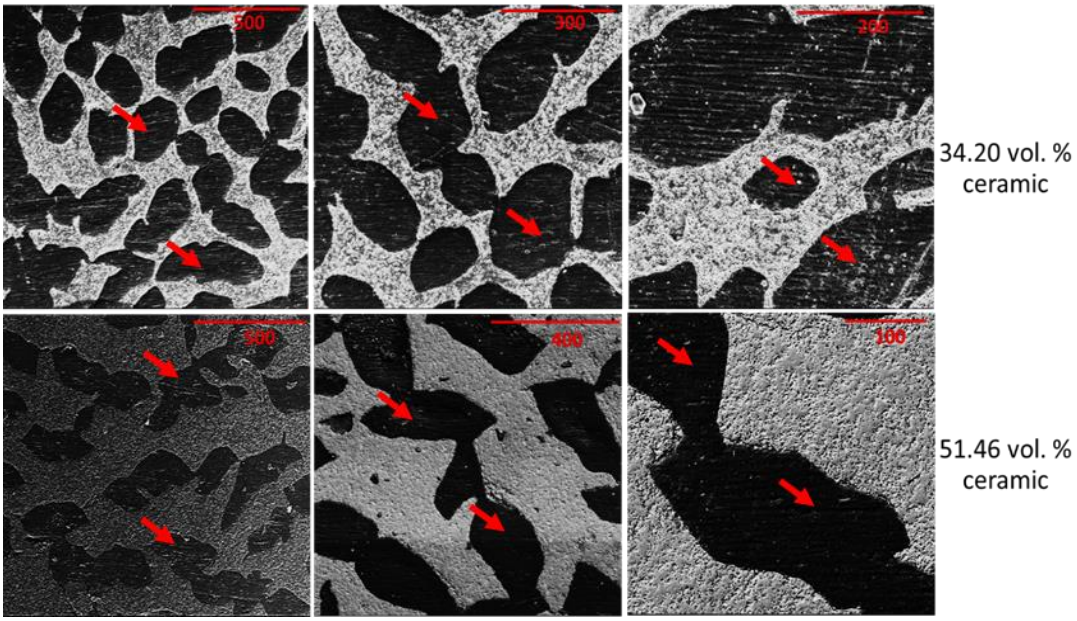

Figure 7-7. SEM images illustrating the effect of simulated toothbrushing on the Al_2O_3-PC interpenetrating phase composites. The darker areas represent the polymer parts and the lighter areas represent the alumina parts. The red arrows indicate the effect of the toothbrushing (polymer part of the composites).

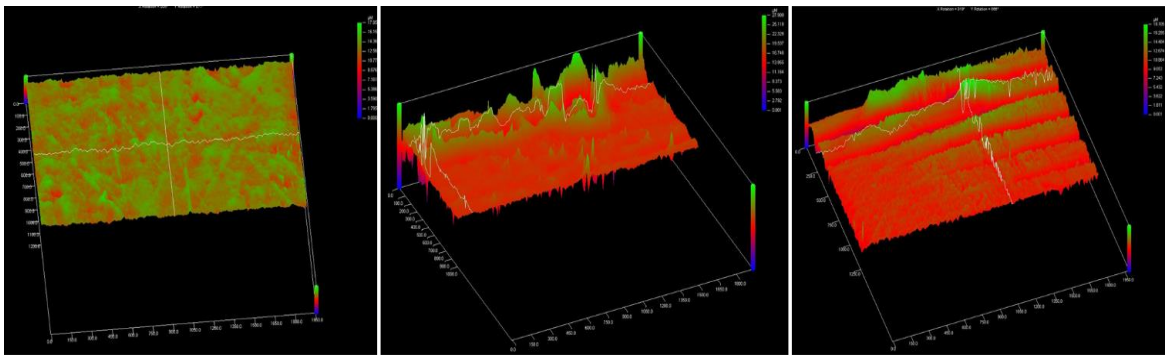

Figure 7-8. 3D profilometry images illustrating the effect of simulated toothbrushing in alumina, PC and UDMA-TEGDMA surfaces respectively.

7.2.4 Surface volume loss after simulated toothbrushing testing

Non-contact profilometry was used to record surface loss following brushing and Figure 7-9 shows the amount of surface loss in µm that occurred with simulated toothbrushing.

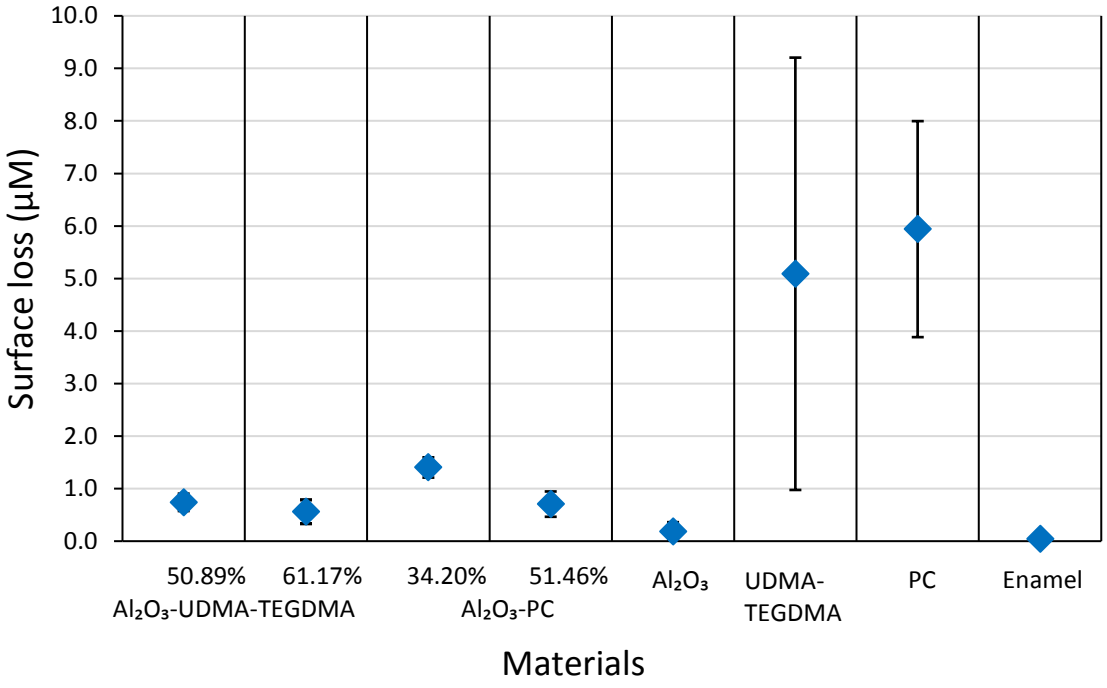

Figure 7-9. Mean and SD (µm) for surface loss after toothbrushing of the Al_2O_3-UDMA-TEGDMA and Al_2O_3-PC interpenetrating phase composites, alumina, UDMA-TEGDMA and PC polymers and enamel under test.

When looking at the results of the surface loss, all materials showed surface loss following simulated toothbrushing. Enamel and alumina showed the least amount of surface loss of all specimens. The pure polymers showed the highest loss of all the specimens. Al_2O_3-UDMA-TEGDMA composite with 50.89 vol.% ceramic fraction and Al_2O_3-PC interpenetrating phase composite with 51.46 vol.% ceramic fraction showed similar loss values. Al_2O_3-PC composite containing 34.20 vol.% demonstrated the highest

surface loss measurements and the Al_2O_3-UDMA-TEGDMA composite containing 61.17 vol.% showed the least surface loss among all of the composite materials. This demonstrates there is less surface loss with increasing ceramic phase volume fraction within the composite materials.

7.3 Discussion

In the present study a range of four varying novel biomimetic ceramic/polymer interpenetrating phase composite materials were evaluated in addition to their constituent raw materials. Zinelis *et al.* (2005) investigated the surface roughness characteristics (Ra, Rq, Rz and Rmax) and hardness of aesthetic bracket raw materials (polymers and alumina ceramics) from different bracket manufacturers using profilometry and Vickers hardness testing. The authors found that alumina ceramic raw material had higher roughness and hardness measurements when compared to polycarbonate. However, there was variability among polycarbonate bracket raw materials provided by different manufacturers (Forestadent, Germany and Ormco, USA).

7.3.1 Hardness of the ceramic/polymer interpenetrating phase composites

Hardness is defined as the resistance to a permanent surface indentation and it affects the wear resistance of a material (Xie *et al.*, 2000). In orthodontics, sufficient hardness is essential for the appliance to maintain surface structural integrity in the presence of loads such as archwire sliding, high torqueing moments, masticatory forces produced by chewing hard food and daily toothbrushing. Nevertheless, ceramics with a high hardness

value might not be desirable as dental materials since they may result in unwanted abrasion of the opposing teeth.

In the present study, the results indicate that a ceramic/polymer interpenetrating phase composite with a lower ceramic fraction results in a lower hardness, as can be seen in Figures 7-1 and 7-2. The lowest measured hardness was 0.82 GPa for the 34.20 vol.% Al_2O_3-PC interpenetrating phase composite and the highest was 1.62 GPa for the 60.17 vol.% Al_2O_3-UDMA-TEGDMA composite material. These values are between those of the dense alumina (8.76 GPa) and pure polymers (0.13 and 0.17 GPa for PC and UDMA-TEGDMA respectively).

When the results for the composites are considered with respect to the hardness of enamel (2.45 GPa), it would suggest the use of such materials as orthodontic brackets would cause little or no wear to the opposing teeth. This is unlike other commercial and non-commercially available ceramics and ceramic/polymer composites such as Enamic (3.31 GPa), polymer-infiltrated zirconia (3.93 GPa), zirconia (13.94 GPa) and lithium disilicate glass ceramics (10 GPa) (Zhang *et al.*, 2012; Min *et al.*, 2016; Li and Sun, 2018), or commercially available ceramic brackets which are much harder than enamel (Swartz, 1988) where the surface hardness for each is such that wear of opposing enamel would take place to varying degrees if occlusal interferences are present as previously reported *in vivo* and *in vitro* (Viazis, 1989).

In the present study, hardness was affected by the ceramic volume fraction and also where the indenter contacted the ceramic/polymer interpenetrating composite surface.

Not only might the ceramic volume fraction directly affect the hardness because there is more of it, but with increasing ceramic content the pore size reduces, and the ceramic wall sizes increase. Any range of values for any specimen where the indenter head appears to fit only within the pore filled with polymer was not used in this study.

The hardness of Al_2O_3-PC interpenetrating phase composites was also measured with the load applied in two planes with respect to the freezing direction of the porous ceramic preform to evaluate the effects of their anisotropy (Figure 7-2). There was only a small mean difference of 0.02 GPa between the two hardness values for the composite containing 51.46 vol.% ceramic fraction. However, for the Al_2O_3-PC interpenetrating phase composites containing 34.20 vol.% ceramic fraction, there was an increase of 0.17 GPa when comparing the hardness obtained as the load was applied perpendicular to the freezing direction as opposed to that obtained as the load was applied parallel to the freezing direction. This difference may indicate the effect of the larger and more rounded honeycomb-like shaped pores filled with polymer in the Al_2O_3-PC interpenetrating phase composite containing 34.20 vol.%, as a result of the larger ice crystals formed during freeze-casting. Higher hardness values were previously reported for human enamel to be obtained in the perpendicular direction too (Zhang *et al.,* 2014). In terms of direction it might be worth commenting that it is perhaps not surprising the hardness is little different, especially with increasing ceramic content for the same reason as above, i.e. the pore size reduces, and the ceramic wall thickness increases with respect to the size of the indenter head.

In the present study, the hardness of human enamel was determined to be 2.45 GPa. This result is lower than those presented in previous studies which evaluated the hardness for enamel to range from 3 to 5.3 GPa (Cuy *et al.*, 2002; Mahoney *et al.*, 2000; Min *et al.*, 2016; Park *et al.*, 2008; He and Swain, 2007; Xu *et al.*, 1998). This large difference can be the result of the hierarchical structure and anisotropy of the enamel (Ang *et al.*, 2009), use of different hardness machines, different loads (Chuenarrom *et al.*, 2009), different locations and teeth from which the specimens were obtained (Roy and Basu, 2008), and different specimen preparations (Wu *et al.*, 2017).

7.3.2 Simulated toothbrushing

Toothbrushing is essential for removal of plaque and debris in order to contribute to good oral health. During orthodontic treatment, orthodontic attachments and arch wires act as barriers and trap food, which makes maintenance of good oral hygiene more challenging (Jenkins, 1972 ; Rafe *et al.*, 2006; Erbe *et al.*, 2013). The British Dental Association recommendation for individual oral hygiene is toothbrushing at least twice daily for at least two minutes (British Dental Association, 2018). However, toothbrushing can cause hard dental tissue loss (Eisenburger and Addy, 2002) and can cause wear of polymeric orthodontic brackets due to their relatively lower hardness (Zinelis *et al.*, 2005).

In the present study, the toothbrushing regimen mimicked a twice-daily oral hygiene pattern of a two minute toothbrushing cycle on twenty teeth in total. In this study, the force applied was standardised at 200 g, as was toothpaste concentration, brushing

technique and model of brush. Other studies have used loads of 100 g (Takahashi *et al.*, 2013), 170 g (Heintze and Forjanic, 2005) or 500 g (Suzuki *et al.*, 2009) depending on purposes of the studies., for example, higher load (500 g) was used in abrasion studies. The 200 g force was chosen as it simulates the applied force during everyday toothbrushing as an average obtained from the literature (Zero, 1996; Lefever *et al.*, 2012) and because any force higher than that had been shown to be of little significance for plaque removal (McCracken *et al.*, 2003; Van der Weijden and Hioe, 2005). Colgate® Total was chosen as it is a commonly used toothpaste in the UK (Ganss *et al.*, 2009) and an Oral-B manual toothbrush was used due to its standardised shape and previous utilisation (Bellamy *et al.*, 2014). The amount of suspension used in each cycle (25 g dentifrice, 40 g deionised water) was prepared in accordance with the study by Schemehorn *et al.* (2011).

7.3.3 Initial surface roughness before toothbrushing

For dental composite materials, the surface roughness characteristics will depend on factors such as type of monomer, filler content, filler size, filler type and preparation methods (Heintze and Forjanic, 2005; Takahashi *et al.*, 2013; Kamonkhantikul *et al.*, 2014). Surface roughness influences clinical performance, aesthetic characteristics and can affect bacterial accumulation (Voltarelli *et al.*, 2010; Lee *et al.*, 2009; Quirynen *et al.*, 1996; Bollenl *et al.*, 1997). For polymeric orthodontic brackets, surface roughness plays an important role in the discoloration of the bracket caused during clinical use (Leibrock *et al.*, 1997). It is also possible that in orthodontics surface roughness can affect friction (Kusy *et al.*, 1988) and potentially orthodontic tooth movement (Marques *et al.*, 2010;

Liu *et al.*, 2013). Choi *et al.* (2015) found that changes in surface roughness of orthodontic appliances showed a similar pattern to those observed in frictional force. Indeed there are reports in the literature that the clinical use of orthodontic archwires and brackets in the oral environment can increase their surface roughness (Alcock *et al.*, 2009; Mendes *et al.*, 2014).

Currently there is little data on the effect of toothbrushing on the surface roughness of orthodontic bracket materials. In the present study, the roughness parameters assessed were Ra, Rmax, Rp and Rq, as these parameters have been previously used to determine the surface characteristics of orthodontic raw materials by Zinelis *et al.* (2005). The Proscan non-contact profilometre consists of a white light source that transmits white light through a lens and then splits the light beam into a full spectral field (Sleibi *et al.,* 2018). This methodology is non-invasive and utilises the different refractive indices of the components of white light to measure height differences in sample topography.

When looking at the surface roughness results before brushing, the mean Ra value for the dense alumina specimens and PC were 0.84 µm and 0.23 µm respectively, which is lower than that found previously for polycrystalline alumina 2.69 µm and for PC 0.94 to 1.20 µm (Zinelis *et al.*, 2005). However, this might be explained by the use of different measuring methods (contact vs. non-contact surface profilometry as used in the present study) and subsequent specimen preparation procedures. When considering enamel specimens before brushing, the Ra value was found to be 0.09 µm, which is comparable to the values obtained by previous research by de Melo Monteiro *et al.* (2016) (0.05 to

0.07 µm), but lower than the results obtained by Mahardhika *et al.* (2017) (0.16 µm) and by Azevedo *et al.* (2008) (1.18 to 1.50 µm).

The ceramic/polymer interpenetrating phase composite Ra surface roughness values ranged from 0.69 to 1.71 µm, while the Rmax results ranged from 4.02 to 12.74 µm, which corroborates the findings of the study by Grossman *et al.* (2004), who evaluated and compared Ra and Rmax surface roughness values obtained with a profilometer for six aesthetic resin based restorative materials. The Ra results ranged from 0.35 to 1.51 µm, while the Rmax results ranged from 1.60 to 16.1 µm.

7.3.4 Effect of simulated toothbrushing on the surface roughness

When considering the surface roughness values following simulated toothbrushing, all of the materials under test showed an increase in all surface roughness parameters except for the dense alumina. This is in accordance with the findings of other studies (Mahardhika *et al.*, 2017; Bolay *et al.*, 2012; de Melo Monteiro *et al.*, 2016). However, unlike the present study, Heintze and Forjanic (2005) found the roughness of the enamel decreased after simulated toothbrushing, and by as much as 40%. This might be attributed to their use of different sample polishing procedures, brushing regimes, tooth paste and brushing force, for example 170 g versus the 200 g used in the current study.

When looking at the Ra results for the new ceramic/polymer interpenetrating phase composites, the mean difference for surface roughness of any specimen after the simulated toothbrushing ranged from 0.18 to 0.65 µm, which is unlikely to be clinically significant. The roughness observed is likely as a result of the direct contact of the

bristles of the brush with the material surface, as well as the effect of the toothpaste (Dyer *et al.*, 2000). The gradual polishing of the ceramic fraction of the composites, and the more rapid abrasion of the polymer phase might lead to this increase in the material roughness (Figure 7-3). The composites' resistance to wear by toothbrushing is affected by the inorganic filler phase, the resin matrix and the chemical link between these two inorganic and organic phases (Sulong and Aziz, 1990). Heintze and Forjanic (2005) also found that hybrid composite materials showed the highest increase in mean roughness after toothbrushing when compared with 21 other dental materials. Furthermore, Kamonkhantikul *et al.* (2014) evaluated roughness of composite material and their results showed a variable surface roughness increase after toothbrushing, depending on the filler particle size in each material.

For the biomimetic ceramic/polymer interpenetrating phase composites in the present study, the difference in roughness increased after brushing as the ceramic content increased, as can be seen in Figures 7-3, 7-4, 7-5 and 7-6. A possible explanation for this is the unique honeycomb-like microstructure of the biomimetic ceramic/polymer interpenetrating phase composite. Increasing the ceramic content (Figure 7-7) of the initial porous ceramic scaffold leads to smaller pores into which the polymer is forced during fabrication of the composite material. This results in more opportunities for irregularities at the ceramic-polymer interface as the polymer preferentially wears with toothbrushing. The images in Figure 7-7 and 7-8 confirm that the simulated toothbrushing has a greater effect on the softer polymer within ceramic/polymer interpenetrating phase composites. Interestingly, during the initial polishing process of

the specimens prior to testing, the 61.17 vol.% ceramic fraction specimens were the most difficult to polish, in large part due to the higher ceramic content. Perhaps unsurprisingly, with all of the surface roughness measurements (Ra, Rq, Rmax and Rq) for enamel, PC and the 61.17 vol.% Al_2O_3- UDMA-TEGDMA composite, there was a statistically significant difference between the pre and post brushing results, while for the dense alumina there was no statistically significant difference, as can be seen in Figures 7-3, 7-4, 7-5 and 7-6.

Although 50.89 vol.% Al_2O_3-UDMA-TEGDMA and 51.46 vol.% Al_2O_3- PC composite materials contain almost the same amount of ceramic, they showed a different surface roughness change following 2 years simulating toothbrushing. This surface roughness difference shows the significant effect that the polymer type has on the final composite materials. Moreover, when the ceramic contents decreased to 34.20 vol.% for the Al_2O_3-PC interpenetrating phase composites, no statistically significant difference before and after toothbrushing for all the roughness parameters was observed.

For the dense alumina, the surface roughness measures Ra, Rz and Rq did decrease slightly, with toothbrushing and this may be because ceramic is such a hard material that it was instead polished by the toothbrushing resulting in a smoother surface. This decrease in the roughness of dental ceramics after toothbrushing has previously been reported in the literature by Heintze and Forjanic (2005). With the pure polymers it was different. The highest post toothbrushing surface roughness was seen for the pure polymers. For enamel, the surface roughness value also increased to 0.29 μm.

7.3.5 Surface loss after simulated toothbrushing

The characterisation and measurement of hard tissue loss due to the oral environment factors is important in dental research (Imfeld, 1996). This process is significantly important for interpenetrating phase composites (as the experimental composites in the present study) as their surfaces are characterised by hybrid microstructures with irregular peaks and valleys that cannot be easily defined (Wiegand *et al.*, 2007). Toothbrushing has an abrasive effect on the teeth and can result in tooth tissue loss (Meyers *et al.*, 2000; Forbes-Haley *et al.*, 2016). Polymeric orthodontic brackets, such as polycarbonate brackets, are characterised by a low resistance to wear compared to human enamel (Zinelis *et al.*, 2005; Kato *et al.*, 2014).

In the present study all of the specimens showed surface loss following toothbrushing, with pure polymers showing significant surface loss, and enamel and dense alumina showing much less surface loss (Figure 7-9). For the dense alumina, the surface loss was only 0.12 µm and this would support the fact that ceramic is a hard material that is not susceptible to significant wear by toothbrushing. The highest surface loss was observed with the pure polymers, supporting the fact that these materials demonstrate less resistance to wear. For the ceramic/polymer interpenetrating phase composites, as the ceramic volume fraction increased, so the surface loss decreased. This can be explained by the fact that ceramic is much more resistant to surface loss caused by toothbrushing.

7.4 Summary

The hardness, surface roughness and surface loss data for the novel ceramic/polymer interpenetrating phase composites ranged between that of the pure polymers and the dense alumina. Indeed, the values observed for the composites were more comparable to enamel than either of their constituent raw materials. Following abrasion testing the mean difference in surface loss over 2 years of simulated toothbrushing was less than 1.5 µm for any of the ceramic/polymer interpenetrating phase composite specimens. Higher surface hardness and less surface loss after toothbrushing was observed with the higher ceramic content composites. The mean difference surface roughness (Ra) value of any of the ceramic/polymer interpenetrating phase composites over 2 years of simulated toothbrushing ranged from 0.18 to 0.65 µm, which is unlikely to be clinically significant. There is an observed overlap in the results between the various ceramic/polymer interpenetrating phase composite materials. It can be seen that as the ceramic content increased in each composite group, the difference in the roughness values increased. The results of the present study suggest that such exposure to toothbrushing can cause an increase in the variety, type and number of surface irregularities and hence an increase in the material surface roughness.

Chapter 8. Discussion

The primary objective of this study is to produce a biomimetic ceramic/polymer composite material, characterised by a multi-level graded structure of a ceramic component infiltrated with a polymer. Current commercially available dental ceramics and composites are both isotropic and unable to emulate the natural structure of dentine and enamel. The secondary objective is to investigate the mechanical and surface properties of the fabricated composite materials with respect to the ceramic/polymer final volume ratio. An efficient biomimetic ceramic/polymer interpenetrating phase composite material with a modulus of elasticity comparable to dentine, wear behaviour comparable to enamel and reduced brittleness compared to dental ceramics is desirable. The benefits of such a material could include improved orthodontic bonding and debonding, less abrasion of opposing teeth, improved wear resistance and fewer in-service bracket failures.

The approach used in this research to fabricate biomimetic ceramic/polymer composite materials with anisotropy similar to that of natural teeth was freeze-casting. The ceramic material under investigation was alumina and the two polymers were UDMA-TEGDMA and PC. Infiltration of the UDMA-TEGDMA polymer into the ceramic framework was by vacuum impregnation, while heat pressing was used with PC, and laboratory tests were used to investigate the mechanical and surface properties of the fabricated materials.

8.1 Interpenetrating approach

The findings of the literature review (Chapter 2) support the trial to develop and characterise interpenetrating phase composite materials for orthodontic applications. Although previous studies have investigated their use in restorative dentistry and for teaching purposes, no such studies were found that have customised their fabrication for orthodontic use.

Aesthetic orthodontic brackets are becoming ever more popular, such that they are now part of the routine orthodontic armamentarium in the treatment of adult patients (Christensen and Luther, 2015). Aesthetic bracket materials can be divided into two groups: ceramics and polymers. Ceramic brackets are the most popular nowadays as they provide the best aesthetics (Jena *et al.*, 2007). However, they are not without problems, principally a low fracture toughness leading to increased in-service failures, high hardness which can result in iatrogenic damage to opposing teeth (Karamouzos *et al.*, 1997) and also a risk of enamel damage at debond (Jeiroudi, 1991; Årtun, 1997; Karamouzos *et al.*, 1997; Jena *et al.*, 2007; Kitahara-Céia *et al.*, 2008; Eslamian *et al.*, 2011). Polymeric brackets also initially have good aesthetic properties, but suffer from low abrasivity, a tendency to discolour, and creep over time leading to loss of torque transfer (Sadat-Khonsari *et al.*, 2004; Ali *et al.*, 2011; Lee, 2011).

Hybrid aesthetic orthodontic brackets are commercially available, but they comprise two distinct bulk phases separated by a single interface, i.e. a ceramic bracket body and tie wings with a single polymeric bracket base (Kusy, 1998). The main disadvantage of these

brackets is delamination of the polymer base during treatment, which results in longer chairside time as a consequence of the need to replace the brackets, and greater discomfort to patients (Olsen *et al.*, 1997; Elekdag-Turk *et al.*, 2009).

A more recent experimental approach has been to fabricate orthodontic brackets from aesthetic CAD/CAM restorative composite materials. The results showed that the brackets can provide torque transfer comparable to commercially available alumina ceramic brackets, but with improved strength and toughness (Alrejaye *et al.*, 2016). However, the authors used traditional polymer-based composite materials (Paradigm MZ100 and Lava Ultimate, 3M ESPE) and interpenetrating phase ceramic/ceramic composite materials (glass/alumina, Mark II feldspathic porcelain, and zirconia/alumina, In-Ceram YZ, VITA Zahnfabrik). These materials differ from our composite material in their structure and manufacturing method as the composites tested in this study are biomimetic interpenetrating phase ceramic/polymer composite materials.

To fabricate a ceramic/polymer interpenetrating phase composite with a graduated structure, porous ceramic preforms that can be infiltrated with a second phase need to be created. In this study, the aim is to produce a composite consisting of a continuous ceramic phase rather than being randomly distributed in a polymeric phase. In this way it is hoped that both phases could be integrated into each other to create a multi-level structure. This approach would then overcome the delamination problem and low wear resistance of previously adapted hybrid aesthetic orthodontic brackets. In the present work, porous ceramic preforms were produced and subsequently infiltrated with polymer to produce a ceramic/polymer interpenetrating phase composite material.

Previous studies have demonstrated that interpenetrating composite materials can demonstrate mechanical properties comparable to those of human dentine and enamel, with the more flexible polymer phase acting as the toughening material (Coldea *et al.*, 2013; Petrini *et al.*, 2013; Nguyen *et al.*, 2014; Okada *et al.*, 2014).

8.2 Fabrication method

In Chapter 4 an *in vitro* study was presented that evaluated the technique of freeze-casting as the method of fabricating the porous ceramic preforms. Freeze-casting provides the advantages of creating porous scaffolds with tailored porosities, pore morphology and size, open interconnectivity and an anisotropic structure (Scotti and Dunand, 2018). Moreover, porous ceramic preforms produced by freeze-casting could then be infiltrated with a second phase material in order to improve the mechanical properties and make it suitable for use in orthodontics (Petrini *et al.*, 2013).

Ceramics have been used extensively in the construction of aesthetic restorative materials for more than 100 years(Li *et al.*, 2014) and are very popular raw materials for fabricating ceramic orthodontic brackets. Alumina is characterised by being bioinert, providing good aesthetics, stiffness and hardness. It can also form a suspension when mixed with water and therefore produce well-defined microstructures after freeze-casting (Sofie and Dogan, 2001; Deville *et al.*, 2015). Water was used as the suspension medium in this study as it has been used successfully in other studies using freeze-casting (Sofie and Dogan, 2001; Scotti and Dunand, 2018). In addition, not only could the suspensions be easily prepared at room temperature, but the ice crystals formed during

freeze-casting were also lamellar in structure due to the directional freeze-casting, meaning the resulting pores in the ceramic scaffold could potentially be easily infiltrated with a second polymeric phase (Deville *et al.*, 2015; Scotti and Dunand, 2018).

In addition to the water, an additive binder gelatine was used in this study. Structures produced by the combination of gelatine and freeze-casting have previously been reported to result in a unique honeycomb-like structure in the final scaffold (Fukushima *et al.*, 2008; Koch *et al.*, 2003; Fukushima *et al.*, 2014; Matsunaga *et al.*, 2017). The reason for this is probably as a result of the increased resistance the gelatine affords in the aqueous suspension during the freeze-casting process, which prevents the ice crystals created adopting their more usual plate-like or lamellar structure within the ceramic suspension.

The freeze-casting apparatus used in the present study was considered suitable for consistently producing graded porous scaffolds, as the rod temperatures were controlled within a closed system. The ceramic samples were fabricated to a height of 20 mm, which was considered sufficient for structural and mechanical characterisation. A temperature gradient of -10 to +20°C was chosen to produce the biomimetic ceramic/polymer interpenetrating phase composites, which means that the ceramic particles were rejected by the freezing front from the bottom of the sample near the cooling plate to the top (Barr and Luijten, 2010). This set-up resulted in a graduated porous microstructure that could be easily infiltrated with the second, polymer phase. By contrast, homogenous freeze-casting using a uniform temperature across the sample leads to the production of a scaffold with randomly oriented porosity, which would be

more difficult for any second phase to penetrate, thereby limiting its clinical usefulness (Fu *et al.*, 2008) as a result of the effect on the subsequent mechanical properties.

Different volumes of initial solid ceramic loadings were chosen for this study (10, 15, 20, 25, 30 and 35 vol.%). This range was considered to be ideal for the production of porous ceramic scaffolds that could subsequently be infiltrated with polymer (Preiss *et al.*, 2012). The porosity of the freeze-cast preforms was tuned by adjusting the initial solid ceramic loading with the final porosity value being linearly dependent upon the solid loading (Figure 4-7).

8.3 Microstructure

The principal objective of this study was to fabricate a material capable of mimicking natural tooth structure. Teeth are unique in being able to withstand masticatory loading throughout an individual's lifetime. Porous alumina scaffolds were produced by gelation freeze-casting that were characterised by a biomimetic anisotropic honeycomb-like structure. This is thought to be due to the addition of water soluble gelatine to the initial ceramic suspension. SEM images (Figure 4-5) revealed the honeycomb-like cylindrical pores to be of varying size as a result of the ceramic particles being expelled by the freezing front of water molecules. In other words the ceramic particles were gradually packed together between the growing ice crystals in the gelatine-based aqueous ceramic suspension (Fukushima *et al.*, 2008; Deville, 2010).

Such a honeycomb-like structure could be said to mimic to some extent the distribution of the dental organic phase within the inorganic phase seen at the dentine-enamel

junction in natural teeth (Amizuka *et al.*, 1992), and in the outer layer of the enamel (Wang *et al.*, 2012). This structure is thought to provide mechanical properties that are significantly better than those achieved with other scaffold structures such as lamellar and dendritic (Wegst *et al.*, 2010; Scotti and Dunand, 2018). This is thought to be due to the higher interconnected open porosities compared to those typically seen in freeze-cast porous scaffolds using other binders such as Polyvinyl alcohol (Preiss *et al.*, 2012). Previous studies have found that composites with interpenetrating phases and a honeycomb-like microstructure can demonstrate good mechanical and tribological properties, especially in terms of strength and wear, when compared to those with a lamellar structure (Lakes, 1993; Coldea *et al.*, 2013; Fukushima *et al.*, 2014; Long *et al.*, 2014; Zhang *et al.*, 2015).

MicroCT images (Figure 4-6) illustrated a graded growth pattern of the ice crystals starting from the freezing bottom plate to the uppermost porous surface. This phenomenon has previously been reported by other workers in the field (Deville, 2010; Lasalle *et al.*, 2012). Notably, the effect of increasing gelatine concentrations (2.5 to 10 vol.%) only changed the pore structure (Figure 4-2).

8.4 Polymer infiltration

In Chapter 5 the relationship between initial ceramic loading and polymer infiltration was investigated. In the present study UDMA-TEGDMA and PC polymers were used as the organic infiltrated phase since they are widely used in dentistry. The combination of UDMA-TEGDMA was based on the work by Okada *et al.,* (2014). UDMA has also been

previously investigated as a single-phase orthodontic bracket material (Sideridou *et al.*, 2003; Faltermeier *et al.*, 2007a; Krauss *et al.*, 2010), but TEGDMA monomer was used as a low viscosity diluent to promote better infiltration of the ceramic scaffold by the high viscosity UDMA (Floyd and Dickens, 2006). Polymerisation of UDMA and TEGDMA monomer occurred *in situ*. This process depends on free radical addition polymerisation (McCabe and Walls, 2013) yielding a highly cross-linked polymer network. However, such polymerisation is not only associated with volumetric shrinkage (Kleverlaan and Feilzer, 2005), but it also displays a susceptibility to oxygen inhibition leading to premature termination of the reaction and the continued presence of unreacted monomer (Shawkat *et al.*, 2009). Additionally, UDMA is a thermal setting polymer that is characterised by hydrophobicity. This property can result in debonding or weakening of the bond between the inorganic filler and the organic matrix, with a subsequent reduction in the mechanical properties and wear resistance (Peutzfeldt, 1997).

Polycarbonate (PC) is a polymer that has been widely used to fabricate orthodontic brackets (Russell, 2005; Krauss *et al.*, 2010). PC is bio-inert and has good aesthetic properties (Xu *et al.*, 2017). However, single phase PC orthodontic brackets have relatively poor mechanical properties (Kusy, 1998). Despite this, PC, a thermoplastic material (Freitag *et al.*, 1991; Brydson, 1999), was used in this study as an alternative to UDMA-TEGDMA polymer. It was infiltrated into the porous ceramic preforms by applying both heat and pressure.

The heat was necessary in order to reduce the viscosity of PC and allow it to flow more easily into the preform. Application of sufficient pressure was important to ensure

thorough penetration of the polymer into the narrow pores of the ceramic preforms. Too much pressure however would lead to failure of the ceramic preform.

The density of the novel biomimetic ceramic/polymer interpenetrating phase composites was found to change with the initial solid ceramic loading. This is in agreement with previous studies on dental interpenetrating phase composite materials (He and Swain, 2011; Coldea *et al.*, 2013). The density of the fabricated biomimetic ceramic/polymer composites ranged between 1.7 and 3.4 g/cm^3 (Figures 5-15 and 5-16), which is higher than that of feldspathic porcelain (2.5 g/cm^3) commonly used in restorative dentistry (Borba *et al.*, 2011).

8.5 Mechanical properties

The ideal material for use as an orthodontic bracket should provide adequate strength and toughness and with a minimum of surface changes during a course of treatment. Mechanically the material would have to withstand the effects of the bonding and debonding processes and without affecting the tooth to which it was bonded, the presence of the archwires in the bracket slot, the different types of ligation, the forces of mastication and contact with the opposing teeth. It would also be important for the initial aesthetic appearance to be maintained throughout the duration of the treatment.

In Chapter 6 the *in vitro* study investigated the effect of the ceramic/polymer ratio on the mechanical properties namely: compressive strength, flexural strength, elastic modulus and fracture toughness. It would seem that when using the process of gelation freeze-casting it is possible to tailor the desired mechanical properties into the final

ceramic/polymer interpenetrating phase composite. The mechanical properties of the novel biomimetic ceramic/polymer interpenetrating phase composites were found to change with the initial solid ceramic loading, which is in agreement with previous studies on dental interpenetrating phase composite materials (He and Swain, 2011; Coldea *et al.*, 2013).

The compressive strength in the present study ranged from 26.31 to 274.91 MPa (Figures 6-1 and 6-2), which although lower than dense alumina (2358.08 MPa), is higher than that of enamel (62 to 89 MPa), and comparable to that of the dentine (194 to 224 MPa) (Chun *et al.*, 2014). The biomimetic ceramic/polymer composite materials containing more than 30 vol.% ceramic fraction showed lower compressive strength compared to dense alumina and higher strength compared to polymers. Interestingly the interpenetrating nature of the composite lead to the samples maintaining much of their shape after testing to failure. By contrast, the pure alumina samples, although demonstrating the highest compressive strength values, underwent catastrophic and sudden failure at the maximum, fracturing into many small particles. The pure polymers had the lowest compressive strengths and were relatively easily compressed with a resultant flattening and loss of shape.

The flexural strength of the biomimetic ceramic/polymer composite, when the force was applied parallel to the direction of freezing, was found to range from 28.28 to 145.65 MPa when the ceramic volume fraction increased from 18.83 to 61.17 vol.% (Figures 6-3 and 6-4). This would suggest that the greater the inorganic content in the novel composite material, the higher its flexural strength, which is in agreement with previous

studies on dental composite materials (Inoue *et al.*, 1994; Kim *et al.*, 2002). Moreover, these values are higher than those reported for feldspathic porcelain (69 MPa) (Giordano II *et al.*, 1995), slightly higher than traditional dental composite (103 to 107 MPa) (Yao *et al.*, 2014) , but lower than that seen with sintered polycrystalline alumina brackets (280 MPa) (Swartz, 1988). In this study, dense alumina showed a mean flexural strength value of 249.3 ± 72 MPa, and once again underwent catastrophic failure on testing. Similarly the two polymers showed lower flexural strengths and underwent a slow but noticeable deformation on compression testing. The novel biomimetic ceramic/polymer interpenetrating phase composites containing more than 50 vol.% ceramic fraction showed an intermediate flexural strength and again the specimen shape was maintained after testing to failure. This indicates a strengthening mechanism of the ceramic phase by the polymer phase.

The modulus of elasticity describes the rigidity of the material. It was calculated from the results of the three-point bend test and for the novel composites was found to range from 1.48 to 16.56 GPa (Figures 6-5 and 6-6). Although this is much lower than that of relatively pure alumina, 118.50 GPa, these values were higher than those recorded for the polymer used for infiltration (1.17 GPa for UDMA-TEGDMA and 1.50 GPa for PC), and comparable to dentine, 10 to 15 GPa (Kinney *et al.*, 2003). This finding agrees with previous work that showed the modulus of elasticity to fall with increasing ceramic porosity (Asmani *et al.*, 2001).

Both flexural and compressive strength values demonstrated anisotropy dependant on the direction of application of the force relative to the direction of freeze-casting, i.e.

whether it was parallel or perpendicular to the direction of freeze-casting (Figures 6-7 and 6-8). A higher strength was observed when the load was applied perpendicular to the direction of freeze-casting. These results can be attributed to the alignment of the ceramic walls and therefore polymer infiltrate within the composite, which resembles the effect seen with enamel and dentine (Kinney *et al.*, 2003; Miura *et al.*, 2009), and is unlike the pure ceramics or polymers found in currently available monolithic aesthetic orthodontic brackets.

Fracture toughness is the measure of a material's ability to absorb strain energy prior to fracture (Anstis *et al.*, 1981) . The reported fracture toughness values for enamel and dentine are approximately 0.72 to 1.28 and 2.20 to 3.10 MPa.m^{½} respectively (Bajaj and Arola, 2009; Lawn and Lee, 2009; Min *et al.*, 2016). The mean values for the fracture toughness of the biomimetic ceramic/polymer interpenetrating phase composites in the present study ranged between 2.17 MPa.m^{½} and 4.86 MPa.m^{½} (Figures 6-7 and 6-8). Previous studies have reported the fracture toughness of polycrystalline alumina to be in the range of 3.5 to 4.4 MPa.m½ (Gogotsi, 2003; Guazzato *et al.*, 2004a) and for monocrystalline alumina to be 2.1 to 2.5 MPa.m^{½} (Anstis *et al.*, 1981; Iwasa and Brandt, 1986). The importance of fracture toughness, which is related to the force or energy for crack propagation in the case of aesthetic orthodontic brackets, is in the ability of the bracket to resist unwanted in-service failure, and this is most commonly at the tie wing (Kusy, 1988; Scott, 1988). This is because ceramics used for brackets are brittle materials that fail by crack propagation (Scott, 1988; Birnie, 1990), and ceramic brackets have historically shown a tendency for tie wing fracture (Johnson *et al.*, 2005). Once a crack

occurs at the surface of ceramic material, stress concentration increases at the crack tip and the crack propagates in almost a straight path due to lack of interfaces and other energy absorption mechanisms. The addition of a more flexible phase might reduce the stress concentration, lead to crack propagation along a more irregular path and thereby absorb more energy. In this way the fracture toughness is increased. This is the main advantage of composite materials compared to monolithic ceramic materials. The interaction of physical property differences between the different phases and the reduced stress concentration give composites their superior fracture strengths (Moon *et al.*, 2009).

The observed fracture toughness values for the ceramic/polymer interpenetrating phase composites in this study, being at the higher end of values previously reported for the polycrystalline alumina most commonly used in orthodontic brackets, would suggest the tie wings of a bracket made from the freeze-cast composite might be more resistant to in-service failure.

8.6 Surface properties

Surface properties including hardness, roughness and volume loss after simulated toothbrushing were measured and reported in Chapter 7. The relationship between the ceramic/polymer ratio and the hardness, roughness and surface loss following toothbrushing were all investigated. Hardness values of the ceramic/polymer interpenetrating phase composites ranged between 0.99 and 1.62 GPa (Figures 7-1 and 7-2), which is lower than that of enamel (3.43 GPa), Enamic (3.31 GPa) (Min *et al.*, 2016),

zirconia (13.94 GPa) (Zhang *et al.*, 2012), traditional dental composite (0.73 to 1.60 GPa) (El-Safty *et al.*, 2012) and lithium disilicate glass ceramics (10.00 GPa) (Smith *et al.*, 2014).

This would suggest that the ceramic/polymer interpenetrating phase composites produced in this study would be a suitable material for oral use when opposing teeth enamel, as it would lead to less enamel abrasion than presently available orthodontic ceramic brackets. Moreover, the surface hardness values observed were much higher than the currently available polyurethane aesthetic orthodontic brackets, where surface hardness is reported to be between 0.18 and 0.19 GPa (Ali *et al.*, 2011). This would suggest that aesthetic brackets made from the novel ceramic/polymer infiltrated composite would show much improved wear resistance over currently available polymeric aesthetic brackets. However, having a lower surface hardness than stainless-steel and nickel titanium alloys, used as bracket and archwire materials, might lead to higher rates of wear and therefore insufficient slot wire engagement (Eliades and Bourauel, 2005). The fact that teeth move with currently available polymeric brackets would suggest this would be equally effective in the case of brackets made from this novel ceramic/polymer interpenetrating phase composites.

In the present study all samples were brushed for 2 hrs and 50 mins to simulate normal toothbrushing over an average 2 year course of orthodontic treatment. The surface roughness values were evaluated before and after toothbrushing (Figures 7-3, 7-4, 7-5 and 7-6). The results illustrated that the pure dense alumina blocks showed the least change in the surface roughness, as might be expected.

While the highest changes were observed with the pure PC and UDMA-TEGDMA specimens. The novel biomimetic ceramic/polymer composite material showed surface properties change values that were the closest to those of enamel. With respect to surface loss, pure alumina and enamel were the most resistant to loss, while the UDMA-TEGDMA and PC specimens demonstrated the greatest surface loss (Figures 7-9). Once again, the novel biomimetic ceramic/polymer composites showed characteristics that more closely resembled enamel rather than either the pure ceramic or the polymer.

In summary, highly porous ceramic materials with interconnected pores were fabricated and subsequently infiltrated with a polymer to produce ceramic/polymer interpenetrating phase composites that could potentially be useful in orthodontic applications. The microstructural and mechanical properties of these composites can be modified by changing the initial ceramic solid loading and subsequent polymer type. The novel composite materials produced were found to have an interpenetrating structure of organic polymer and inorganic ceramic phases in an anisotropic form. Changes to the processing parameters were found to have an effect on the physical and mechanical properties of these materials. The final composites were found to possess mechanical properties part-way between those of enamel and pure alumina at one end and polymers at the other. They certainly would appear to show promise as potential aesthetic orthodontic bracket materials.

Chapter 9. Conclusions and further work

9.1 Conclusions

The results from this study provide compelling *in vitro* evidence for the novel ceramic/polymer interpenetrating phase composites, produced using the technique of freeze-casting, to be potential orthodontic bracket materials. They comprise an interconnected network of inorganic and organic phases and represent a relatively new and promising concept for use in aesthetic orthodontic brackets. The polymer rich surface could aid in safe bonding and debonding, whilst the relatively ceramic rich surface will provide wear resistance. The combination of the two materials in the bulk of the bracket will reduce in-service failures and eliminate creep. The ultimate aim would be to more closely imitate the structural properties and the mechanical behaviour of natural teeth.

By the use of gelatine freeze-casting, a carefully controlled freezing gradient and subsequent processing through the four consecutive steps (i.e. ceramic suspension preparation, ice crystal formation, sublimation and finally sintering), it was possible to fabricate a graded porous ceramic scaffold with an aligned microstructure. The result was unidirectional interconnected pores in 3D honeycomb-like structure along the whole body of the scaffold, as illustrated by SEM and MicroCT imaging. The role of different initial solid ceramic loadings on the scaffold microstructure was determined. The gelatine concentration in the initial gelatine/alumina suspension played an important role in defining subsequent preform structure and porosity. These findings

were corroborated by SEM and MicroCT imaging. Micro-CT images also confirmed good interpenetration of the polymer phase into the pores of the ceramic preform (Figure 5-10 and 5-12). Resultant anisotropy was achieved in the ceramic/polymer composites. There was an increase in porosity and a corresponding decrease in ceramic content by volume through the length of the preforms, progressing from the ceramic rich layer (bottom level) to the polymer rich layer (top level).

As might be expected, the observed density of the ceramic/polymer interpenetrating phase composites increased linearly with an increase in initial ceramic solid loading. There was also a correlation between the mechanical properties and the final ceramic/polymer volumes of the interpenetrating phase composites. The compressive strength of the final ceramic/polymer composites fabricated with initial solid ceramic loading of 30 vol.% was the highest when compared to other volumes of ceramic. However, the flexural strengths and the modulus of elasticity of the composite material showed a relative increase when ceramic volume fractions were increased. Fracture toughness properties were higher when ceramic/polymer interpenetrating phase composites with 50 vol.% ceramic ratios were measured. Initial results show that ceramic/polymer interpenetrating phase composites with a ceramic ratio of 50 vol.% show the greatest promise for the potential use as aesthetic orthodontic brackets.

The hardness, surface roughness and surface loss measurements of the interpenetrating phase composites were observed to be part way between those of the pure polymers and the pure alumina, and were more comparable to those of enamel.

To date there have been no reports regarding the use of the gelatine freeze-casting technique for the fabrication of biomimetic composite materials for use as aesthetic orthodontic brackets.

9.2 Further work

The novel ceramic/polymer interpenetrating phase composites produced in this research show great promise as aesthetic orthodontic bracket materials. Further research to optimise their properties might include:

1. An investigation into methods of improving polymer penetration into the ceramic scaffold. This might include alterations in the constituent ratios of UDMA-TEGDMA to alter the viscosity. Similarly, in the case of PC, penetration could be investigated by further alterations in the pressure/temperature conditions in the hot-pressing technique. The use of thermal and light polymerisation could also be studied.
2. Although mechanical properties of the ceramic/polymer interpenetrating phase composites were investigated in this research, it would also be worth investigating the optical properties in both the short and longer term. This would include colour stability. Aesthetic brackets would be expected to have an in-service life of approximately two years, during which time they are exposed to the oral environment. Therefore, they are exposed to changes in temperature and humidity, and ranging from dry to total immersion. The effect of saliva, intra oral microbes and different foodstuffs could also therefore be studied.
3. The ability to bond to human enamel and in particular the ease of debond could be investigated along with the fracture characteristics of the final ceramic/polymer interpenetrating phase composite.

4. The examination of the fatigue life of the novel ceramic/polymer interpenetrating phase composites is very important factor affecting the survival of the composite as an orthodontic bracket material as these materials will be exposed to thermocycling in an aggressive saliva environment in the oral cavity, leading to a stress development and drop in strength properties. Dynamic and static fatigue experiments can be performed in dry and wet environments *in vitro* with different loading cycles at different rates over time and the subsequent strength and crack growth can be then calculated.
5. An evaluation of friction that can be produced when the ceramic/polymer interpenetrating phase composites are in contact with different types of arch wires should be determined so that the appropriate force to acquire the optimal tooth movement during sliding mechanics in the oral cavity can be predicted. The use an Instron universal testing machine to move these ceramic/polymer interpenetrating phase composites along an arch wires with different sizes and material and verify their behaviour in vitro is recommended.
6. The ability of the novel ceramic/polymer interpenetrating phase composites to maintain morphologic integrity after application of orthodontic force should be evaluated along with the resistance to deformation due to torsional force application. This can be achieved by subjecting brackets produced from the ceramic/polymer interpenetrating phase composites to torque, using a rectangular stainless steel archwire and subsequently the moments and degrees of torsion necessary to fracture the brackets will be determined and compared with those of commercially available orthodontic brackets.

References

Abanto-Bueno, J. & Lambros, J. 2002. Investigation of crack growth in functionally graded materials using digital image correlation. *Engineering Fracture Mechanics,* 69**,** 1695-1711.

Aird, J. & Durning, P. 1987. Fracture of polycarbonate edgewise brackets: a clinical and SEM study. *British Journal of Orthodontics,* 14**,** 191-195.

Aknin, P. C.; Nanda, R. S.; Duncanson, M. G.; Currier, G. F. & Sinha, P. K. 1996. Fracture strength of ceramic brackets during arch wire torsion. *American Journal of Orthodontics and Dentofacial Orthopedics,* 109**,** 22-27.

Al-Omiri, M. K. & Abu Alhaija, E. S. 2006. Factors affecting patient satisfaction after orthodontic treatment. *Angle Orthodontist,* 76**,** 422-431.

Al-Radha, A. S. D.; Dymock, D.; Younes, C. & O'Sullivan, D. 2012. Surface properties of titanium and zirconia dental implant materials and their effect on bacterial adhesion. *Journal of Dentistry*, 40, 149-153.

Albakry, M.; Guazzato, M. & Swain, M. V. 2003. Biaxial flexural strength, elastic moduli, and x-ray diffraction characterization of three pressable all-ceramic materials. *Journal of Prosthetic Dentistry,* 89**,** 374-380.

Alcock, J. P.; Barbour, M. E.; Sandy, J. R. & Ireland, A. J. 2009. Nanoindentation of orthodontic archwires: The effect of decontamination and clinical use on hardness, elastic modulus and surface roughness. *Dental Materials,* 25**,** 1039-1043.

Ali, O.; Makou, M.; Papadopoulos, T. & Eliades, G. 2011. Laboratory evaluation of modern plastic brackets. *European Journal of Orthodontics,* 34**,** 595-602.

Alkire, R. G.; Bagby, M. D.; Gladwin, M. A. & Kim, H. 1997. Torsional creep of polycarbonate orthodontic brackets. *Dental Materials,* 13**,** 2-6.

Alrejaye, N.; Pober, R. & Giordano II, R. 2016. Torsional strength of computer-aided design/computer-aided manufacturing–fabricated esthetic orthodontic brackets. *Angle Orthodontist,* 87**,** 125-130.

Alt, V.; Hannig, M.; Wöstmann, B. & Balkenhol, M. 2011. Fracture strength of temporary fixed partial dentures: CAD/CAM versus directly fabricated restorations. *Dental Materials,* 27**,** 339-347.

Amitay–Sadovsky, E. & Wagner, H. D. 1999. Hardness and Young's modulus of transcrystalline polypropylene by Vickers and Knoop microindentation. *Journal of Polymer Science Part B: Polymer Physics,* 37**,** 523-530.

Amizuka, N.; Uchida, T.; Fukae, M.; Yamada, M. & Ozawa, H. 1992. Ultrastructural and immunocytochemical studies of enamel tufts in human permanent teeth. *Archives of Histology and Cytology,* 55**,** 179-190.

An, Y.; Han, J.; Zhang, X.; Han, W.; Cheng, Y.; Hu, P. & Zhao, G. 2016. Bioinspired high toughness graphene/ZrB2 hybrid composites with hierarchical architectures spanning several length scales. *Carbon,* 107**,** 209-216.

Ang, S. F.; Scholz, T.; Klocke, A. & Schneider, G. A. 2009. Determination of the elastic/plastic transition of human enamel by nanoindentation. *Dental Materials,* 25**,** 1403-1410.

Angolkar, P. V.; Kapila, S.; Duncanson, M. G. & Nanda, R. S. 1990. Evaluation of friction between ceramic brackets and orthodontic wires of four alloys. *American Journal of Orthodontics and Dentofacial Orthopedics,* 98**,** 499-506.

Anstis, G.; Chantikul, P.; Lawn, B. R. & Marshall, D. 1981. A critical evaluation of indentation techniques for measuring fracture toughness: I, direct crack measurements. *Journal of the American Ceramic Society,* 64**,** 533-538.

Arabi, N. & Zamanian, A. 2013. Effect of cooling rate and gelatin concentration on the microstructural and mechanical properties of ice template gelatin scaffolds. *Biotechnology and Applied Biochemistry,* 60**,** 573-579.

Arash, V.; Rabiee, M.; Rakhshan, V.; Khorasani, S. & Sobouti, F. 2015. In vitro evaluation of frictional forces of two ceramic orthodontic brackets versus a stainless steel bracket in combination with two types of archwires. *Journal of Orthodontic Science,* 4**,** 42-46.

Arici, N.; Akdeniz, B. S. & Arici, S. 2015. Comparison of the frictional characteristics of aesthetic orthodontic brackets measured using a modified in vitro technique. *Korean Journal of Orthodontics,* 45**,** 29-37.

Arici, S. & Regan, D. 1997. Alternatives to ceramic brackets: the tensile bond strengths of two aesthetic brackets compared ex vivo with stainless steel foil-mesh bracket bases. *British Journal of Orthodontics,* 24**,** 133-138.

Årtun, J. 1997. A post-treatment evaluation of multibonded ceramic brackets in orthodontics. *European Journal of Orthodontics,* 19**,** 219-228.

Asmani, M.; Kermel, C.; Leriche, A. & Ourak, M. 2001. Influence of porosity on Young's modulus and Poisson's ratio in alumina ceramics. *Journal of the European Ceramic Society,* 21**,** 1081-1086.

Asmussen, E. & Peutzfeldt, A. 1990. Mechanical properties of heat treated restorative resins for use in the inlay/onlay technique. *European Journal of Oral Sciences,* 98**,** 564-567.

Asmussen, E. & Peutzfeldt, A. 1998. Influence of UEDMA, BisGMA and TEGDMA on selected mechanical properties of experimental resin composites. *Dental Materials,* 14**,** 51-56.

ASTM, I. 2011. Standard Test Method for Measurement of Fracture Toughness1. *In.*: American Society for Testing and Materials.

ASTM, I. 2016. Standard Test Methods for Determination of Water Absorption and Associated Properties by Vacuum Method for Pressed Ceramic Tiles and Glass Tiles and Boil Method for Extruded Ceramic Tiles and Non-tile Fired Ceramic Whiteware Products1. *In: C373 − 16´1.*

Azevedo, A. M. d.; Panzeri, H.; Prado, C. J. d.; De-Mello, J. D. B.; Soares, C. J. & Fernandes-Neto, A. J. 2008. Assessment in vitro of brushing on dental surface roughness alteration by laser interferometry. *Brazilian Oral Research,* 22**,** 11-17.

Azzeh, E. & Feldon, P. J. 2003. Laser debonding of ceramic brackets: a comprehensive review. *American Journal of Orthodontics and Dentofacial Orthopedics,* 123**,** 79-83.

Bajaj, D. & Arola, D. D. 2009. On the R-curve behavior of human tooth enamel. *Biomaterials,* 30**,** 4037-4046.

Bajaj, D.; Nazari, A.; Eidelman, N. & Arola, D. D. 2008. A comparison of fatigue crack growth in human enamel and hydroxyapatite. *Biomaterials,* 29**,** 4847-4854.

Balkenhol, M.; Mautner, M. C.; Ferger, P. & Wöstmann, B. 2008. Mechanical properties of provisional crown and bridge materials: chemical-curing versus dual-curing systems. *Journal of Dentistry,* 36**,** 15-20.

Banks, P.; Elton, V.; Jones, Y.; Rice, P.; Derwent, S. & Odondi, L. o. 2010. The use of fixed appliances in the UK: a survey of specialist orthodontists. *Journal of Orthodontics,* 37**,** 43-55.

Barg, S.; Koch, D. & Grathwohl, G. 2009. Processing and properties of graded ceramic filters. *Journal of the American Ceramic Society,* 92**,** 2854-2860.

Barr, S. A. & Luijten, E. 2010. Structural properties of materials created through freeze casting. *Acta Materialia,* 58**,** 709-715.

Baysan, A.; Sleibi, A.; Ozel, A. & Anderson., P. 2018. The quantification of surface roughness on root caries using Noncontact Optical Profilometry—An *in vitro* study. *Lasers in Dental Science,* 2, 229-237.

Bazakidou, E.; Nanda, R. S.; Duncanson Jr, M. G. & Sinha, P. 1997. Evaluation of frictional resistance in esthetic brackets. *American Journal of Orthodontics and Dentofacial Orthopedics,* 112**,** 138-144.

Bellamy, P. G.; Harris, R.; Date, R. F.; Mussett, A. J.; Manly, A.; Barker, M. L.; Hellin, N. & West, N. X. 2014. In situ clinical evaluation of a stabilised, stannous fluoride dentifrice. *International Dental Journal,* 64**,** 43-50.

Bergström, K.; Halling, A. & Wilde, B. 1998. Orthodontic care from the patients' perspective: perceptions of 27-year-olds. *European Journal of Orthodontics,* 20**,** 319-329.

Best, A. D.; Shroff, B.; Carrico, C. K. & Lindauer, S. J. 2016. Treatment management between orthodontists and general practitioners performing clear aligner therapy. *Angle Orthodontist,* 87**,** 432-439.

Beun, S.; Glorieux, T.; Devaux, J.; Vreven, J. & Leloup, G. 2007. Characterization of nanofilled compared to universal and microfilled composites. *Dental Materials,* 23**,** 51-59.

Birnie, D. 1990. Ceramic brackets. *British Journal of Orthodontics,* 17**,** 71-75.

Bishara, S. E. 2000. Ceramic brackets and the need to develop national standards. *American Journal of Orthodontics and Dentofacial Orthopedics,* 117**,** 595-597.

Bishara, S. E. & Fehr, D. E. 1997. Ceramic brackets: something old, something new, a review. *Seminars in Orthodontics,* 3**,** 178-88.

Bishara, S. E.; Fehr, D. E. & Jakobsen, J. R. 1993. A comparative study of the debonding strengths of different ceramic brackets, enamel conditioners, and adhesives. *American Journal of Orthodontics and Dentofacial Orthopedics,* 104**,** 170-179.

Bishara, S. E.; Fonseca, J. M.; Fehr, D. E. & Boyer, D. B. 1994. Debonding forces applied to ceramic brackets simulating clinical conditions. *Angle Orthodontist,* 64**,** 277-282.

Bishara, S. E.; Olsen, M. E.; VonWald, L. & Jakobsen, J. R. 1999. Comparison of the debonding characteristics of two innovative ceramic bracket designs. *American Journal of Orthodontics and Dentofacial Orthopedics,* 116**,** 86-92.

Bishara, S. E.; Ortho, D.; Olsen, M. E. & VonWald, L. 1997. Evaluation of debonding characteristics of a new collapsible ceramic bracket. *American Journal of Orthodontics and Dentofacial Orthopedics,* 112**,** 552-559.

Bishara, S. E. & Trulove, T. S. 1990a. Comparisons of different debonding techniques for ceramic brackets - an *in vitro* study .1. Background and methods. *American Journal of Orthodontics and Dentofacial Orthopedics,* 98**,** 145-153.

Bishara, S. E. & Trulove, T. S. 1990b. Comparisons of different debonding techniques for ceramic brackets: An in vitro study: Part II. Findings and clinical implications. *American Journal of Orthodontics and Dentofacial Orthopedics,* 98**,** 263-273.

Blalock, K. A. & Powers, J. M. 1995. Retention capacity of the bracket bases of new esthetic orthodontic brackets. *American Journal of Orthodontics and Dentofacial Orthopedics,* 107**,** 596-603.

Bolay, S.; Cakir, F. Y. & Gurgan, S. 2012. Effects of toothbrushing with fluoride abrasive and whitening dentifrices on both unbleached and bleached human enamel surface in terms of roughness and hardness: An *in vitro* study. *Journal of Contemporry Dental Practice,* 13**,** 584-9.

Bollenl, C. M.; Lambrechts, P. & Quirynen, M. 1997. Comparison of surface roughness of oral hard materials to the threshold surface roughness for bacterial plaque retention: a review of the literature. *Dental Materials,* 13**,** 258-269.

Borba, M.; Cesar, P. F.; Griggs, J. A. & Della Bona, A. 2011. Adaptation of all-ceramic fixed partial dentures. *Dental Materials,* 27**,** 1119-1126.

Bordeaux, J. M.; Moore, R. N. & Bagby, M. D. 1994. Comparative evaluation of ceramic bracket base designs. *American Journal of Orthodontics and Dentofacial Orthopedics,* 105**,** 552-560.

Bos, A.; Hoogstraten, J. & Prahl-Andersen, B. 2003. Expectations of treatment and satisfaction with dentofacial appearance in orthodontic patients. *American Journal of Orthodontics and Dentofacial Orthopedics,* 123**,** 127-132.

Bouville, F.; Maire, E.; Meille, S.; Van de Moortele, B.; Stevenson, A. J. & Deville, S. 2014. Strong, tough and stiff bioinspired ceramics from brittle constituents. *Nature Materials,* 13**,** 508-514.

Boyd, R. L. 2008. Esthetic orthodontic treatment using the Invisalign appliance for moderate to complex malocclusions. *Journal of Dental Education,* 72**,** 948-967.

Boyd, R. L.; Oh, H.; Fallah, M. & Vlaskalic, V. 2006. An update on present and future considerations of aligners. *Journal of the California Dental Association,* 34**,** 793-805.

Braden, M. & Davy, K. 1986. Water absorption characteristics of some unfilled resins. *Biomaterials,* 7**,** 474-475.

Braly, A.; Darnell, L.; Mann, A.; Teaford, M. & Weihs, T. 2007. The effect of prism orientation on the indentation testing of human molar enamel. *Archives of Oral Biology,* 52**,** 856-860.

Brantley, W. & Eliades, T. 2001. *Orthodontic Materials- Scientific and Clinical Aspects*, New York: Thieme Stuttgart.

British Dental Association. 2018. *Myth busters on brushing your teeth* [Online]. Available: https://bda.org/public/myth-busters-on-brushing-teeth [Accessed 21/03 2018].

British Orthodontic Society, B. 2018. *Public-Patients/Orthodontics-for-Children-Teens/Treatment-brace-types/Fixed-appliances/Lingual.* [Online]. Available: https://www.bos.org.uk/Public-Patients/Orthodontics-for-Children-Teens/Treatment-brace-types/Fixed-appliances/Lingual [Accessed 18/01/2019 2018].

Britton, J. C.; Mcinnes, P.; Weinberg, R.; Ledoux, W. R. & Retief, D. H. 1990. Shear bond strength of ceramic orthodontic brackets to enamel. *American Journal of Orthodontics and Dentofacial Orthopedics,* 98**,** 348-353.

Brydson, J. A. 1999. *Plastics Materials*, Elsevier.

BSI 2007. Advanced technical ceramics. Mechanical properties of monolithic ceramics at room temperature. Vickers, Knoop and Rockwell superficial hardness. *In*.: BSI.

BSI 2008. Dentistry. Ceramic materials.

Burrow, S. J. 2009. Friction and resistance to sliding in orthodontics: a critical review. *American Journal of Orthodontics and Dentofacial Orthopedics,* 135**,** 442-447.

Buzzitta, V. A. J.; Hallgren, S. E. & Powers, J. M. 1982. Bond strength of orthodontic direct-bonding cement-bracket systems as studied *in vitro*. *American Journal of Orthodontics and Dentofacial Orthopedics,* 81**,** 87-92.

Cacciafesta, V.; Sfondrini, M. F.; Ricciardi, A.; Scribante, A.; Klersy, C. & Auricchio, F. 2003. Evaluation of friction of stainless steel and esthetic self-ligating brackets in various bracket-archwire combinations. *American Journal of Orthodontics and Dentofacial Orthopedics,* 124**,** 395-402.

Campbell, S. D.; Pelletier, L. B.; Pober, R. L. & Giordano, R. A. 1995. Dimensional and formation analysis of a restorative ceramic and how it works. *Journal of Prosthetic Dentistry,* 74**,** 332-340.

Carrion-Vilches, F. J.; Bermudez, M.-D. & Fructuoso, P. 2015. Static and kinetic friction force and surface roughness of different archwirebracket sliding contacts. *Dental Materials Journal,* 34**,** 648-653.

Cedro, M. K.; Moles, D. R. & Hodges, S. J. 2010. Adult orthodontics—who's doing what?. *Journal of Orthodontics,* 37**,** 107-117.

Cesarano, J.; Aksay, I. A. & Bleier, A. 1988. Stability of aqueous α ‐ Al2O3 suspensions with poly (methacrylic acid) polyelectrolyte. *Journal of the American Ceramic Society,* 71**,** 250-255.

Chaiyabutr, Y.; Giordano, R. & Pober, R. 2009. The effect of different powder particle size on mechanical properties of sintered alumina, resin ‐ and glass ‐ infused alumina. *Journal of Biomedical Materials Research Part B: Applied Biomaterials,* 88**,** 502-508.

Chan, Y.; Ngan, A. & King, N. 2011. Nano-scale structure and mechanical properties of the human dentine–enamel junction. *Journal of Mechanical Behavior of Biomedical Materials,* 4**,** 785-795.

Chen, P.-Y.; McKittrick, J. & Meyers, M. A. 2012. Biological materials: Functional adaptations and bioinspired designs. *Progress in Materials Science,* 57**,** 1492-1704.

Chen, P. Y.; Lin, A. Y. M.; Lin, Y. S.; Seki, Y.; Stokes, A. G.; Peyras, J.; Olevsky, E. A.; Meyers, M. A. & McKittrick, J. 2008. Structure and mechanical properties of selected biological materials. *Journal of the Mechanical Behavior of Biomedical Materials,* 1**,** 208-226.

Cheng, M.-q.; Wahafu, T.; Jiang, G.-f.; Liu, W.; Qiao, Y.-q.; Peng, X.-c.; Cheng, T.; Zhang, X.-l.; He, G. & Liu, X.-y. 2016. A novel open-porous magnesium scaffold with controllable microstructures and properties for bone regeneration. *Scientific Reports,* 6**,** 24134.

Choi, S.-H.; Kang, D.-Y. & Hwang, C. J. 2013. Surface roughness of three types of modern plastic bracket slot floors and frictional resistance. *Angle Orthodontist,* 84**,** 177-183.

Choi, S.; Hwang, E. Y.; Park, H. K. & Park, Y. G. 2015. Correlation between frictional force and surface roughness of orthodontic archwires. *Scanning,* 37**,** 399-405.

Christel, M., Heller, Torre , Peille 1989. Mechanical properties and short term in vivo evaluation of yttrium-oxide-partially-stabilized zirconia. *Journal of Biomedical Materials Research,* 23**,** 4-61.

Christensen, L. & Luther, F. 2015. Adults seeking orthodontic treatment: expectations, periodontal and TMD issues. *British Dental Journal,* 218**,** 111-117.

Chuenarrom, C.; Benjakul, P. & Daosodsai, P. 2009. Effect of indentation load and time on Knoop and Vickers microhardness tests for enamel and dentin. *Materials Research,* 12**,** 473-476.

Chun, K.; Choi, H. & Lee, J. 2014. Comparison of mechanical property and role between enamel and dentin in the human teeth. *Journal of Dental Biomechanics,* 5.

Clements, K. M.; Bollen, A.-M.; Huang, G.; King, G.; Hujoel, P. & Ma, T. 2003. Activation time and material stiffness of sequential removable orthodontic appliances. Part

2: dental improvements. *American Journal of Orthodontics and Dentofacial Orthopedics,* 124**,** 502-508.

Coldea, A.; Swain, M. V. & Thiel, N. 2013. Mechanical properties of polymer-infiltrated-ceramic-network materials. *Dental Materials,* 29**,** 419-426.

Creekmore, T. 1989. Lingual orthodontics—its renaissance. *American Journal of Orthodontics and Dentofacial Orthopedics,* 96**,** 120-137.

Crooks, M.; Hood, J. & Harkness, M. 1997. Thermal debonding of ceramic brackets: an in vitro study. *American Journal of Orthodontics and Dentofacial Orthopedics,* 111**,** 163-172.

Cunningham, S. J.; Gilthorpe, M. S. & Hunt, N. P. 2000. Are orthognathic patients different?. *European Journal of Orthodontics,* 22**,** 195-202.

Cuy, J. L.; Mann, A. B.; Livi, K. J.; Teaford, M. F. & Weihs, T. P. 2002. Nanoindentation mapping of the mechanical properties of human molar tooth enamel. *Archives of Oral Biology,* 47**,** 281-291.

de Hazan, Y. 2012. Porous ceramics, ceramic/polymer, and metal‐doped ceramic/polymer nanocomposites via freeze casting of photo‐curable colloidal fluids. *Journal of the American Ceramic Society,* 95**,** 177-187.

de Melo Monteiro, G. Q.; de Oliveira, I. L. M.; de Brito, O. F. F.; Guedes, B. P.; de Amorim, M. S. M. L. & Maia, A. M. A. 2016. Chromatic and surface alterations in enamel subjected to brushing with desensitizing whitening toothpaste. *European Journal of General Dentistry,* 5**,** 115-121.

De Santis, R.; Mollica, F.; Prisco, D.; Rengo, S.; Ambrosio, L. & Nicolais, L. 2005. A 3D analysis of mechanically stressed dentin-adhesive-composite interfaces using X-ray micro-CT. *Biomaterials,* 26**,** 257-270.

Della Bona, A.; Corazza, P. H. & Zhang, Y. 2014. Characterization of a polymer-infiltrated ceramic-network material. *Dental Materials,* 30**,** 564-569.

Deville, S. 2008. Freeze-casting of porous ceramics: A review of current achievements and issues. *Advanced Engineering Materials,* 10**,** 155-169.

Deville, S. 2010. Freeze-Casting of Porous Biomaterials: Structure, Properties and Opportunities. *Materials,* 3**,** 1913-1927.

Deville, S. 2013. Ice-templating, freeze casting: Beyond materials processing. *Journal of Materials Research,* 28**,** 2202-2219.

Deville, S.; Maire, E.; Lasalle, A.; Bogner, A.; Gauthier, C.; Leloup, J. & Guizard, C. 2009. In Situ X-Ray Radiography and Tomography Observations of the Solidification of Aqueous Alumina Particle Suspensions-Part I: Initial Instants. *Journal of the American Ceramic Society,* 92**,** 2489-2496.

Deville, S.; Maire, E.; Lasalle, A.; Bogner, A.; Gauthier, C.; Leloup, J. & Guizard, C. 2010. Influence of particle size on ice nucleation and growth during the ice‐templating process. *Journal of the American Ceramic Society,* 93**,** 2507-2510.

Deville, S.; Meille, S. & Seuba, J. 2015. A meta-analysis of the mechanical properties of ice-templated ceramics and metals. *Science and Technology of Advanced Materials,* 16**,** 043501.

Deville, S.; Saiz, E.; Nalla, R. K. & Tomsia, A. P. 2006a. Freezing as a path to build complex composites. *Science,* 311**,** 515-518.

Deville, S.; Saiz, E. & Tomsia, A. P. 2006b. Freeze casting of hydroxyapatite scaffolds for bone tissue engineering. *Biomaterials,* 27**,** 5480-5489.

Deville, S.; Saiz, E. & Tomsia, A. P. 2007. Ice-templated porous alumina structures. *Acta Materialia,* 55**,** 1965-1974.

Diamond, S. 2000. Mercury porosimetry: an inappropriate method for the measurement of pore size distributions in cement-based materials. *Cement and Concrete Research*, 30**,** 1517-1525.

Ding, S.; Zeng, Y. P. & Jiang, D. 2007. Fabrication of mullite ceramics with ultrahigh porosity by gel freeze drying. *Journal of the American Ceramic Society,* 90**,** 2276-2279.

Djeu, G.; Shelton, C. & Maganzini, A. 2005. Outcome assessment of Invisalign and traditional orthodontic treatment compared with the American Board of Orthodontics objective grading system. *American Journal of Orthodontics and Dentofacial Orthopedics,* 128**,** 292-298.

Dobrin, R.; Kamel, I. & Musich, D. 1975. Load-deformation characteristics of polycarbonate orthodontic brackets. *American Journal of Orthodontics,* 67**,** 24-33.

Douglass, J. B. 1989. Enamel wear caused by ceramic brackets. *American Journal of Orthodontics and Dentofacial Orthopedics,* 95**,** 96-98.

Dyer, D.; Addy, M. & Newcombe, R. 2000. Studies in vitro of abrasion by different manual toothbrush heads and a standard toothpaste. *Journal of Clinical Periodontology,* 27**,** 99-103.

Eisenburger, M. & Addy, M. 2002. Erosion and attrition of human enamel in vitro part I: interaction effects. *Journal of Dentistry,* 30**,** 341-347.

El-Safty, S.; Akhtar, R.; Silikas, N. & Watts, D. 2012. Nanomechanical properties of dental resin-composites. *Dental Materials,* 28**,** 1292-1300.

Elekdag-Turk, S.; Isci, D.; Ozkalayci, N. & Turk, T. 2009. Debonding characteristics of a polymer mesh base ceramic bracket bonded with two different conditioning methods. *European Journal of Orthodontics,* 31**,** 84-89.

Eliades, T. 2007. Orthodontic materials research and applications: Part 2. Current status and projected future developments in materials and biocompatibility. *American Journal of Orthodontics and Dentofacial Orthopedics,* 131**,** 253-262.

Eliades, T. & Bourauel, C. 2005. Intraoral aging of orthodontic materials: the picture we miss and its clinical relevance. *American Journal of Orthodontics and Dentofacial Orthopedics,* 127**,** 403-412.

Erbe, C.; Klukowska, M.; Tsaknaki, I.; Timm, H.; Grender, J. & Wehrbein, H. 2013. Efficacy of 3 toothbrush treatments on plaque removal in orthodontic patients assessed with digital plaque imaging: A randomized controlled trial. *American Journal of Orthodontics and Dentofacial Orthopedics,* 143**,** 760-766.

Erdogan, F. & Joseph, P. F. 1989. Toughening of ceramics through crack bridging by ductile particles. *Journal of the American Ceramic Society,* 72**,** 262-270.

Eslamian, L.; Borzabadi-Farahani, A.; Mousavi, N. & Ghasemi, A. 2011. A comparative study of shear bond strength between metal and ceramic brackets and artificially aged composite restorations using different surface treatments. *European Journal of Orthodontics,* 34**,** 610-617.

Evans, A. G. 1978. A general approach for the statistical analysis of multiaxial fracture. *Journal of the American Ceramic Society,* 61**,** 302-308.

Facenda, J. C.; Borba, M. & Corazza, P. H. 2018. A literature review on the new polymer‐infiltrated ceramic‐network material (PICN). *Journal of Esthetic and Restorative Dentistry*.

Faltermeier, A.; Behr, M. & Mossig, D. 2007a. In vitro colour stability of aesthetic brackets. *European Journal of Orthodontics,* 29**,** 354-358.

Faltermeier, A.; Rosentritt, M.; Faltermeier, R. & Müßig, D. 2007b. Influence of fibre and filler reinforcement of plastic brackets: an in vitro study. *European Journal of Orthodontics,* 29**,** 304-309.

Feldner, J. C.; Sarkar, N. K.; Sheridan, J. J. & Lancaster, D. M. 1994. *In vitro* torque-deformation characteristics of orthodontic polycarbonate brackets *American Journal of Orthodontics and Dentofacial Orthopedics,* 106**,** 265-272.

Feldon, P. J.; Murray, P. E.; Burch, J. G.; Meister, M. & Freedman, M. A. 2010. Diode laser debonding of ceramic brackets. *American Journal of Orthodontics and Dentofacial Orthopedics,* 138**,** 458-462.

Fernandez, L. & Canut, J. A. 1999. In vitro comparison of the retention capacity of new aesthetic brackets. *European Journal of Orthodontics,* 21**,** 71-77.

Ferracane, J. L. 1995. Current trends in dental composites. *Critical Reviews in Oral Biology & Medicine,* 6**,** 302-318.

Ferracane, J. L. 2005. Developing a more complete understanding of stresses produced in dental composites during polymerization. *Dental Materials,* 21**,** 36-42.

Floyd, C. J. E. & Dickens, S. H. 2006. Network structure of bis-GMA- and UDMA-based resin systems. *Dental Materials,* 22**,** 1143-1149.

Forbes-Haley, C.; Jones, S. B.; Davies, M. & West, N. X. 2016. Establishing the Effect of Brushing and a Day's Diet on Tooth Tissue Loss in Vitro. *Dentistry Journal,* 4**,** 25.

Forsberg, C. M. & Hagberg, C. 1992. Shear bond strength of ceramic brackets with chemical or mechanical retention. *British Journal of Orthodontics,* 19**,** 183-9.

Foster, J. & Walker, R. 1974. *Dental filling materials*. US Pat. 3825518 patent application.

Franklin, S. & Garcia-Godoy, F. 1993. Shear bond strengths and effects on enamel of two ceramic brackets. *Journal of Clinical Orthodontics,* 27**,** 83-88.

Freilich, M. A.; Karmaker, A. C.; Burstone, C. J. & Goldberg, A. J. 1998. Development and clinical applications of a light-polymerized fiber-reinforced composite. *Journal of Prosthetic Dentistry,* 80**,** 311-318.

Freitag, D.; Fengler, G. & Morbitzer, L. 1991. Routes to new aromatic polycarbonates with special material properties. *Angewandte Chemie International Edition in English,* 30**,** 1598-1610.

Frohberg, P.; Nguyen, T. N. P. & Ulrich, J. 2016. New Aspects in the Formulation of Drugs Based on Three Case Studies. *Molecules,* 21**,** 577.

Fu, Q.; Rahaman, M. N.; Dogan, F. & Bal, B. S. 2008. Freeze casting of porous hydroxyapatite scaffolds. II. Sintering, microstructure, and mechanical behavior. *Journal of Biomedical Materials Research Part B-Applied Biomaterials,* 86B**,** 514-522.

Fujita, K. 1979. New orthodontic treatment with lingual bracket mushroom arch wire appliance. *American Journal of Orthodontics,* 76**,** 657-675.

Fukasawa, T.; Ando, M.; Ohji, T. & Kanzaki, S. 2001a. Synthesis of porous ceramics with complex pore structure by freeze-dry processing. *Journal of the American Ceramic Society,* 84**,** 230-232.

Fukasawa, T.; Deng, Z. Y.; Ando, M.; Ohji, T. & Goto, Y. 2001b. Pore structure of porous ceramics synthesized from water-based slurry by freeze-dry process. *Journal of Materials Science,* 36**,** 2523-2527.

Fukasawa, T.; Deng, Z. Y.; Ando, M.; Ohji, T. & Kanzaki, S. 2002. Synthesis of Porous Silicon Nitride with Unidirectionally Aligned Channels Using Freeze‐Drying Process. *Journal of the American Ceramic Society,* 85**,** 2151-2155.

Fukushima, M.; Nakata, M. & Yoshizawa, Y.-i. 2008. Fabrication and properties of ultra highly porous cordierite with oriented micrometer-sized cylindrical pores by gelation and freezing method. *Journal of the Ceramic Society of Japan,* 116**,** 1322-1325.

Fukushima, M.; Nakata, M.; Zhou, Y.; Ohji, T. & Yoshizawa, Y.-i. 2010. Fabrication and properties of ultra highly porous silicon carbide by the gelation-freezing method. *Journal of the European Ceramic Society,* 30**,** 2889-2896.

Fukushima, M.; Ohji, T.; Hyuga, H.; Matsunaga, C. & Yoshizawa, Y.-i. 2017. Effect of gelatin gel strength on microstructures and mechanical properties of cellular ceramics created by gelation freezing route. *Journal of Materials Research,* 32**,** 3286-3293.

Fukushima, M. & Yoshizawa, Y.-i. 2015. Fabrication of highly porous nickel with oriented micrometer-sized cylindrical pores by gelation freezing method. *Materials Letters,* 153**,** 99-101.

Fukushima, M.; Yoshizawa, Y. & Ohji, T. 2014. Macroporous Ceramics by Gelation-Freezing Route Using Gelatin. *Advanced Engineering Materials,* 16**,** 607-620.

Furusawa, T.; Minatoya, T.; Okudera, T.; Sakai, Y.; Sato, T.; Matsushima, Y. & Unuma, H. 2016. Enhancement of mechanical strength and in vivo cytocompatibility of porous β-tricalcium phosphate ceramics by gelatin coating. *International Journal of Implant Dentistry,* 2**,** 4.

Gajewski, V. E.; Pfeifer, C. S.; Fróes-Salgado, N. R.; Boaro, L. C. & Braga, R. R. 2012. Monomers used in resin composites: degree of conversion, mechanical properties and water sorption/solubility. *Brazilian Dental Journal,* 23**,** 508-514.

Gang, B. & Chung-Yuen, H. 1990. Effects of interface debonding on the toughness of ductile-particle reinforced ceramics. *International Journal of Solids and Structures,* 26**,** 631-642.

Ganss, C.; Schlueter, N.; Preiss, S. & Klimek, J. 2009. Tooth brushing habits in uninstructed adults—frequency, technique, duration and force. *Clinical Oral Investigations,* 13**,** 203.

Gaudillere, C.; Garcia‐Fayos, J.; Balaguer, M. & Serra, J. M. 2014. Enhanced oxygen separation through robust freeze‐cast bilayered dual‐phase membranes. *ChemSusChem,* 7**,** 2554-2561.

Gaudillere, C. & Serra, J. M. 2016. Freeze-casting: Fabrication of highly porous and hierarchical ceramic supports for energy applications. *Boletin De La Sociedad Espanola De Ceramica Y Vidrio,* 55**,** 45-54.

Gazit-Rappaport, T.; Haisraeli-Shalish, M. & Gazit, E. 2010. Psychosocial reward of orthodontic treatment in adult patients. *European Journal of Orthodontics,* 32**,** 441-446.

Géminard, J.-C. & Bertin, E. 2010. Aging of the frictional properties induced by temperature variations. *Physical Review E,* 82**,** 056108.

Ghafari, J.; Skanchy, T. L. & Mante, F. 1992. Shear bond strengths of two ceramic brackets. *Journal of Clinical Orthodontics,* 26**,** 491-3.

Giancotti, A.; Greco, M. & Mampieri, G. 2006. Extraction treatment using Invisalign Technique. *Progress in Orthodontics,* 7**,** 32-43.

Gioka, C. & Eliades, T. 2004. Materials-induced variation in the torque expression of preadjusted appliances. *American Journal of Orthodontics and Dentofacial Orthopedics,* 125**,** 323-328.

Giordano II, R. A.; Pelletier, L.; Campbell, S. & Pober, R. 1995. Flexural strength of an infused ceramic, glass ceramic, and feldspathic porcelain. *Journal of Prosthetic Dentistry,* 73**,** 411-418.

Giordano, R. A. 1998. Method for fabricating odontoforms and dental restorations having infused ceramic network. *In*.: Google Patents.

Giordano, R. A. 2000. Method for fabricating ceramic network material. *In*.: Google Patents.

Giordano, R. A.; Pelletier, L.; Campbell, S. & Pober, R. 1995. Flexural strength of an infused ceramic, glass-ceramic, and feldspathic porcelain. *Journal of Prosthetic Dentistry,* 73**,** 411-418.

Goel, V. K.; Khera, S. C. & Singh, K. 1990. Clinical implications of the response of enamel and dentin to masticatory loads. *Journal of Prosthetic Dentistry,* 64**,** 446-454.

Gogotsi, G. A. 2003. Fracture toughness of ceramics and ceramic composites. *Ceramics International,* 29**,** 777-784.

Goodson, J.; Shoher, I.; Imber, S.; Som, S. & Nathanson, D. 2001. Reduced dental plaque accumulation on composite gold alloy margins. *Journal of Periodontal Research,* 36**,** 252-259.

Grauer, D. & Proffit, W. R. 2011. Accuracy in tooth positioning with a fully customized lingual orthodontic appliance. *American Journal of Orthodontics and Dentofacial Orthopedics,* 140**,** 433-443.

Green, D. J. & Colombo, P. 2003. Cellular ceramics: intriguing structures, novel properties, and innovative applications. *MRS bulletin,* 28**,** 296-300.

Grossman, E.; Rosen, M. & Cleaton-Jones, P. 2004. Surface roughness values for resin based materials. *Journal of the South African Dental Association,* 59**,** 274, 276, 278-9.

Gu, J.; Tang, J. S.; Skulski, B.; Fields Jr, H. W.; Beck, F. M.; Firestone, A. R.; Kim, D.-G. & Deguchi, T. 2017. Evaluation of Invisalign treatment effectiveness and efficiency compared with conventional fixed appliances using the Peer Assessment Rating index. *American Journal of Orthodontics and Dentofacial Orthopedics,* 151**,** 259-266.

Guazzato, M.; Albakry, M.; Ringer, S. P. & Swain, M. V. 2004a. Strength, fracture toughness and microstructure of a selection of all-ceramic materials. Part I. Pressable and alumina glass-infiltrated ceramics. *Dental Materials,* 20**,** 441-448.

Guazzato, M.; Albakry, M.; Ringer, S. P. & Swain, M. V. 2004b. Strength, fracture toughness and microstructure of a selection of all-ceramic materials. Part II. Zirconia-based dental ceramics. *Dental Materials,* 20**,** 449-456.

Guerrero, A. P.; Guariza Filho, O.; Tanaka, O.; Camargo, E. S. & Vieira, S. 2010. Evaluation of frictional forces between ceramic brackets and archwires of different alloys compared with metal brackets. *Brazilian Oral Research,* 24**,** 40-45.

Habelitz, S.; Marshall, S.; Marshall Jr, G. & Balooch, M. 2001. Mechanical properties of human dental enamel on the nanometre scale. *Archives of Oral Biology,* 46**,** 173-183.

Habibi, M.; Nik, T. H. & Hooshmand, T. 2007. Comparison of debonding characteristics of metal and ceramic orthodontic brackets to enamel: an *in vitro* study. *American Journal of Orthodontics and Dentofacial Orthopedics,* 132**,** 675-679.

Hammel, E.; Ighodaro, O.-R. & Okoli, O. 2014. Processing and properties of advanced porous ceramics: An application based review. *Ceramics International,* 40**,** 15351-15370.

Han, J. C.; Hu, L. Y.; Zhang, Y. M. & Zhou, Y. F. 2009. Fabrication of Ceramics with Complex Porous Structures by the Impregnate-Freeze-Casting Process. *Journal of the American Ceramic Society,* 92**,** 2165-2167.

Harzer, W.; Bourauel, C. & Gmyrek, H. 2004. Torque capacity of metal and polycarbonate brackets with and without a metal slot. *European Journal of Orthodontics,* 26**,** 435-441.

Hayasaki, H.; Okamoto, A.; Iwase, Y.; Yamasaki, Y. & Nakata, M. 2004. Occlusal contact area of mandibular teeth during lateral excursion. *International Journal of Prosthodontics,* 17**,** 72-76.

He, L.-H. & Swain, M. 2011. A novel polymer infiltrated ceramic dental material. *Dental Materials,* 27**,** 527-534.

He, L. H. & Swain, M. V. 2007. Nanoindentation derived stress-strain properties of dental materials. *Dental Materials,* 23**,** 814-821.

He, L. H. & Swain, M. V. 2008. Understanding the mechanical behaviour of human enamel from its structural and compositional characteristics. *Journal of the Mechanical Behavior of Biomedical Materials,* 1**,** 18-29.

He, L. H.; Yin, Z. H.; van Vuuren, L. J.; Carter, E. A. & Liang, X. W. 2013. A natural functionally graded biocomposite coating - Human enamel. *Acta Biomaterialia,* 9**,** 6330-6337.

Heintze, S. & Forjanic, M. 2005. Surface roughness of different dental materials before and after simulated toothbrushing in vitro. *Operative Dentistry,* 30**,** 617.

Hohoff, A.; Seifert, E.; Fillion, D.; Stamm, T.; Heinecke, A. & Ehmer, U. 2003. Speech performance in lingual orthodontic patients measured by sonagraphy and auditive analysis. *American Journal of Orthodontics and Dentofacial Orthopedics,* 123**,** 146-152.

Hohoff, A.; Stamm, T. & Ehmer, U. 2004. Comparison of the effect on oral discomfort of two positioning techniques with lingual brackets. *Angle Orthodontist,* 74**,** 226-233.

Hollister, S. J. 2005. Porous scaffold design for tissue engineering. *Nature Materials,* 4**,** 518 - 524

Holt, M. H.; Nanda, R. S. & Duncanson, M. G. 1991. Fracture-resistance of ceramic brackets during arch wire torsion. *American Journal of Orthodontics and Dentofacial Orthopedics,* 99**,** 287-293.

Hornberger, H.; Marquis, P. M.; Christiansen, S. & Strunk, H. P. 1996. Microstructure of a high strength alumina glass composite. *Journal of Materials Research,* 11**,** 855-858.

Hosoya, Y.; Marshall, S.; Watanabe, L. & Marshall, G. 2000. Microhardness of carious deciduous dentin. *Operative Dentistry,* 25**,** 81-89.

Hu, L.; Wang, C.-A.; Huang, Y.; Sun, C.; Lu, S. & Hu, Z. 2010. Control of pore channel size during freeze casting of porous YSZ ceramics with unidirectionally aligned channels using different freezing temperatures. *Journal of the European Ceramic Society,* 30**,** 3389-3396.

Imfeld, T. 1996. Dental erosion. Definition, classification and links. *European Journal of Oral Sciences,* 104**,** 151-155.

Inoue, M.; Finger, W. & Mueller, M. 1994. Effect of filler content of restorative resins on retentive strength to acid-conditioned enamel. *American Journal of Dentistry,* 7**,** 161-6.

Ireland, A.; Sherriff, M. & McDonald, F. 1991. Effect of bracket and wire composition on frictional forces. *European Journal of Orthodontics,* 13**,** 322-328.

ISO 2017. Dentistry -- Dentifrices -- Requirements, test methods and marking. *In: 11609:2017.*

ISO, E. 2003. 604. *Plastics–determination of compressive properties (ISO 604: 2002)*.

Iwasa, M. & Brandt, R. 1986. Fracture toughness of single crystal alumina. *In:* WD, K. (ed.) *Structure and properties of MgO and Al2O3. Advances in ceramics.* Columbus: American Ceramic Society.

Jeiroudi, M. T. 1991. Enamel fracture caused by ceramic brackets. *American Journal of Orthodontics and Dentofacial Orthopedics,* 99**,** 97-99.

Jena, A.; Duggal, R. & Mehrotra, A. 2007. Physical Properties and Clinical Characteristics of Ceramic Brackets: A Comprehensive Review. *Trends in Biomaterials and Artificial Organs,* 20**,** 101-115.

Jenkins, G. 1972 Current concepts concerning the development of dental caries. *International Dental Journal,* 22**,** 350-61.

Jeremiah, H.; Bister, D. & Newton, J. 2010. Social perceptions of adults wearing orthodontic appliances: a cross-sectional study. *European Journal of Orthodontics,* 33**,** 476-482.

Jing, L.; Zuo, K. H.; Zhang, F. Q.; Chun, X.; Fu, Y. F.; Jiang, D. L. & Zeng, Y. P. 2010. The controllable microstructure of porous Al2O3 ceramics prepared via a novel freeze casting route. *Ceramics International,* 36**,** 2499-2503.

Johal, A.; Alyaqoobi, I.; Patel, R. & Cox, S. 2014. The impact of orthodontic treatment on quality of life and self-esteem in adult patients. *European Journal of Orthodontics,* 37**,** 233-237.

Johnson, G.; Walker, M. P. & Kula, K. 2005. Fracture strength of ceramic bracket tie wings subjected to tension. *Angle Orthodontist,* 75**,** 95-100.

Johnston, N. J.; Price, R.; Day, C. J.; Sandy, J. R. & Ireland, A. J. 2009. Quantitative and qualitative analysis of particulate production during simulated clinical orthodontic debonds. *Dental Materials,* 25**,** 1155-1162.

Jones, R. & Todhunter, R. 2010. *Casting Process*.

Jongsma, L.; Kleverlaan, C. & Feilzer, A. 2012. Clinical success and survival of indirect resin composite crowns: results of a 3-year prospective study. *Dental Materials,* 28**,** 952-960.

Kamonkhantikul, K.; Arksornnukit, M.; Takahashi, H.; Kanehira, M. & Finger, W. J. 2014. Polishing and toothbrushing alters the surface roughness and gloss of composite resins. *Dental Materials,* 33**,** 599-606.

Kang, H. W.; Tabata, Y. & Ikada, Y. 1999. Fabrication of porous gelatin scaffolds for tissue engineering. *Biomaterials,* 20**,** 1339-1344.

Kapur Wadhwa, R.; Kwon, H. K. & Close, J. M. 2004. Frictional resistances of different bracket-wire combinations. *Australian Orthodontic Journal,* 20**,** 25.

Karamouzos, A.; Athanasiou, A. E. & Papadopoulos, M. A. 1997. Clinical characteristics and properties of ceramic brackets: a comprehensive review. *American Journal of Orthodontics and Dentofacial Orthopedics,* 112**,** 34-40.

Kato, M.; Miyoshi, K.; Suzuki, T.; Tabuchi, M.; Miyazawa, K. & Goto, S. 2014. Changes in physical properties of new, non-BPA containing, polymeric orthodontic bracket materials over time: A 2-year clinical study. *Orthodontic Waves,* 73**,** 41-47.

Katona, T. R. 1997. A comparison of the stresses developed in tension, shear peel, and torsion strength testing of direct bonded orthodontic brackets. *American Journal of Orthodontics and Dentofacial Orthopedics,* 112**,** 244-251.

Kearns, H.; Sandham, J.; Bryan Jones, W. & Lagerström, L. 1997. Electrothermal debonding of ceramic brackets: an ex vivo study. *British Journal of Orthodontics,* 24**,** 237-242.

Keim, R.; Gottlieb, E.; Vogels 3rd, D. & Vogels, P. 2014. 2014 JCO study of orthodontic diagnosis and treatment procedures, Part 1: results and trends. *Journal of Clinical Orthodontics,* 48**,** 607.

Keith, O.; Kusy, R. P. & Whitley, J. Q. 1994. Zirconia brackets: an evaluation of morphology and coefficients of friction. *American Journal of Orthodontics and Dentofacial Orthopedics,* 106**,** 605-614.

Kelly, J. R. 1999. Clinically relevant approach to failure testing of all-ceramic restorations. *Journal of Prosthetic Dentistry,* 81**,** 652-661.

Kelly, J. R.; Campbell, S. D. & Bowen, H. K. 1989. Fracture-surface analysis of dental ceramics. *Journal of Prosthetic Dentistry,* 62**,** 536-541.

Kerosuo, H.; Hausen, H.; Laine, T. & Shaw, W. C. 1995. The influence of incisal malocclusion on the social attractiveness of young adults in Finland. *European Journal of Orthodontics,* 17**,** 505-512.

Kim, K. H.; Ong, J. L. & Okuno, O. 2002. The effect of filler loading and morphology on the mechanical properties of contemporary composites. *Journal of Prosthetic Dentistry,* 87**,** 642-649.

Kim, Y. 2017. Study on the perception of orthodontic treatment according to age: A questionnaire survey. *The Korean Journal of Orthodontics,* 47**,** 215-221.

Kinney, J. H.; Marshall, S. J. & Marshall, G. W. 2003. The mechanical properties of human dentin: A critical review and re-evaluation of the dental literature. *Critical Reviews in Oral Biology & Medicine,* 14**,** 13-29.

Kitahara-Céia, F. M. F.; Mucha, J. N. & dos Santos, P. A. M. 2008. Assessment of enamel damage after removal of ceramic brackets. *American Journal of Orthodontics and Dentofacial Orthopedics,* 134**,** 548-555.

Kleverlaan, C. J. & Feilzer, A. J. 2005. Polymerization shrinkage and contraction stress of dental resin composites. *Dental Materials,* 21**,** 1150-1157.

Kluemper, G. T.; Hiser, D. G.; Rayens, M. K. & Jay, M. J. 2002. Efficacy of a wax containing benzocaine in the relief of oral mucosal pain caused by orthodontic appliances. *American Journal of Orthodontics and Dentofacial Orthopedics,* 122**,** 359-365.

Knight, C. A.; Hallett, J. & DeVries, A. 1988. Solute effects on ice recrystallization: an assessment technique. *Cryobiology,* 25**,** 55-60.

Knösel, M.; Klang, E.; Helms, H.-J. & Wiechmann, D. 2014. Lingual orthodontic treatment duration: performance of two different completely customized multi-bracket appliances (Incognito and WIN) in groups with different treatment complexities. *Head & Face Medicine,* 10**,** 46.

Koch, D.; Andresen, L.; Schmedders, T. & Grathwohl, G. 2003. Evolution of porosity by freeze casting and sintering of sol-gel derived ceramics. *Journal of Sol-Gel Science and Technology,* 26**,** 149-152.

Krauss, J.; Faltermeier, A.; Behr, M. & Proff, P. 2010. Evaluation of alternative polymer bracket materials. *American Journal of Orthodontics and Dentofacial Orthopedics,* 137**,** 362-367.

Kraut, J.; Radin, S.; Trowbridge, H.; Emling, R. & Yankell, S. 1991. Clinical evaluations on thermal versus mechanical debonding of ceramic brackets. *Journal of Clinical Dentistry,* 2**,** 92-96.

Kravitz, N. D.; Kusnoto, B.; BeGole, E.; Obrez, A. & Agran, B. 2009. How well does Invisalign work? A prospective clinical study evaluating the efficacy of tooth movement with Invisalign. *American Journal of Orthodontics and Dentofacial Orthopedics,* 135**,** 27-35.

Krell, K. V.; Courey, J. M. & Bishara, S. E. 1993. Orthodontic bracket removal using conventional and ultrasonic debonding techniques, enamel loss, and time requirements. *American Journal of Orthodontics and Dentofacial Orthopedics,* 103**,** 258-266.

Kuang, J.; Dai, Z.; Liu, L.; Yang, Z.; Jin, M. & Zhang, Z. 2015. Synergistic effects from graphene and carbon nanotubes endow ordered hierarchical structure foams with a combination of compressibility, super-elasticity and stability and potential application as pressure sensors. *Nanoscale,* 7**,** 9252-9260.

Kuncio, D.; Maganzini, A.; Shelton, C. & Freeman, K. 2007. Invisalign and traditional orthodontic treatment postretention outcomes compared using the American Board of Orthodontics objective grading system. *Angle Orthodontist,* 77**,** 864-869.

Kuo, E. & Miller, R. J. 2003. Automated custom-manufacturing technology in orthodontics. *American Journal of Orthodontics and Dentofacial Orthopedics,* 123**,** 578-581.

Kusy, R. P. 1988. Morphology of polycrystalline alumina brackets and its relationship to fracture-toughness and strength. *Angle Orthodontist,* 58**,** 197-203.

Kusy, R. P. 1998. The future of orthodontic materials: the long-term view. *American Journal of Orthodontics and Dentofacial Orthopedics,* 113**,** 91-95.

Kusy, R. P. & Whitley, J. Q. 1990. Effects of surface roughness on the coefficients of friction in model orthodontic systems. *Journal of Biomechanics,* 23**,** 913-925.

Kusy, R. P. & Whitley, J. Q. 2005. Degradation of plastic polyoxymethylene brackets and the subsequent release of toxic formaldehyde. *American Journal of Orthodontics and Dentofacial Orthopedics,* 127**,** 420-427.

Kusy, R. P.; Whitley, J. Q.; Mayhew, M. J. & Buckthal, J. E. 1988. Surface roughness of orthodontic archwires via laser spectroscopy. *Angle Orthodontist,* 58**,** 33-45.

Kusy, R. R. 2002. Orthodontic biomaterials: From the past to the present. *Angle Orthodontist,* 72**,** 501-512.

Lakes, R. 1993. Materials with structural hierarchy. *Nature,* 361**,** 511-515.

Landi, E.; Valentini, F. & Tampieri, A. 2008. Porous hydroxyapatite/gelatine scaffolds with ice-designed channel-like porosity for biomedical applications. *Acta Biomaterialia,* 4**,** 1620-1626.

Lasalle, A.; Guizard, C.; Maire, E.; Adrien, J. & Deville, S. 2012. Particle redistribution and structural defect development during ice templating. *Acta Materialia,* 60**,** 4594-4603.

Launey, M. E.; Munch, E.; Alsem, D.; Barth, H.; Saiz, E.; Tomsia, A. P. & Ritchie, R. O. 2009. Designing highly toughened hybrid composites through nature-inspired hierarchical complexity. *Acta Materialia,* 57**,** 2919-2932.

Launey, M. E.; Munch, E.; Alsem, D. H.; Saiz, E.; Tomsia, A. P. & Ritchie, R. O. 2010. A novel biomimetic approach to the design of high-performance ceramic–metal composites. *Journal of the Royal Society Interface,* 7**,** 741-753.

Lawn, B. R.; Evans, A. & Marshall, D. 1980. Elastic/plastic indentation damage in ceramics: the median/radial crack system. *Journal of the American Ceramic Society,* 63**,** 574-581.

Lawn, B. R. & Lee, J. J. W. 2009. Analysis of fracture and deformation modes in teeth subjected to occlusal loading. *Acta Biomaterialia,* 5**,** 2213-2221.

Lee, E.-J.; Koh, Y.-H.; Yoon, B.-H.; Kim, H.-E. & Kim, H.-W. 2007. Highly porous hydroxyapatite bioceramics with interconnected pore channels using camphene-based freeze casting. *Materials Letters,* 61**,** 2270-2273.

Lee, H.; Jang, T.-S.; Song, J.; Kim, H.-E. & Jung, H.-D. 2017. The production of porous hydroxyapatite scaffolds with graded porosity by sequential freeze-casting. *Materials,* 10**,** 367.

Lee, S.-P.; Lee, S.-J.; Lim, B.-S. & Ahn, S.-J. 2009. Surface characteristics of orthodontic materials and their effects on adhesion of mutans streptococci. *Angle Orthodontist,* 79**,** 353-360.

Lee, S.; Novitskaya, E. E.; Reynante, B.; Vasquez, J.; Urbaniak, R.; Takahashi, T.; Woolley, E.; Tombolato, L.; Chen, P.-Y. & McKittrick, J. 2011. Impact testing of structural biological materials. *Materials Science & Engineering C-Materials for Biological Applications,* 31**,** 730-739.

Lee, Y. B. Y.-K. 2011. Aesthetic colour performance of plastic and ceramic brackets -- an in vitro study. *Journal of Orthodontics,* 38**,** 167-74.

Lefever, D.; Perakis, N.; Roig, M.; Krejci, I. & Ardu, S. 2012. The effect of toothbrushing on surface gloss of resin composites. *American Journal of Dentistry,* 25**,** 54-8.

Leibrock, A.; Rosentritt, M.; Lang, R.; Behr, M. & Handel, G. 1997. Colour stability of visible light-curing hybrid composites. *European Journal of Prosthodontics and Restorative Dentistry,* 5**,** 125-130.

Leung, B. T.; Tsoi, J. K.; Matinlinna, J. P. & Pow, E. H. 2015. Comparison of mechanical properties of three machinable ceramics with an experimental fluorophlogopite glass ceramic. *Journal of Prosthetic Dentistry,* 114**,** 440-446.

Li, J.; Zhang, X.-H.; Cui, B.-C.; Lin, Y.-H.; Deng, X.-L.; Li, M. & Nan, C.-W. 2017. Mechanical performance of polymer-infiltrated zirconia ceramics. *Journal of Dentistry,* 58**,** 60-66.

Li, J. C. & Dunand, D. C. 2011. Mechanical properties of directionally freeze-cast titanium foams. *Acta Materialia,* 59**,** 146-158.

Li, R. W. K.; Chow, T. W. & Matinlinna, J. P. 2014. Ceramic dental biomaterials and CAD/CAM technology: state of the art. *Journal of Prosthodontic Research,* 58**,** 208-216.

Li, W. & Sun, J. 2018. Effects of Ceramic Density and Sintering Temperature on the Mechanical Properties of a Novel Polymer-Infiltrated Ceramic-Network Zirconia Dental Restorative (Filling) Material. *Medical Science Monitor: International Medical Journal of Experimental and Clinical Research,* 24**,** 3068.

Li, W.; Wang, S. & Zhang, Y. 2015. The effectiveness of the Invisalign appliance in extraction cases using the the ABO model grading system: a multicenter randomized controlled trial. *International Journal of Clinical and Experimental Medicine,* 8**,** 8276.

Lin, M.; Xu, F.; Lu, T. J. & Bai, B. F. 2010. A review of heat transfer in human tooth-Experimental characterization and mathematical modeling. *Dental Materials,* 26**,** 501-513.

Liu, X.; Lin, J. & Ding, P. 2013. Changes in the surface roughness and friction coefficient of orthodontic bracket slots before and after treatment. *Scanning,* 35**,** 265-272.

Liu, X.; Xue, W.; Shi, C. & Sun, J. 2015. Fully interconnected porous Al2O3 scaffolds prepared by a fast cooling freeze casting method. *Ceramics International,* 41**,** 11922-11926.

Loftus, B. P.; Ârtun, J.; Nicholls, J. I.; Alonzo, T. A. & Stoner, J. A. 1999. Evaluation of friction during sliding tooth movement in various bracket-arch wire combinations. *American Journal of Orthodontics and Dentofacial Orthopedics,* 116**,** 336-345.

Long, C. G.; Su, Y. & Shen, C. 2014. Mechanical and Tribological Properties of Polytetrafluoroethylene filled Polyoxymethylene/Aluminum Foam Interpenetrating Phase Composites. *Advanced Materials Research,* 835-836**,** 285-289.

Lu, K.; Kessler, C. S. & Davis, R. M. 2006. Optimization of a nanoparticle suspension for freeze casting. *Journal of the American Ceramic Society,* 89**,** 2459-2465.

Maganzini, A. L. 2006. Outcome assessment of Invisalign and traditional orthodontic treatment and subsequent commentaries. *American Journal of Orthodontics and Dentofacial Orthopedics,* 129**,** 456.

Mahardhika, A.; Noerdin, A. & Eriwati, Y. The effects of brushing on human enamel surface roughness after NaF gel and theobromine gel exposure. Journal of Physics: Conference Series, 2017. IOP Publishing, 012007.

Mahler, W. & Bechtold, M. F. 1980. Freeze-formed silica fibres. *Nature,* 285**,** 27.

Mahoney, E.; Holt, A.; Swain, M. & Kilpatrick, N. 2000. The hardness and modulus of elasticity of primary molar teeth: an ultra-micro-indentation study. *Journal of Dentistry,* 28**,** 589-594.

Mansor, N.; Jia, J.; Miller, T.; Suter, T.; Jorge, A. B.; Gibbs, C.; Shearing, P. R.; McMillan, P. F.; Mattevi, C. & Shaffer, M. 2016. Graphitic carbon nitride-graphene hybrid nanostructure as a catalyst support for polymer electrolyte membrane fuel cells. *ECS Transactions,* 75**,** 885-897.

Mante, F.; Brantley, W.; Dhuru, V. & Ziebert, G. 1993. Fracture toughness of high alumina core dental ceramics: the effect of water and artificial saliva. *International Journal of Prosthodontics.,* 6**,** 546-52.

Marques, I. S. V.; Araújo, A. M.; Gurgel, J. A. & Normando, D. 2010. Debris, roughness and friction of stainless steel archwires following clinical use. *Angle Orthodontist,* 80**,** 521-527.

Marshall Jr, G. W.; Marshall, S. J.; Kinney, J. H. & Balooch, M. 1997. The dentin substrate: structure and properties related to bonding. *Journal of Dentistry,* 25**,** 441-458.

Matsui, S.; Umezaki, E.; Komazawa, D.; Otsuka, Y. & Suda, N. 2015. Evaluation of mechanical properties of esthetic brackets. *Journal of Dental Biomechanics,* 6.

Matsunaga, C.; Fukushima, M.; Hyuga, H. & Yoshizawa, Y.-i. 2017. Fabrication of porous silica ceramics by gelation-freezing of diatomite slurry. *Journal of the European Ceramic Society,* 37**,** 5259-5264.

McCabe, J. F. & Walls, A. W. 2013. *Applied Dental Materials*, John Wiley & Sons.

McCollough, C. H.; Leng, S.; Yu, L. & Fletcher, J. G. 2015. Dual and multi energy CT: principles, technical approaches, and clinical applications. *Radiology,* 276**,** 637-653.

McCracken, G.; Janssen, J.; Swan, M.; Steen, N.; De Jager, M. & Heasman, P. 2003. Effect of brushing force and time on plaque removal using a powered toothbrush. *Journal of Clinical Periodontology,* 30**,** 409-413.

McKittrick, J.; Chen, P. Y.; Tombolato, L.; Novitskaya, E. E.; Trim, M. W.; Hirata, G. A.; Olevsky, E. A.; Horstemeyer, M. F. & Meyers, M. A. 2010. Energy absorbent natural materials and bioinspired design strategies: A review. *Materials Science & Engineering C-Materials for Biological Applications,* 30**,** 331-342.

McNeill, I. & Rincon, A. 1993. Thermal degradation of polycarbonates: Reaction conditions and reaction mechanisms. *Polymer Degradation and Stability,* 39**,** 13-19.

Meguro, D.; Hayakawa, T.; Kawasaki, M. & Kasai, K. 2006. Shear bond strength of calcium phosphate ceramic brackets to human enamel. *Angle Orthodontist,* 76**,** 301-305.

Melsen, B. 2012. *Adult Orthodontics*, Wiley-Blackwell.

Mendes, B. d. A. B.; Ferreira, R. A. N.; Pithon, M. M.; Horta, M. C. R. & Oliveira, D. D. 2014. Physical and chemical properties of orthodontic brackets after 12 and 24 months: in situ study. *Journal of Applied Oral Science,* 22**,** 194-203.

Meyers, I.; McQueen, M.; Harbrow, D. & Seymour, G. 2000. The surface effect of dentifrices. *Australian Dental Journal,* 45**,** 118-124.

Meyers, M. A.; Chen, P.-Y.; Lin, A. Y.-M. & Seki, Y. 2008. Biological materials: structure and mechanical properties. *Progress in Materials Science,* 53**,** 1-206.

Meyers, M. A.; Chen, P.-Y.; Lopez, M. I.; Seki, Y. & Lin, A. Y. 2011. Biological materials: A materials science approach. *Journal of the Mechanical Behavior of Biomedical Materials,* 4**,** 626-657.

Mianger, V. 2016. *Adults seeking more orthodontic treatment* [Online]. Dentistry.co.uk. Available: https://www.dentistry.co.uk/2016/07/25/survey-reveals-rising-number-of-adults-seeking-ortho-treatment/ [Accessed 31/10/2018 2018].

Min, J.; Arola, D. D.; Yu, D. D.; Yu, P.; Zhang, Q. Q.; Yu, H. Y. & Gao, S. S. 2016. Comparison of human enamel and polymer-infiltrated-ceramic network material "ENAMIC" through micro- and nano-mechanical testing. *Ceramics International,* 42**,** 10631-10637.

Mistakidis, I.; Katib, H.; Vasilakos, G.; Kloukos, D. & Gkantidis, N. 2015. Clinical outcomes of lingual orthodontic treatment: a systematic review. *European Journal of Orthodontics,* 38**,** 447-458.

Miura, J.; Maeda, Y.; Nakai, H. & Zako, M. 2009. Multiscale analysis of stress distribution in teeth under applied forces. *Dental Materials,* 25**,** 67-73.

Miyawaki, S.; Yasuhara, M. & Koh, Y. 1999. Discomfort caused by bonded lingual orthodontic appliances in adult patients as examined by retrospective questionnaire. *American Journal of Orthodontics and Dentofacial Orthopedics,* 115**,** 83-88.

Miyazaki, T. & Hotta, Y. 2011. CAD/CAM systems available for the fabrication of crown and bridge restorations. *Australian Dental Journal,* 56**,** 97-106.

Möller, M.; Klocke, A.; Sadat-Khonsari, R.; Schlegel, V. & Kahl-Nieke, B. 2009. Torque stability of plastic brackets following multiple loading and artificial material aging–an *in vitro* comparison. *Journal of Orofacial Orthopedics/Fortschritte der Kieferorthopädie,* 70**,** 385.

Moon, R. J.; Hoffman, M.; Rödel, J.; Tochino, S. & Pezzotti, G. 2009. Evaluation of crack-tip stress fields on microstructural-scale fracture in Al–Al2O3 interpenetrating network composites. *Acta Materialia,* 57**,** 570-581.

Moraes, M. C. C. d. S.; Elias, C. N.; Duailibi Filho, J. & Oliveira, L. G. d. 2004. Mechanical properties of alumina-zirconia composites for ceramic abutments. *Materials Research,* 7**,** 643-649.

Moran, K. I. 1987. Relative wire stiffness due to lingual versus labial interbracket distance. *American Journal of Orthodontics and Dentofacial Orthopedics,* 92**,** 24-32.

Moretti, E.; Zinzi, M.; Carnielo, E. & Merli, F. 2017. Advanced polycarbonate transparent systems with aerogel: Preliminary characterization of optical and thermal properties. *Energy Procedia,* 113**,** 9-16.

Mörmann, W. & Swain, M. 2014. The CAD/CAM material of the future. *In:* Sirona (ed.) *Dental Visionist.* Sirona.

Mozafari, M.; Moztarzadeh, F.; Rabiee, M.; Azami, M.; Maleknia, S.; Tahriri, M.; Moztarzadeh, Z. & Nezafati, N. 2010. Development of macroporous nanocomposite scaffolds of gelatin/bioactive glass prepared through layer solvent casting combined with lamination technique for bone tissue engineering. *Ceramics International,* 36**,** 2431-2439.

Munch, E.; Launey, M. E.; Alsem, D. H.; Saiz, E.; Tomsia, A. P. & Ritchie, R. O. 2008. Tough, Bio-Inspired Hybrid Materials. *Science,* 322**,** 1516-1520.

Munch, E.; Saiz, E.; Tomsia, A. P. & Deville, S. 2009. Architectural Control of Freeze-Cast Ceramics Through Additives and Templating. *Journal of the American Ceramic Society,* 92**,** 1534-1539.

Naleway, S. E.; Christopher, F. Y.; Porter, M. M.; Sengupta, A.; Iovine, P. M.; Meyers, M. A. & McKittrick, J. 2015. Bioinspired composites from freeze casting with clathrate hydrates. *Materials & Design,* 71**,** 62-67.

Naleway, S. E.; Fickas, K. C.; Maker, Y. N.; Meyers, M. A. & McKittrick, J. 2016. Reproducibility of ZrO2-based freeze casting for biomaterials. *Materials Science and Engineering: C,* 61**,** 105-112.

Nattrass, C. & Sandy, J. 1995. Adult orthodontics—a review. *British Journal of Orthodontics,* 22**,** 331-337.

Newton, J. T.; Prabhu, N. & Robinson, P. G. 2003. The impact of dental appearance on the appraisal of personal characteristics. *International Journal of Prosthodontics,* 16.

Nguyen, J.-F.; Migonney, V.; Ruse, N. D. & Sadoun, M. 2012. Resin composite blocks via high-pressure high-temperature polymerization. *Dental Materials,* 28**,** 529-534.

Nguyen, J. F.; Ruse, D.; Phan, A. C. & Sadoun, M. J. 2014. High-temperature-pressure Polymerized Resin-infiltrated Ceramic Networks. *Journal of Dental Research,* 93**,** 62-67.

Nguyen, P. T. & Ulrich, J. 2014. Fast Dispersible Cocoa Tablets: A Case Study of Freeze‐Casting Applied to Foods. *Chemical Engineering & Technology,* 37**,** 1376-1382.

Niesz, D. E. 1996. A review of ceramic powder compaction. *KONA Powder and Particle Journal,* 14**,** 44-51.

Nishio, C.; Mendes, A. D.; Almeida, M. A. D.; Tanaka, E.; Tanne, K. & Elias, C. N. 2009. Evaluation of esthetic brackets' resistance to torsional forces from the archwire. *American Journal of Orthodontics and Dentofacial Orthopedics,* 135**,** 42-48.

Noguchi, H.; Sakane, M.; Watanabe, A.; Tsukanishi, T.; Wadano, Y. & Yamazaki, M. 2014. A novel unidirectional porous hydroxyapatite in canines. *Bioinspired, Biomimetic and Nanobiomaterials,* 3**,** 228-234.

Obata, A.; Tsumura, T.; Niwa, K.; Ashizawa, Y.; Deguchi, T. & Ito, M. 1999. Super pulse CO2 laser for bracket bonding and debonding. *European Journal of Orthodontics,* 21**,** 193-198.

Ogaard, B. 2004. Enamel effects during bonding-debonding and treatment with fixed appliances. *Risk Management in Orthodontics: Experts' Guide to Malpractice***,** 19-46.

Ohji, T. & Fukushima, M. 2012. Macro-porous ceramics: processing and properties. *International Materials Reviews,* 57**,** 115-131.

Okada, K.; Kameya, T.; Ishino, H. & Hayakawa, T. 2014. A novel technique for preparing dental CAD/CAM composite resin blocks using the filler press and monomer infiltration method. *Dental Materials Journal,* 33**,** 203-209.

Olsen, M. E.; Bishara, S. E. & Jakobsen, J. R. 1997. Evaluation of the shear bond strength of different ceramic bracket base designs. *Angle Orthodontist,* 67**,** 179-182.

Olsen, M. E.; Bishara, S. E.; Ortho, D.; Boyer, D. B. & Jakobsen, J. R. 1996. Effect of varying etching times on the bond strength of ceramic brackets. *American Journal of Orthodontics and Dentofacial Orthopedics,* 109**,** 403-409.

Özcan, M.; Finnema, K. & Ybema, A. 2008. Evaluation of failure characteristics and bond strength after ceramic and polycarbonate bracket debonding: effect of bracket base silanization. *European Journal of Orthodontics,* 30**,** 176-182.

Öztürk, F.; Ersöz, M.; Öztürk, S. A.; Malkoç, S. & Hatunoğlu, E. 2015. Micro-CT evaluation of microleakage under orthodontic ceramic brackets bonded with different

bonding techniques and adhesives. *European Journal of Orthodontics,* 38**,** 163-169.

Pabari, S.; Moles, D. R. & Cunningham, S. J. 2011. Assessment of motivation and psychological characteristics of adult orthodontic patients. *American Journal of Orthodontics and Dentofacial Orthopedics,* 140**,** e263-e272.

Paepegaey, A.-M.; Barker, M. L.; Bartlett, D. W.; Mistry, M.; West, N. X.; Hellin, N.; Brown, L. J. & Bellamy, P. G. 2013. Measuring enamel erosion: A comparative study of contact profilometry, non-contact profilometry and confocal laser scanning microscopy. *Dental Materials,* 29**,** 265-1272.

Papageorgiou, S. N.; Gölz, L.; Jäger, A.; Eliades, T. & Bourauel, C. 2016. Lingual vs. labial fixed orthodontic appliances: systematic review and meta‐analysis of treatment effects. *European Journal of Oral Sciences,* 124**,** 105-118.

Park, H.; Choi, M.; Choe, H. & Dunand, D. C. 2017. Microstructure and compressive behavior of ice-templated copper foams with directional, lamellar pores. *Materials Science and Engineering a-Structural Materials Properties Microstructure and Processing,* 679**,** 435-445.

Park, K. H.; Bayome, M.; Park, J. H.; Lee, J. W.; Baek, S.-H. & Kook, Y.-A. 2015. New classification of lingual arch form in normal occlusion using three dimensional virtual models. *The Korean Journal of Orthodontics,* 45**,** 74-81.

Park, S.; Quinn, J.; Romberg, E. & Arola, D. 2008. On the brittleness of enamel and selected dental materials. *Dental Materials,* 24**,** 1477-1485.

Pauls, A.; Nienkemper, M.; Schwestka-Polly, R. & Wiechmann, D. 2017. Therapeutic accuracy of the completely customized lingual appliance WIN. *Journal of Orofacial Orthopedics/Fortschritte der Kieferorthopädie,* 78**,** 52-61.

Peko, C.; Groth, B. & Nettleship, I. 2010. The effect of polyvinyl alcohol on the microstructure and permeability of freeze‐cast alumina. *Journal of the American Ceramic Society,* 93**,** 115-120.

Pereira, C.; Demarco, F.; Cenci, M.; Osinaga, P. & Piovesan, E. 2003. Flexural strength of composites: influences of polyethylene fiber reinforcement and type of composite. *Clinical Oral Investigations,* 7**,** 116-119.

Petrini, M.; Ferrante, M. & Su, B. 2013. Fabrication and characterization of biomimetic ceramic/polymer composite materials for dental restoration. *Dental Materials,* 29**,** 375-381.

Peutzfeldt, A. 1997. Resin composites in dentistry: the monomer systems. *European Journal of Oral Sciences,* 105**,** 97-116.

Plotino, G.; Grande, N. M.; Bedini, R.; Pameijer, C. H. & Somma, F. 2007. Flexural properties of endodontic posts and human root dentin. *Dental Materials,* 23**,** 1129-1135.

Porter, M. M.; McKittrick, J. & Meyers, M. A. 2013. Biomimetic Materials by Freeze Casting. *JOM,* 65**,** 720-727.

Prakobna, K.; Berthold, F.; Medina, L. & Berglund, L. A. 2016. Mechanical performance and architecture of biocomposite honeycombs and foams from core–shell holocellulose nanofibers. *Composites Part A: Applied Science and Manufacturing,* 88**,** 116-122.

Pratten, D. H.; Popli, K.; Germane, N. & Gunsolley, J. C. 1990. Frictional resistance of ceramic and stainless steel orthodontic brackets. *American Journal of Orthodontics and Dentofacial Orthopedics,* 98**,** 398-403.

Preiss, A.; Su, B.; Collins, S. & Simpson, D. 2012. Tailored graded pore structure in zirconia toughened alumina ceramics using double-side cooling freeze casting. *Journal of the European Ceramic Society,* 32**,** 1575-1583.

Pudyani, P. S. & Widiarsanti, S. 2016. Effects of silane application on the shear bond strength of ceramic orthodontic brackets to enamel surface. *Dental Journal (Majalah Kedokteran Gigi),* 49**,** 189-194.

Quirynen, M.; Bollen, C. M.; Papaioannou, W.; Van Eldere, J. & van Steenberghe, D. 1996. The influence of titanium abutment surface roughness on plaque accumulation and gingivitis: short-term observations. *International Journal of Oral & Maxillofacial Implants,* 11.

Rafe, Z.; Vardimon, A. & Ashkenazi, M. 2006. Comparative study of 3 types of toothbrushes in patients with fixed orthodontic appliances. *American Journal of Orthodontics and Dentofacial Orthopedics,* 130**,** 92-95.

Rahaman, M. N. & Fu, Q. 2008. Manipulation of porous bioceramic microstructures by freezing of suspensions containing binary mixtures of solvents. *Journal of the American Ceramic Society,* 91**,** 4137-4140.

Rahiotis, C. & Schricker, S. 2017. Bonding with glass ionomer cements and resin-modified glass ionomer cements. *Orthodontic Applications of Biomaterials.* Elsevier.

Rashid, H. 2014. The effect of surface roughness on ceramics used in dentistry: A review of literature. *European Journal of Dentistry,* 8**,** 571-9.

Rasmussen, S. T.; Patchin, R. E.; Scott, D. B. & Heuer, A. H. 1976. Fracture properties of human enamel and dentin. *Journal of Dental Research,* 55**,** 154-164.

Redd, T. & Shivapuja, P. 1991. Debonding ceramic brackets: effects on enamel. *Journal of Clinical Orthodontics,* 25**,** 475.

Reed, B. B.; Choi, K.; Dickens, S. H. & Stansbury, J. W. 1997. Effect of resin composition on kinetics of dimethacrylate photopolymerization. *Abstracts of Papers of the American Chemical Society,* 214**,** 41-POLY.

Reynolds, I. R. 1975. A review of direct orthodontic bonding. *British Journal of Orthodontics* 2 171 – 175.

Rezwan, K.; Chen, Q.; Blaker, J. & Boccaccini, A. R. 2006. Biodegradable and bioactive porous polymer/inorganic composite scaffolds for bone tissue engineering. *Biomaterials,* 27**,** 3413-3431.

Ritchie, R. O.; Knott, J. F. & Rice, J. 1973. On the relationship between critical tensile stress and fracture toughness in mild steel. *Journal of the Mechanics and Physics of Solids,* 21**,** 395-410.

Rodríguez-Parra, J. M.; Moreno, R. & Nieto, I. M. 2012. Effect of cooling rate on the microstructure and porosity of alumina produced by freeze casting. *Journal of the Serbian Chemical Society,* 77**,** 1775-1785.

Rose, L. F. 1987. Crack reinforcement by distributed springs. *Journal of the Mechanics and Physics of Solids,* 35**,** 383-405.

Rossini, G.; Parrini, S.; Castroflorio, T.; Deregibus, A. & Debernardi, C. L. 2014. Efficacy of clear aligners in controlling orthodontic tooth movement: a systematic review. *Angle Orthodontist,* 85**,** 881-889.

Rosvall, M. D.; Fields, H. W.; Ziuchkovski, J.; Rosenstiel, S. F. & Johnston, W. M. 2009. Attractiveness, acceptability, and value of orthodontic appliances. *American Journal of Orthodontics and Dentofacial Orthopedics,* 135**,** 276. e1-276. e12.

Roy, S. & Basu, B. 2008. Mechanical and tribological characterization of human tooth. *Materials Characterization,* 59**,** 747-756.

Rummel, V.; Wiechmann, D. & Sachdeva, R. 1999. Precision finishing in lingual orthodontics. *Journal of Clinical Orthodontics,* 33**,** 101.

Russell, J. 2005. Current products and practice: aesthetic orthodontic brackets. *Journal of Orthodontics,* 32**,** 146-163.

Sadat-Khonsari, R.; Moshtaghy, A.; Schlegel, V.; Kahl-Nieke, B.; Möller, M. & Bauss, O. 2004. Torque deformation characteristics of plastic brackets: a comparative study. *Journal of Orofacial Orthopedics/Fortschritte der Kieferorthopädie,* 65**,** 26-33.

Santana, I. L.; Gonçalves, L. M.; Ribeiro, J. J. S.; Mochel Filho, J. R.; Júnior, C. & Alves, A. 2011. Thermal behavior of direct resin composites: glass transition temperature and initial degradation analyses. *Revista Odonto Ciência,* 26**,** 50-55.

Saunders, C. & Kusy, R. P. 1994. Surface topography and frictional characteristics of ceramic brackets. *American Journal of Orthodontics and Dentofacial Orthopedics,* 106**,** 76-87.

Schemehorn, B. R.; Moore, M. H. & Putt, M. S. 2011. Abrasion, polishing, and stain removal characteristics of various commercial dentifrices in vitro. *Journal of Clinical Dentistry,* 22**,** 11.

Schulze, K. A.; Marshall, S. J.; Gansky, S. A. & Marshall, G. W. 2003. Color stability and hardness in dental composites after accelerated aging. *Dental Materials,* 19**,** 612-619.

Schumacher, H.; Bourauel, C. & Drescher, D. 1990. The friction behavior of the ceramic bracket in arch wire-guided tooth movement. *Fortschritte der Kieferorthopadie,* 51**,** 259-265.

Scott, G. E. 1988. Fracture-toughness and surface cracks - the key to understanding ceramic brackets. *Angle Orthodontist,* 58**,** 5-8.

Scott, P.; Fleming, P. & DiBiase, A. 2007. An update in adult orthodontics. *Dental Update,* 34**,** 427-438.

Scotti, K. L. & Dunand, D. C. 2018. Freeze casting–A review of processing, microstructure and properties via the open data repository, FreezeCasting. net. *Progress in Materials Science,* 94, 243-305.

Scully, C. 2018. Number of UK adults seeking braces is rising. *British Dental Journal,* 5**,** 4.

Seghi, R.; Denry, I. & Rosenstiel, S. 1995. Relative fracture toughness and hardness of new dental ceramics. *Journal of Prosthetic Dentistry,* 74**,** 145-150.

Senden, D. J.; Krop, S.; van Dommelen, J. & Govaert, L. 2012. Rate‐and temperature‐dependent strain hardening of polycarbonate. *Journal of Polymer Science Part B: Polymer Physics,* 50**,** 1680-1693.

Shah, S. G. & Kishen, J. M. C. 2011. Fracture Properties of Concrete-Concrete Interfaces Using Digital Image Correlation. *Experimental Mechanics,* 51**,** 303-313.

Shalish, M.; Cooper-Kazaz, R.; Ivgi, I.; Canetti, L.; Tsur, B.; Bachar, E. & Chaushu, S. 2011. Adult patients' adjustability to orthodontic appliances. Part I: a comparison between Labial, Lingual, and Invisalign™. *European Journal of Orthodontics,* 34**,** 724-730.

Sharifi, L.; Ghanbarnezhad, S.; Ghofrani, S. & Mirhosseini, S. 2014. „High Porous Alumina Bodies: Production and Properties via Gelcasting Technique". *International Journal of Advanced Science and Technology,* 65**,** 59-70.

Shawkat, E. S.; Shortall, A. C.; Addison, O. & Palin, W. M. 2009. Oxygen inhibition and incremental layer bond strengths of resin composites. *Dental Materials,* 25**,** 1338-1346.

Sideridou, I.; Tserki, V. & Papanastasiou, G. 2003. Study of water sorption, solubility and modulus of elasticity of light-cured dimethacrylate-based dental resins. *Biomaterials,* 24**,** 655-665.

Sinha, P. K. & Nanda, R. S. 1997a. The effect of different bonding and debonding techniques on debonding ceramic orthodontic brackets. *American Journal of Orthodontics and Dentofacial Orthopedics,* 112**,** 132-137.

Sinha, P. K. & Nanda, R. S. 1997b. Esthetic orthodontic appliances and bonding concerns for adults. *Dental Clinics of North America,* 41**,** 89-109.

Sleibi, A.; Tappuni, AR.; Davis, GR.; Anderson, P. & Baysan, A. 2018. Comparison of efficacy of dental varnish containing fluoride either with CPP-ACP or bioglass on root caries: *ex vivo* study. *Journal of Dentistry,* 73, 2018–2096.

Smith, C. M.; Jiang, D.; Gong, J. & Yin, L. 2014. Determination of the mechanical behavior of lithium disilicate glass ceramics by nanoindentation & scanning probe microscopy. *Materials Chemistry and Physics,* 148**,** 1036-1044.

Sofie, S. W. 2007. Fabrication of functionally graded and aligned porosity in thin ceramic substrates with the novel freeze-tape-casting process. *Journal of the American Ceramic Society,* 90**,** 2024-2031.

Sofie, S. W. & Dogan, F. 2001. Freeze casting of aqueous alumina slurries with glycerol. *Journal of the American Ceramic Society,* 84**,** 1459-1464.

Souza, D. F.; Nunes, E. H.; Pimenta, D. S.; Vasconcelos, D. C.; Nascimento, J. F.; Grava, W.; Houmard, M. & Vasconcelos, W. L. 2014. Synthesis and structural evaluation of freeze-cast porous alumina. *Materials Characterization,* 96**,** 183-195.

Spears, I.; Van Noort, R.; Crompton, R.; Cardew, G. & Howard, I. 1993. The effects of enamel anisotropy on the distribution of stress in a tooth. *Journal of Dental Research,* 72**,** 1526-1531.

Springate, S. D. & Winchester, L. J. 1991. An evaluation of zirconium oxide brackets: a preliminary laboratory and clinical report. *British Journal of Orthodontics,* 18**,** 203-9.

Stamm, T.; Wiechmann, D.; Heinecken, A. & Ehmer, U. 2000. Relation between second and third order problems in lingual orthodontic treatment. *Journal of Lingual Orthodontics,* 1.

Stawarczyk, B.; Liebermann, A.; Eichberger, M. & Güth, J.-F. 2016. Evaluation of mechanical and optical behavior of current esthetic dental restorative CAD/CAM composites. *Journal of the Mechanical Behavior of Biomedical Materials,* 55**,** 1-11.

Strabala, K. W. 2009. *The Effects of Combined Compression and Aging on the Properties of Glassy Polycarbonate.* University of Nebraska.

Stratmann, U.; Schaarschmidt, K.; Wegener, H. & Ehmer, U. 1996. The extent of enamel surface fractures. A quantitative comparison of thermally debonded ceramic and

mechanically debonded metal brackets by energy dispersive micro-and image-analysis. *European Journal of Orthodontics,* 18**,** 655-662.

Strobl, K.; Bahns, T. L.; Wiliham, L.; Bishara, S. E. & Stwalley, W. 1992. Laser-aided debonding of orthodontic ceramic brackets. *American Journal of Orthodontics and Dentofacial Orthopedics,* 101**,** 152-158.

Studart, A. R. 2012. Towards High-Performance Bioinspired Composites. *Advanced Materials,* 24**,** 5024-5044.

Studart, A. R.; Gonzenbach, U. T.; Tervoort, E. & Gauckler, L. J. 2006. Processing routes to macroporous ceramics: A review. *Journal of the American Ceramic Society,* 89**,** 1771-1789.

Suliman, S. N.; Trojan, T. M.; Tantbirojn, D. & Versluis, A. 2014. Enamel loss following ceramic bracket debonding: A quantitative analysis in vitro. *Angle Orthodontist,* 85**,** 651-656.

Sulong, M. Z. A. M. & Aziz, R. A. 1990. Wear of materials used in dentistry: a review of the literature. *Journal of Prosthetic Dentistry,* 63**,** 342-349.

Sutton, M. A.; Cheng, M. Q.; Peters, W. H.; Chao, Y. J. & McNeill, S. R. 1986. Application of an optimized digital correlation method to planar deformation analysis. *Image and Vision Computing,* 4**,** 143-150.

Suzuki, T.; Kyoizumi, H.; Finger, W. J.; Kanehira, M.; Endo, T.; Utterodt, A.; Hisamitsu, H. & Komatsu, M. 2009. Resistance of nanofill and nanohybrid resin composites to toothbrush abrasion with calcium carbonate slurry. *Dental Materials Journal,* 28**,** 708-716.

Swain, M.; Coldea, A.; Bilkhair, A. & Guess, P. 2016. Interpenetrating network ceramic-resin composite dental restorative materials. *Dental Materials,* 32**,** 34-42.

Swartz, M. 1988. Ceramic brackets. *Journal of Clinical Orthodontics,* 22**,** 82-8.

Szepes, A.; Ulrich, J.; Farkas, Z.; Kovács, J. & Szabó-Révész, P. 2007. Freeze-casting technique in the development of solid drug delivery systems. *Chemical Engineering and Processing: Process Intensification,* 46**,** 230-238.

Takahashi, R.; Jin, J.; Nikaido, T.; Tagami, J.; Hickel, R. & Kunzelmann, K.-H. 2013. Surface characterization of current composites after toothbrush abrasion. *Dental Materials Journal,* 32**,** 75-82.

Tang, X.; Cai, J.; Lin, B.; Yao, L. & Lin, F. 2015. Motivation of adult female patients seeking orthodontic treatment: an application of Q-methodology. *Patient Preference and Adherence,* 9**,** 249-256.

Tehranchi, A.; Fekrazad, R.; Zafar, M.; Eslami, B.; Kalhori, K. A. & Gutknecht, N. 2011. Evaluation of the effects of CO2 laser on debonding of orthodontics porcelain brackets vs. the conventional method. *Lasers in Medical Science,* 26**,** 563-567.

Thorstenson, G. & Kusy, R. 2003. Influence of stainless steel inserts on the resistance to sliding of esthetic brackets with second-order angulation in the dry and wet states. *Angle Orthodontist,* 73**,** 167-175.

Tillman, M.; Yeomans, J. A. & Dorey, R. A. 2014. The effect of a constraint on the sintering and stress development in alumina thick films. *Ceramics International,* 40**,** 9715-9721.

Tilson, T. 1994. *Evaluation of the fracture toughness of the Japanese Yttrium-stabilized Zirconia orthodontic brackets and possible clinical implications* M,The Ohio State University, Columbus

Tobler, R. & Reed, R. 1977. Fracture mechanics parameters for a 5083-0 aluminum alloy at low temperatures. *Journal of Engineering Materials and Technology,* 99**,** 306-312.

Tocchio, R. M.; Williams, P. T.; Mayer, F. J. & Standing, K. G. 1993. Laser debonding of ceramic orthodontic brackets. *American Journal of Orthodontics and Dentofacial Orthopedics,* 103**,** 155-162.

Tong, H. & Gryte, C. 1985. Mechanism of lamellar spacing adjustment in directionally frozen agar gels. *Colloid and Polymer Science,* 263**,** 147-155.

Tselepis, M.; Brockhurst, P. & West, V. C. 1994. The dynamnic frictional resistance between orthodontic brackets and arch wires. *American Journal of Orthodontics and Dentofacial Orthopedics,* 106**,** 131-138.

Ural, Ç.; Külünk, T.; Külünk, Ş. & Kurt, M. 2010. The effect of laser treatment on bonding between zirconia ceramic surface and resin cement. *Acta Odontologica Scandinavica,* 68**,** 354-359.

Van der Veen, M.; Attin, R.; Schwestka‐Polly, R. & Wiechmann, D. 2010. Caries outcomes after orthodontic treatment with fixed appliances: do lingual brackets make a difference?. *European Journal of Oral Sciences,* 118**,** 298-303.

Van der Weijden, G. & Hioe, K. 2005. A systematic review of the effectiveness of self‐performed mechanical plaque removal in adults with gingivitis using a manual toothbrush. *Journal of Clinical Periodontology,* 32**,** 214-228.

Van Meerbeek, B.; De Munck, J.; Yoshida, Y.; Inoue, S.; Vargas, M.; Vijay, P.; Van Landuyt, K.; Lambrechts, P. & Vanherle, G. 2003. Adhesion to enamel and dentin: current status and future challenges. *Operative Dentistry,* 28**,** 215-235.

Viazis, A. D. 1989. Enamel wear from ceramic and stainless steel orthodontic brackets. *Orthodontike Epitheorese,* 1**,** 167-74.

Viazis, A. D.; Chabot, K. A. & Kucheria, C. S. 1993. Scanning electron-microscope (sem) evaluation of clinical failures of single-crystal ceramic brackets. *American Journal of Orthodontics and Dentofacial Orthopedics,* 103**,** 537-544.

Viazis, A. D.; Delong, R.; Bevis, R. R.; Rudney, J. D. & Pintado, M. R. 1990. Enamel abrasion from ceramic orthodontic brackets under an artificial oral environment. *American Journal of Orthodontics and Dentofacial Orthopedics,* 98**,** 103-109.

Voltarelli, F. R.; Santos-Daroz, C. B. d.; Alves, M. C.; Cavalcanti, A. N. & Marchi, G. M. 2010. Effect of chemical degradation followed by toothbrushing on the surface roughness of restorative composites. *Journal of Applied Oral Science,* 18**,** 585-590.

Waltimo, A. & Kononen, M. 1995. Maximal bite force and its association with signs and symptoms of craniomandibular disorders in young Finnish nonpatients. *Acta Odontologica Scandinavica,* 53**,** 254-258.

Walton, D. K.; Fields, H. W.; Johnston, W. M.; Rosenstiel, S. F.; Firestone, A. R. & Christensen, J. C. 2010. Orthodontic appliance preferences of children and adolescents. *American Journal of Orthodontics and Dentofacial Orthopedics,* 138**,** 698. e1-698. e12.

Wang, C.; Li, Y.; Wang, X.; Zhang, L. & Fu, B. 2012. The enamel microstructures of bovine mandibular incisors. *Anatomical Record: Advances in Integrative Anatomy and Evolutionary Biology,* 295**,** 1698-1706.

Wang, S.; Liang, Z.; Pham, G.; Park, Y.-B.; Wang, B.; Zhang, C.; Kramer, L. & Funchess, P. 2007. Controlled nanostructure and high loading of single-walled carbon nanotubes reinforced polycarbonate composite. *Nanotechnology,* 18**,** 095708.

Wang, W. N.; Meng, C. L. & Tarng, T. H. 1997. Bond strength: a comparison between chemical coated and mechanical interlock bases of ceramic and metal brackets. *American Journal of Orthodontics and Dentofacial Orthopedics,* 111**,** 374-381.

Waschkies, T.; Oberacker, R. & Hoffmann, M. 2011. Investigation of structure formation during freeze-casting from very slow to very fast solidification velocities. *Acta Materialia,* 59**,** 5135-5145.

Wegst, U. G.; Bai, H.; Saiz, E.; Tomsia, A. P. & Ritchie, R. O. 2015. Bioinspired Structural Materials. *Nature Materials,* 14**,** 23-36.

Wegst, U. G. K.; Schecter, M.; Donius, A. E. & Hunger, P. M. 2010. Biomaterials by freeze casting. *Philosophical Transactions of the Royal Society a-Mathematical Physical and Engineering Sciences,* 368**,** 2099-2121.

Weinkamer, R. & Fratzl, P. 2011. Mechanical adaptation of biological materials - The examples of bone and wood. *Materials Science & Engineering C-Materials for Biological Applications,* 31**,** 1164-1173.

Weir, T. 2017. Clear aligners in orthodontic treatment. *Australian Dental Journal,* 62**,** 58-62.

West, N. X.; Jandt, K. D.; Addy, M.; Embery, G.; Edgar, W. M. & Orcharson, R. 2000. Methodologies and instrumentation to measure tooth wear: Future perspectives. *In:* Addy, M., Embery, G., Edgar, W. M. & Orcharson, R. (eds.) *In Tooth Wear and Sensitivity.* London: Martin Dunitz Ltd.

Wiechmann, D.; Rummel, V.; Thalheim, A.; Simon, J.-S. & Wiechmann, L. 2003. Customized brackets and archwires for lingual orthodontic treatment. *American Journal of Orthodontics and Dentofacial Orthopedics,* 124**,** 593-599.

Wiegand, A.; Wegehaupt, F.; Werner, C. & Attin, T. 2007. Susceptibility of acid-softened enamel to mechanical wear–ultrasonication versus toothbrushing abrasion. *Caries Research,* 41**,** 56-60.

Wilson, R.; Elliott, J. & Dowker, S. 1999. Rietveld refinement of the crystallographic structure of human dental enamel apatites. *American Mineralogist,* 84**,** 1406-1414.

Winchester, L. 1992a. Aesthetic brackets: to perfect or to reject?. *Dental Update Publication,* 19**,** 107-114.

Winchester, L. 1992b. Methods of debonding ceramic brackets. *British Journal of Orthodontics,* 19**,** 233-237.

Wong, C. & Bollampally, R. S. 1999. Thermal conductivity, elastic modulus, and coefficient of thermal expansion of polymer composites filled with ceramic particles for electronic packaging. *Journal of Applied Polymer Science,* 74**,** 3396-3403.

Wriedt, S.; Schepke, U. & Wehrbein, H. 2007. The discoloring effects of food on the color stability of esthetic brackets - an *in vitro* study. *Journal of Orofacial Orthopedics-Fortschritte Der Kieferorthopadie,* 68**,** 308-320.

Wu, J.; Luo, B.; Liu, X. & Zhang, L. 2018. Control of the structure and mechanical property of porous WS2 scaffold during freeze casting. *Journal of Porous Materials,* 25**,** 37-43.

Wu, X.; Liu, Y.; Li, X.; Wen, P.; Zhang, Y.; Long, Y.; Wang, X.; Guo, Y.; Xing, F. & Gao, J. 2010. Preparation of aligned porous gelatin scaffolds by unidirectional freeze-drying method. *Acta Biomaterialia,* 6**,** 1167-1177.

Wu, Y.-Q.; Arsecularatne, J. A. & Hoffman, M. 2017. Attrition-corrosion of human dental enamel: A review. *Biosurface and Biotribology,* 3**,** 196-210.

Xie, D.; Brantley, W.; Culbertson, B. & Wang, G. 2000. Mechanical properties and microstructures of glass-ionomer cements. *Dental Materials,* 16**,** 129-138.

Xing, Z.; Li, J.; Wang, Q.; Zhou, W.; Tian, G.; Pan, K.; Tian, C.; Zou, J. & Fu, H. 2013. A floating porous crystalline TiO_2 ceramic with enhanced photocatalytic performance for wastewater decontamination. *European Journal of Inorganic Chemistry,* 2013**,** 2411-2417.

Xu, H.; Smith, D.; Jahanmir, S.; Romberg, E.; Kelly, J.; Thompson, V. & Rekow, E. 1998. Indentation damage and mechanical properties of human enamel and dentin. *Journal of Dental Research,* 77**,** 472-480.

Xu, X. & Burgess, J. O. 2003. Compressive strength, fluoride release and recharge of fluoride-releasing materials. *Biomaterials,* 24**,** 2451-2461.

Xu, X.; He, L.; Zhu, B.; Li, J. & Li, J. 2017. Advances in polymeric materials for dental applications. *Polymer Chemistry,* 8**,** 807-823.

Yan, J.; Taskonak, B. & Mecholsky, J. J., Jr. 2009. Fractography and fracture toughness of human dentin. *Journal of the Mechanical Behavior of Biomedical Materials,* 2**,** 478-484.

Yao, J.; Li, J.; Wang, Y. & Huang, H. 2014. Comparison of the flexural strength and marginal accuracy of traditional and CAD/CAM interim materials before and after thermal cycling. *Journal of Prosthetic Dentistry,* 112**,** 649-657.

Yap, A. U. J.; Low, J. S. & Ong, L. 2000. Effect of food-simulating liquids on surface characteristics of composite and polyacid-modified composite restoratives. *Operative Dentistry,* 25**,** 170-176.

Yeh, Y. & Feeney, R. E. 1996. Antifreeze proteins: Structures and mechanisms of function. *Chemical Reviews,* 96**,** 601-617.

Yogesh, g.; Vikram, S.; Shruti, S.; Aarathi, S.; Sankalp, V. & Marceliano-Alves, M. 2016. Dissipation of temperature during electro thermal debonding- an in vitro study. *International Journal of Current Research,* 8**,** 27747-27751.

Yook, S.-W.; Yoon, B.-H.; Kim, H.-E.; Koh, Y.-H. & Kim, Y.-S. 2008. Porous titanium (Ti) scaffolds by freezing TiH2/camphene slurries. *Materials Letters,* 62**,** 4506-4508.

Yoon, B. H.; Park, C. S.; Kim, H. E. & Koh, Y. H. 2007. In situ synthesis of porous silicon carbide (SiC) ceramics decorated with SiC nanowires. *Journal of the American Ceramic Society,* 90**,** 3759-3766.

Young, R. 1974. Implications of atomic substitutions and other structural details in apatites. *Journal of Dental Research,* 53**,** 193-203.

Zamanian, A.; Farhangdoust, S.; Yasaei, M.; Khorami, M. & Hafezi, M. 2014. The effect of particle size on the mechanical and microstructural properties of freeze‐casted

macroporous hydroxyapatite scaffolds. *International Journal of Applied Ceramic Technology,* 11**,** 12-21.

Zaslansky, P.; Zabler, S. & Fratzl, P. 2010. 3D variations in human crown dentin tubule orientation: A phase-contrast microtomography study. *Dental Materials,* 26**,** E1-E10.

Zero, D. T. 1996. Etiology of dental erosion–extrinsic factors. *European Journal of Oral Sciences,* 104**,** 162-177.

Zhang, L.; Le Coz-Botrel, R.; Beddoes, C.; Sjostrom, T. & Su, B. 2017. Gelatin freeze casting of biomimetic titanium alloy with anisotropic and gradient pore structure. *Biomedical Materials,* 12.

Zhang, Q. C.; Yang, X. H.; Li, P.; Huang, G. Y.; Feng, S. S.; Shen, C.; Han, B.; Zhang, X. H.; Jin, F.; Xu, F. & Lu, T. J. 2015. Bioinspired engineering of honeycomb structure - Using nature to inspire human innovation. *Progress in Materials Science,* 74**,** 332-400.

Zhang, Y.; Allahkarami, M. & Hanan, J. C. 2012. Measuring residual stress in ceramic zirconia-porcelain dental crowns by nanoindentation. *Journal of the Mechanical Behavior of Biomedical Materials,* 6**,** 120-127.

Zhang, Y.; Hu, L.; Han, J. & Jiang, Z. 2010. Freeze casting of aqueous alumina slurries with glycerol for porous ceramics. *Ceramics International,* 36**,** 617-621.

Zhang, Y.; Zuo, K. & Zeng, Y.-P. 2009. Effects of gelatin addition on the microstructure of freeze-cast porous hydroxyapatite cerarmics. *Ceramics International,* 35**,** 2151-2154.

Zhou, K.; Zhang, Y.; Zhang, D.; Zhang, X.; Li, Z.; Liu, G. & Button, T. W. 2011. Porous hydroxyapatite ceramics fabricated by an ice-templating method. *Scripta Materialia,* 64**,** 426-429.

Zinelis, S.; Eliades, T.; Eliades, G.; Makou, M. & Silikas, N. 2005. Comparative assessment of the roughness, hardness, and wear resistance of aesthetic bracket materials. *Dental Materials,* 21**,** 890-894.

Zou, J.; Zhang, Y. & Li, R. 2011. Effect of Suspension State on the Pore Structure of Freeze‐Cast Ceramics. *International Journal of Applied Ceramic Technology,* 8**,** 482-489.

Zuo, K. H.; Zeng, Y.-P. & Jiang, D. 2008. Properties of microstructure-controllable porous yttria-stabilized ziroconia ceramics fabricated by freeze casting. *International Journal of Applied Ceramic Technology,* 5**,** 198-203.

Zuo, K. H.; Zhang, Y.; Zeng, Y.-P. & Jiang, D. 2011. Pore-forming agent induced microstructure evolution of freeze casted hydroxyapatite. *Ceramics International,* 37**,** 407-410.

Appendix

DENTAL MATERIALS 34 (2018) 934–1002

Available online at www.sciencedirect.com

ScienceDirect

journal homepage: www.intl.elsevierhealth.com/journals/dema

Fabrication and characterisation of a novel biomimetic anisotropic ceramic/polymer-infiltrated composite material

Sara Al-Jawoosh[a,*], Anthony Ireland[b], Bo Su[a]

[a] Biomaterials Engineering Group, Bristol Dental School, University of Bristol, Lower Maudlin Street, Bristol, BS1 2LY, UK

[b] Child Dental Health, Bristol Dental School, University of Bristol, Lower Maudlin Street, Bristol, BS1 2LY, UK

ARTICLE INFO

Article history:
Received 2 October 2017
Received in revised form
11 March 2018
Accepted 23 March 2018

Keywords:
Biomimetic composite
Porous ceramic
Microstructure
Gelatine
Polymer
Freeze casting
Orthodontic brackets
Vickers hardness
Strength
Fracture toughness

ABSTRACT

Objective. To fabricate and characterise a novel biomimetic composite material consisting of aligned porous ceramic preforms infiltrated with polymer.

Method. Freeze-casting was used to fabricate and control the microstructure and porosity of ceramic preforms, which were subsequently infiltrated with 40–50% by volume UDMA-TEGDMA polymer. The composite materials were then subjected to characterisation, namely density, compression, three-point bend, hardness and fracture toughness testing. Samples were also subjected to scanning electron microscopy and computerised tomography (Micro-CT).

Results. Three-dimensional aligned honeycomb-like ceramic structures were produced and full interpenetration of the polymer phase was observed using micro-CT. Depending on the volume fraction of the ceramic preform, the density of the final composite ranged from 2.92 to 3.36 g/cm^3, compressive strength ranged from 206.26 to 253.97 MPa, flexural strength from 97.75 to 145.65 MPa, hardness ranged from 1.46 to 1.62 GPa, and fracture toughness from 3.91 to 4.86 MPa m$^{1/2}$.

Significance. Freeze-casting provides a novel method to engineer composite materials with a unique aligned honeycomb-like interpenetrating structure, consisting of two continuous phases, inorganic and organic. There was a correlation between the ceramic fraction and the subsequent, density, strength, hardness and fracture toughness of the composite material.

1. Introduction

Within both restorative dentistry and orthodontics there is a need for biomimetic materials that more closely approach the properties of natural tooth tissue. In restorative dentistry such a material could be used to restore tooth tissue lost through trauma or caries. A hybrid dental ceramic is commercially available [1,2] for use with CAD/CAM technology to mill dental

Abbreviations: SEM, scanning electron microscopy; h, hours; UDMA, urethane dimethacrylate; TEGDMA, triethylene glycol dimethacrylate; vol., volume; wt., weight; g, gram; mm, millimetre; μm, micrometre; °C, cellulose degrees; MCT, micro computerized tomography; GPa, gigapascal; MPa, megapascal; N, number; SD, standard deviation.

* Corresponding author.
E-mail address: sarah.al-jawoosh@bristol.ac.uk (S. Al-Jawoosh).

https://doi.org/10.1016/j.dental.2018.03.008

restorations. In orthodontics such a material might be more aesthetic and have improved mechanical properties when compared with currently available aesthetic bracket materials.

Orthodontic brackets are used to transmit loads from the archwire to the tooth [3], and are most commonly metallic and bonded to the labial surfaces of the teeth, which makes them highly visible. In the United States, from 1981 to 2013, the number of adults seeking orthodontic treatment grew from 15% to 23% [4] and as a result there have been increasing demands for more aesthetic, non-metallic bracket materials. Currently available aesthetic orthodontic brackets are either made from a polymer e.g. polycarbonate or polyurethane, or a ceramic, usually alumina, and the latter are either mono or polycrystalline in structure [5,6].

Polymeric brackets, although aesthetically good at the start of treatment, are not popular due to poor dimensional stability under applied load (creep), staining and low wear resistance [3,5]. Although ceramic brackets do not suffer from these same disadvantages, they are brittle with a tendency to fracture in-service, have a high surface hardness which can lead to abrasion of opposing teeth, and there is an increased risk of enamel fracture during bracket removal [7,8].

An ideal aesthetic orthodontic bracket would combine the advantages and none of the disadvantages of currently available polymeric and ceramic brackets. These would include improved wear resistance, whilst minimising damage to opposing teeth, good stain resistance, good dimensional stability with minimal creep, and ease of removal from the tooth surface at completion of treatment. Although brackets comprising two material phases have been produced in the past, they are essentially a ceramic bracket with a thin polymeric bonding base. Such a bracket still possesses many of the unwanted properties of ceramic brackets, namely brittleness and wear of opposing teeth. In addition, the polymeric base can delaminate during clinical service, leading to loss of tooth control and the need to bond a new replacement bracket [9,10]. Consequently, the development of a composite material that exhibits the advantages of both polymeric and ceramic brackets in a single interconnected network, is therefore desirable.

Certain naturally occurring biomaterials, including enamel and dentine, exhibit an interconnected dual phase structure leading to enhanced mechanical properties, which enable them to meet the biological functional needs of the organism [11]. Dental enamel is the hardest, most mineralised structure in the human body. It is composed of 96%–97% hydroxyapatite, 1% collagen and 2%–3% water. Throughout a lifetime, enamel can endure the forces of mastication over millions of cycles [12,13]. By contrast, dentine is a porous mineralised structure that is composed of 70% hydroxyapatite, 20% collagen and 10% water by weight [14]. Because dentine is very tough, and enamel is much harder and more brittle, they need to be joined together to provide a biomechanically compatible system.

The aim of the present study is to produce a novel biomimetic ceramic/polymer composite for use as a possible orthodontic bracket material. The novelty of such a material would be defined by its unique microstructure, characterised by two continuous interconnected inorganic and organic phases as shown in Fig. 1. The polymer rich surface attached to the tooth surface will aid bonding and debonding, and the ceramic rich surface, directly exposed to the oral environment, will provide the mechanical stability and durability in clinical use. In this way the final composite material will ideally combine the desirable properties of both ceramics and polymers, creating a durable, safe and aesthetically pleasing orthodontic bracket.

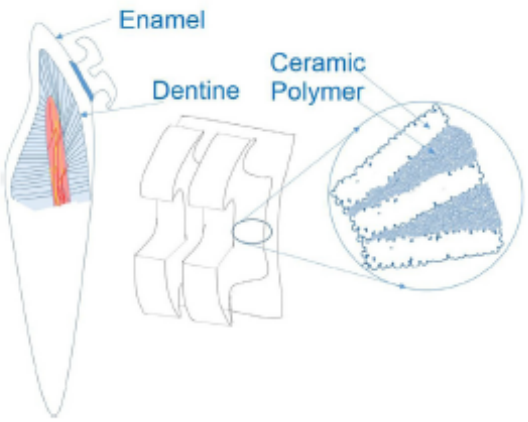

Fig. 1 – Schematic of the structure of the central incisor with the anisotropic feature of the biomimetic composite orthodontic bracket.

Freeze-casting is a well-established technique that can be used to fabricate porous scaffolds with complex microstructures. The process utilises the directional solidification of a ceramic suspension in a double-sided cooling/freezing device. The suspension is placed in a mould between two cooled surfaces, one of which is colder than the other and from where ice crystals begin to form in a unidirectional fashion. As the suspension continues to freeze the ice crystals grow from the coldest to the less cold surface. In doing so they compress the ceramic particles within the suspension to form an interconnected scaffold, which is then freeze dried and sintered. The technique is relatively simple, cost efficient, environmentally friendly and offers the ability to produce a porous material with a controlled-size and interconnection of the pores. A large number of processing parameters are used to tailor the final architecture of the porous scaffold, by controlling the crystal growth of ice [15,16].

The principal aim of the current study was to produce a ceramic/polymer-infiltrated composite material using the freeze-casting technique, followed by its infiltration with UDMA-TEGDMA polymer. The effect of the ceramic solid loading used during the freeze casting phase on the microstructure, physical and mechanical properties of the final ceramic polymer composite were then investigated.

2. Materials and methods

In this study, two novel experimental biomemetic ceramic/polymer composites were investigated. These were, EBCI = experimental biomemetic composite with 30 vol.% ceramic in the aqueous suspension, and EBCII = experimental biomemetic composite with 35 vol.% ceramic in the aqueous suspension.

2.1. Suspension preparation

Alumina powder (CT3000, Almatis AC, Inc. Germany) with an average particle size of 0.6 μm, was mixed with 0.6 wt% dispersant (Dolapix CE 64, Zschimmer & Schwarz GmbH, Germany) and distilled water to create two aqueous suspensions containing 30 and 35 vol.% ceramic. These were then ball-milled in polyethylene bottles, using zirconia media in a ball-milling machine (SRT6, Stuart, UK) overnight, in order to break down any agglomerations and achieve a homogenous dispersion. Gelatine powder (Type A, G250, Sigma–Aldrich, UK) was used as a binder to increase the strength of the green ceramic scaffold and was added in a ratio of 2.5 wt.% with respect to the ceramic powder dry weight. The final aqueous solutions of alumina, dispersant and gelatine were then ball-milled once more in a roller mixer machine (SRT6, Stuart, UK) in an oven (Thermo-Scientific, UK), and heated to 55 °C for 4 h prior to freeze casting.

2.2. Freeze-casting

Following ball milling the gelatine–alumina aqueous suspensions were poured into custom-made non-porous cylindrical moulds (diameter: 60 mm, height: 65 mm). Each mould was made of a 20-mm thick acrylic ring, which acted to insulate the suspension, and a disc-shaped base made of copper, which was used as a freezing temperature carrier. The mould was then placed in a custom-built freeze-casting machine and the process of freeze-casting was carried out as described by Preiss et al. [17]. The temperatures were controlled using band heaters (MI, Watlow, USA) and thermocouples (Type J, Watlow, USA). The top rod was cooled using an immersion cooler (FT200, Julabo, Germany), while the bottom was cooled using a separate immersion probe cooler (Polyscience, Illinois, USA). The bottom rod was cooled at a controlled rate of 1 °C/min to −10 °C, whilst the temperature of the top rod was kept at 20 °C. Subsequent sublimation of the ice took place in a vacuum in a Modulo Freeze Dryer (Edwards, Modulyo, UK) at −55 °C and 10^{-1} mbar for 48 h. The ceramic green body was then carefully removed and sintered in a high-temperature furnace (Model BRF17/4M, Elite Thermal Systems Ltd., UK) at a rate of 2 °C/min up to a temperature of 400 °C, which was then maintained for 2 h, followed by continued heating at a rate of 10 °C/min up to 1600 °C, and maintained for a further 2 h. The samples were then removed from the furnace after 24 h and allowed to cool to room temperature overnight.

2.3. Polymer infiltration

Once sintered, the porous scaffolds were chemically treated with pre-hydrolysed 3-(trimethoxysilyl) propyl methacrylate coupling agent (Sigma- Aldrich, USA), to promote chemical bonding between the inorganic and organic phases of the final ceramic/polymer hybrid. The porous ceramic scaffolds were then infiltrated with the organic phase under vacuum. The monomers were prepared by adding equal volumes of UDMA and TEGDMA and 1 vol.% of Luperox Benzoyl peroxide (Sigma–Aldrich, UK) as a heat activator. A self-contained vacuum impregnation system (Cast N'Vac Castable Vacuum System, Buehler, USA) was used to backfill the porous ceramic samples at a vacuum pressure of 4×10^{-2} mbar. The monomer/ceramic samples were then carefully placed in an oven at 50 °C for 2 h, followed by 60 °C for 3 h, 70 °C for 6 h and finally at 90 °C for 12 h, to promote heat polymerisation of the infiltrates.

2.4. Cutting procedures

An Accutom-50 (Struers, UK) precise cutting machine was used to prepare the samples using a diamond saw (Beuhler, USA), cutting them into various sizes dependant on the test to be performed. The second stage of sample preparation involved polishing using a grinding machine (Tegra Pol 15, Struers, UK) with different sequential silicon carbide papers under water cooling to a final 2400 grit. The samples were then placed in an ultrasonic water bath for 30 minutes (Grant Scientific, UK) to remove any debris and unwanted particles.

2.5. Ceramic fraction measurements

The ceramic fractions were determined by weighing the ceramic/polymer specimens and then heating them in an oven (Elite thermal systems Ltd., UK) to a temperature of 600 °C in order to ensure complete removal of the organic polymer phase. Once cooled to room temperature over 24 h, the specimens were then reweighed and the weight fractions determined. The volume fractions could then be calculated from the specific densities of the principal constituents (alumina = 3.96 g/cm^3, polymer = 1.21 g/cm^3).

2.6. Densities

The densities of the composite specimens were obtained using the Archimedes' method according to ASTM standard, C373–16, USA [18]. Rectangular blocks (4 × 4 × 8 mm) were prepared and the densities were calculated according to the following formula:

$$\text{Density} = \frac{\text{Dryweight} \times (\rho_{water} - \rho_{air})}{\text{Dryweight} - \text{Suspendedweight}},$$

where ρ_{water} and ρ_{air} are the density of deionised water and air respectively.

2.7. Sample imaging

The samples were imaged using SEM (FEI Quanata 400, FEI, USA) after being coated with a gold palladium mixture (Emitech K575X, Quorum Technology Ltd, UK). Images of the samples were also produced using a Micro-CT scanner (Nikon XTH320 CT scanner, Japan), with isotropic voxels and a spatial resolution of 13 μm. These Micro-CT images were used to reconstruct three-dimensional models of the scaffolds. The three-dimensional reconstruction of the model of each scaffold was performed from the stacking of the two-dimensional images using specialised software (Simpleware, UK).

2.8. Compressive strengths

Five rectangular specimens (4 × 4 × 8 mm) of each ceramic/polymer composite material were tested using a

universal testing machine (Zwick Roell Z020, Ulm, Germany). The compression force was directed along the long axis of the specimens and in the same direction as the freeze-casting, with the polymer rich surface at the top and the ceramic rich surface at the bottom. The compressive strength σ_C was calculated according to the following formula, where F is the load at fracture and A is the cross-sectional area:

$$\sigma c = \frac{F}{A}$$

2.9. Flexural strength and elastic modulus

A three-point bend test was used to determine the flexural strength of the fabricated composite samples. Each sample (1.8 × 4 × 18 mm) was placed into a computer-controlled universal testing machine according to British Standard, BS EN ISO 6872, 2008 [19]. For this test the samples were divided into two groups. In one group the force was directed parallel to the direction of freeze-casting and in the second group the force was applied perpendicular to the direction of freeze-casting. Once the maximum load was reached, all the samples were removed and checked to make sure that the fracture point was at the centre of the sample. Flexural strength, σ_f, was calculated according to the formula:

$$\sigma f = \frac{3FL}{2WH^2}$$

where F is the load at fracture, L the span length, W the specimen width and H the specimen height.

The elastic modulus was determined from the three-point bend test results using the formula:

$$E = \frac{F * l^3}{4 * D * W * H^3}$$

where D is the deflection corresponding to load.

2.10. Hardness

Surface hardness was measured using a micro-based indentation system (Duramin Ver 0.08, Struers, UK) under a load of 9.807 Newton with a calibrated Vickers indenter according to the Standards of Advanced Technical Ceramics, EN843-4: 2005 [20]. Six rectangular specimens (4 × 10 × 12 mm) were subjected to a maximum load for 20 s parallel to the direction of freeze casting. 30 determinations were made for each material. Indentation diagonals were measured by light microscopy. Any indentations with an irregular shape were rejected.

2.11. Fracture toughness

Six rectangular specimens of each composite sample (32 × 8 × 4 mm) were polished and pre-notched with a high-speed cutting machine according to the standards for a single-edge-notched beam, ASTM 1820.15.A,USA [21]. A razor blade and diamond paste were then employed to sharpen the notch and extend it an additional 200–350.89 μm. The final length of the notch was measured with an optical microscope. All the samples were loaded in a universal testing machine (Zwick Roell Z020, Ulm, Germany) parallel to the direction of freeze casting. The fracture toughness K_{1C} was calculated according to the formula:

$$K_{1C} \frac{Fl}{BW^{22}} f\left(\frac{\dot{\alpha}}{w}\right)$$

F is the load at fracture, L is the span length, B is the breadth of the beam, W is the width of the beam, and a is the length of the notch. Geometrical factor $f(\dot{\alpha}/w)$ can be calculated by the following equation:

$$f\left(\frac{\alpha}{w}\right) = 3\left(\frac{\alpha}{w}\right)^{1/2} x\left(1.99 - \left(\frac{\alpha}{w}\right) x\left(1 - \left(\frac{\alpha}{w}\right)\right) x2.15 - 3.93\left(\frac{\dot{\alpha}}{w}\right) + 2.7\left(\frac{\dot{\alpha}}{w}\right)^2\right) /2\left(1 + 2\left(\frac{\dot{\alpha}}{w}\right)\right) x\left(1 - \left(\frac{\alpha}{w}\right)\right)^{3/2}$$

2.12. Statistical analysis

The data were analysed using Stata version 14 (Stata Corp, College Station, Texas, USA) with a predetermined significance level of alpha = 0.05. Summary statistics are illustrated in Table 1 along with the means and 95% confidence intervals of the means and the results of the Shapiro–Wilks test. The data were found to be normally distributed in the majority of cases. Therefore t-tests were used for direct comparison of the two materials EBCI and EBCII for each characterisation test.

3. Results

The principal aim of this study was to fabricate a biomimetic composite material with fully interconnected networks of ceramic and polymer, and an intimate ceramic/polymer interface. Two different ceramic concentrations were prepared in the aqueous ceramic suspensions, 30 and 35 vol.%, with a 2.5% gelatine concentration by dry weight in each case. The slurries were then freeze-cast followed by sublimation, sintering and polymer infusion to create the ceramic/polymer specimens for testing. The use of gelatine as a binder in combination with freeze casting, promotes the formation of a three-dimensional honeycomb-like structure with pores in the micrometre range, as illustrated in Fig. 2.

3.1. Ceramic fraction and densities

As the initial ceramic suspension concentration increased from 30 to 35 vol.%, the ceramic volume of the final composite was observed to rise from 50.89% (EBCI) to 61.17% (EBCII). By increasing the ceramic volume fraction of the composite by 10%, the mean densities increased from 2.9 g/cm^3 to 3.4 g/cm^3, although this increase was not statistically significant (p = 0.069) (Table 1). Micro-CT confirmed this trend, with

Table 1 – Summary data tables for EBCI and EBCII including means, SD, 95% confidence intervals of the means, Shapiro–Wilk test (Prob > z) for normality and independent t-test p values.

Property under test	Ceramic/polymer-infiltrated composite										
	EBCI					EBCII					
	N	Mean	SD	[95% conf. interval]	SWilk prob > z	N	Mean	SD	[95% conf. interval]	SWilk prob > z	p Value
Density (g/cm^3)	5	2.92	0.33	2.52–3.33	0.47	5	3.36	0.32	2.96–3.76	0.58	0.069
Compressive strength (MPa)	5	253.97	19.23	230.06–277.84	0.35	5	206.26	20.29	181.06–231.46	0.89	0.005
Flexural strength parallel to freezing direction (MPa)	30	97.73	21.12	89.84–105.61	0.08	21	145.65	32.50	128.62–162.68	0.10	0.001
Flexural strength perpendicular to freezing direction (MPa)	6	111.57	7.36	103.84–119.30	0.59	6	129.18	13.96	114.52–143.83	0.50	0.021
Modulus of elasticity (GPa)	18	15.53	4.50	13.28–17.76	0.06	15	16.56	4.06	14.31–18.81	0.68	0.498
Hardness (GPa)	6	1.46	0.11	1.35–1.58	0.06	6	1.62	0.09	1.51–1.71	0.54	0.026
Fracture toughness (MPa m$^{1/2}$)	6	4.86	1.03	3.77–5.94	0.17	6	3.91	0.42	3.47–4.34	0.23	0.063

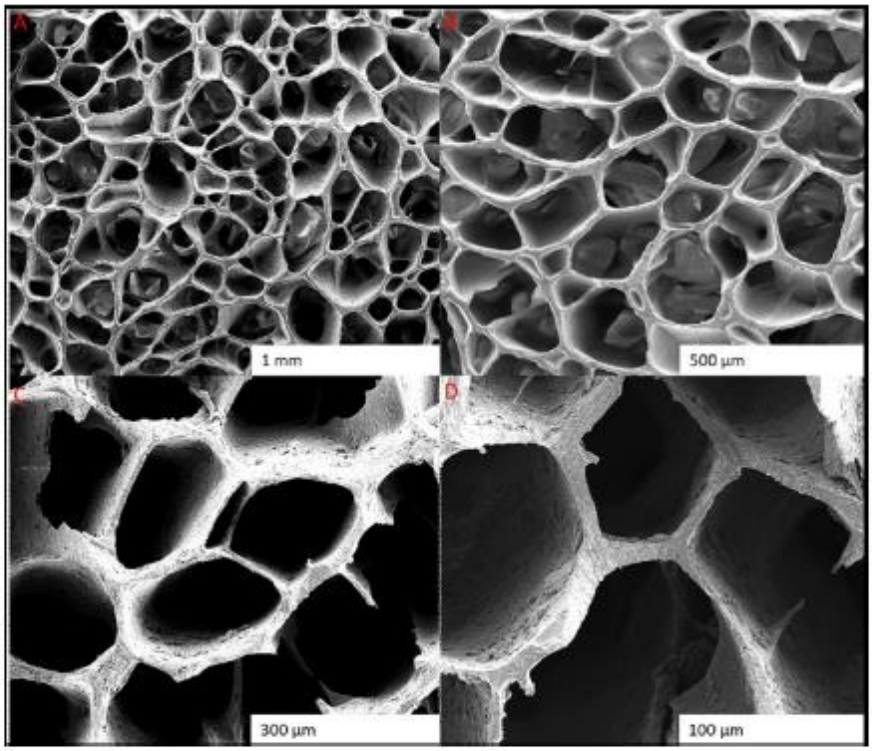

Fig. 2 – SEM images showing the honeycomb-like structure of the porous ceramic scaffold in cross section, perpendicular to the freezing direction and at four different magnifications (A ×50, B ×75, C ×180 and D ×300).

the % volumes for ECBI and ECBII being 51.27% and 62.91% respectively.

3.2. *Micro-CT sample imaging*

Micro-CT examination revealed the structure of the composite material as a fully interconnected network of a polymeric phase within a ceramic network phase. Three-dimensional reconstruction of the ceramic and polymer networks showed almost a complete infiltration of the polymer phase in the ceramic porous preform (Fig. 3).

3.3. *Compressive strength*

Unlike density, the compressive strength of the novel biomimetic composite fell as the fraction volume of ceramic in the composite increased, with the mean compres-

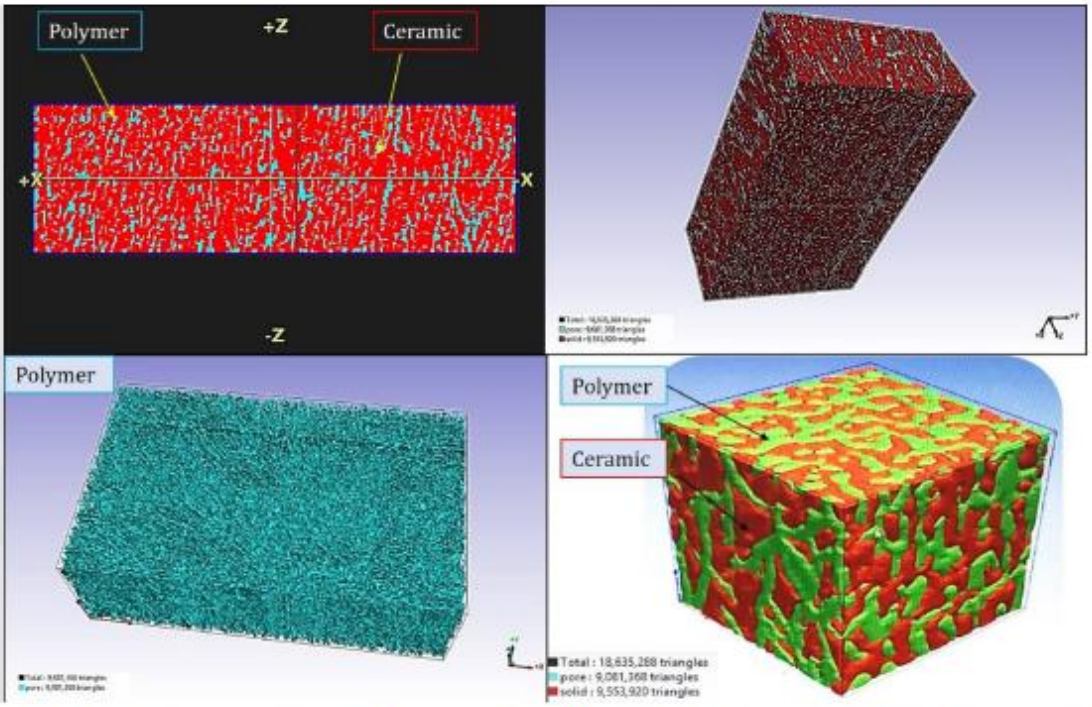

Fig. 3 – Micro-CT images representing the final composite material. Different colours represent different substances; red represents the ceramic phase, green represents the polymer phase and black represents air (less than 2%).

sive strength for EBCII being 206.26 MPa and for EBCI 253.97 MPa. This difference was statistically significant ($p = 0.005$) (Table 1).

3.4. *Flexural strength*

With increasing volume fraction of ceramic, the mean flexural strength of the hybrid composite increased from 97.73 to 145.65 MPa parallel to the direction of freeze casting, which was statistically significant ($p = 0.001$), and from 111.57 to 129.18 MPa perpendicular to the direction of freeze casting, which was also statistically significant ($p = 0.021$).

3.5. *Elastic modulus*

The elastic modulus of each of the composite materials, EBCI and EBCII were similar with mean values of 15.53 and 16.56 GPa respectively, which were not statistically significantly different ($p = 0.498$).

3.6. *Hardness*

As the ceramic suspension concentration increased there was again little change in the observed mean hardness values, which were 1.46 GPa and 1.62 GPa for the EBCI and EBCII respectively. The results were not statistically significantly different ($p = 0.026$)

3.7. *Fracture toughness*

There was a trend for a small reduction in observed mean fracture toughness from 4.86 to 3.91 GPa as the ceramic volume fraction increased for EBCI and EBCII, but this effect was not statistically significant ($p = 0.063$).

4. Discussion

The principal aim of this research was to develop a new composite material composed of ceramic and polymer networks using a novel fabrication method. Rather than one continuous organic polymer phase filled with inorganic particles, as in conventional dental composites, the new composite material possesses co-continuous interpenetrating phases of ceramic and polymer, with an anisotropic microstructure (Fig. 3). The advantage of such a composite is that its use as an orthodontic bracket material might overcome some of the disadvantages of currently available monolithic ceramic or filled polymeric orthodontic aesthetic brackets, whilst retaining the advantages of each. It is anticipated that such a new composite material could provide good bonding and debonding properties to enamel via the organic phase, fewer in service fractures and good wear resistance to brushing via the inorganic phase, but less wear to opposing teeth.

Freeze casting is a technique that can be used to create a porous ceramic scaffold through the solidification of a

ceramic suspension across a temperature gradient, followed by sublimation and sintering [22]. Alumina powder was used in the present study as it is the most popular ceramic material used to fabricate orthodontic brackets. This is due to its biocompatibility, aesthetics, high wear resistance, and high mechanical strength [23]. In the present study, the porous ceramic scaffolds created comprised anisotropic honeycomb-like porous micro-structures, rather than the lamellar pore structure typically seen with freeze casting [24]. This was due to the use of gelatine as a binder and is in agreement with another study that investigated the production of a microporous ceramic with a very high porosity and a honey-comb like structure [20]. The characteristic honeycomb-like structure is believed to be formed as a result of the gelatine gelation effect during the freezing process [25]. This mimics to some extent the distribution of the dental organic phase within the inorganic phase seen at the dentine–enamel junction in teeth [26]. The SEM images (Fig. 2) reveal honeycomb-like cylindrical pores perpendicular to the freezing direction, with various sizes of pore formed as result of the ceramic particles being expelled by the freezing water molecules. This leads to the ceramic particles becoming packed between the growing ice crystals in the gelatine-based ceramic suspension [15,25].

Gelatine is a biopolymer that is widely used in composite materials due to its non-toxicity, biological origin and desirable mechanical properties. It is a denatured collagen which undergoes physical gelation at temperatures below 15–20 °C, forming a weakly crosslinked network. The way it creates the honeycomb-like scaffold is probably as a result of the increased resistance it affords, preventing the ice crystals created during the freeze-casting process adopting their more usual plate-like morphology, and therefore lamellar structure within the ceramic suspension. Composites with interpenetrating phases and a honeycomb-like microstructure can demonstrate good mechanical and tribological properties, especially shear strength and wear, when compared to those with a lamellar structure [2,27–30].

In the present study UDMA and TEGDMA were used as the organic phase, since both are widely used as dental polymers for restorative purposes. UDMA has also previously been investigated as a single phase orthodontic bracket material [31–33]. TEGDMA monomer was used as a low viscosity diluent to promote better infiltration of the ceramic scaffold by the high viscosity UDMA [34].

The density and mechanical properties of the novel composite materials were found to change with increasing ceramic volume fraction, which is in agreement with previous studies on hybrid composite Dent Mater [2,35]. The compressive strength in the present study ranged from 206.26 to 253.97 MPa, which although lower than 94% alumina (2100 MPa) [36], is higher than that of enamel 62 to 89 MPa, and comparable to that of the dentine 194–224 MPa [37]. The flexural strength of the biomimetic ceramic/polymer composite parallel to the direction of freezing was found to be 97.73 MPa and 145.65 MPa for EBCI and EBCII respectively. This would suggest that the greater the inorganic content in the novel composite material the higher its flexural strength, and is in agreement with previous studies on dental composite materials [38,39]. Moreover, these values are higher than that found for feldspathic porcelain (65 MPa), and slightly higher than the traditional dental composite (139 MPa), but lower than data provided for sintered poly-crystalline alumina brackets (280 MPa) [40,41].

The flexural strength demonstrated anisotropy dependant on the direction of application of the force relative to the direction of freeze casting i.e. whether it was parallel or perpendicular to the direction of freeze casting. A higher strength was observed when the load was applied perpendicular to the direction of freeze casting. These results can be attributed to the arrangement of the ceramic walls and therefore polymer infiltrate within the composite, which resembles the effect seen with enamel and dentine [42,43], and is unlike the pure ceramics or polymers found in currently available monolithic aesthetic orthodontic brackets.

The elastic modulus was calculated from the results of the three-point bend test and was found to range from 15.53 GPa to 16.56 GPa. Although this is much lower than that of relatively pure alumina (300 GPa), it is to be expected of a very porous ceramic scaffold and agrees with previous work [44] that has shown elastic modulus to fall with increasing ceramic porosity.

Hardness is defined as the resistance to a permanent surface indentation and affects the material's wear resistance [45]. In this study, the hardness values of the composite material ranged between 1.46 GPa and 1.62 GPa, which is lower than that of enamel and other Dent Mater such as enamic, zirconia and lithium disilicate glass ceramics, which are 3.43, 3.31, 13.94 and 10 GPa respectively [46,47]. This would suggest that the novel ceramic/polymer composite produced in the present study would be a suitable material for oral use when opposing enamel, as it would lead to less enamel abrasion than presently available orthodontic ceramic brackets [40]. However, the surface hardness values observed were much higher than is seen with currently available polyurethane aesthetic orthodontic brackets, where surface hardness is reported to be between 0.18 and 0.19 GPa [48]. This would suggest that aesthetic brackets made from the novel ceramic/polymer infiltrated composite would show much improved wear resistance over currently available polymeric aesthetic brackets. Although having a lower surface hardness than stainless steel and nickel titanium alloys, used as bracket and archwire materials, has been suggested might lead to higher rates of wear and therefore insufficient slot–wire engagement [49], the fact that teeth move with currently available polymeric brackets would suggest this would be equally effective in the case of brackets made from this novel composite material.

Fracture toughness is the measure of a material's ability to absorb strain energy prior to fracture [50]. The reported fracture toughness values for enamel and dentine are approximately 0.72 to 1.28 and 2.2 to 3.1 MPa $m^{1/2}$ respectively [46,51,52]. The mean values for the fracture toughness of the two ceramic/polymer-infiltrated composite materials, EBCII and EBCI in the present study, were 3.91 MPa $m^{1/2}$ and 4.86 MPa $m^{1/2}$. Previous studies have reported the fracture toughness of polycrystalline alumina to be in the range of 3.0–5.3 MPa [53] and for monocrystalline alumina to be 2.4–4.5 MPa [54]. The importance of fracture toughness in the

case of aesthetic orthodontic brackets is in the ability of the bracket to resist unwanted in-service failure, and this is most commonly at the tie wing. The observed fracture toughness values for the ceramic/polymer infiltrated composite in this study, being at the higher end of values previously reported for polycrystalline alumina, the most commonly used material in orthodontic ceramic brackets, would suggest the tie wings of a bracket made from the freeze cast composite might be more resistant to failure.

Currently available aesthetic orthodontic brackets are made either from monolithic ceramic, with the disadvantages of a high surface hardness and brittle nature, or a polymer (filled or unfilled) with a low surface hardness and poor wear resistance. The novel composite materials produced in the current study were found to have an interpenetrating structure of organic polymer and inorganic ceramic phases and in an anisotropic form. Changes in the processing parameters was found to have an effect on the physical and mechanical properties of the novel ceramic/polymer infiltrated composite produced and the null hypothesis was rejected in the case of compressive strength, flexural strength and surface hardness. Further work is required on the ceramic loadings to optimise the properties for orthodontic use. In this way it is hoped that such a material will have none of these disadvantages of a currently available aesthetic orthodontic brackets, whilst retaining their aesthetic advantages.

5. Conclusion

This study has demonstrated that the use of the freeze-casting technique and a ceramic-gelatine suspension can produce porous ceramic scaffolds with interconnected pores in a three-dimensional honeycomb-like structure. By the interpenetration of a polymer into the sintered three dimensional ceramic scaffold, composite materials with two continuous ceramic and polymer phases, and different ceramic volume fractions were produced. Imaging characterisation and analysis confirmed that the new composite materials were different from the traditional composites and ceramics currently used in dentistry. It was also shown that by controlling the solid loading in the initial ceramic aqueous suspension, the physical and mechanical properties of the final composite material can be altered. There was a correlation between the physical and mechanical properties of the ceramic/polymer composite materials, their composition and their microstructure, although the effects were not always statistically significant.

Acknowledgements

We sincerely thank the Higher committee of Education Development in Iraq, Baghdad, Iraq for providing the financial support, Dr. Steven Rae for his help in fracture toughness measurements (ACCIS, Department of Aerospace Engineering, University of Bristol, UK) and the Wolfson Bioimaging Facility (University of Bristol, UK) for their help in obtaining the SEM images.

REFERENCES

[1] He L-H, Swain M. A novel polymer infiltrated ceramic dental material. Dent Mater 2011;27(6):527–34.
[2] Coldea A, Swain MV, Thiel N. Mechanical properties of polymer-infiltrated-ceramic-network materials. Dent Mater 2013;29(4):419–26.
[3] Proffit WR, Fields HW, Sarver DM. Contemporary orthodontics. 5th ed; 2012. Mosby, Inc. an affiliate of Elisive Inc.
[4] Christensen L, Luther F. Adults seeking orthodontic treatment: expectations, periodontal and TMD issues. Br Dent J 2015;218(3):111–7.
[5] Feldner JC, Sarkar NK, Sheridan JJ, Lancaster DM. In-vitro torque-deformation characteristics of orthodontic polycarbonate brackets. Am J Orthod Dentofac Orthop 1994;106(3):265–72.
[6] Kusy RR. Orthodontic biomaterials: from the past to the present. Angle Orthod 2002;72(6):501–12.
[7] Buzzitta VAJ, Hallgren SE, Powers JM. Bond strength of orthodontic direct-bonding cement-bracket systems as studied in vitro. Am J Orthodont Dentofac Orthop 1982;81(2):87–92.
[8] Douglass JB. Enamel wear caused by ceramic brackets. Am J Orthod Dentofac Orthop 1989;95(2):96–8.
[9] Olsen ME, Bishara SE, Jakobsen JR. Evaluation of the shear bond strength of different ceramic bracket base designs. Angle Orthod 1997;67(3):179–82.
[10] Elekdag-Turk S, Isci D, Ozkalayci N, Turk T. Debonding characteristics of a polymer mesh base ceramic bracket bonded with two different conditioning methods. Eur J Orthod 2009;31(1):84–9.
[11] Munch ME, Launey DH, Alsem E, Saiz AP, Tomsia RO. Tough, bio-inspired hybrid materials. Science 2008;322(5907):1516–20.
[12] Nancy A. Ten Cate's oral histology: development, structure, and function. 7th. ed. Saint Louis: Mosby Inc.; 2008.
[13] He LH, Yin ZH, van Vuuren LJ, Carter EA, Liang XW. A natural functionally graded biocomposite coating — human enamel. Acta Biomater 2013;9(5):6330–7.
[14] Zaslansky P, Zabler S, Fratzl P. 3D variations in human crown dentin tubule orientation: a phase-contrast microtomography study. Dent Mater 2010;26(1):E1–10.
[15] Deville S. Freeze-casting of porous biomaterials: structure, properties and opportunities. Materials 2010;3(3):1913–27.
[16] Zhang Y, Zuo K, Zeng Y-P. Effects of gelatin addition on the microstructure of freeze-cast porous hydroxyapatite cerarmics. Ceram Int 2009;35(6):2151–4.
[17] Preiss A, Su B, Collins S, Simpson D. Tailored graded pore structure in zirconia toughened alumina ceramics using double-side cooling freeze casting. J Eur Ceram Soc 2012;32(8):1575–83.
[18] A. International, Standard test methods for determination of water absorption and associated properties by vacuum method for pressed ceramic tiles and glass tiles and boil method for extruded ceramic tiles and non-tile fired ceramic whiteware products 1, C373 – 16′1, 2016.
[19] BSI. Dentistry. Ceramic materials. BSI; 2008.
[20] BSI. Advanced technical ceramics. Mechanical properties of monolithic ceramics at room temperature. Vickers, Knoop and Rockwell superficial hardness. BSI; 2007.
[21] A. International. Standard test method for measurement of fracture toughness 1. American Society for Testing and Materials; 2011.
[22] Deville S. Freeze-casting of porous ceramics: a review of current achievements and issues. Adv Eng Mater 2008;10(3):155–69.

[23] de Sá e Benevides de Moraes MCC, Elias CN, Filho JD, de. Oliveira LG. Mechanical properties of alumina–zirconia composites for ceramic abutments. Mater Res 2004;4(4):643–9.
[24] Park H, Choi M, Choe H, Dunand DC. Microstructure and compressive behavior of ice-templated copper foams with directional, lamellar pores. Mater Sci Eng 2017;679:435–45.
[25] Fukushima M, Nakata M, Yoshizawa Y-I. Fabrication and properties of ultra highly porous cordierite with oriented micrometer-sized cylindrical pores by gelation and freezing method. J Ceram Soc Japan 2008;116(1360):1322–5.
[26] Amizuka N, Uchida T, Fukae M, Yamada M, Ozawa H. Ultrastructural and immunocytochemical studies of enamel tufts in human permanent teeth. Arch Histol Cytol 1992;5(2):179–90.
[27] Long CG, Su Y, Shen C. Mechanical and tribological properties of polytetrafluoroethylene filled polyoxymethylene/aluminum foam interpenetrating phase composites. In: Kim YH, Yarlagadda P, editors. Research in materials and manufacturing technologies. 2016. p. 285–9. Pts 1-32014.
[28] Zhang QC, Yang XH, Li P, Huang GY, Feng SS, Shen C, et al. Bioinspired engineering of honeycomb structure — using nature to inspire human innovation. Prog Mater Sci 2015;74:332–400.
[29] Lakes R. Materials with structural hierarchy. Nature 1993;361(6412):511–5.
[30] Fukushima M, Yoshizawa Y, Ohji T. Macroporous ceramics by gelation-freezing route using gelatin. Adv Eng Mater 2014;6(6):607–20.
[31] Sideridou I, Tserki V, Papanastasiou G. Study of water sorption, solubility and modulus of elasticity of light-cured dimethacrylate-based dental resins. Biomaterials 2003;24(4):655–65.
[32] Faltermeier A, Behr M, Mossig D. In vitro colour stability of aesthetic brackets. Eur J Orthod 2007;9(4):354–8.
[33] Krauss J, Faltermeier A, Behr M, Proff P. Evaluation of alternative polymer bracket materials. Am J Orthod Dentofac Orthop 2010;137(3):362–7.
[34] Floyd CJE, Dickens SH. Network structure of bis-GMA- and UDMA-based resin systems. Dent Mater 2006;2(12):1143–9.
[35] He L-H, Purton D, Swain M. A novel polymer infiltrated ceramic for dental simulation. J Mater Sci Mater Med 2011;22(7):1639–43.
[36] ACCURATUS, Aluminum oxide, Al_2O_3 ceramic properties. http://accuratus.com/alumox.html.
[37] Chun KJ, Choi HH, Lee JL. Comparison of mechanical property and role between enamel and dentin in the human teeth. J Dent Biomech 2014;5.
[38] Mueller IWFM. Effect of filler content of restorative resins on retentive strength to acid-conditioned enamel. Am J Dent 1994;7(3):161–6.
[39] Kim KH, Ong JL, Okuno O. The effect of filler loading and morphology on the mechanical properties of contemporary composites. J Prosthet Dent 2002;87(6):642–9.
[40] Sakaguchi R, Powers J. Craig's restorative dental materials. 13 ed. St. Louis: Mosby; 2012.
[41] Swartz M. Ceramic brackets. J Clin Orthod 1988;22(2):82–8.
[42] Miura J, Maeda Y, Nakai H, Zako M. Multiscale analysis of stress distribution in teeth under applied forces. Dent Mater 2009;25(1):67–73.
[43] Kinney JH, Marshall SJ, Marshall GW. The mechanical properties of human dentin: a critical review and re-evaluation of the dental literature. Crit Rev Oral Biol Med 2003;14(1):13–29.
[44] Asmani M, Kermel C, Leriche A, Ourak M. Influence of porosity on Young's modulus and Poisson's ratio in alumina ceramics. J Eur Ceram Soc 2001;21(8):1081–6.
[45] Vallittu P. Non-metallic biomaterials for tooth repair and replacement. Cambridge: Woodhead; 2012.
[46] Min J, Arola DD, Yu DD, Yu P, Zhang QQ, Yu HY, et al. Comparison of human enamel and polymer-infiltrated-ceramic network material ENAMIC through micro- and nano-mechanical testing. Ceram Int 2016;42(9):10631–7.
[47] Zhang Y, Allahkarami M, Hanan JC. Measuring residual stress in ceramic zirconia-porcelain dental crowns by nanoindentation. J Mech Behav Biomed Mater 2012;6:120–7.
[48] Ali O, Makou M, Papadopoulos T, Eliades G. Laboratory evaluation of modern plastic brackets. Eur J Orthod 2012;4(5):595–602.
[49] Graber T, Bjorn U, Zachrisson B, Büyükyilmaz T. Orthodontics—current principles and technique. Mosby; 2005.
[50] Brantley W, Eliades T. Orthodontic materials, scientific and clinical aspect. New York: Thieme Stuttgart; 2001.
[51] Bajaj D, Arola DD. On the R-curve behavior of human tooth enamel. Biomaterials 2009;30(23–24):4037–46.
[52] Lawn BR, Lee JJW. Analysis of fracture and deformation modes in teeth subjected to occlusal loading. Acta Biomater 2009;5(6):2213–21.
[53] Hertzberg RW. Deformation and fracture mechanics of engineering materials. 2nd ed. John Wiley & Sons; 1983.
[54] Iwasa M, Brandt R. Fracture toughness of single crystal alumina. In: Kingery WD, editor. Structure and properties of MgO and Al_2O_3. Advances in ceramics. Columbus: American Ceramic Society; 1986. p. 767–78.